Structural Studies of Fullerene Derivatives [60]PCBM and All 19 Isomers of Bis[60]PCBM

Tong Liu

Submitted in partial fulfillment of

the requirements of the Degree of

Doctor of Philosophy

School of Physics and Astronomy
Queen Mary, University of London
2019

Statement of Originality

I, Tong Liu, confirm that the research included within this thesis is my own work or that where it has been carried out in collaboration with, or supported by others, that this is duly acknowledged below and my contribution indicated. Previously published material is also acknowledged below.

I attest that I have exercised reasonable care to ensure that the work is original, and does not to the best of my knowledge break any UK law, infringe any third party's copyright or other Intellectual Property Right, or contain any confidential material.

I accept that the College has the right to use plagiarism detection software to check the electronic version of the thesis.

I confirm that this thesis has not been previously submitted for the award of a degree by this or any other university.

The copyright of this thesis rests with the author and no quotation from it or information derived from it may be published without the prior written consent of the author.

Signature:

Date: 26.09.2019

Publications

1. W. Shi, X. Hou, **T. Liu**, X. Zhao, A. B. Sieval, J. C. Hummelen, and T. J. S. Dennis, "Separation and Electric Characterisation of all 18 Isomers BisPCBM", *Chemical Communications*, 2017, **53**(5), 975-978.

2. **T. Liu**, I. Abrahams, and T. J. S. Dennis, "Structural Identification of 19 Purified Isomers of the OPV Acceptor Material bisPCBM by ^{13}C NMR and UV–Vis Absorption Spectroscopy and High-Performance Liquid Chromatography", *Journal of Physical Chemistry A*, 2018, **122**(16), 4138-4152.

Acknowledgments

Abstract

Bis[60]PCBM is a molecule with two identical asymmetric addends bridging double bonds on the fullerene C_{60}, giving rise to 58 nominal structural isomers. However, symmetry, chirality and steric hindrance reasons leave 19 possible isomers. Considering bond-type involved gives one C_1 and one C_2 isomers for the *cis*-3, *trans*-3 and *trans*-2 bonds; one C_1 and two C_s isomers for the *cis*-2 and *trans*-4 bonds; two C_1 isomers for the *e* bonds; one isomer of C_{2v} and C_{2h} symmetry for the *trans*-1 bonds.

The mixture of bis[60]PCBM was separated into individual components through high-pressure liquid chromatography. An initial single-pass HPLC treatment separated the mixture into 7 resolved fractions, of which three comprised a single isomer. A multi-stage peak-recycling HPLC process which involved several complimentary columns was devised to separate all isomers. The mixture was purified into 19 isomers (same number as possible isomers). Characterisation by UV-Vis absorption spectroscopy showed that some were similar, while others were different. This placed the isomers into 7 groups, two of which contained two isomers and the other five contained three isomers – the same in number and size for each bond-type as identified from the molecular structures, suggesting that there is a link between the shape of the spectra and the bond type of the isomer. A similar link was reported in the literature for symmetric fullerene bis-adducts, allowing assignment of the 7 isomer groups to their respective bond types. ^{13}C NMR spectroscopy allowed for the C_{2v}, C_{2h}, and the unique (C_1) isomers in each of the five three-membered bond-type groups to be associated with their corresponding

HPLC fraction. This left 6 groups, each two unidentified isomers with both being either C_1, C_2, or C_s, which cannot be distinguished by ^{13}C NMR spectra. HPLC retention times for members of the three-membered groups had the order of symmetric-asymmetric-symmetric. Hence, the two same-symmetry isomers in each group had widely spaced retention times. As HPLC columns separate based on molecular polarity. By arranging the same-symmetry isomers in order of polarity inversely orders then in HPLC retention time, which allowed for their identification. By these analyses, every one of the 19 purified HPLC fractions was associated with its corresponding structural isomer.

Structural identification via ^{13}C NMR spectroscopy was aided by benchmarking several DFT methods against the spectrum of [60]PCBM. The ωB97X method performed particularly well, and Dunning-type, outperformed Pople-type, basis sets. Agreement between experiment and simulation allowed all resonances to be assigned to their corresponding carbon atoms with high confidence.

Table of Contents

List of Figures

List of Abbreviations

BHJ	bulk heterojunction
OPV	organic photovoltaics
HOMO	highest occupied molecular orbital
LUMO	lowest unoccupied molecular orbital
FCC	face centred cubic
UV-Vis	ultraviolet and visible light absorption spectroscopy
NMR	nuclear magnetic resonance
HPLC	high-pressure liquid chromatography
DFT	density functional theory
IUPAC	international union for pure and applied chemistry
CV	cyclic voltammetry
TMS	trimethylsilane
MB	methyl butanoate
ATP	attached proton test
GIAO	gauge independent atomic orbitals
MAE	mean absolute error

1   Introduction

1.1   The thesis

The fullerene derivative methyl 4-[61-phenyl,3'*H*-cyclopropa-1,9-(C$_{60}$-*I*$_h$)[5,6]-fullerenyl]butanoate, originally named M1-OMe[1] is more commonly known as phenyl C$_{61}$ butyric acid methyl ester – simply by the acronym thereof, PCBM[2] or [60]PCBM.[3] It is one of the most important n-type molecules in organic electronics principally as the archetypal electron acceptor in bulk heterojunction (BHJ) photovoltaics.[4-10] Moreover, it has also been widely used in photodetectors[11-17], light emitting diodes[18-25], transistors[26-30], and perovskite-based organic-inorganic hybrid solar cells[31-36]. [60]PCBM was first reported by Hummelen, Wudl and co-workers in 1995 as one of six examples of the synthesis of novel homo- and methano-bridged cyclo-additions to the fullerene C$_{60}$ and, as mentioned above. It was identified at the time by the name of M1-OMe.[1] The initial motivation of that research was to increase the solubility of C$_{60}$ (whose concentration in 'good' solvents is micromolar) for potential bio-molecular applications. However, as

mentioned above, this molecule has re-named as [60]PCBM and been having a new and spectacular life in organic electronics.

From Equation 1-1, the power conversional efficiency (η) of organic photovoltaics (OPV) scales linearly with the open circuit voltage (V_{OC})[37].

$$\eta = \frac{V_{OC} \times J_{SC} \times FF}{P_{IN}}$$ **Equation 1-1**

V_{OC}, J_{SC}, FF and P_{IN} are the open circuit voltage, short circuit current, the fill factor and the power of the incident light. Furthermore, empirically the V_{OC} of OPVs scales reasonably linearly with the energy difference between the highest occupied molecular orbital (HOMO) of the donor material and the lowest unoccupied molecular orbital (LUMO) of the acceptor material.[38-40] Therefore, increasing the LUMO of acceptor material and/or lowering the HOMO of donor material leads to increase the efficiency. The two effective approaches that can be employed to raising the LUMO of acceptor and decreasing HOMO of the donor. Decreasing the HOMO of the donor would increase the HOMO-LUMO gap of the donor which would decrease the maximum wavelength of the absorption – losing some red and orange radiation, it is not beneficial for the improvement of the efficiency.

Over the last 15 years, improvement of the performance of the donor material has advanced steadily. Over the same period, the acceptor material has remained almost exclusively the fullerene adduct like [60]PCBM[41, 42] and some other related species like [70]PCBM[43] and bis[60]PCBM[44] etc. In this work, I concentrate on improving the properties of acceptor material.

C_{60} has many properties that make it an almost ideal acceptor material.[45] Its spherical shape means that it cannot interface with a donor polymer in an

unfavourable orientation. It has a low lying triply degenerate LUMO (t_{1u}) and low lying triply degenerate LUMO+1 (t_{1g}).[46] Thus, C_{60} may readily accept up to 12 electrons. It has a well-defines face centred cubic (FCC) crystal structure[47], which has beneficial effects on charge transport within the fullerene phase, enhancing device current. At high concentration, C_{60} forms aggregates which is essential for BHJ formation as this results in interlinked fullerene domains and donor polymer domains. Unfortunately, C_{60} also has some drawbacks. It has very low solubility[48], which results in processability problems – primarily through oversized aggregates (the single fullerene domain that are larger than the thickness of the active layer). The high symmetry of C_{60} leads to many optically (dipole) forbidden transitions.

In 1992 Wudl and co-workers demonstrated that the ultrafast electron transferred from a polymer to C_{60}[49], but the development of a working OPV device was hindered by the abovementioned solubility issues. This group later (in 1995) synthesised [60]PCBM with the intention to increase the solubility of C_{60} (by a factor of 10) for use as a HIV protease inhibitor.[1] However, the higher solubility of [60]PCBM than C_{60} make it successfully as an acceptor in an OPV device.[50] This paper not only revealed the successful use of a fullerene in an OPV device, in employing a mixture of a donor and acceptor, it also was the first demonstration of a bulk heterojunction. On top of the increase in solubility, the additional group of [60]PCBM reduces the molecular symmetry to C_s which makes all optical modes dipole allowed. This advantage is not as great as might be expected. This is because away from the addition site the perturbation to the cage is small, so most modes only become weakly allowed.[51]

With [60]PCBM showing promising properties as an electron acceptor material, a matching donor material was needed to work with [60]PCBM. Ideally, such a

donor should have wide absorption across the visible spectrum while having a LUMO level slightly above that of [60]PCBM. This is because a wide absorption range is needed to maximise utilisation of most solar radiation available at the earth's surface, and a nearly matching LUMO level is needed to minimise energy loss following charge separation while maintaining spontaneity of the transfer. The polymer Poly(3-hexylthiophene-2,5-diyl) (P3HT) has proven to be useful in this expectation.[52] Its HOMO-LUMO gap is 1.68 eV[53] which means that all solar radiation with a wavelength below 738 nm can photo excite it, and its LUMO level (–3.52 eV) is 0.23 eV above the LUMO level of [60]PCBM.[54] Nevertheless, there is still space for further improvement that a new acceptor could be employed with a higher LUMO than that of [60]PCBM. For this reason, several other fullerene derivatives have been developed.

Other fullerenes have subsequently been employed as an acceptor material for organic solar cells including [70]PCBM[55] and [84]PCBM[56], as well as the mixture of bis and tris versions of [60]PCBM (bis[60]PCBM and tris[60]PCBM[57]). [70]PCBM has been proved reasonably successful because of its lower symmetry, but it suffers from a lower LUMO than that of [60]PCBM, as well as [84]PCBM. Tris[60]PCBM mixture yields a high 200 meV increase in LUMO level compared with [60]PCBM, but even with this increase, the efficiency of tris[60]PCBM-based OPVs is still lower than that of those made from [60]PCBM. The reason is said to relate to a lowering of transport capabilities with the increasing number of addends.[27] Although the efficiency of bis[60]PCBM-based OPVs is higher than that of its [60]PCBM-based analogue, it is still lower than expected from a pure isomer-based OPVs with increased-LUMO V_{OC} for the same reason.[44] Together with varying the fullerene, there is much published work on C_{60} bisadduct-based

OPV devices involving varying the parts of the addends. Examples include variants on bis[60]PCBM where aryl groups other than phenyl[58-62], n-alkyl chains replace butyl[60, 63] and end groups other than methyl esters has been employed.[59-61, 64-79] Methods other than cyclopropa-additions of attaching the addends to the fullerene have also been employed. These include dihydronaphalyl-based derivative[80-82], fulleropyrrolidine derivatives[83-86] and quinooxaline based derivatives.[87-91] Again, like the cyclopropa-additions, these have also been synthesised with numerous variations of attached functional groups.[92] However, although these changes may affect the performance of the altered molecules in electronic devices, they all exit as the mixture of many isomers.

Although bis[60]PCBM-based OPVs have higher efficiencies, it has potential to be considerably better. This is because (as will be shown in Chapter 4) it is synthesised as a mixture of 19 structural isomers. Each isomer will have a different LUMO level[93] – some above and some below the average LUMO level for the bis[60]PCBM mixture. Making BHJ-OPVs only with isomers that have high LUMOs would produce devices with higher V_{OC}s to get higher efficiencies. Making devices with pure isomers would also have advantages on the current side as it could improve the morphology of active layer. Through Equation 1-1, the efficiency also scales linearly with the J_{SC}. As a mixture of 19 different isomers, it would have a poorly defined crystal structure. Hence, the hopping of the electron from within the fullerene phase from the charge separation site towards the cathode would be somewhat inefficient. In addition, using a single isomer would remove the energetic disorder associated with the mixture. This is because all molecules in the fullerene phase would have exactly the same LUMO level which is helpful for electron transition compared with varied LUMO levels of the mixture.

With this, it can be claimed that using pure isomer of bis[60]PCBM potentially will increase V_{OC} via employing isomers with the highest LUMO levels, and also increase J_{SC} via improved morphology.

Despite these advantages of using single purified isomers being known for more than a decade, there are very few reports in the literature on employing them in organic electronic devices. One fullerene bis-adduct that has been separated into purified isomers is indene C_{60} bis-adduct ([60]ICBA). Cao *et al.*[94] separated [60]ICBA into to its individual isomers, characterised them by ultraviolet and visible light absorption spectroscopy (UV-Vis), ^1H and ^{13}C NMR spectroscopy. They also employed the individual isomers into OPV devices. However, this still leaves one major problem. They isolated the three *trans*-2 isomers of [60]ICBA from the mixture, and each other, but they did not determine which one of the three possible *trans*-2 isomers corresponded to each of the three high-pressure liquid chromatography (HPLC) fractions. Isomers of the C_{70}-based analogue of [70]ICBA have also been purified (by Leihua Hu and co-workers[95]. Again, these were characterised by UV-Vis spectroscopy, ^1H and ^{13}C nuclear magnetic resonance (NMR) spectroscopy. The OPV devices based on them were fabricated and characterised. There were reported as iso-3(2)-$IC_{70}BA$ and iso-5-$IC_{70}BA$, which affords little information on which one of the more-than-20 possible isomers of $IC_{70}BA$ was used in their devices.

Addressing this problem about the lack of identification for the specific molecular structure of these even few purified isomers of [60]ICBA and [70]ICBM with their corresponding HPLC-purified samples was a major aim of my PhD investigations. Here I used UV-Vis and ^{13}C NMR spectroscopic analyses, together with developing, describing and quantifying a reliably method of determining the HPLC

retention time order of same-symmetry isomers, to associate every one of the 19 possible structural isomers of bis[60]PCBM to its corresponding HPLC-purified sample. Hence, the thesis of this work is that, in order for these ideas to be tested and improved for devices achievement, samples of individual purified isomers of bis[60]PCBM must be made available to researchers in the field, and that in order for them to draw meaningful conclusions on why some isomers are better or worse than others, they need to know the molecular structure of each purified sample they are using.

1.2 The outline of the work

In the year of September 1985, in order to collect the products of laser ablation of graphite, a series of experiments were originally set up for the investigation of the formation mechanisms of long-chain carbon molecules which were found in interstellar space. However, the experiments were not only successful to obtain the long-chain carbon molecules, but also accidentally made a remarkable discovery of a very stable molecule. That stable molecule composed 60 carbons atoms which gave a relative molecular mass of 720 amu. In order to find out the molecular structure of this molecule, a truncated icosahedral molecular structure was proposed to present this molecule which contained 60 carbons. Unfortunately, it was not possible to obtain enough material for structural identification as these experiments were only produced by millisecond timescale for each laser pulse and detected in microscopic quantities by mass spectroscopy. In August 1990, another research group who was working on the diffuse interstellar bands of astrophysical chemistry found the method to synthesise this stable molecule in the macroscopic

quantities. This finding then allowed confirmation of the proposed molecular structure after gaining enough material.

The discovery of fullerene that showed elemental carbon could form a ball structure that has given rise to a revolution in carbon chemistry, as it was claiming that carbon can only crystallised into two allotropes of diamond and graphite before the discovery of fullerene. This finding awarded the Nobel Prize in chemistry in 1996. A brand-new branch of science 'nanotechnology' had been developed based on fullerene materials. This includes the applications of fullerene-like carbon allotrope, the development of fullerene chemistry, the application of fullerene derivatives and so on.

This thesis contains an investigation on such fullerene derivative, bis[60]PCBM, which principally has potential application as an n-type material in organic electronics. This molecule could exist in literally hundreds of isomeric forms. Initially, following a method that was devised to separate the as-produced isomers mixture into its individual purified isomers from Dennis[93] and Shi.[96] After which the molecular structure of each of the purified isomers was identified. With this information, researcher who follow and put purified isomers into organic electronic devices may know which particular isomer (molecular structure) they are using. This work was conducted between September 2015 and September 2019 in the School of Physics and Astronomy, Queen Mary University of London.

The remainder of this chapter contains an historical account of fullerene, from the first imaginative prediction, through its serendipitous discovery, the steps that led to the availability of macroscopic samples. Issues relating to fullerene nomenclature will also be discussed.

Chapter 2 presents some theoretical aspects of the principles behind the methods that used in this thesis. They include general spectroscopy with an emphasis on ultraviolet and visible light absorption spectroscopy, nuclear magnetic resonance spectroscopy and high-pressure liquid chromatography.

Chapter 3 presents the ^{1}H, ^{13}C and 2D NMR spectra of the fullerene mono-adduct [60]PCBM. Apart from the 2D spectrum, these spectra were previously published in the literature, but the analyses were incomplete. For example, several of the proton resonances were previously described as 'multiplets' despite they were being expected to comprise simple spin-spin coupling components (e.g., 1:2:1 triplets). The multiplets resulted from 2nd-order spin-spin coupling effects which were not even previously mentioned. These are fully analysed in this Chapter and give insights into the orientational dynamics and conformer populations of the butyl chain of the ester group. In addition, there were several previously unknown ^{13}C resonances which are identified. This leads to the identification of all resonances that include the fullerene carbons on the molecule's mirror plane for the first time. The 2D spectrum allowed for the unambiguous assignment of all ^{13}C resonances from the carbons with attached hydrogens to their respective carbon atoms on the molecule. Finally, simulations of the ^{13}C NMR spectrum using modified ωB97X density functional theory (DFT) allowed the assignment of the carbon atoms of the fullerene to their corresponding resonances to be made with a high degree of confidence.

Chapter 4 Following the purification method that provided in the published account[93, 96], this Chapter demonstrates the finding of the 19th missing isomer of F1.1, these resulted in having samples of all the isomers from the mixture, then those isomers were studied in the following Chapter. The results show that despite

the potential of hundreds of possible bis[60]PCBM isomers, only 19 of them actually form.

Chapter 5 presents the characterisation of bis[60]PCBM by UV-Vis and ^{13}C NMR spectroscopic methods. Rather than studying the frontier energy levels (which was a part of the project led by another student[96]), I used my own synthesised and purified samples, recorded and analysed their UV-vis spectra, which were then used, in conjunction with the ^{13}C NMR spectra with the primary aim of identifying the molecular structure of the isomers that correspond to each of the isomer-pure samples obtained from the work presented in Chapter 4. The results show that all the isomers are cyclopropa-fullerenes (methano-bridged). This means no homo-fullerene are formed (in which may bridge either two intra-pentagonal single bonds, two intra-hexagonal double bonds, or a combination of bridging one single and one double bond). This drastically reduced the number of possible bis[60]PCBM isomers to only 58. With this, this chapter also presents all 58 potential isomers, and then shows how symmetry, chirality and steric hindrance reduce the number of possible isomers to only 19. Hence, this chapter explains why there are only 19 isomers and goes on to allow for the association of every one of the 19 possible isomers to its corresponding one of the 19 purified HPLC fractions.

The thesis is summarised in the 6th and final Chapter.

1.3   The discovery of fullerenes

In the year of 1970, Osawa firstly reported the assumption of C_{60} in his article[97], then it was further presented in a book which was discussing the super aromaticity by Yoshida and Osawa in 1971.[98] Initially, in 1966, a similarly imaginative paper

which conjectured the possibility of making large hollow carbon cages [99, 100] were reported by Jones. But the concept of C_{60} was not clearly formed at that time. In 1971, Huckel calculations of C_{60} was published by Bochvar and Gal'pern.[101] Then the graph theory was used to deduce an algebraic solution of the Huckel calculations from Davidson in 1981.[102] Overall the discovery of C_{60} came by an accident – from observing the experiments that were set up for the chemical processes in the interstellar medium material.

From the early 1970s, professor Kroto was focusing on the research of unsaturated carbon in his laboratory. The specific topic was unstable closed-shell species which contain multiple C-S, C-Si, C-P, and C-C bonds.[103] These molecules were produced from specially synthesised precursors by thermolysis, and characterised by spectroscopic techniques such as infra-red, microwave and photoelectron. Then some improvements were achieved in molecular radio-astronomy at the same period of time. The finding of many unidentified molecules from black clouds smeared across in the galaxy was observed.[104] Compared with this discovery, the second-row elements in the period table formed compounds, and long chain carbon molecules which contained C-C multiple bonds were also being detected and under investigation from interstellar space. Walton and co-workers devised the synthesis of long chain polyynylcyanides, including HC_5N, HC_7B and HC_9N. The microwave spectra of these molecules were recorded, and radio-astronomy led to the identification in dark molecular clouds[105]. The discovery of these attracted attentions from researchers of the origin form of these molecules. For the observation of huge quantities of carbon-based dust was periodically cast off from variable red-giant stars, this led to the researchers came up with the idea of long-chain carbon molecules might be present in the dust grains in circumstellar shells.

In the year of 1979, a powerful technique which allowed mass spectroscopy worked on measurement of short-lived unstable species was developed by Smalley and co-workers at Rice University. The original interest from Smalley was the research of tiny clusters of silicon and germanium atoms by focussing a laser beam on the solid target. These experiments were considered valuable for the discovery of useful applications in semiconductor technology. By the chance of visiting Smalley's laboratory, Kroto came up with the ideas that the experiment environment of focussing the laser on a graphite target can be similar to that of in the outer atmospheres of carbon stars, and this might lead to the formation of long chain carbon molecules. In the summer of 1984, a basic graphite laser vaporisation experiment was carried out by a research group in Standard Oil Company of New Jersey.[106] They surprisingly discovered carbon clusters ranging from C_{30} to C_{190}.[106] with only even numbered. However, none of those carbon clusters was identified to be special.

The characterisations of the products from laser-vaporised graphite experiment were commenced at Rice University in September 1985. The measurements of using atmospheres of ammonia, hydrogen, oxygen and so on to produce and detect long-chain carbon molecules were successful. The results demonstrated that the chemistry in red-giant stars could be the reasons to form interstellar carbon grains. In addition, as measurements continued, a special peak in the mass spectrum at mass 720 amu from a carbon cluster which corresponded to a C_{60} cluster appeared to get people's attention. In order to investigate this product, the following experiments were set to optimise the experiment conditions which could only form this carbon cluster. However, there was always a small amount of a cluster (mass 840 amu) appeared with the carbon cluster of mass 720 amu in the spectrum.

Afterwards, the molecular structure of C_{60} was proposed to be a truncated icosahedral structure.[107] The arguments for this molecular structure were from the reasons that observed from experiment, (a) C_{60} seemed very stable to further cluster nucleation; (b) the truncated icosahedron model satisfied the valency of every carbon atom, resulting in a closed electronic shell; (c) the structure of being a closed cage eliminated all unsatisfied edge-bonds, making the molecule unreactive to further growth and (d) the isolation of the pentagonal faces (having no abutting pentagons) reduced the bond strain from a curved surface. The isolation of the pentagons also explained the presence of C_{70} in the spectra – C_{60} is the smallest possible cage molecule with no abutting pentagons, and C_{70} is the second smallest. However, the solid evidence of C_{60} only came from the dominance of a peak in the mass spectrum at 720 amu, the special nature of the proposed structure would remain widely unaccepted for the next 5 years.

Almost 5 years to the day after the truncated icosahedral structure that was proposed for cluster C_{60}[107], the first macroscopic samples of C_{60} were synthesised, isolated and characterised by Kratschmer and Huffman.[108] They discovered that a solid material could be evaporated out of deposits which obtained from arc-processed graphite at 300°C. This evaporated material can give a red solution after dissolving in benzene, and black crystals after the evaporation of the solvent. The analysis of X-ray and electron diffraction showed that this material consisted on arrays of 7Å diameter spheroids in a hexagonal-close-packed lattice, with separations of 3Å. The UV-Vis light absorption spectrum and mass spectrum of the material together with the infra-red spectrum were also characterised. The characteristic 4-line spectrum from infra-red clearly indicated that they were expected from extremely high symmetry molecule. Many of the features of C_{60}

were also present in C_{70}. These results provided convincing proof of the structural proposal for both C_{60} and C_{70}.

In a separated group study of similarly arc-processed carbon, Kroto also obtained a red solution with the mass spectroscopy shown that the material contained C_{60}. Then the experiments were designed to extract the material via a Soxhlet procedure and chromatograph by using hexane/alumina. Afterwards, C_{60} and C_{70} were separated from each other giving magenta and red solutions, respectively. There was only one line from ^{13}C NMR spectroscopy of the magenta solution. This can provide that all 60 carbon atoms were in the equivalent environment – a significant proof that C_{60} molecule is a truncated icosahedral structure. There is an alternative structure that would give a single line in the ^{13}C NMR spectrum for C_{60}, which is that all C_{60} carbons are on the perimeter of a C_{60} mono-cyclic ring. However, this assumption was effectively eliminated by the ^{13}C NMR spectrum of C_{70}, which showed 5 lines with an intensity ratio of 10:20:10:20:10 from the 70 carbon atoms.[51] these proved that this line pattern can only come from a proposed D_{5h} C_{70} cage structure.[109] The comparison of ^{13}C NMR spectroscopy from C_{60} and C_{70} confirmed the proposed 5-membered and 6-membered ring structure.

1.4   Fullerene nomenclature

The original name given to C_{60} was buckminsterfullerene.[107] It was named on honour of the American architect Richard Buckminster Fuller, who was famous for his design of buildings with geodesic construction that has hexagonal and pentagonal topologies – like C_{60}.

Fullerene C_{60} contains 60 carbon atoms in the arrangement of pentagon and hexagons forming a truncated icosahedron as show in Figure 1-1(a)(b). The bonds making up the pentagonal face are all single sigma bonds of length about 1.45 Å and those joining hexagonal faces are all double bonds of length 1.40 Å with substantial π character[47]. As any carbon atoms are identical, so anyone could be labelled as 1st, following the ring spiral order to the end of 60th carbon.

(a)   (b)
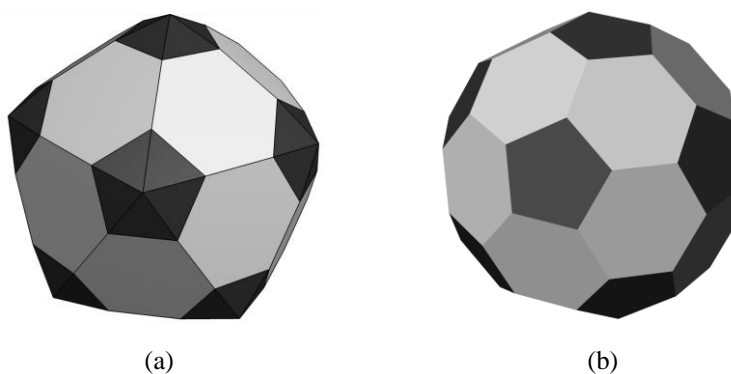
Figure 1-1 The truncated icosahedron structure.

There are two ways it can go for labelling the C_{60} carbon atoms, that is following the edge of pentagon or hexagon. The general principle of which way to go is that the spiral should be as small as possible.[110] As going around a pentagon is tighter than the hexagon, the correct numbering system begins with a spiral around pentagon. Figure 1-2 and Figure 1-3 show the diagrams of C_{60} with all the carbons properly numbered in 2D and 3D presentation. Then each bonding on C_{60} can be labelled according to the two carbon atom numbers at each end of the bond. With this, the double bond with the lowest starting number is between carbons C1 and C9, and it termed the 1,9-bond.
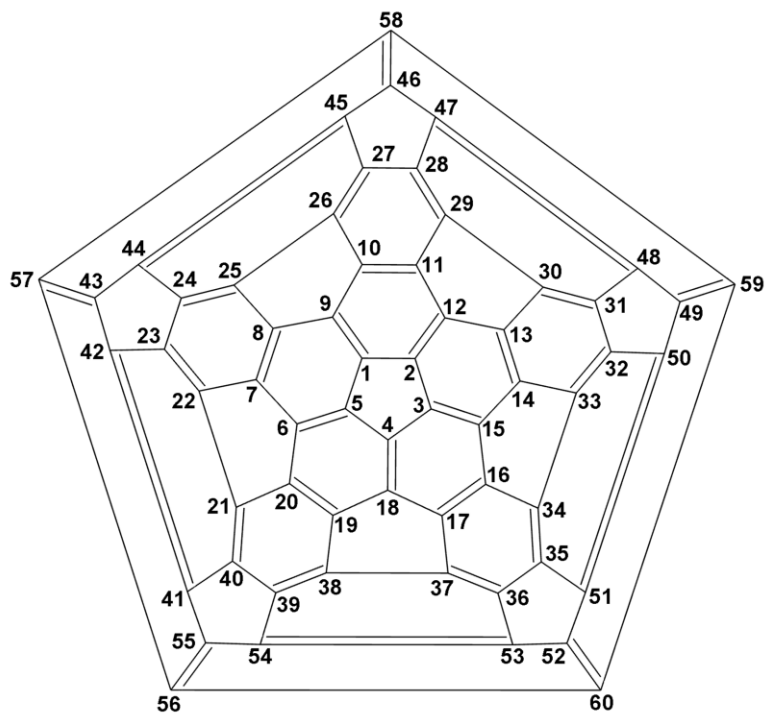
Figure 1-2 The systematic numbering for (C₆₀-*I*ₕ)[5,6]fullerene in 2D.
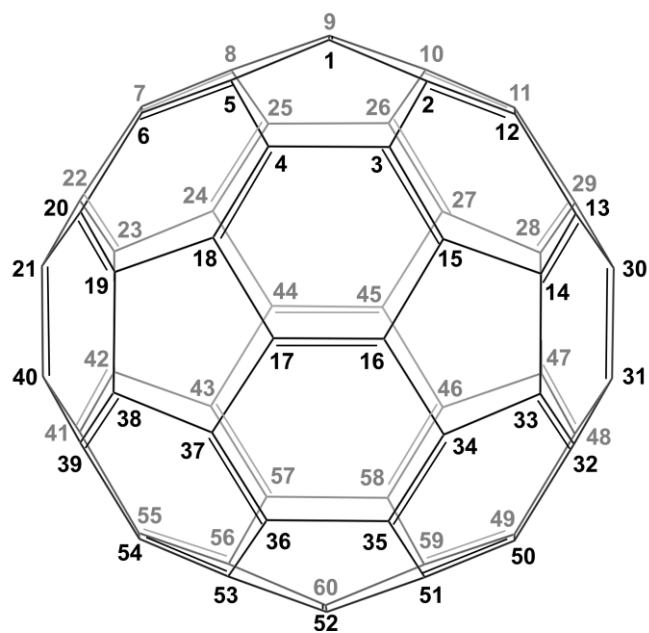
Figure 1-3 The systematic numbering for (C₆₀-*I*ₕ)[5,6]fullerene in 3D.

Following the International Union for Pure and Applied Chemistry (IUPAC) systematic rules on nomenclature, the systematic name for buckminsterfullerene is: hentriacontacyclo[29.29.0.0^{2,14}.0^{3,12}.0^{4,59}.0^{5,10}.0^{6,58}.0^{7,55}.0^{8,53}.0^{9,21}.0^{11,20}.0^{13,18}.0^{15,30}.0^{16,28}.0^{17,25}.0^{19,24}.0^{22,52}.0$^{23.50}$.0^{26,49}.0^{27,47}.0^{29,45}.0^{32,44}.0^{33,60}.0^{34,57}.0^{35,43}.0^{36,56}.0^{37,41}.0^{38,54}.0^{39,51}.0^{40,48}.0^{42,46}]hexaconta-1,3,5(10),6,8,11,13(18),14,16,19,21,23,25,27,29(45),30,32(44),33,35(43),36,38(54),39(51),40(48),41,46,49,52,55,57,59-triacontaene. The numbers in the bracket refer to the connectivity of the hexagonal and pentagonal rings, and the remainder refer to the positions of the 30 double bonds.

This name is clearly too lengthy and complicated for general use. Furthermore, the huge number of potential derivatives of C_{60} requires a simplified nomenclature system for fullerenes. As such, the IUPAC system has recommended that the icosahedral isomer of buckminsterfullerene be named as $(C_{60}$-$I_h)$[5,6]fullerene. "[5,6]fullerene" indicates that buckminsterfullerene is comprised of only pentagons and hexagons; "C_{60}" indicates that the molecule is comprised of 60 carbon atoms only; "I_h" indicates that buckminsterfullerene is the only one of the 1812 [5,6]fullerene isomers of C_{60} that has I_h symmetry. This naming method also applied on the other fullerenes. For example, the equivalent name for C_{70} is $(C_{70}$-$D_{5h(6)})$[5,6]fullerene. In this case, there are two [5,6]fullerene isomers of C_{70} with D_{5h} symmetry. The "(6)" indicates that it refers to the isomer where the pentagon on the principle axis are surrounded by hexagons (as opposed to the other $(C_{70}$-$D_{5h(5)})$[5,6]fullerene isomer that a non-isolated pentagon isomer in which the pentagon on the principle axis is surrounded by pentagons). The [5,6] part of the name also allows for the naming of fullerene with other than a hexagonal/pentagonal topology. One example would be: $(C_{48}$-$O_h)$[4,6,8]fullerene,

an all-carbon cage of 48 carbon atoms that has octahedral symmetry and is comprised of octagons, hexagons and squares. The molecular structures of these four fullerenes: $(C_{60}\text{-}I_h)$[5,6]fullerene, $(C_{70}\text{-}D_{5h(6)})$[5,6]fullerene, $(C_{70}\text{-}D_{5h(5)})$[5,6]fullerene, and $(C_{48}\text{-}O_h)$[4,6,8]fullerene are shown in Figure 1-4.

(a)	(b)	(c)	(d)
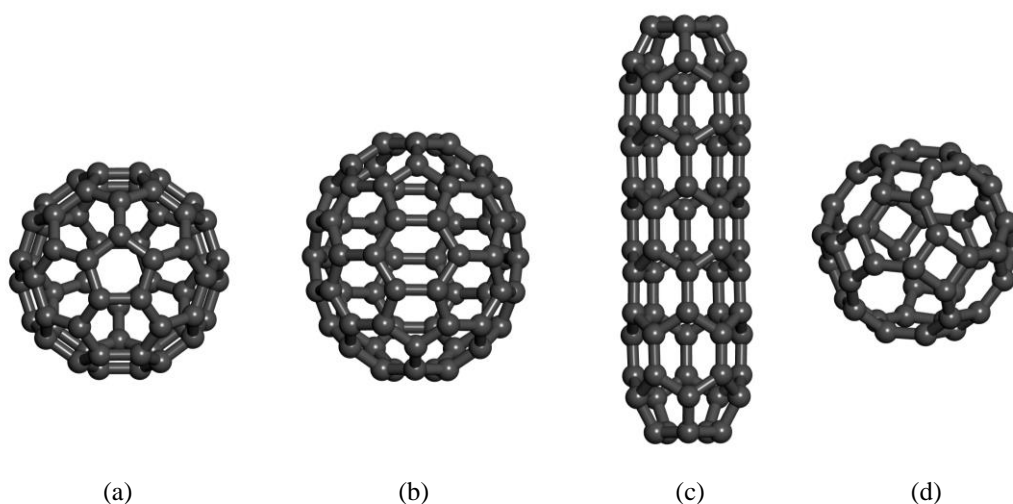
Figure 1-4 The molecular structures of four fullerenes.
(a) $(C_{60}\text{-}I_h)$[5,6]fullerene, (b) $(C_{70}\text{-}D_{5h(6)})$[5,6]fullerene, (c) $(C_{70}\text{-}D_{5h(5)})$[5,6]fullerene and (d) $(C_{48}\text{-}O_h)$[4,6,8]fullerene.

1.5   Note on nomenclature for the isomers of bis[60]PCBM

Literally there are hundreds of structural isomers of bis[60]PCBM. These include cyclopropa-fullerenes bridging double bonds in fullerenes, homo-fullerenes bridging single bonds, and numerous combinations of these. For instance, with one addend giving a cyclopropa-fullerene and the other is a homo-fullerene. However, as will be shown later in this thesis, all the isomers are in fact cyclopropa-fullerenes for bis[60]PCBM. Hence, this discussion on nomenclature and the number of isomers will be limited to isomers of this type. The trivial name of the mono-

analogue of bis[60]PCBM is [60]PCBM. Methyl 4-[61-phenyl, 3'H-cyclopropa-1,9-(C_{60}-I_h)[5,6]-fullerenyl]butanoate is the proper IUPAC system name of [60]PCBM, which shows the name of the molecule information fully. Its molecular structure is shown in Figure 1-5. The short version, [60]PCBM means **P**henyl C_{61} **B**utyric acid **M**ethyl ester for the mono-adduct of fullerene, which describes the molecule from left to right. This is a simple way to present the molecule structure, which can be extended to other fullerenes by including the fullerene used (e.g., for [70]PCBM and [84]PCBM). In addition, another short form of $PC_{61}BM$ can also be seen from literatures showing the same thing of mono-adduct of fullerene. Ideally the IUPAC naming system should be also used for bis[60]PCBM. This is because it uses strict rules that can be used to draw the structure without any misunderstanding. However, as can be seen in the simple example of [60]PCBM the proper name is very long. Extending it to an asymmetric bis-adduct would not only need a second addend to be included in the name, it would also need showing the relative orientations of two addends (R/S isomerism). There is an example of applying IUPAC on one of the isomers of bis[60]PCBM can be:

dimethyl 4,4'-[61(R)62(S)-diphenyl, 3'H3"H-dicyclopropa-1(R),9(S):49(R),59(S)-(C_{60}-I_h)[5,6]fullerendiyl]-dibutanoate.

To avoid using such long and tedious names, a short naming system for bis-adduct, bis[60]PCBM, with a method of counting for different positions for the two addends and two relative orientations of these two addends with low ambiguity is needed.
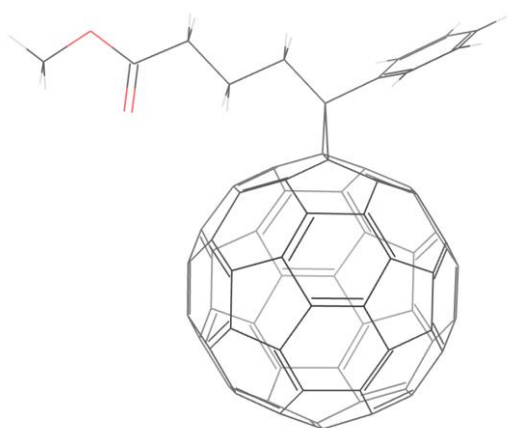
Figure 1-5 The molecular structure of [60]PCBM.

In the literature, there is one method in which the two addends are *cis* and *trans* depending on whether the two addends are in the same hemisphere (*cis*) or in the opposite hemisphere (*trans*) with equatorial (*e*) if the second addend is on the equator.[111] There are three different *cis* double bonds depending on how far the second addend is to the first addend (*cis*-1, *cis*-2 and *cis*-3). For the *trans* double bonds, these give four different bonds (*trans*-1, *trans*-2, *trans*-3 and *trans*-4). The equatorial bonds give a *e* type of double bond for the two same symmetrical addends of fullerenes (for example, $C_{60}(NCOOEt)_2$, $C_{62}(COOEt)_4$ and $C_{62}(anisyl)_4$), or two different double bonds with *e'* and *e''* for two different symmetrical addends (for example, $C_{61}(COOEt)_2(NCOOEt)_2$ and $C_{62}(anisyl)_2(COOEt)_2$) which depend on whether the double bond is vertical which is the *e'* or horizontal which is the *e''*.[112] This method is easy to understand and presents the molecular structure of bis-adduct fullerene, however, it can only be applied on symmetrical addends of fullerenes with horizontal mirror plane. As can be seem in Figure 1-6 (a) and (b), the solid double bond is equal to dot double bond in same colour and those two

double bonds are equivalent to the other two double bonds behind, so there are 4

equivalent double bonds for each bond type except for *trans*-1 and *e* double bonds.

This gives 8 or 9 distinguishable isomers which are easy to be named.

(a)   (b)
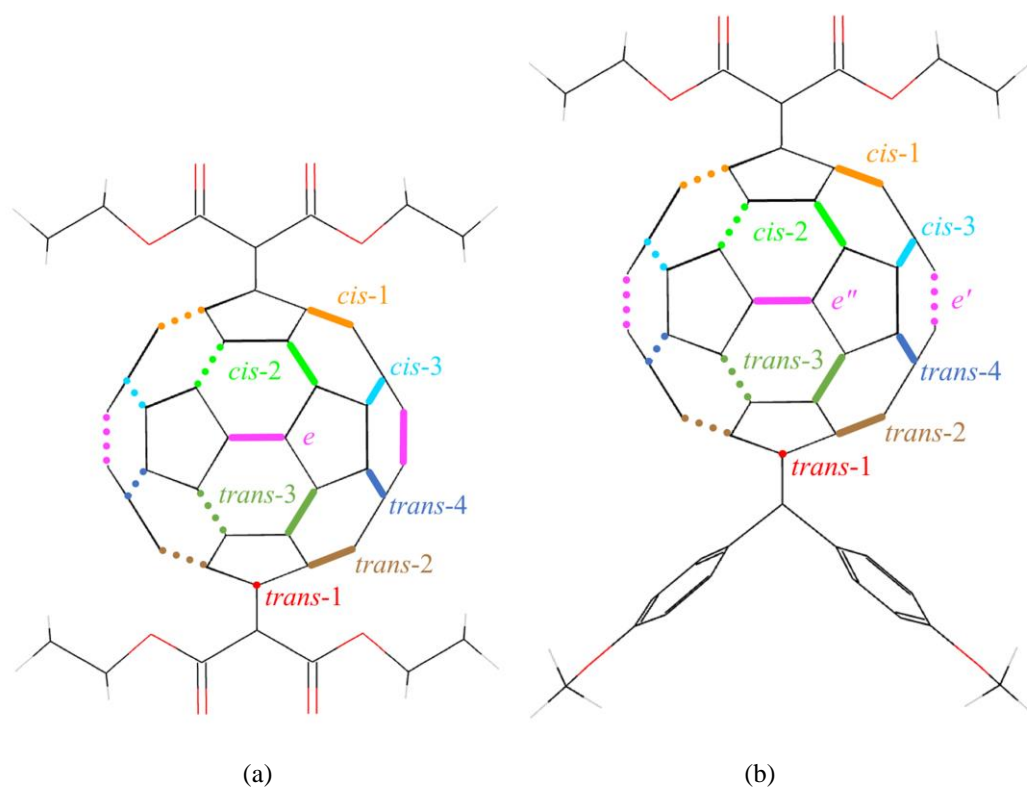
Figure 1-6 The 8 or 9 different bond types on C$_{60}$ cage.
For (a) two symmetrical addends, e.g., C$_{62}$(COOEt)$_4$, (b) two different symmetrical
addends, e.g., C$_{62}$(anisyl)$_2$(COOEt)$_2$.

Unfortunately, this system can be only applied on bis-adduct with symmetrical

addends to fullerene with horizontal mirror plane. As can be seen from Figure 1-7,

the solid bonds on the right of the molecule can be distinguished from the dot

double bonds on the left because the asymmetrical addend reducing the symmetry

of the molecule. But in general, those double bonds behind are also different giving

4 distinguishable double bonds for each of *cis*-1, *cis*-2, *cis*-3, *e*, *trans*-3 and *trans*-

2 bond type (the *trans*-1 bond type is different because there is only one *trans*-1

bond). Because of this, an extension is required to the naming system to tell the

difference between the 4 bonds of each double bond type.
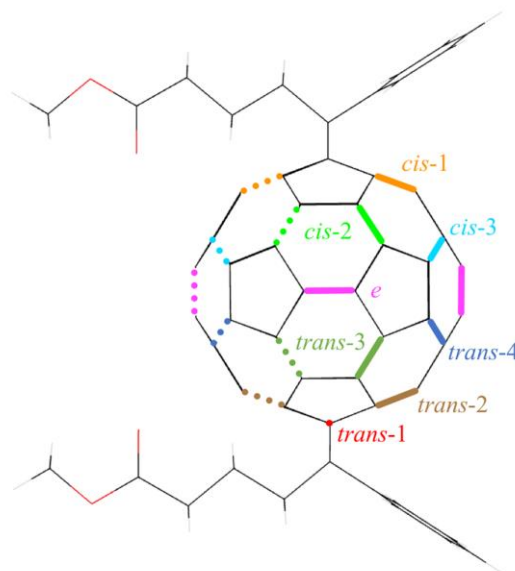
Figure 1-7 The 8 different bond types on C$_{60}$ for two same asymmetrical addends of bis[60]PCBM.

For symmetrical bis-adduct, except for the sole *trans*-1 bond, there are four symmetrically equivalent bonds of each type (left, right, and mirrored behind). However, for asymmetrical bis-adducts, such as bis[60]PCBM, the bond types on the right are not equivalent to those on the left (indicated by solid and dotted lines), and those behind are, in general, enantiomers of those in front – yielding four generally symmetrically inequivalent bonds of each non-*trans*-1 type.

So, a short form name is needed like [60]PCBM for bis[60]PCBM, replacing the

cis and *trans* double bonds (Figure 1-7) by IUPAC numbers. The reason for doing

this is that it is short and easy to define all double bonds in the way that everybody

could unmistakably understand. To count the two relative orientations from the

second adduct to the first adduct which always bonds to the 1,9 double bond on

each double bond. *Endo* and *exo* were suggested in the literature, where by the

phenyl rings point towards each other (*endo-endo*), away from each other (*exo-*

exo), or one phenyl ring points towards the ester of the second addend (*endo-exo*

or *exo-endo*).[113] However, there are several problems with this definition. Firstly, *endo* and *exo* are not properly used. This is because *endo* and *exo* should be used to distinguish relative orientations towards (*endo*) or away (*exo*) from the largest bridge on a bicyclo-ring. Secondly and more importantly, the naming method is ambiguous, because whether an isomer can be named *exo-exo* depends on how you look the molecule for *cis*-3 and *trans*-3 and *trans*-2 bond isomers which do not have mirror plane. That is two people checking the same isomer could reach two different conclusions with both being consistent with this naming system.

A naming system for the isomers was developed in our laboratory by a senior PhD student, Wenda Shi, which appears in this thesis. In that system, the isomers were named according to the bond numbering of the second addend (as the 1st isomer adds across the 1,9 bond in all bis[60]PCBM isomers by definition). The two isomers for each double bond were then distinguished by adding the suffix cis and trans depending on the orientation of the two addends relative to each other. It is also noted that the cis/trans nomenclature of Shi[96] is not only different from that used by Hirsch[112], it is also another non-standard use of this type of stereoisomerism. Early on in my PhD, I was asked to carry out this same analysis for myself. However, when doing so, I came to different conclusions for several of the isomers. That as for several of the isomers that has previously been named as trans, I had named them as cis, and vice versa. After re-checking, it seems that this naming method is ambiguous – just like the *endo-exo* system mentioned above. As such, using the previous naming system whether an isomer was cis or trans, depends on your point of view.

As an example, Figure 1-8 below shows the meaning of cis and trans in Shi's naming system[96]. The molecule (a) illustrates a cis relative orientation of the two

addends and the molecule (b) illustrates a trans relative orientation. However, both figures are of the same isomers but in two different orientations. This problem exists for all the isomers except for the two polar isomers. It was the two polar isomers that Shi to illustrate in his naming system, but this is the one and only case where names are unambiguous.

(a)   (b)
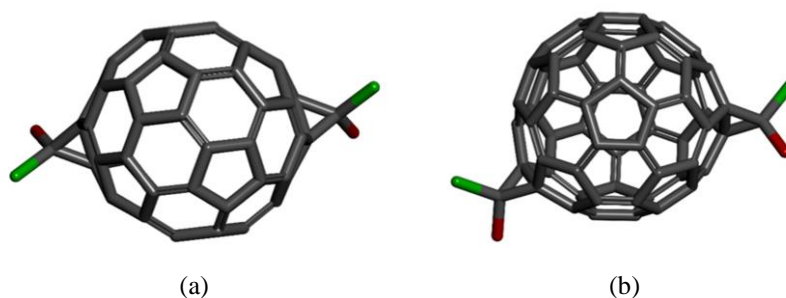
Figure 1-8 An illustration of the problem with the previous naming system for asymmetrical fullerene bis-adducts.
The molecule (a) shows cis arrangement of the two addends, and the molecule (b) shows a trans arrangement; but both are of the same isomer.

This problem can be overcome by defining a rule to decide on the 'correct' orientation to use. However, this has the problem that we would need a different rule for each isomer. As such, a new naming system is needed to remove this ambiguity – and indeed, remove all other forms or ambiguity.

Overcoming this problem requires a simple naming system that has lower ambiguity. As [60]PCBM and bis[60]PCBM are very commonly used in the literature, we will keep this part of the name in place of the very long IUPAC name, but replace the *cis*/*trans*/*e* system which cannot distinguish the four different bonds of each bond type with the IUPAC numbering system that is easy to distinguish. With the first addend attached to 1,9 bond as it is for every bis[60]PCBM isomer, the four *cis*-2 double bonds are, for example, 3,15; 4,18; 24,25 and 26,27, where

the second addend could be attached. The relative orientations can be represented with molecular symmetry. Applying this system to the simple example of the two polar (*trans*-1 bond) isomers, we name them as (C_{2h})1,9;52,60-bis[60]PCBM and (C_{2v})1,9;52,60-bis[60]PCBM. As mentioned above, the first addend can only be attached to 1,9 bond in every bis[60]PCBM isomer. So, these names can be further shorten by leaving out the 1,9 bond and leaving it implied by the bis part of bis[60]PCBM – (C_{2h})52,60-bis[60]PCBM. More naming details of all the isomers of bis[60]PCBM are presented in chapter 5.

The first partial chromatography of bis[60]PCBM mixture was acquired on a silica column using toluene as eluent by Bouwer in 2012.[113] His chromatogram indicated that the mixture could be separated into several fractions and that those fractions shows evidence of consisting of several unresolved sub-fractions. This was similar to the later published Stage 1 Figure by Shi et al.[93] However, Bouwer did not achieve full separation of any individual isomers. The following purification work was undertaken by my supervisor (John Dennis) and senior PhD student (Wenda Shi) in Queen Mary University of London, that the mixture of bis[60]PCBM was separated into 18 individual isomers and the electronic properties was characterised. Nevertheless, this still not the fully purification for the bis[60]PCBM mixture. During the my study of possible molecular structures for bis[60]PCBM, it expected to obtain 19 isomers instead of 18. Hereafter, the missing 19th isomer was found and isolated from the bis[60]PCBM mixture in my own purification work.

The electronic characterisation of bis[60]PCBM of previous 18 isomers was carried out as a joint project with two other fellow students (Wenda Shi and Xueyan Hou). The UV-Vis absorption spectra were used to measure the HOMO-LUMO gap of 18 isomers combining with cyclic voltammetry (CV) measurement to work

out the LUMO levels. These results are presented in the paper[93] and the thesis of Shi[96] and further reported with additional analysis in the recently submitted thesis of Hou.[114]

Shi and Hou assisted me in my part of the UV-Vis project which was comparing the spectra with other fullerene bis-adducts that had been reported in the literature. Although they reported our joint findings of this in their respective thesis, they were not as detailed as it discussed in this thesis. For example, both Shi and Hou had included both horizontal (e′) and vertical (e″) equatorial isomers as they discussed in the literature. However it is not as is established in this thesis, note that for bis[60]PCBM the horizontal (e′) and vertical (e″) equatorial isomers cannot be distinguished. These works were published in a joint paper.[93] In this thesis, it was established that the previous analysis of the number of isomers had several flaws including that there were 18 isomers. The new analysis presented here showed that there should be 19 isomers, and using principles established in this thesis I was able to predict the HPLC behaviour of the missing isomer and successfully locate and purify it. With this, and in conjunction with the new NMR analyses, I was able to confidently assign which isomer corresponds to which HPLC fraction. With this information, those who use purified isomers in their research can know which isomer they are using and/or can purify a specific isomer from the isomer mixture.

2 Theory

2.1 Liquid chromatography

Liquid chromatography is by far the most common method of separating fullerenes and fullerene derivatives[47, 51, 115-122]. Several stationary phases have been tested with the objective of increasing productivity through increasing the selectivity between the different components of the as-produced fullerene mixture and reducing the cost of separation.

2.1.1 The mechanism of HPLC

HPLC relies on a pump to push a liquid solvent (termed the 'mobile phase') at high pressure (typically 100 bar) from a reservoir through a column containing granules of an adsorbent material[123] (termed the 'stationary phase'). The granules are typically 5 μm diameter silica beads which may be coated with monolayers of other materials for the purpose of enhancing their adsorption properties.[124] After passing

through the column, the mobile phase passes through a detector (usually a small fixed wavelength UV absorption spectrophotometer) before being collected.

With pure mobile phase running through the column, a small amount of a solution of the sample mixture is injected onto the column, via an injection valve. This is followed by continuing elution by pure mobile phase. With this, the components of the mixture are adsorbed onto the adsorbent material of the stationary phase initially near the top of the column. As the mobile phase flows past at high pressure, it desorbs the components off the stationary phase, and they flow with the mobile phase a little way down to the column before they are adsorbed again onto the stationary phase. This adsorption-desorption process continues until the components of the mixture come off the end of the column. During this process, each component in the mixture interacts slightly different with the adsorbent material in the column. That is, some components stick for longer onto the adsorbent material before being washed off than the others. This is because there are different flow rates for the different components of the mixture through the column, it leads to the separation of the components when they flow through the column.

Once removed from the column, the separated solution of the sample mixture passes through the detector which digitises the signal to be both recorded and displayed on a computer screen. By monitoring the progress of the separation on the screen, the operator can direct the individual separated samples into each of an array of sample collection bottles via a fraction collection valve at appropriate times. A flow scheme of HPLC purification process is shown in Figure 2-1.
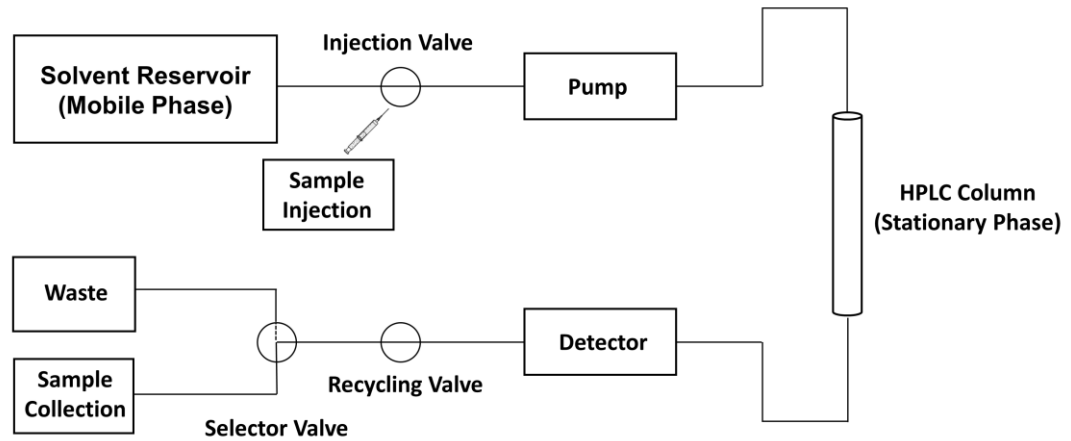
Figure 2-1 Normal single-pass mode of HPLC purification.

2.1.2 Peak-recycling HPLC

Peak-recycling HPLC is a variation of normal single-pass HPLC which allows for

the separation of components with very poor resolution on the HPLC column. The

working principle of peak-recycling HPLC is, after detection, the mobile phase

containing partially separated components of the mixture are redirected back to the

injection valve via a recycling valve to be re-injected back onto the column. While

the machine is left in peak-recycling mode, no mobile phase leaves the system and

no new mobile phase enters the system. In the peak-recycling mode, the mobile

phase still in the system cycles through the column many times until the machine

is switched out of recycling mode, then the normal HPLC is resumed. This peak-

recycling mode has the effect of producing a many-fold increase in column length

(for example, cycling 4 times through the column produces the equivalent

separation of having a column 4 times as long). There are three major advantages

to this. First, a column 4 times as long would cost considerably more money.

Second, a column 4 times as long would have a prohibitively high back pressure,

requiring a much stronger and more expensive HPLC machine. Third, as no new solvent flows through the system during recycling mode, there is a very considerable saving in solvent costs.

There are two factors that could contribute to the efficiency of separation. They are (1) the difference of the retention time between two successive peaks, and (2) the width of those two peaks. The further apart the two peaks are in the retention time and/or the narrower the peaks are, the more efficient the separation of the peaks.

The first factor is related to the materials being used. That is, primarily to the solvent, the solute and the stationary phase. The second factor is related to the instrument. Peak broadening is largely related to dispersion on the column. There is also dispersion within the instrument. This arises through laminar flow in the tubing, and re-mixing in the pump cylinders and detector flow cell. However, as the internal volume of the instrument is about 0.5% of that of the column, the instrument dispersion can be neglected.

A peak in the HPLC profile has a reasonably Gaussian-type shape. The longer time of the sample is on the column the wider the peak becomes. There are three major factors that contribute to dispersion on the column. The first of these is so-called eddy diffusion. This is related to that there are multiple pathways which the molecules of the solute may randomly take in going down the column. The difference in pathlength of these different pathways leads to peak broadening. This type broadening is related to the size and uniformity of the particles of the stationary phase – the smaller and more uniform the particle, the lower the effect of eddy diffusion. The second broadening effect is longitudinal diffusion. It comes about by that there is a short cylinder of high concentration of solute injected onto the column, which then works its way down to the column during elution with the

43

mobile phase. Random Brownian-motion of the particles sees them diffuse into areas of lower concentration, which are behind and in front of the short cylinder of solute. With this, the cylinder broadens. By the effect that the longer the solute is on the column the greater the peak broadening. As such, the peak broadening may be reduced by using a higher mobile phase velocity (faster flow rate). The final broadening factor comes from that there is a finite time for the solute to equilibrate between the mobile and stationary phases. That is some of the solute molecule becomes relatively stuck on the stationary phase, while other move relatively freely in the mobile phase between stationary phase particles. As the chromatography proceeds, the free molecules will become stuck on later stationary phase particles while the previously stuck molecules become free. The overall effect is a broadening the solute cylinder along the column. Contrary to longitudinal diffusion, this mass transfer-related broadening may be reduced by reducing the mobile phase velocity. These three broadening factors can be expressed mathematically as the van Deemter Equation[125] which related the HPLC 'plate height', H, (the lower the better) to these three factors and the mobile phase velocity, u:

$$H = A + B/u + Cu$$ **Equation 2-1**

The A term is related to *eddy diffusion* and being a function of path difference only, it is not dependent on the mobile phase velocity. The B term is related to *longitudinal diffusion* and its effect inversely related to the mobile phase velocity. The C term is related to the equilibration time and increases linearly with mobile phase velocity.

Assuming the A term is minimised though good quality column manufacturing, then from the van Deemter equation, it can be seen that longitudinal diffusion is

the dominant factor at low flow rates. Whereas, as mobile phase velocity increases there is a rapid geometric decrease in longitudinal diffusion and a monotonic increase in the *C* term. Combing these effects, there is an optimal mobile phase velocity that gives optimal separation efficiency.

During my PhD I did not determine the flow rate that needed for optimal separation efficiency. This is because the optimisation separation efficiency does not take time into account. What I was interested in was obtaining purified samples as quickly as possible. Hence, the purification was done at a faster, but sub-optimal, flow rate. Although this resulted in more stages in the purification, the decrease in time needed to complete each stage more than made up for this. This time-optimised flow rate had previously been determined by my supervisor.

Returning to peak-recycling HPLC, consider two fractions, Fraction 1 and Fraction 2 have one minute width respectively, with retentions times start at 6.0 and 6.5 min in the HPLC profile. This would result in a single composite peak of width 1.5 min. The resolution of these peaks may be calculated from the following formula[125]:

$$resolution = \Delta t_{1,2}/w_{av}$$ **Equation 2-2**

$\Delta t_{1,2}$ is the retention time difference of Faction 1 and Fraction 2, and w_{av} is the average width of the two peaks. Two closely spaced peaks would not be fully resolved unless the difference in their retention times was at least equal to their widths (giving a resolution of 1.0). In the above example of two overlapping peaks the resolution would be 0.5/1 = 0.5.

Peak-recycling HPLC effectively increases the length of the column. Hence, the number of theoretical plates of the column increases linearly with the number of cycles. Assuming a Gaussian-type shape peak, the number of theoretical plates (*N*)

of a column is related to the retention time (t_R), and full width (*W*) of an HPLC

peak as follows[125]:

$$N = 16(t_R/W)^2$$

<div align="right">**Equation 2-3**</div>

As such, the number of theoretical plates incorporates the effect of column

dispersion discussed above. The resolution of a column may also be expressed in

terms of the number of plates *N* as follows[125]:

$$resolution = \frac{\sqrt{N}}{4}\left(\frac{t_2}{t_1} - 1\right)$$

<div align="right">**Equation 2-4**</div>

With this, after two cycles (*N* goes to *2N*) the resolution increases by a factor of $\sqrt{2}$

to 0.7, and doubles to an effectively fully separated resolution of 1.0 after 4 cycles.

That is, two peaks that are only half-separated after single-pass HPLC may be fully

resolved from each after 4 cycles of peak-recycling HPLC. Figure 2-2 shows the

HPLC system in peak-recycling mode.
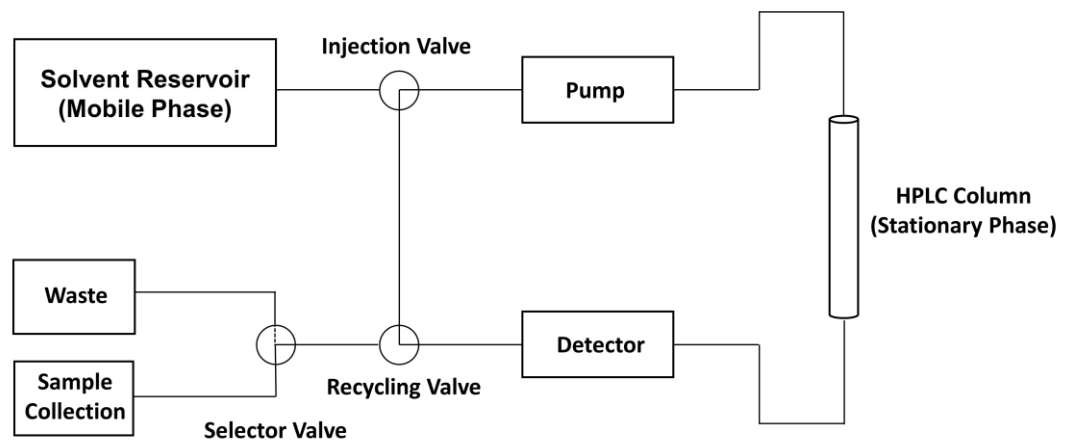
Figure 2-2 Peak-recycling mode of HPLC purification. While recycling, there is no solvent consumption.

2.1.3 Early stationary phases via column chromatography

In 1990, C_{60} and C_{70} were the first fullerenes to be purified.[51] Indeed, at the time they were thought to be the only fullerenes. Their purification was achieved through column chromatography on alumina in hexane solution.[51] However, the solubility of fullerenes in hexane is extremely low, and even using very large 10 cm diameter column that packed with about 2 kg of alumina. It was only able to purify about 100 mg per purification run and required the consumption of about 15 litres of high-purity hexane. As each separation run took about 3 hours to complete, and each day could only make 2 production runs. Although this is an effective method for separating these fullerenes, the technique is laborious and time-consuming. An additional drawback of using alumina column was that fullerene tended to oxidise in light when it in contact with the alumina stationary phase. Nevertheless, this was the primary method of purifying fullerenes during the first 5 years of their macroscopic availability.

The more traditional column chromatography stationary phase of silica was not successful for fullerenes separation as no matter what mobile phase was employed. C_{60}/C_{70} had very short retention times and the separation was very low.[126] Traditional reverse-phase stationary phases such as octadecyl silica (C18) have been used with limited success. Increases in solubility through using aromatic solvents are negated by decreases in separation. Therefore, it may be countered by using mixtures of a solvent and a counter-solvent. For instance, toluene/acetonitrile and toluene/methanol. This is because acetonitrile gives good separation of higher fullerenes and methanol gives a shorter retention time. Hence, the ratio of acetonitrile or methanol in the toluene has influences on the selectivity and on the duration of separation.[127] However, a drawback of using solvent mixtures in

preparative HPLC is that the solvent mixture cannot be recovered to be reused (for example, by rotavaporation). Hence, solvent mixtures can only be used once, and then discarded.

2.1.4 Stationary phases for HPLC

The first successful HPLC column for fullerenes was the 'buckyclutcher'.[128] This column used silica beads coated with a nitro-styrene based moiety which is shown in Figure 2-3(a), so that the fullerene would adhere. This column allowed for the use of pure aromatic eluents such as toluene to be used which is an enhancement.

Following the buckyclutcher, several other reverse-phase coatings were developed for the fullerene research. Principal among these were the 'buckyprep'[129] and 'PBB' columns. The buckyprep comprised a pyrene unit that connected to a silicate group via a propyl linkage (in Figure 2-3(b)), whereas the PBB had the silicate group linked to a pentabromobenzene group (in Figure 2-3(c)). Additionally, these two columns could operate in a complementary fashion. That is the components which cannot be separated on one column may often be separated on the other. A development of the buckyprep column is the PYE[130] which has a slightly shorter linkage (show in Figure 2-3(d)) between the silicate and the pyrene unit ($-CH_2-CH_2-$ rather than $-CH_2-CH_2-CH_2-$). This shorter linkage results in approximate halving of the retention time with only a small reduction in the separation.

A further development of the buckyprep column is the modified buckyprep or "buckyprep-M" which replaces the pyrene group with a phenothiazinyl group shown in Figure 2-3(e). Although it is not relevant to the purifications of the fullerene derivatives studied in this thesis, this column was devised for the

48

purification of high-polarity fullerenes – metal-containing endohedral fullerenes in

particular.
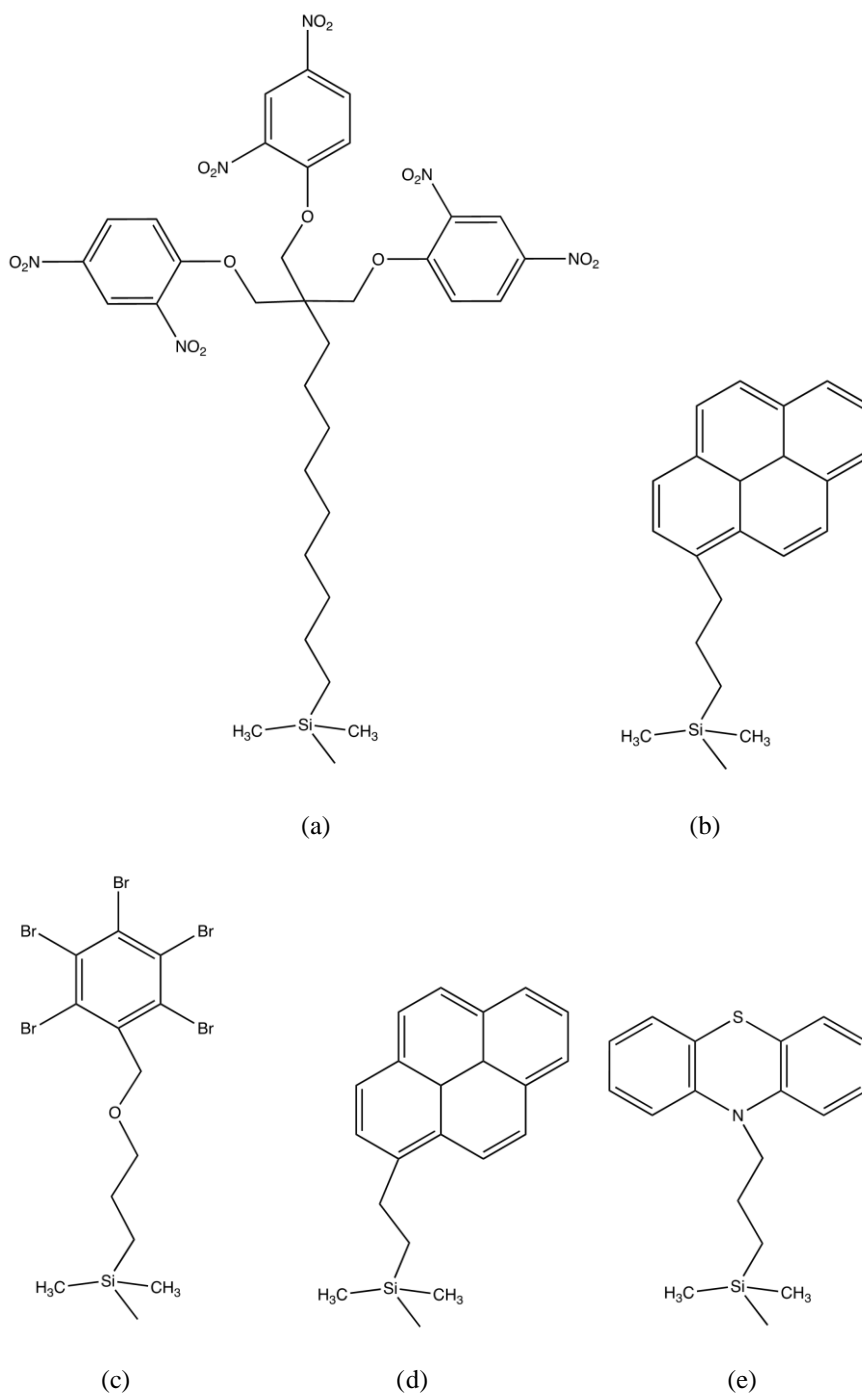
Figure 2-3 The molecular structures of 5 stationary phases.
(a) buckyclutcher, (b) buckyprep, (c) PBB, (d) PYE and (e) buckyprep-M.

In this work, A Japan Analytical Industries LC908 peak recycling HPLC with three preparative columns were used: a Cosmosil 20 mm i.d. × 250 mm 5PYE, a Cosmosil 20 mm i.d. × 250 mm 5PBB (both manufactured by Nakalai Tesque), and a Sunfire 19 mm i.d. × 150 mm 5 mm bare silica (manufactured by Waters). The toluene eluent flow rate was at 18 mL min^{-1}.

Although it is not relevant to stationary phases, it is worth mentioning that, unlike many materials, the solubility of fullerenes in many common eluents has its peak near 280 K[48]. This explains why better results obtained in winter. Unfortunately for fullerene research, although column ovens are readily available, column fridges are not.

2.2   General spectroscopy

The electromagnetic spectrum ranges from very long radio waves to extremely short gamma rays. The spectrum is divided into seven different parts; which from long to short wavelengths are called (1) radio, (2) microwaves, (3) infra-red, (4) visible, (5) ultraviolet, (6) *x*-rays and (7) γ-rays. If the relatively very narrow visible region is combined with the much broader ultraviolet region, then the wavelength of the centres of each of the resulting 6 parts is 100 to 1000 times shorter than that of the next. For example, $\lambda_{\mu w}$ is about 100 times longer than λ_{IR}, which is about 100 times longer than λ_{UV-Vis}, etc. In addition, each of these 6 parts may be associated with the energy changes of difference molecular phenomenon. That are: Radio waves bring about nuclear spin-flip transitions as studies by nuclear magnetic resonance spectroscopy; microwaves excite molecular rotations (measured by microwave spectroscopy) and also excite electronic spin-flip

transitions (measured by electron spin resonance spectroscopy); infra-red radiation excites molecular vibrations through bond stretching and bending (they are measured by Infra-red and Raman spectroscopic methods); UV-Vis radiation excite valence electronic transitions to higher energy states within the molecule (measured by UV-Visible absorption spectroscopy) or even brings about their complete removal from the molecule (measured by UV photoelectron spectroscopy); x-rays perform a similar role to UV-Vis radiation but to the core electrons of molecules (measured by x-ray absorption spectroscopy and x-ray photoelectron spectroscopy).

Spectroscopy is an experimental technique whereby radiation of an appropriate wavelength is shone onto a sample of a molecule, so the particular property of the sample is being measured. The radiation is absorbed at specific wavelengths that correspond to the specific energy changes related to the property within the molecules. The spectrum which shown as a plot of intensity of the absorbed radiation against its wavelength, is a 'fingerprint' of that molecule with regard to the property being measured.

2.2.1 UV-Vis absorption spectroscopy

When a UV-Vis photon interacts with a molecule and is absorbed, the valence electrons in the molecule are excited into higher energy levels.[131] UV-Visible light has enough energy to promote electrons to a higher electronic state, that is from the highest occupied molecular orbital (HOMO) to the lowest unoccupied molecular orbital (LUMO). The energy difference between the HOMO and the LUMO is called the HOMO-LUMO gap (E_{gap}). The energy of the photon must match the E_{gap} for the photon to be absorbed. At shorter wavelengths (higher photon energies),

deeper valence electron transitions may occur (for example, HOMO to LUMO+1, HOMO–1 to LUMO and HOMO–1 to LUMO+1), but still the photon energy must match the energy gap between the various levels. Thus, molecules with different chemical structures have different energy gaps and different absorption spectra. The most common transitions that fall in the UV-Vis range are π-π* and n-π*. π orbitals arise due to double bonds, and n orbitals are for non-bonding electrons. π* are anti-bonding π orbitals. Thus, the best UV-Vis absorption is by molecules that contain double bonds. π orbitals adjacent to each other that are connected, called conjugation typically increases absorption. The σ-σ* transitions which associated with single bonds have higher energy and fall in the deep UV, so they are less useful for routine use. This is particularly so for fullerenes, which have a very large number of π-orbitals that in turn give a high degree of conjugation.

The absorption of a UV-Vis photon not only excites an electronic transition, it may also excite a large number of vibrations within the molecule. The range of excited vibrational modes gives a range of slightly higher electronic transition energies (as they add to the energy of the electronic transition). Conversely, the absorption of a photon in exciting an electronic transition may de-excite vibration of the molecule – giving a similar range of energies on the low-energy side of the electronic transition energy. Hence, the UV-Vis absorption spectrum has the appearance of broad bands or shoulders on the UV-Vis structure due to those numerous vibrational states of a molecule. Molecules with absorption in the visible region are coloured, including all the isomers of bis[60]PCBM. The colour of a compound arises because those wavelengths of light are selectively transmitted through the sample, and thus they are not absorbed.

The UV-Vis machine used for taking the spectra of all isomers of bis[60]PCBM is Shimadzu UV-2600 spectrophotometer. The range, scanning rate, step size and path length are 325 – 800 nm, 30 nm min^{-1}, 0.2 nm, and 10 mm, respectively.

2.3 NMR Theory

In this section, the origin of the NMR signal will be discussed in terms of the energy states of spin ½ particles in a magnetic field, and the nuclear spin-flip transitions between them. Issues relating to the sensitivity of the technique and methods to improve the signal will also be discussed. This will be followed by a discussion on the origin, nature and usefulness in relation to molecular structure identification of the 'chemical shift' in NMR spectroscopy.

2.3.1 Origin of the NMR signal

When placed in a magnetic field, spin $I = $½ nuclei, such as ^{1}H and ^{13}C, give rise to two spin-based states α ($I = $ –½) and β ($I = $ +½). The energy difference between these two states is related to the applied magnetic field strength B_0[132] by the following relationship:

$$\Delta E = \gamma \hbar B_0$$ <div style="text-align:right">**Equation 2-5**</div>

γ is the nuclear magnetogyric ratio which are 42.5775 and 10.7084 MHz T^{-1} for ^{1}H and ^{13}C, respectively. $\hbar$ is the reduced Planck Constant which equals to 1.0546×10^{-34} J·s. According to the Equation 2-5, the energy difference increases with the applied field as shown in Figure 2-4.
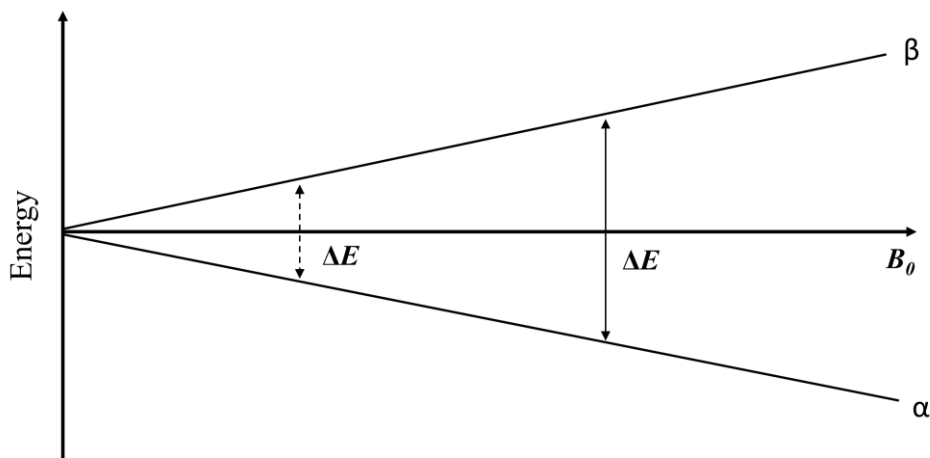
Figure 2-4 A diagram showing the evolution of the α and β nuclear spin states with increasing applied magnetic field B_0.
Transitions between the α and β states at two different values for B_0 are shown, it indicates how the transition energy ΔE is proportional B_0.

If a sample in an external magnetic field is irradiated with electromagnetic radiation, and the frequency of that radiation corresponds to the difference in energy between α and β states ($\nu = \Delta E/h$), then the resonance occurs causing nuclear spin flip transitions. Once the radiation is turned off, the spins decay back to their original states causing emission of radiation at the same frequencies as those previously absorbed. That is, corresponding to the energy difference between the β and α states. The NMR spectrum is a plot of the intensity of the emission versus the emission frequency, and hence consists of a signal peak at each resonance frequency.

The intensity of the emission is related to the population difference between the α and β states. The populations of the two states obey the Boltzmann distribution:

$$\frac{N_\alpha}{N_\beta} = e^{\frac{E_\beta - E_\alpha}{kT}}$$

Equation 2-6

N is the population in each state. T is the absolute temperature in Kelvin, and k (the Boltzmann constant has a value of 1.381×10^{-23} J K^{-1}).

For NMR spectrometers with the strongest electromagnets which is available, the protons resonate at about 60 MHz. Hence, at room temperature, ΔE is about 10^5 times smaller than kT, which gives rise to a population ratio of about $N_\alpha/N_\beta = 1.00001$. That is, for every 100,000 atoms in the lower α state, there are 99,999 atoms in the higher β state. This means that only one in every 200,000 atoms contribute a net NMR signal. This may be compared to the other spectroscopic technique used in this thesis, UV-Vis absorption spectroscopy, in which ΔE is about 100 times greater kT (giving $N_\alpha/N_\beta \approx 10^{43}$). Here, all atoms are in the lower state (none are in higher states), which means that every atom contributes a signal. This makes the UV-Vis absorption spectroscopy the order of $100,000^2$ (10 billion) times more sensitive that NMR spectroscopy (as signal intensity scales with the population difference squared). Hence, NMR spectroscopy is an extremely insensitive technique. This poor sensitivity is compounded in ^{13}C NMR spectroscopy. This is because the natural abundance of ^{13}C is about 1%. Hence, only one in a hundred carbon atoms can give an NMR signal with the remaining 99% (^{12}C) being NMR silent. Hence, only one in every 20,000,000 carbon atoms gives an NMR signal.

The sensitivity may be improved by increasing the magnetic field strength, but going beyond 60 MHz requires superconducting magnets which dramatically increase the cost of the instrument. For example. The spectrometer used during this thesis has a proton resonance frequency about 600 MHz which is 10 times higher

than that discussed above and gives a 10 times increase in population difference, thereby 100 times increase in sensitivity. However, the cost of such a machine is about £750,000, and a further 50% (900 MHz) increase would cost to about £5,000,000.

The signal to noise ratio may be improved by co-adding spectra. The advantage of this method may be realized by noting that the signals from the various nuclei in the NMR spectrum always occur at the same frequencies. Hence, adding many spectra gives a many-fold increase in the size of the signals. Conversely, the noise in the spectrum is random. Hence, there will be almost as many $+x$ values as there are $–x$ values to average the noise close to zero when co-adding a large number of spectra. This means that co-adding spectra increases the signal and decreases the noise. Co-adding a large number of spectra allows the signal to be distinguished from the noise. However, there is a diminishing returns law which indicates the improvement in the signal-to-noise ratio is proportional to the square root of the number of scans. That is, to improve the signal by a factor of 8 comes at the expense of a 64 times increase in signal acquisition time, and a further increase to a factor of 16 requires a 256 times increase in acquisition time. In this thesis, 4096 spectra (taking about 4 hours per spectrum) were co-added for each ^{13}C NMR spectrum.

2.3.2 Chemical shift NMR

From Equation 2-5 it may seem that NMR spectroscopy only distinguishes nuclei based on their magnetogyric ratios. This is because on a given spectrometer B_0, like $\hbar$, is a constant. So, NMR may distinguish different elements and different isotopes of the same element, but cannot distinguish one ^{13}C nucleus from another. This

would restrict its usefulness to elemental and isotopic analysis only. In fact, NMR spectroscopy is one of the most powerful analytical tools in chemistry. This is because in chemistry, the nuclei are in atoms, and the atoms join to make up molecules. That is, the nuclei are surrounded by electrons in atoms and in molecules. These electrons are also magnetic particles which interact with the external magnetic field inducing the ring currents in the atoms and bonds of molecules. In diamagnetic materials that have closed electronic valence shells, these ring currents act to the oppose to the external magnetic field. In doing so, they partially 'shield' the nuclei from the external field. Hence, the nuclei feel an *effective* external field, B_{eff}, that is slightly reduced by the shielding from that of the applied external field, B_0. As the degree of shielding depends on the electronic arrangement around the nuclei (i.e., on the chemical environment of the nuclei), different chemical environments generally give different effective external magnetic fields. Thereby, the same nuclei in difference chemical environments have different resonance frequencies. Although these changes in frequencies are relatively small (10s to 1000s of Hz compared to a resonance frequency of near 600 MHz), they are easily measured. This change in the resonance frequency through the chemical environment of the nuclei is the basis of chemical shift NMR spectroscopy.

2.3.3 The chemical shift δ

B_{eff} is a shift from B_0 that depends on the chemical environment of the nuclei. As such, B_{eff} depends on B_0. Hence, the resonance frequency of a certain chemical environment is depending on B_0. With this, the same chemical environment on different spectrometers with different applied magnetic fields will produce

different resonance frequencies. In order to make the chemical shift standard, the shifts need to be reported in a relation to a change in frequency, from that of a standard chemical environment measured on the same instrument at the same time, as follows:

$$\delta = \frac{frequence\ of\ the\ signal - frequence\ of\ the\ standard}{frequency\ of\ the\ instrument} \times 10^6 \qquad \textbf{Equation 2-7}$$

With this, the chemical shift δ is independent of the B_0 value of a particular instrument, and hence, it is a constant characteristic for each chemical environment on any instrument. The 10^6 term is used to give more 'numerically familiar' δ values (i.e., 1, 10, or 100 as opposed to 0.000001, 0.00001 or 0.0001). It also the reason that δ is quoted with the pseudo-units of parts per million (ppm), although δ is dimensionless – being $\Delta\nu/\nu$.

For ^1H and ^{13}C measurements, the standard chosen is trimethylsilane (TMS). This is for two reasons. The first is that the high symmetry of this molecule gives only one ^1H and one ^{13}C chemical environment, and hence, only one frequency for each nucleus from both measurements. The second reason is that this molecule has a very high degree of chemical shielding. It means that nuclei in the vast majority of organic molecules are less shielded than they are in TMS. With this, that most organic molecules have a higher B_{eff} than TMS, which in turn gives them a higher resonance frequency which results in positive values for δ.

2.3.4 ^{13}C NMR spectral analysis

The number of resonances and their relative intensities

As each different chemical environment in a molecule gives rise to a unique resonance frequency, the number of resonances in the ^{13}C NMR spectrum of a molecule is equal to the number of different chemical environments in that molecule. The relative intensity of each resonance is related to the number of carbon atoms that are in different chemical environments in the molecule. So the number of resonances and their relative intensities may be obtained by inspection of the molecule. However, this method is not successful with increasing structural complexity. As such, the effect of symmetry operation is combined for more complicated molecules.

As a simple inspection example, consider the carbons in the molecule allene (Figure 2-5). Although this molecule has three carbon atoms, they exist in only two different chemical environments. The left end carbon is clearly in a different chemical environment that the central carbon. This is because the left end carbon has two attached hydrogens and is bonded to only one carbon which has no attached hydrogens. Whereas, the central carbon has no attached hydrogens and is bonded to two other carbon (as opposed to one) and these both have two attached hydrogens. Moreover, the right end carbon is clearly in exactly the same chemical environment as the left end carbon (i.e., this carbon has two attached hydrogens and is bonded to only one carbon which has no attached hydrogens). Therefore, allene gives rise to two resonances in the ^{13}C NMR spectrum with one being twice the intensity as the other.
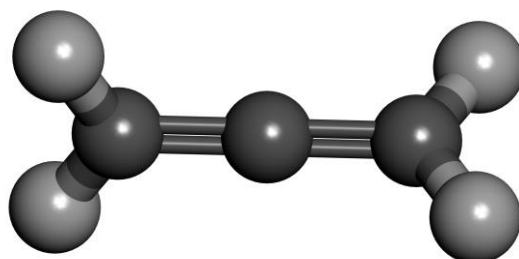
Figure 2-5 The molecular structure of allene.

Molecular symmetry may also be used to determine the number and relative intensities of the resonances. Napthalene can be used as a more complicated example (in Figure 2-6). This molecule has D_{2h} molecular point group symmetry. Of the symmetry operations of this group, E, $C_2(z)$, $C_2(x)$, $C_2(y)$, i, $\sigma_h(xy)$, $\sigma_v(xz)$ and $\sigma_v(yz)$. The $C_2(z)$ and $\sigma_v(yz)$ operations both show that C1=C5, C2=C4, C6=C10 and C7=C9. The $C_2(x)$ and σ_h operations both show that C1=C10, C2=C9, C3=C8, C4=C7 and C5=C6. The $C_2(y)$ and i operations both show that C1=C6, C2=C7, C3=C8, C4=C9 and C5=C10. Finally, the two remaining operations E and $\sigma_v(xz)$ have no effect in generating symmetrically equivalent atoms as both simply map every atom onto themselves. The combined effect of these operations is that C1=C5=C6=C10, C2=C4=C7=C9 and C3=C8, respectively. Hence, the ^{13}C NMR spectrum of naphthalene comprised three separate resonances of which 2 have relative intensity of 4, and the other has a relative intensity of 2. In this thesis, the same type of symmetry analysis was applied to the much more complicated molecules of [60]PCBM and each of the 19 isomers of bis[60]PCBM.
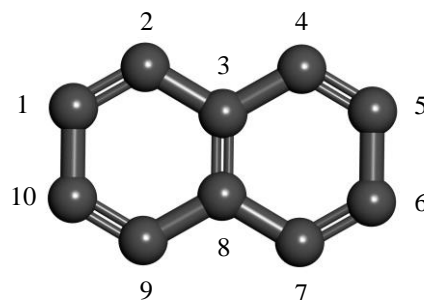
Figure 2-6 The molecular structure of naphthalene.

The chemical shifts of the resonances

Although difference chemical environments have different resonance frequencies, the amount of difference depends on the amount of difference in the environment. In other words, similar chemical environments have similar resonance frequencies, and thereby similar chemical shifts. This gives rise to the notion of *group frequencies*; whereby functional groups may be identified in molecules based on their chemical shifts. For example, protons on OH groups in alcohols, phenols and acids tend to resonate between 2-5, 4-7 and 10-13 ppm, respectively.

2.3.5 Spin-spin coupling

Such as ^1H and ^{13}C, magnetic nuclei have magnetic fields associated with them. when the magnetic nuclei were placed in an external applied magnetic field, effectively half of the nuclei align with the field and another half align against the field. Those nuclei that align with the field produce a relatively tiny induced magnetic field that adds to the external applied field. Conversely, the nuclei that align against the field produce a relatively tiny induced magnetic field that subtracts

from the external applied field. As such, if a nucleus of interest in a sample that has a single neighbouring magnetic nucleus, the results in local magnetic fields in the sample that are slightly higher than B_0 (from those with a neighbours with an aligned spins) and slightly lower than B_0 (from those with neighbours with anti-aligned spins). As the nucleus of interest has half its neighbours adding and half subtracting, the magnetic energy levels of the nucleus of interest are each split into two levels, giving two resonance frequencies of equal intensity, that is a 1:1 doublet signal. Similarly, if the nucleus of interest has two identical magnetic neighbours, then both can add, both can subtract and there are two combinations that cancel each other out. This gives a 1:2:1 triplet signal. However, if the two neighbours are not identical, then the result is two doublets (a doublet of doublets).

3   NMR spectroscopy of [60]PCBM

3.1   The prediction of ^{13}C NMR spectrum pattern

The molecular structure of [60]PCBM with the carbon labels shown in Figure 1-3 and Figure 3-1 are used for the explanation in this thesis. It has C_s point group symmetry whereby four of the cyclopropa-fullerene equatorial carbons C21, C30, C31 and C40, the bridge carbon C61, the methyl butanoate (MB) group (Me, B1, B2, B3 and B4) and the phenyl ring carbons Ph1 and Ph4 lie on the mirror plane, and the remainder of the fullerene and phenyl groups are bisected by the mirror plane. Hence, [60]PCBM generates 42 distinguishable chemical environments of carbon atoms. These should give rise to 4 resonances from the phenyl ring group (all sp^2), with phenyl carbons Ph1 and Ph4 having single-intensity resonances (being on the mirror plane) and the others having double-intensity resonances (as Ph2/Ph6 and Ph3/Ph5 are each mirrored pairs). There are 5 resonances from the methyl butanoate group (each of unitary integrated-intensity). Of these, 4 are sp^3

hybridized carbons (from Me, B2, B3 and B4) and one is sp^2 (from B1 carbon)

hybridized carbon.

(a)   (b)
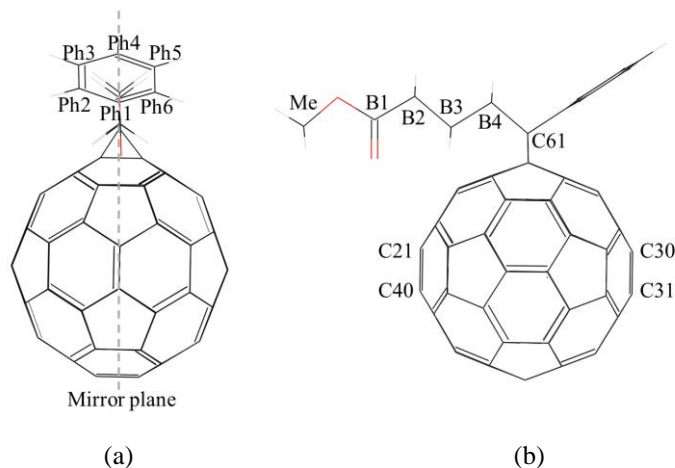
Figure 3-1 The molecular structure of [60]PCBM that has C_s point group symmetry.
The 6 carbons on the phenyl ring are labelled as Ph1–Ph6 in the front view (a); carbons on methyl butanoate group are labelled as Me, B1, B2, B3 and B4; the bridge carbon labelled as C61; 4 equatorial carbons are labelled as C21, C30, C31 and C40 in the side view (b).

Furthermore, there should be 33 resonances from the cyclopropa-fullerene. These

comprise one single-intensity resonance from the bridge carbon (C61), one double-

intensity resonance from two bridgehead carbons (C1 and C9) on the C_{60}, 4 single-

intensity resonances, one from each of the four equatorial fullerene carbons on the

mirror plane, and 27 double-intensity resonances from those either side of the

mirror plane. The fullerene resonances result from sp^2 hybridized carbon region

except for the resonances from the bridge carbon C61 and the two symmetrically

equivalent bridgehead carbons, which are each sp^3 hybridized. The details are list

in Table 3-1.

Table 3-1 The ^{13}C NMR spectrum prediction for [60]PCBM that has C_s point group symmetry.

carbon	hybridization	
	sp^2	sp^3
C_{60}	$27\times2+4\times1$	1×2
phenyl ring	$2\times2+2\times1$	--
C61	--	1×1
MB	1×1	4×1
In total	$29\times2+7\times1$	$1\times2+5\times1$

According to the typical group resonance values[133] with the ^{13}C NMR resonances prediction, we expect the following qualitative spectrum for [60]PCBM. In the sp^3 region from 20 – 90 ppm, it should comprise a total of 6 carbon resonances. These are, 3 single-intensity resonances from the –CH$_2$–CH$_2$–CH$_2$– group between 20 and 40 ppm – with the middle carbon B3 having the lowest chemical shift, one single-intensity line from the methyl carbon of the methyl butanoate near 50 ppm, one single-intensity resonance from the fullerene bridge carbon (C61) also near 50 ppm, one double-intensity resonance from the two mirrored bridgehead carbons on C$_{60}$ cage near 70 ppm. In the sp^2 region (above 120 ppm), it should comprise 36 resonances in total. These are, 4 resonances from the phenyl group between 125 and 135 ppm, of which 2 are single-intensity resonances and 2 are of double-intensity. Moreover, 31 resonances from the fullerene between 135 and 150 ppm, of which 27 are double-intensity resonances and 4 are single-intensity, and one single-intensity line from the carbonyl carbon of the methyl butanoate group near 170 ppm.

Based on the prediction for the ^{13}C NMR spectrum of [60]PCBM, next is trying to find the agreement with the experimental ^{13}C NMR data that is illustrated below. This will also give a clue for identifying the carbons from the molecular structure of [60]PCBM.

3.2   The ^{13}C NMR spectrum

The experimental ^{13}C NMR of [60]PCBM in solution state is recorded on the Bruker AvanceNEO 600 MHz spectrometer, the spectrum is shown in Figure 3-2. To aid in the interpretation of this spectrum, some empty space in sp^3 region between 24 – 33, 35 – 51, 53 – 79 ppm and in sp^2 region between 139 – 141, 143.5 – 144 and 149 – 171 ppm, the empty area between the sp^2 and sp^3 regions (81 – 125 ppm), as well as the relatively gigantic lines due to the solvent CS_2 (at 192.20 ppm) are omitted. The deuterated benzene that was used as a signal lock in the NMR experiment (at 128.06 ppm) is kept with [60]PCBM ^{13}C NMR resonances. The lines of noise are labelled with star on top: toluene lines at 125.73, 128.59 and 129.31 ppm; the short noise line from 137.6 ppm which is not from toluene and does not exist in other repeating ^{13}C NMR spectra.

In general, the ^{13}C NMR spectrum presented here (Figure 3-2) is in line with the above prediction. There are 6 resonances in the sp^3 region ranging from 22.90 to 80.04 ppm, 4 phenyl ring carbons line between 128.55 and 136.93 ppm, fullerene lines between 137.99 and 148.86 ppm, and a carbonyl carbon resonance at 171.73 ppm as list in Table 3-2.
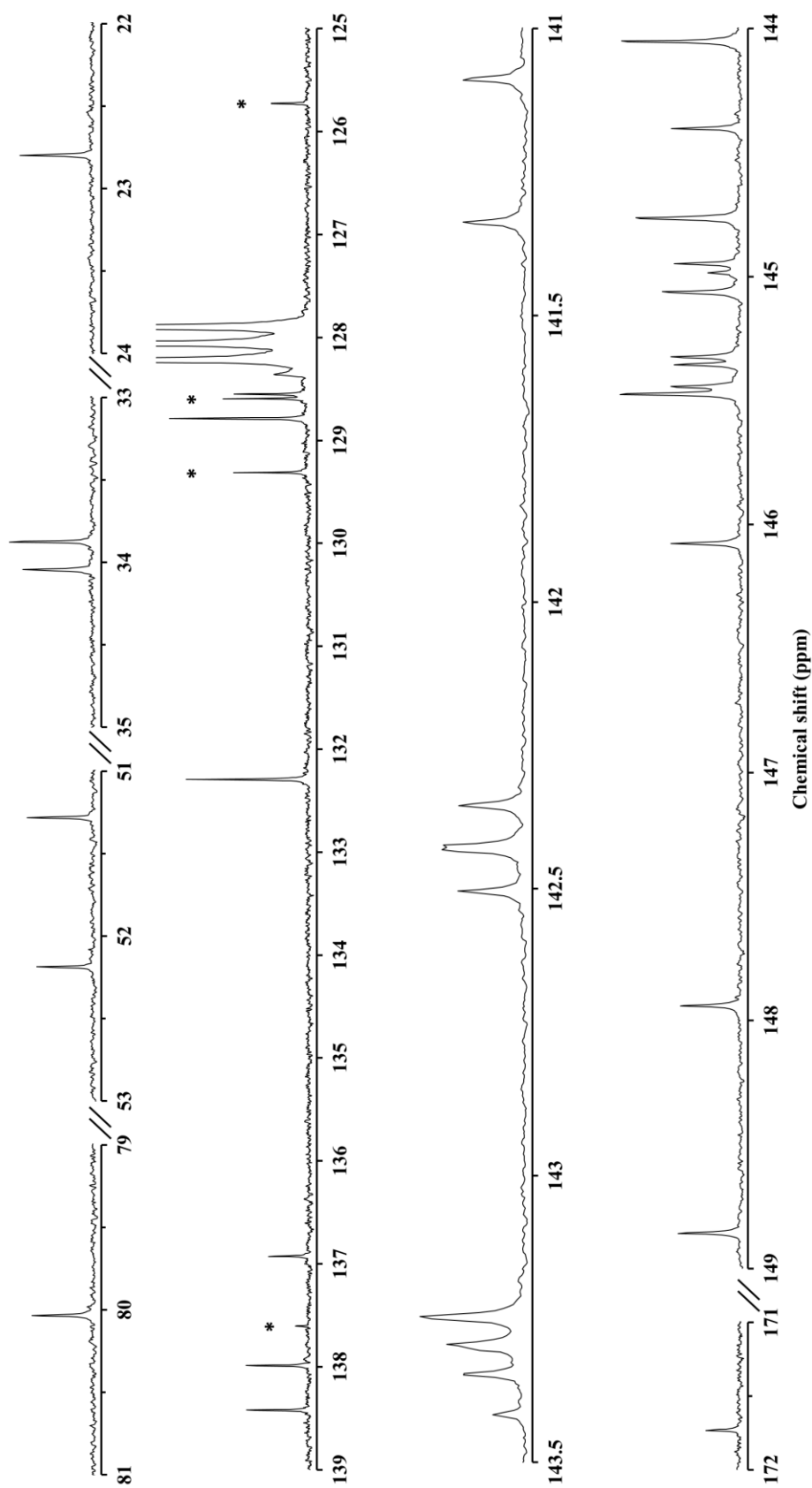
Figure 3-2 The ¹³C NMR spectrum (600 MHz) of [60]PCBM.
Resonances below 81 ppm and above 125 ppm respectively originate from sp^3 and sp^2 hybridized carbons.

67

The sp^3 region constants with the prediction of ^{13}C NMR spectrum of [60]PCBM, the double-intensity resonance at 80.04 ppm is from bridgehead carbons (cyclopropa-fullerene carbons C1 and C9). The two close resonances near 52 ppm are from the bridge carbon (C61) and the methyl carbon. However, it cannot be determined which resonance is which carbon atom only based on the ^{13}C NMR spectrum. The 2D NMR spectrum is assisted which is detailed in Section 3.4, the resonance at 51.28 ppm that has associated hydrogens (at 3.50 ppm; and hence, this resonance that is assigned to the methyl carbon – leaving the resonance at 52.19 ppm to be assigned to the bridge carbon. The two end carbons (B4 and B2) of the $-CH_2-CH_2-CH_2-$ part of the MB group occur at 34.05 and 33.87 ppm (again, determined via the 2D NMR spectrum), with the B2 carbon has slightly higher intensity as it has a neighbour carbon attached with an oxygen and the middle carbon (B3) of that chain occurs at 22.90 ppm.

Table 3-2 The chemical shift of ^{13}C NMR spectrum of [60]PCBM. The relative intensity of each resonance is labelled in the parentheses.

hybridization	chemical shift/ppm
sp^3	22.90(2), 33.87(2), 34.05(2), 51.28(2), 52.19(2), 80.04(2).
sp^2	128.55(1), 128.79(2), 132.30(2), 136.93(1), 137.95(2), 138.38(2), 141.05(2), 141.30(2), 142.32(2), 142.38(2), 142.39(2), 142.47(2), 143.21(4), 143.26(3), 143.31(2), 143.38(1), 144.02(4), 144.36(2), 144.72(4), 144.91(2), 144.95(1), 145.03(3), 145.29(2), 145.32(2), 145.40(2), 145.44(4), 146.04(2), 147.91(2), 148.83(2), 171.72(1).

The first four resonances in the sp^2 region occur at 128.55(1C), 128.79(2C), 132.30(2C) and 136.93(1C) ppm are the 4 resonances from the phenyl ring carbons. Three of these resonances (128.55, 128.79 and 132.30 ppm) ascribed to the phenyl ring group have intensities greater than expected based on their degeneracy as

shown in Figure 3-2. This behaviour results from the faster relaxation of these three ^{13}C nuclei environments (Ph2/Ph6, Ph3/Ph5 and Ph4) by their attached hydrogens. By this reasoning, the single-intensity resonances at 128.55 and 136.93 ppm are respectively assigned to phenyl ring carbon Ph4 and Ph1, on the basis that Ph4, having an attached hydrogen, has considerably greater intensity than Ph1 carbon. The double degenerate resonances at 128.79 and 132.30 ppm may be respectively assigned to phenyl ring carbons Ph3/Ph5 and Ph2/Ph6 based on typical group frequencies. In addition, the 2D NMR of [60]PCBM confirms these assignments, will explain in Section 3.4. The total number of sp^2 chemical shift shown from 125 to 172 ppm region is 30 which is lower than the 36 expected. However, integration analysis list in Table 3-2 indicates that there are several accidental coincidences of lines. The lines at 143.21, 144.02, 144.72 and 145.44 ppm are all of intensity 4 – indicating that each is a coincidence of two double-intensity lines; and the lines at 143.26 and 145.03 ppm are of intensity 3 – both indicating the coincidences of a double and single intensity lines. With these analyses, resonances from all 58 sp^2 fullerene carbons are fully accounted for. This includes those of the 4 single-intensity resonances, which originate from the 4 equatorial carbons on the mirror plane (C21, C30, C31 and C40) that occur at 143.26, 143.38, 144.95 and 145.03 ppm. Although, which of these carbons corresponds to which resonance cannot be determined from the spectrum alone, these 4 resonances forms a useful 'fingerprint' for the later benchmarking of DFT simulations in the fullerene region. The last resonance at 171.72 ppm which is well-separated from the other resonances and is typical of carbonyl carbon. Hence, it is readily assigned to B1 of the methyl butanoate group.

3.3 The ^{1}H NMR spectrum

The experimental ^{1}H NMR of [60]PCBM in solution state is recorded on the Bruker AvanceNEO 600 MHz spectrometer. The digital resolution is given from the acquisition parameters as: *resolution* = TD/(AQ×SI). TD is the data acquisition size, AQ is the acquisition time, and SI is Fourier transform size. With both TD and SI being the same, at 64K, and AQ being 2.6477449 s, the digital resolution is about 0.4 (or ± 0.2) Hz. The full spectrum is shown in Figure 3-3. The inserts on top show enlargements of individual resonances that indicate spin-spin couplings with matched intensities. With the starts on top of several signals, the full spectrum exhibits some other resonances from contaminants which are the toluene from the solvent of the sample and benzene used as a signal lock. The resonances from toluene are a singlet at 2.26 ppm from the methyl group, a triplet at 7.09 ppm from phenyl hydrogens attached to phenyl carbon Ph4, the coincidence of a doublet from symmetry equivalent phenyl carbons Ph2/Ph6 and a triplet from symmetry equivalent phenyl carbons Ph3/Ph5 near 7.01 ppm. The benzene line appear at 7.20 ppm. The resonances shown in Figure 3-3 are from [60]PCBM is confirmed by several indicators. The resonances occur at the chemical shifts which are expected, their integrations are all consistent with the number of hydrogens expected of [60]PCBM – with all in near-integer ratios, and finally, they are consistent with the previous report from the original synthesis[1] in the literature.
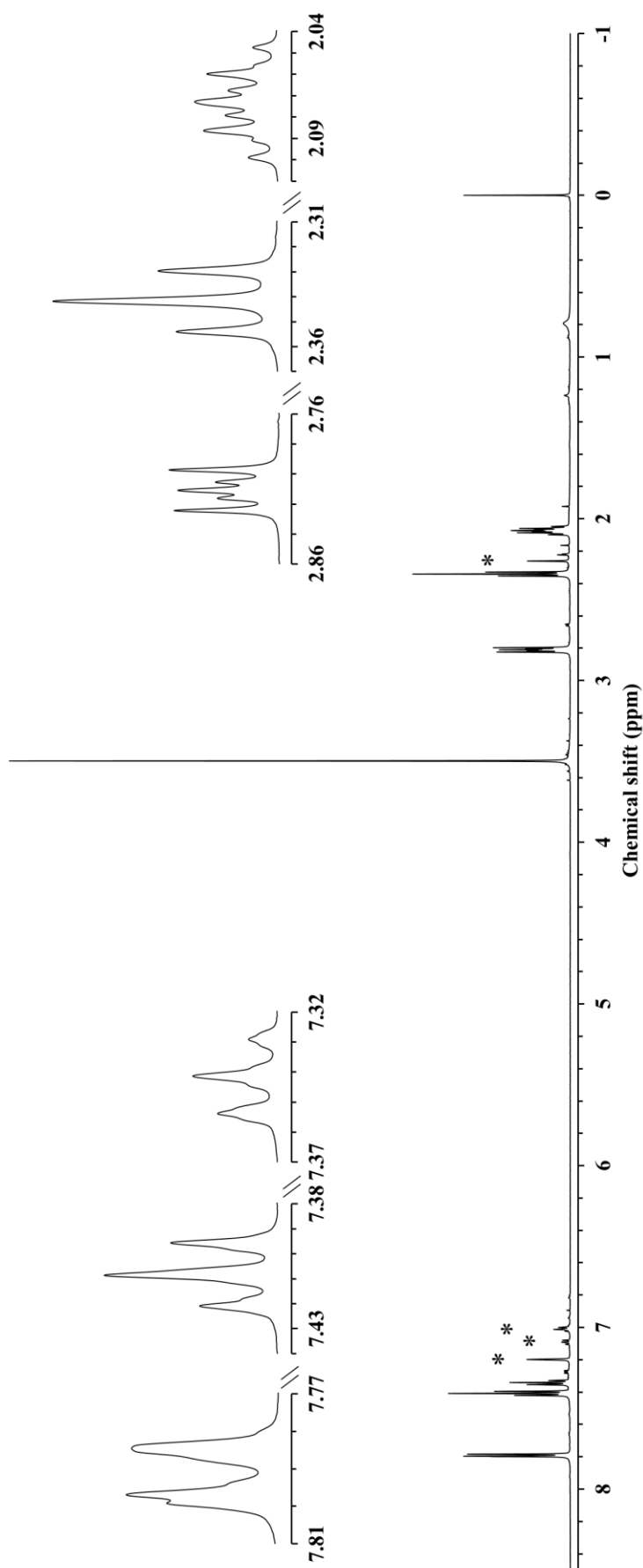
Figure 3-3 The ¹H NMR spectrum (600 MHz) for [60]PCBM.

The insets indicate spin-spin splitting of resonances from the phenyl ring (left) and the ($-CH_2-CH_2-CH_2-$) part of the methyl butanoate group (right). Resonances from residual toluene and benzene solvents are indicated with *, and the singlet at 0 ppm is the TMS reference.

The full ^{1}H NMR resonances of [60]PCBM are a singlet of integration 3 appear at 3.50 ppm is from the three methyl protons shown as a huge peak in Figure 3-3, The remaining three resonances at 2.81, 2.34 and 2.07 ppm, all of integration-2 are from the $-CH_2-CH_2-CH_2-$ part. These show as a 5-peak multiplet, a 1:2:1 triplet and a 9-peak multiplet, respectively. The two multiplets of the $-CH_2-CH_2-CH_2-$ chain in the top right insert of Figure 3-3 show clearly the 2nd-order spin-spin interactions. In the left insert of Figure 3-3, the resonances from phenyl group of [60]PCBM occur at 7.79 and 7.41 ppm as two double of doublets and a triplet of triplets of integration 1 occurs at 7.34 ppm. The detailed is analysed below.

The methyl butanoate group ($-CH_2-CH_2-CH_2-$ part) of [60]PCBM: Based on the typical group resonance values[133], the ^{1}H resonance with the lowest chemical shift (2.07 (m, 2H) ppm) may be assigned to the hydrogens that attached to the central carbon (B3) and the resonance with the highest value of chemical shift (2.81 (m, 2H) ppm) assigned to the hydrogens that attached to the end carbon (B4) which has the neighbour of the cyclopropa-fullerene bridge carbon C61. Leaving the resonance appear at 2.34 (tt, 2H) ppm is assigned to the hydrogens from the other end carbon B2.

At 1st-order, the resonance at 2.81 ppm from the two chemically equivalent hydrogens that attached to the carbon B4 of the MB group is expected to show spin-spin coupling to the two chemically equivalent hydrogens attached to the neighbouring carbon B3. As such, it should comprise a 1:2:1 triplet of integration 2 with a spin-spin coupling constant $^3J \approx 8$ Hz. However, what is observed from the spectrum recorded in Figure 3-3 for the hydrogens attached on carbon B4 is roughly a 2:1:2:1:2 quintet at first sight. This presence indicates that the two hydrogens attached on B4 are not magnetically equivalent to each other. Similarly,

the two hydrogens attached on carbon B3 are also magnetically inequivalent. Hence, this system is showing 2nd-order spin-spin couplings between the hydrogens that attach on B4 and B3 carbons. Moreover, this situation presented for hydrogens attached on carbon B4 is a 4-spin AA′BB′-type system, where A and A′ represent the two chemically equivalent but magnetically inequivalent attached hydrogens, and B and B′ represent their analogues attached to the neighbouring carbon B3. This situation generally yields 4 coupling constants as $^3J_{AB}$, $^3J_{AB'}$, $^2J_{AA'}$ and $^2J_{BB'}$ which are represented for $^3J_{4,3}$, $^3J_{4,3'}$, $^2J_{4,4'}$ and $^2J_{3,3'}$, respectively. Generally, the AA′BB′ system yields a spectrum that comprises 10 lines for the hydrogens which are attached on carbon B4 of $-CH_2-CH_2-CH_2-$ chain, resulting from a doublet, and two separate AB-type quartets. However, the measured spectrum contains 7 lines. The close inspection of the insert of 5-line multiplet from Figure 3-3 shows that there are two very weak outer lines. Such a pattern is explained by Edgar W. Garbisch[134] Jr who had represented the situation where $^2J_{AA'}$ and $^2J_{BB'}$ are equal to each other within the experimental error, and this leads to the coincidences of 3 lines. As mentioned above, the spectrum of the hydrogens attached on B4 carbon may be analysed in terms of three features. Firstly, it is an intense doublet (2.79 and 2.83 ppm) which is centred on ν_A and has a separation of ($^3J_{AB}$ + $^3J_{AB'}$). Secondly, it is an AB-type quartet – again centred on ν_A. However, with $^2J_{AA'}$ = $^2J_{BB'}$, the two outer lines are coincidental in our case. This has the appearance of a doublet (2.80 and 2.82 ppm) of total width of ($^3J_{AB}$ − $^3J_{AB'}$). The third is another AB-type quartet centred on ν_A, which again has the two central lines coincidental. This yields another triplet (2.76, 2.81 and 2.86 ppm) with the separation of ($^2J_{AA'}$ + $^2J_{BB'}$), this time the inner line is much more intense than the outer lines.

Applying these analyses to the present spectrum, it indicates that: $\nu_A = 1683.8$ Hz

on the instrument used, corresponding a chemical shift of $\delta = 2.81$ ppm from TMS.

The splitting of the intense doublet indicated that $^3J_{AB} + {}^3J_{AB'} = {}^3J_{4,3} + {}^3J_{4,3'} = 16.4(2)$

Hz. The width of the 1st quartet indicates that $^3J_{AB} - {}^3J_{AB'} = {}^3J_{4,3} - {}^3J_{4,3'} = 6.8(2)$ Hz.

From these it can be established that $^3J_{4,3}$ and $^3J_{4,3'}$ are 11.6(2) Hz and 4.8(2) Hz,

respectively. Although it is not possible to determine which value is corresponds

to $^3J_{4,3}$ or $^3J_{4,3'}$ at this stage. From the shape and spacings of the 2nd quartet showing

that $^2J_{AA'} + {}^2J_{BB'} = 27.5(2)$ Hz, with the fact that $^2J_{AA'} = {}^2J_{BB'}$ in this case, it is

established that $^2J_{4,4'} = {}^2J_{3,3'} = 13.8(2)$ Hz. In order to test these analyses, the form

of the spectrum of this multiplet was simulated using the WinDNMR computer

program[135] for an AA′BB′ system. The simulation used the 4-spin coupling

constants established above together with the experimental ν_A–ν_B difference of 430

Hz, the instrumental resolution (taken from the FWHM of the TMS line). The

simulated result is shown in Figure 3-4 which is remarkably like the experimental

spectrum of this multiplet. The splittings and relative intensities, including the 2nd-

order unevenness of those intensities of the simulation is effectively

indistinguishable from the experimental spectrum. This suggests that all the

couplings for the protons on ester carbon B4 founded from the 2nd-order analysis

are reliable.

$^2J_{4,4'} + {}^2J_{3,3'} = 27.5(2)$ Hz

$^3J_{4,3} + {}^3J_{4,3'} = 16.4(2)$ Hz

$^3J_{4,3} - {}^3J_{4,3'} = 6.8(2)$ Hz
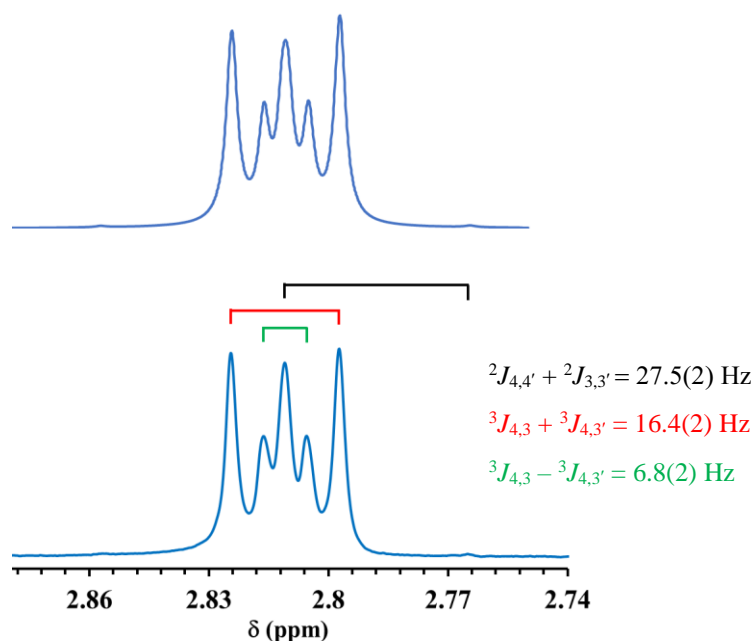
Figure 3-4 WinDNMR[135] simulation (top) of the experimental spectrum (bottom) of hydrogens attached on B4 carbon of the methyl butanoate group. It based on an AA′BB′ system with $^3J_{4,3}$, $^3J_{4,3'}$ and $^2J_{4,4'}$ being 11.6, 4.8 and 13.8 Hz, respectively. The $\nu_4 - \nu_3$ being the experimental 430 Hz.

The presence of 2nd-order couplings which is founded on the hydrogens attached on carbon B4 strongly suggests that the three staggered conformers (*gauche*, *anti*, and *gauche'*) are unevenly populated. This is because, at 2nd-order, equal population of all three conformers yields the 1st-order 1:2:1 triplet. Staggered conformers, being considerably more stable than eclipsed conformers, are far more likely to be populated. This means that there is a preferred conformer resulting from hinderance to free rotation about the carbon B3–B4 bond of the MB group resulting from the proximity of this bond, which joins the rest of the long ester group to the relatively huge cyclopropa-fullerene cage. A reasonable estimate of the relative populations of the three staggered conformers may be obtained via the computer program MestReJ[136] using a Colucci-Jungk-Gandour analysis.[137]

Although this program has empirical data for an ester substituent, it, not unreasonably, has none for a phenyl cyclopropa-fullerenyl group. However, making the reasonable substitution of phenyl group gives $^3J_{AB} = 3.4$ Hz for the *anti* and *gauche* conformers and $^3J_{AB} = 14.4$ Hz for the *gauche'* conformer; and $^3J_{AB'} = 14.4$ Hz for the *anti* conformer and $^3J_{AB'} = 3.4$ Hz for the *gauche* and *gauche'* conformers. A population analysis based on these figures suggests that the '*anti*' conformer is occupied for about 75 % of the time; with occupation times of the two *gauche* conformers being equal at about 12.5 % each. This is because a 75:12.5:12.5 ratio gives $^3J_{4,3} = (0.75 \times 14.4 + 0.125 \times 3.4 + 0.125 \times 3.4) = 11.7$ Hz and gives $^3J_{4,3'} = (0.75 \times 3.4 + 0.125 \times 3.4 + 0.125 \times 14.4) = 4.8$ Hz. Both are consistent with the experimental values of 11.6(2) and 4.8(2) Hz, respectively. This also resolves the issue of which of $^3J_{4,3}$ or $^3J_{4,3'}$ equals to 11.6 or 4.8 Hz ($^3J_{4,3}$ is 11.6 Hz and $^3J_{4,3'}$ is 4.8 Hz). It suggests that there is a strong preference for the '*anti'* conformer; whereby, the carbon B4 of the MB group lies along the mirror plane. However, there is a small probability of rotation about the B3-B4 bond through the eclipsed conformer to the gauche staggered conformers on either side – but there is negligible probability of further rotation to the through the conformer with the phenyl cyclopropa-fullerene groups and the remainder of the ester group being eclipsed.

The protons on carbon B2 of the MB group at the other end of the –CH$_2$–CH$_2$– CH$_2$– chain closely resembles a 1st-order 1:2:1 triplet with a chemical shift of 2.34 ppm. with a $^3J_{3,2}$ coupling of 7.4(2) Hz through protons on the middle carbon B3. The presence of this triplet indicates that the populations of the three conformers of the 4-spin couplings type discussed above are effectively equally populated (i.e., there is free rotation about the carbon B2–B3 bond). Closer analysis indicated that

there is also what appears to be a $^4J_{2,4}$ coupling to carbon B4 with a coupling constant 1.7(2) Hz. Hence, this resonance appears as a triplet of triplet.

The resonance of the protons on the middle carbon B3 of the MB group has a chemical shift of 2.07 ppm with showing the presence of 9 components. However, as these protons are coupled to those on B4 with its 2nd-order couplings and to those on carbon B2 with its 1st order couplings, the coupling constants of the protons on this carbon are those already determines ($^2J_{3,3'}$ = 13.8(2) Hz, $^3J_{3,4}$ = 11.6(2) Hz, $^3J_{3,4'}$ = 4.8(2) Hz, $^3J_{3,2}$ = 7.4(2) Hz).

For the phenyl group of [60]PCBM:

The three ^{1}H resonances for the phenyl group of [60]PCBM occur at 7.79(ddd 2H), 7.41(ddd 2H) and 7.34(tt 1H) ppm were assigned to the hydrogens attached to the carbons Ph2/Ph6, Ph3/Ph5 and Ph4, respectively.

The resonance at 7.34 ppm of integration 1 is assigned to phenyl carbon Ph4 (*para* position) and shows as a triplet of triplets with coupling constants of $^3J_{4,3}$= 7.5 Hz and $^4J_{4,2}$ = 1.3 Hz.

The resonance at 7.41 ppm has an integration of 2, and is assigned to the hydrogens attached on the symmetrically equivalent carbons Ph3/Ph5 (*meta* position). This resonance is reported in the literature as a 1:2:1 triplet.[1] However, closer analysis reveals that it is a double doublet of doublets in which one line from each doublet is practically co-incident – giving the effect of a triplet. This is evidence by the fact that the intense 'central' line is not quite at the centre of the 'triplet'. Hence, two coupling constants were measured $^3J_{3,2}$ = 7.8 Hz and $^3J_{3,4}$ = 7.3 Hz. A doublet of doublets is expected for this resonance because the splitting of hydrogens attached on carbon Ph3 by that of carbon Ph2 is close to but not the same as the splitting of

hydrogens attached on carbon Ph3 by that of carbon Ph4. There is also evidence of further doublet splittings of this resonance by the protons at phenyl carbon Ph6 (as evidences by shoulders) with $^5J_{3,6} = 2.0$ Hz. As with the resonance for the protons attached at carbons Ph2/Ph6, there is evidence of immeasurable 2nd-order effects, as evidenced by weak unresolved shoulders on the lines.

The 7.79 ppm line also has an integration of 2 and is clearly from the hydrogens attached to the symmetrically equivalent carbons Ph2/Ph6 (*ortho* position). At first glance, this resonance shows the doublet of doublets pattern which is expected of this position. However, closer inspection reveals unresolved shoulders which are indicative of weak effects of 2nd-order. This suggesting that $^4J_{2,6}$ and $^4J_{3,5}$ are very close to zero Hz, but not exactly. Although the additional 2nd-order peaks are seen in the figure, unlike for the $–CH_2–CH_2–CH_2–$ chain of the MB group, the effect is so weak that no reliable measurement can be made of their resonance frequencies. Hence, the resonances from Ph2/Ph6 are analysed in terms of their measurable 1st-order spin-spin splitting from the protons at these *ortho*-positioned proton are split by Ph3/Ph5 (*meta* position) with a coupling constant $^3J_{2,3}= 7.8$ Hz, which is further split by the proton at Ph4 (*para* position) with coupling constant $^4J_{2,4} = 1.3$ Hz. However. The coupling constant of $^5J_{2,5}$ which although present, was not resolved sufficiently to be reliably determined from the spectrum.

The summaries of the ^{1}H NMR spectra analyses, including chemical shifts, integrations, assignments (where possible) and spin-spin coupling constants (where appropriate) are respectively given in Table 3-3.

Table 3-3 The ^{1}H NMR spectroscopic data for [60]PCBM as extracted from the ^{1}H spectrum and the 2D spectrum. The apparent septet and nonet both show strong 2nd-order spin-spin interactions from magnetically inequivalent protons.

chemical shift/ppm	Int.	assignment	multiplet	spin-spin coupling constant/Hz			
2.07	2H	CH$_2$-**CH$_2$**-CH$_2$-	2nd-order m	$^2J_{3,3'}$ 13.8	$^3J_{3,4}$ 11.6	$^3J_{3,4'}$ 4.8	$^3J_{3,2}$ 7.4
2.34	2H	-CH$_2$-**CH$_2$**-CO	tt	$^3J_{2,3}$ 7.4	$^4J_{2,4}$ 1.7		
2.81	2H	Ph-C-**CH$_2$**-	2nd-order m	$^2J_{4,4'}$ 13.8	$^3J_{4,3}$ 11.6	$^3J_{4,3'}$ 4.8	
3.50	3H	Me	s				
7.34	1H	*p*-Ph4	tt	$^3J_{4,3}$ 7.3	$^4J_{4,2}$ 1.3		
7.41	2H	*m*-Ph3/Ph5	ddd	$^3J_{3,2}$ 7.8	$^3J_{3,4}$ 7.3	$^5J_{3,6}$ 2.0	
7.79	2H	*o*-Ph2/Ph6	ddd	$^3J_{2,3}$ 7.8	$^4J_{2,4}$ 1.3	$^5J_{2,5}$?	

3.4 2D NMR spectroscopy

The 2D NMR spectrum of [60]PCBM is given in Figure 3-5 which shows the aliphatic hydrogens and Figure 3-6 for the phenyl ring hydrogens.
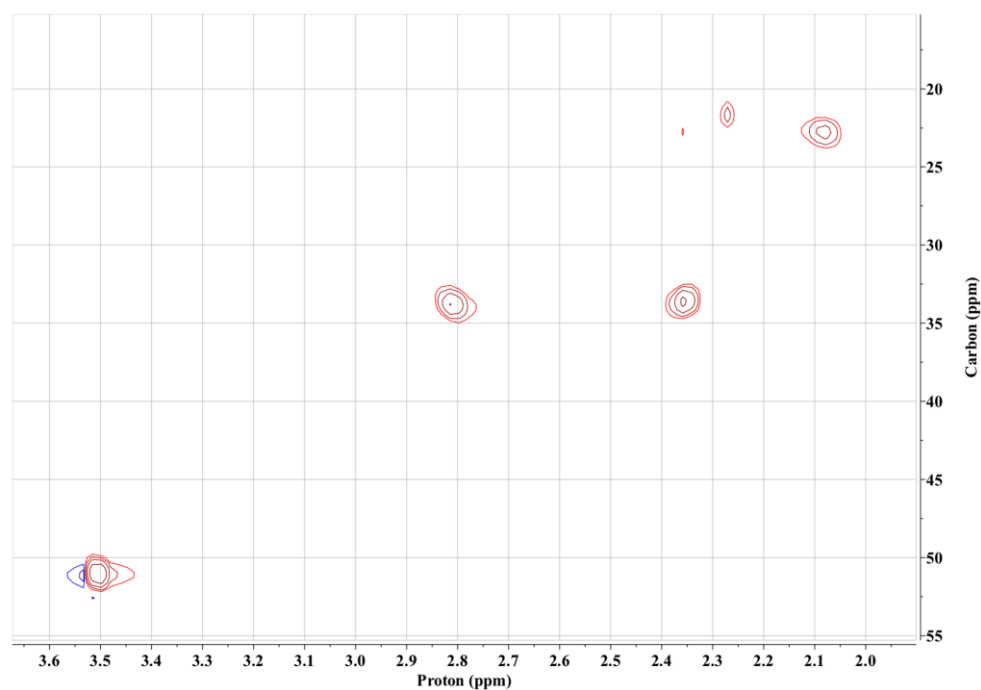
Figure 3-5 2D NMR spectrum of the aliphatic carbons.

79

Based on the typical group frequencies[133], the ^{13}C resonance at 22.90 ppm corresponds to the centre carbon (B3) of the $–CH_2–CH_2–CH_2–$ chain from the analysis in Section 3.2, and Figure 3-5 indicates that the hydrogens attached to that central carbon come from the ^{1}H resonance at 2.07 ppm.

The ^{13}C resonances from the two end-carbons of the $–CH_2–CH_2–CH_2–$ chain, B2 and B4, occur very close together at 33.87 and 34.05 ppm from Figure 3-2. Indeed, the previous reports by Yang et al.[138] and Mens et al.[139] did not resolve these, and hence, did not determine which is which; and although Hummelen et al.[1] resolved them, they were not distinguished in their assignment. It is not surprising that these two carbons are so close. This is because they are both bonded to a CH_2 group (B3 carbon in both cases) and a carbon with no attached hydrogens (B4 carbon is attached to fullerene C61 and B2 carbon is attached to the carbonyl group). Hence, both are in similar chemical environments. However, the difference is enough for them to be distinguished from the 2D spectrum. This spectrum shows that it is the ^{13}C resonance at 34.05 ppm that is associated with the carbon B4 of MB group, and that resonance at 33.87 pm that is associated with carbon B2.

The 2D spectrum can also be used to distinguish cyclopropa-fullerene bridge carbon (C61) from the methyl carbon (both are predicted to occur near 50 ppm. The 2D spectrum clearly indicates that the ^{13}C resonance at 51.28 ppm that is associated with methyl ^{1}H resonance at 3.50 ppm, leaving the 52.19 ppm resonance as being from the bridge carbon C61 which is not present in the 2D spectrum as it has no hydrogens. Further evidence in favour of this conclusion comes from the resonance at 52.19 ppm being of slightly lower intensity than that at 51.28 ppm in ^{13}C NMR spectrum. A lower intensity is expected from the bridge carbon (C61) by reason of having no attached hydrogens, which are an additional course of spin-

lattice relaxation only available to the methyl carbon. The assignment of the resonance at 51.28 ppm to the methyl group is consistent with the previous report, via attached proton test (ATP) NMR spectroscopy, of Mens et al.[139] However, Hummelen et al.[1] misassigne the methyl group to the higher of the two resonances near 50 ppm, and Yang et al. assigned the methyl group to a resonance near 62 ppm, which in not present in our spectrum.

Figure 3-6 2D NMR spectrum of the phenyl carbons.

The spectrum for the aromatic carbons in Figure 3-6 shows that the single-intensity ^{13}C resonance at 128.55 ppm originates from the triplet of integration 1 that is associated with the ^{1}H resonance at 7.34 ppm, and hence, this ^{13}C resonance arises from the phenyl carbon Ph4. The two double-intensity ^{13}C resonances at 128.79 and 132.30 ppm are respectively associated with the ^{1}H resonances at 7.41 and 7.79 ppm. Hence, they are phenyl carbons Ph3/Ph5 that resonate at 128.79 ppm and

Ph2/Ph6 carbons that resonate at 132.30 ppm based on the 2D spectrum. This leaves the single-intensity ^{13}C resonance at 136.93 ppm as originating from the phenyl carbon with no protons (Ph1) (which we had already surmised above based on its lower intensity when compared to the other single intensity resonance (128.55 ppm) from Ph4 in Section 3.2).

According to the analysis from ^{13}C, ^{1}H and 2D NMR spectroscopy, all the carbon atoms on the phenyl C61 butyric acid methyl ester together with two bridgehead carbons can be assigned to their corresponding ^{13}C resonances in this stage, leaving the assignment for fullerene carbons from DFT simulation method in the next section. The summaries of the ^{13}C spectra analyses, including chemical shifts, integrations and assignments (where possible) are respectively given in Table 3-4 below.

Table 3-4 The measured ^{13}C chemical shifts (ppm), integrations and atom assignments for the addend of [60]PCBM based on the conclusion of ^{13}C, ^{1}H and 2D NMR spectroscopy.

chemical shift/ppm	integration	assignment
22.90	1C	B3
33.87	1C	B2
34.05	1C	B4
51.28	1C	methyl carbon
52.19	1C	bridge carbon C61
80.04	2C	bridgehead carbons C1/C9
128.55	1C	Ph4
128.79	2C	Ph3/Ph5
132.30	2C	Ph2/Ph6
136.93	1C	Ph1
171.72	1C	B1

3.5   DFT simulations of the ^{13}C NMR spectrum

Gauge independent atomic orbitals (GIAO) density functional theory (DFT) simulations of the ^{13}C NMR spectrum for [60]PCBM was performed using the Gaussian 16 package.[140] An ωB97X DFT method[141] coupled with a Dunning-type[142] correlation-consistent polarized valence-only triple zeta basis set (cc-pVTZ) was used for the analysis on the ground that when the range separation parameter ω was set to zero. The ωB97X/cc-pVTZ simulated spectrum showed remarkable agreement with the experimental spectrum. For comparison, the spectrum was also simulated by using the B3LYP/6-31G(*d,p*) method[143] as this is arguably the most methods used by other researchers to simulate spectra, and hence acts as a in effect standard to judge the quality of the ωB97X simulation. To make this point, a literature search indicated that in the last two years there were nine papers on simulations ^{13}C NMR of fullerenes or their derivatives. Of these, 6 were performed by using B3LYP as the only method[144-148], another use X3LYP as well as B3LYP[149], and there was one paper using each of the following method Hartree Fork at STO-6-31G[150], wB97XD[151] and HC-PBE[152]. Although B3LYP is the go-to standard, it is not necessarily accurate. Therefore, we also tested against the X3LYP/6-31G method[153] which does not employ polarisation functions, as this was found after considerable benchmarking by Tulyabaev et al. [149] to give the most accurate results for an analogous mono cyclopropa-fullerene ($C_{61}H_2$)[154], based on their trialled exchange and correlation functional and basis set. All simulated spectra were referenced that the first line in each of the three simulated spectra (corresponds to carbon C3 of the ester group) had the same chemical shift as that of the corresponding resonance in the experimental spectrum (22.90 ppm) as shown in Figure 3-7 to Figure 3-9.

As shown in Figure 3-7, in the sp^3 region, the overall (a) experimental pattern comprises a single line near 20 ppm, two very closely spaced lines (0.16 ppm) near 30 ppm, two slightly wider spaced lines (0.91 ppm) near 50 ppm, and a single line near 80 ppm. All these features are qualitatively and quantitatively reproduced in the ωB97X simulated spectrum (b). The general features are also reasonably reproduced in the X3LYP and B3LYP simulations (c) and (d), respectively. However, the spacings between the two close lines are much wider than experiment. with X3LYP being the wider of the two close lines near 30 ppm (2.23 ppm for X3LYP and 1.28 ppm for B3LYP compared to a 0.27 ppm for ωB97X and 0.16 ppm for experiment) and B3LYP being the wider for the two close lines near 50 ppm (2.65 for B3LYP and 1.54 ppm for X3LYP compared to 0.89 ppm for ωB97X and 0.90 ppm for experiment). However, the order of the lines in all simulations agrees with the experimental 2D data, particularly that the methyl carbon has a lower chemical shift than the bridge carbon C61.
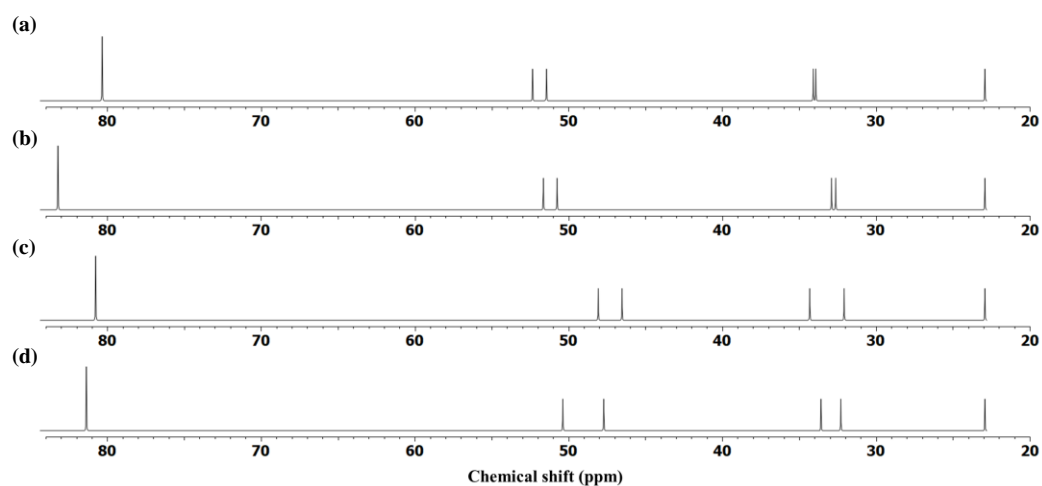
Figure 3-7 The ^{13}C NMR spectrum comparison on sp^3 hybridized carbons of experimental and DFT simulations of [60]PCBM.
(a) Experimental spectrum, (b) ωB97X/cc-pVTZ simulated spectrum, (c) X3LYP/6-31G simulated spectrum and (d) B3LYP/6-31G(*d,p*) simulated spectrum.

In the sp^2 region all the simulations correctly predicts that the first four lines should comprise two lines with single-intensity and two with double-intensity, and that they correspond to the phenyl carbons (Figure 3-8). The order of the lines here also agrees with experiment results except that the single-intensity line from phenyl carbon Ph4 and the double-intensity line from the mirrored Ph3/Ph5 pair of phenyl carbons are reversed from that of the experiment in the ωB97X simulation. However, this is not a significant failure as these two resonances are separated by only 0.24 ppm in experimental spectrum. Similar to the sp^3 region, the general experimental features of two very close lines near 128 ppm, a single double intensity lines near 132 ppm and a single intensity line near 137 ppm are accurately predicted in the simulated spectrum.
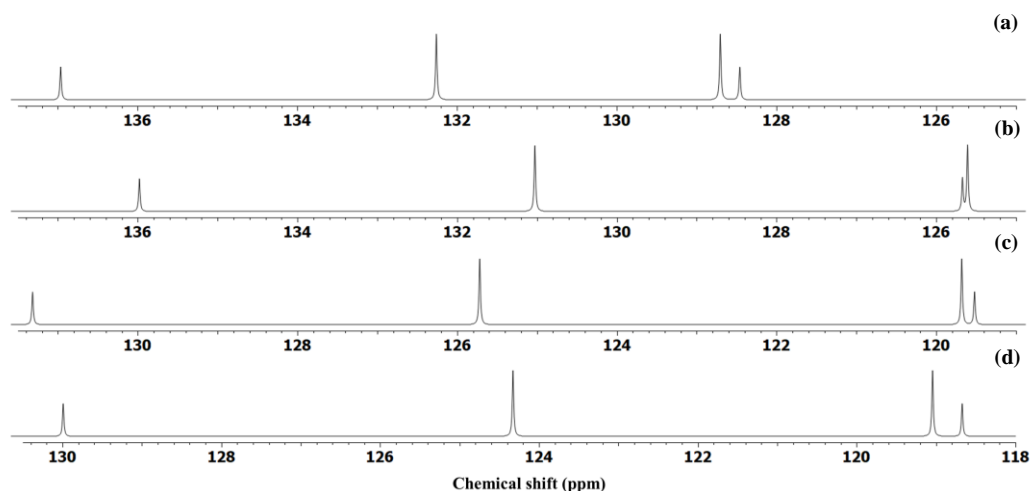
Figure 3-8 The ^{13}C NMR spectrum comparison on phenyl ring sp^2 hybridized carbons of experimental and DFT simulations of [60]PCBM.
(a) Experimental spectrum, (b) ωB97X/cc-pVTZ simulated spectrum, (c) X3LYP/6-31G simulated spectrum and (d) B3LYP/6-31G(d,p) simulated spectrum.

Before turning to the more complicated fullerene sp^2 resonances, it is noted that all simulations accurately predict that the carbonyl resonance should be near 172 ppm. As shown in Figure 3-9, the ωB97X simulation (b) is numerically closest to

experiment being about 3.5 ppm below experimental spectrum for carbonyl carbon. In comparison, the X3LYP and B3LYP simulations are about 8.1 and 13.0 ppm below the experimental value. Nevertheless, the final line in each simulated spectrum is reasonably near the experimental 171.73 ppm and are well separated from the fullerene lines, so there is essentially no doubt that the final line in the spectrum originates from the carbonyl carbon of the ester group as predicted.

The 58 fullerene sp^2 carbons should give rise to 4 single intensity lines from the 4 carbons on [60]PCBM's mirror plane (C21, C30, C31 and C40) and 27 double intensity lines from the carbons split by the mirror plane. Consulting the experimental spectrum reveals that the fullerene resonances occur between 135 and 150 ppm fall into several well-separated groups in Figure 3-9(a). These groups comprise a pair of lines near 138 ppm representing 4 carbon atoms, a pair of lines representing 4 carbon atoms near 141 ppm, a group of three lines near 142.5 ppm representing 8 carbons, 4 lines closely spaced lines near 143 ppm (10 carbons), a wide group of three lines between 144 and 144.8 ppm from 10 carbons, a close group of three lines near 145 ppm from 6 carbons, a cluster of 5 lines from 12 carbons between 145.5 and 146 ppm, and finally a pair of double intensity lines, representing the remaining 4 fullerene sp^2 carbons near 148.5 ppm.

Consulting the ωB97X simulated spectrum in Figure 3-9(b), it reveals the same number of groups of resonances with the same number of carbon atoms in each respective group as that of the experimental spectrum. Furthermore, the distribution of the lines within each group may be matched between the simulated and experimental spectra.
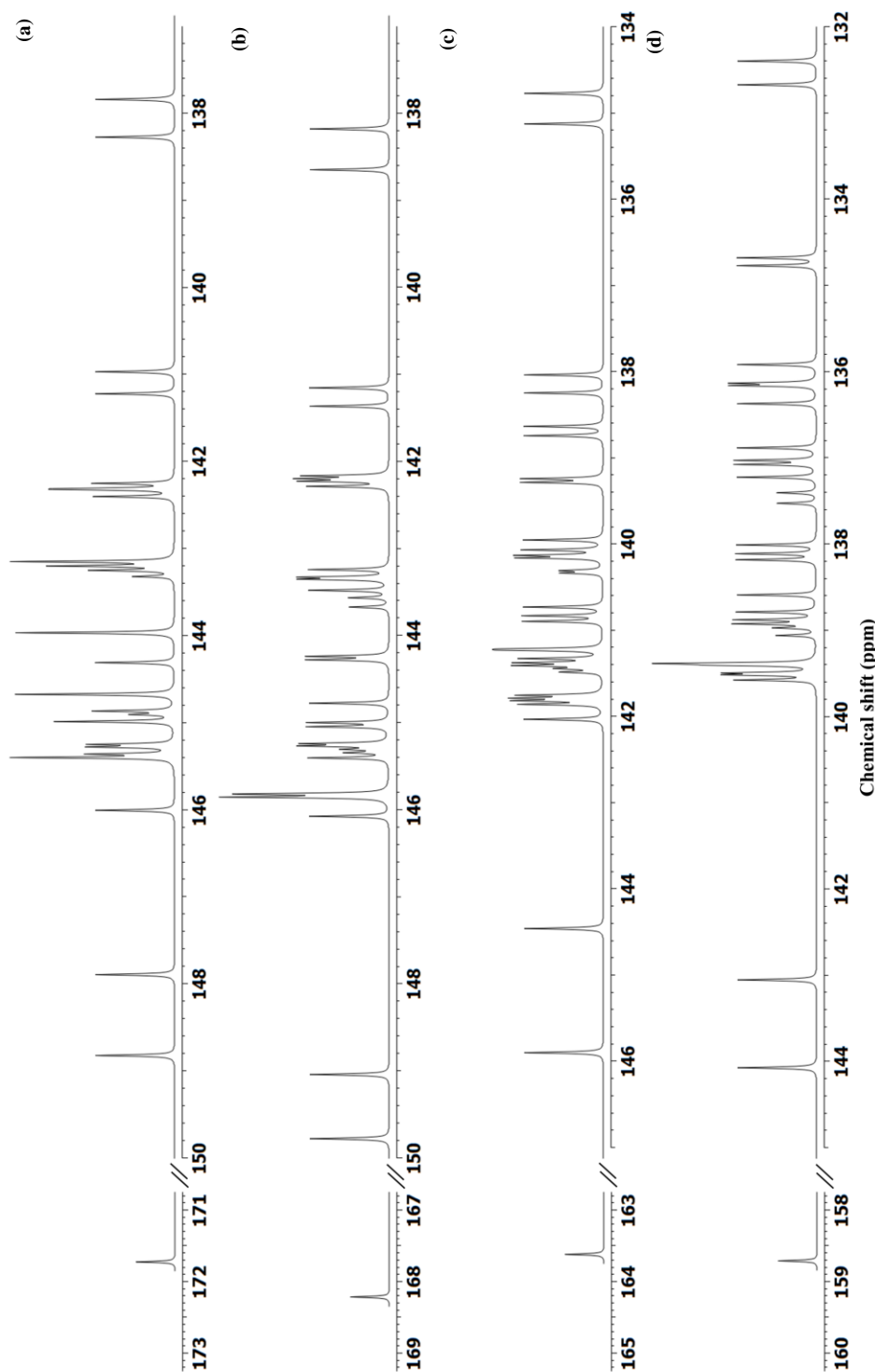
Figure 3-9 The ^{13}C NMR spectrum comparison on fullerene sp^2 hybridized carbons and carbonyl sp^3 hybridized carbons of experimental and DFT simulations of [60]PCBM.

(a) experimental spectrum, (b) ωB97X/cc-pVTZ simulated spectrum, (c) X3LYP/6-31G simulated spectrum, (d) B3LYP/6-31G(d,p) simulated spectrum.

It is also apparent that there is a good agreement of the numerical values of the chemical shifts of the groups of the experimental spectrum with those of the ωB97X spectrum for the fullerene sp^2 resonances. For example, both begin near 138 ppm and end near 149 ppm. There X3LYP and B3LYP spectra also reasonably well qualitatively agree with the experimental spectrum in terms of the separation into distinct groups with resonances that match the number of carbon atoms within each group. In the B3LYP simulation (d) in Figure 3-9, the 1st group (4 carbons), the 2nd group (4 carbons), 3rd group (8 carbons) and the 4th group (10 carbons) are all clearly recognisable, however thereafter there is no so good agreement in respect of groupings until the final group (4 carbons) which is very recognisable. The X3LYP spectrum (c) does slightly less well for the 3rd group, because containing 8 carbons is not as recognisable as it splits into two well separated pair – with the first of those pairs being closer to the 2nd group than it is to the other pair of its group. On a qualitative basis, there is remarkable agreement between the ωB97X spectrum (b) and the experimental spectrum (a) with there being clear matches of all the groups in terms of their number of members and their spacings. The X3LYP and B3LYP also have good qualitative agreement with experiments for the first 4 groups and the last group. However, they are less well in the middle of the spectrum. In addition, ωB97X simulation has excellent quantitative agreement with experiment. The spacing of the first group of fullerene lines is commensurate with the experiment (about 0.4 ppm for both) as the chemical shifts of the members. For example, about 138.3 ppm for ωB97X compared to the experiment at 137.9 ppm – a difference of about 0.4 ppm for both lines. Although the X3LYP and B3LYP agree with experiment on the spacing of the members of this group (at about 0.4 ppm) their chemical shifts vary substantially from

experiment (about 134.8 ppm for X3LYP and 132.4 ppm for B3LYP to compare with 137.9 ppm for experiment – a difference of about 3.1 ppm for X3LYP and 5.5 ppm for B3LYP, respectively). The large numerical values of the chemical shift differences between might suggest that these simulations give large errors when compared to the ωB97X simulation. However, this does not seem to be the case (at lease from the point of view of making line assignments). As mentioned earlier, the resonances in the experimental spectrum of the sp^2 fullerene carbons may be divided into groups, and that to a large extent the simulations may be divided into the same number of groups with the same numbers of members. Hence, it seems that the relative comparisons of resonances are more important for the purpose of assigning the lines than the numerical value of the chemical shifts (although the numerical values may be important for other purposes). Another piece of evidence in support of this view is that the range of sp^2 fullerene carbon chemical shifts is remarkably similar across the simulation methods compared with experiment. That is, this range is about 10.9 ppm in the experimental spectrum, and 11.6, 11.5 and 11.0 ppm for the B3LYP, ωB97X and X3LYP in the simulations, respectively.

With this, I will in the remainder of this section attempt to assign each line in the experimental spectrum to its corresponding carbon atom(s) via comparison of the experimental and simulated spectra. The assignments may be made with a high degree of confidence in where there is substantial agreement across the simulations with experiment in terms of relative spacings of the lines and their line order. In other cases, the arguments will be made that assignments may be made with some confidence. But I stress that such assignment is only tentatively made.

The fullerene resonances begin with a pair of double-intensity lines near 138 ppm and another pair of double-intensity lines near 141 ppm: C11/C12 and C6/C7,

C15/C27 and C18/C24. This feature is clearly seen in all three simulated spectra with very similar chemical shifts and line spacings (but X3LYP and ωB97X performed better than B3LYP on the second group as shown in Figure 3-9). Confidence in this assignment comes from the first two fullerene lines in the Incredible Natural Abundance Double Quantum Transfer Experiment (INADEQUATE) spectrum of 13% ^{13}C-enriched $C_{61}H_2$ having a very similar chemical shift (136.77 ppm and 140.98 ppm) and originating from these same 4 carbon atoms for each line.[154] Hence, the resonances of the first pair – at 137.95 and 138.38 ppm – are respectively assigned to the mirrored pairs C11/C12 and C6/C7 (the carbon labels are shown in Figure 1-3) with a high degree of confidence. And those of the 2nd pair – at 141.05 and 141.30 ppm – are confidently assigned to the C15/C27 and C18/C24 mirrored pairs, respectively.

This occurrence of resonances appearing in pairs is seen throughout the spectrum. It indicates that resonances that would be symmetrically equivalent but for the asymmetry of the addend have very similar chemical shifts. For example, in the two pairs discussed so far, the first pair respectively corresponds to C11 (and its mirror, C12) and C6 (and its mirror, C7). However, C12 and C6 are symmetrically equivalent in the symmetric malonate mono-adducts of C_{60} (as are, of course, C11 and C7)[155], and would be for all cyclopropa-fullerene derivatives with symmetric addends. Similarly, for the second pair, C15/C27 and C18/C24 are symmetrically equivalent in the malonate adducts. This seems reasonable as the perturbation of the chemical of the distant asymmetric addend would be small but noticeable. Confidence in this conclusion comes from observing that in the experimental spectrum, the last two lines near 148 ppm are also seen as a separated pair that is well separated from other lines, which is again a feature clearly observed in the

simulated spectrum. The simulations all show that these two double intensity lines correspond to carbon atoms C2/C10 and C5/C8. As with the other pairs discussed so far, C2 would be symmetrically equivalent to C5 but for the asymmetry of the addend (as are their respective mirrors C10 and C8). Hence, the last two fullerene resonances at 147.91 and 148.83 are confidently assigned to fullerene carbon atoms C5/C8 and C2/C10, respectively.

Returning to an earlier part of the fullerene sp^2 part of the spectrum, following the two initial pairs already discusses, there are is a cluster of 4 lines between 142.3 and 142.5 ppm in the experimental spectrum, all with integrations of 2 carbons. In addition, the two central lines are separated by only 0.01 ppm and give the appearance of a single line of enhanced intensity. Similarly, in the simulated spectrum there is a clear cluster of 8 resonances in two pairs. Based on the closeness of the experimental and simulated spectra for this group, the experimental resonances at 142.32, 142.38, 142.39 and 142.47 ppm are provisionally assigned to fullerene carbons C20/C22 and C13/C29, and C34/C46 and C37/C43, respectively. The next 2 resonances in the spectrum of $C_{61}H_2$[154] correspond to these same 8 carbons and appear in the same order in simulations (as C34/C46/C37/C43 at 142.24 ppm and C13/C29/C20/C22 at 142.78 ppm). Hence, it is confident that the 8 carbons in these 4 lines cluster are indeed fullerene carbons C13, C20, C22, C29, C34, C37, C43 and C46. However, given closeness of the experimental resonances assigned to C13/C29 and C34/C46 (just 0.01 ppm difference) it is also reasonable that the assigned order may be reversed. Indeed, this entire cluster is only 0.15 ppm, it is wider than the mean absolute error (MAE) of the ωB97X simulation is 0.09 ppm which will be explained in Section 3.6 below. As such, it is unreasonable to confidently assign the order of any of the lines in this cluster.

Nevertheless, all three simulated spectra, with their three different exchange functionals, two different correlation functionals and three different basis sets, all assign the carbon in the line order of the above provisional assignment. Despite the complete line order agreement between all three simulations, they are only made tentatively owing to the very narrow range (0.15 ppm) of this group.

Following a gap of almost 1 ppm the experimental spectrum shows, near 143.2 ppm, a cluster of 4 lines indicating that they comprise resonances from 10 carbon atoms. The first in an integration of 4 carbons line at 143.21 ppm, which is an accidental coincidence of two double intensity resonances. The second is at 143.26 ppm and is of integration 3 carbons, representing a coincidence is a single and a double intensity line. The final two lines in this cluster are an integration of 2 line at 143.31 ppm and a single intensity line at 143.38 ppm. This feature is reasonably-well represented in the three simulated spectra in that there is a clear cluster of lines representing resonances 10 carbons. And that two of these resonances are of single intensity. However rather than the experimental 4:3:2:1 intensity patterns, the simulated spectra show a 2:4:2:1:1, 2:2:4:1:1, and 2:2:2:2:1:1 pattern from ωB97X, X3LYP and B3LYP, respectively. Nevertheless, as the simulation indicates these 10 carbons are grouped into only three pairs of lines, and by analysing the pairs we can make reasonable assignments.

The easiest of these pairs to analyse is the two single intensity lines with 0.12 ppm difference, which is wider than the MAE = 0.09 accuracy of the ωB97X spectrum. The simulated order is C40 followed by C31 in the ωB97X simulation. This order is reversed in the X3LYP and B3LYP simulations. However, the values of "Exp.-Cal." for the C40 and C31 in ωB97X (shown in Table 3-5) are within the MAE of the ωB97X, while the reversed order gives larger values that are outside the MAE.

92

This analysis gives confidence in the assignment that the single-intensity component of the triple-intensity line at 143.26 ppm, and the final single intensity line at 143.38 ppm, come from carbons C40 and C31, respectively. The remaining two pairs of this cluster are the off-mirror equatorial carbons (C16/C45 and C17/C44) and the C35/C58 and C36/C57 from all simulations. This cluster of 10 atoms in the spectrum of $C_{61}H_2^{154}$ shows as two lines: one at 143.02 ppm from carbons C35/C58/C36/C57 (which is coincident with the resonances from C31 and C40 already discussed), and a line at 143.15 ppm from the 4 horizontal equatorial carbons C16/C45/C17/C44. These pairs are opposite each other on the same hexagonal ring (the ring C17, C16, C34, C35, C36 and C37), and the C16 and C35 are both bonded to the other member of their pair (C17 and C36, respectively). The simulated spectra suggest that the components of the two pairs have separated chemical shifts. Hence, the accidental coincidence of quadruple intensity is more likely to come from a coincidence of the first member of each pair rather than two members of the same pair. Furthermore, the gap differences of these four resonances are narrower than MAE of ωB97X. Hence, it tentatively assigns the line at 143.21 ppm to C17/C44 and C36/C57. It follows from this discussion that the double intensity component of the triple intensity line at 143.26 ppm may be tentatively assigned to carbons C35/C58. This leaves the double intensity line at 143.31 ppm as tentatively assigned to the equatorial carbons C16/C45.

The next feature in the experimental spectrum is a series of three lines between 144.0 and 144.8 ppm, which have integrations of 4, 2 and 4 representing 10 carbon atoms occur at 144.02, 144.36 and 144.72 ppm. Hence, the first and last lines are each a coincidence of two double intensity lines. This pattern is very closely represented in the corresponding part of the ωB97X simulated spectrum but is not

so recognisable in the other two simulations. In the ωB97X simulated spectra, the coincidences each comprise two very closely spaced double intensity lines (centred on 144.3 ppm and 145.1 ppm) and rather than being fully coincident. Further confidence in these assignments comes from the experimental spectrum of $C_{61}H_2$, which has resonances from these same carbons in the same order as the next three lines in its spectrum.[154] Hence, the integration of 4 carbons line at 144.02 ppm is readily assigned to fullerene carbons C38/C42 and C33/C47, the central integration of 2 carbons line at 144.36 ppm is readily assigned to C14/C28 and the second integration of 4 carbons line, at 144.72 ppm is readily assigned to C54/C55 and C49/C50.

The abovementioned three-line feature is followed in the experimental spectrum by another one, at about 145 ppm. However, this time the integrations are 2, 1 and 3 from 6 carbons, with the latter representing a coincidence of single and double intensity lines. Again, such a series is seen in the simulated spectrum of ωB97X. The spacing between this group of thee lines and the previous three-line group is closer in the simulated spectrum than they are in the experimental spectrum, and the 6 carbons occur as 4 lines with integrations of 2:2:1:1. However, despite the final two resonance of this group not being coincident in the simulated spectra they are very close and the overall the prediction that these three lines comprise two double and two single intensity resonances is correct. As such, the pair of single intensity lines at 144.95 and 145.03 are temporally assigned to the equatorial carbons C30 and C21, respectively. Of these two equatorial carbons on the mirror plane, all three simulations have a similar gap between them, ωB97X gives C21 as having the larger chemical shift, whereas X3LYP and B3LYP have this line with the lower chemical shift. The gap between them are much smaller than the

respective MAEs of the three simulations. On this basis, the single intensity component of the integration 3 line at 145.03 ppm is tentatively assigned to C21, is the single intensity line at 144.95 ppm is tentatively assigned to C30. The remaining resonances in this cluster of three lines, the two double intensity lines at 144.91 and 145.03 ppm, are tentatively assigned based on their order in the ωB97X simulated spectrum to C52/C60 and C19/C23. However, it is noted that C52/C60 comes after C19/C23 in the experimental spectrum of $C_{61}H_2$[154], and that the ωB97X simulation has these two resonances as almost coincident (0.02 ppm separation). Hence, the order of these two lines is possible to be reversed. There is an additional double intensity line in the simulated spectrum in the neighbour of this group. That line belongs to the following group of resonances and will be discussed below.

The 2nd-last grouping of fullerene sp^2 resonances in the experimental spectrum is a cluster of 5 lines representing 12 carbon atoms. It appears as two closely spaced double intensity lines near 145.3 ppm, another two closely spaced lines near 145.4 ppm of which one is double intensity and the other is a coincidence of two double intensity lines (intensity of 4 carbons), and a lone double intensity line near 146.0 ppm. These appear in the ωB97X simulated spectrum as 4 lines with a 2:4:4:2 intensity ratio. Comparison with the experimental spectrum of $C_{61}H_2$[154] suggest that these lines come from: (a) C32/C39/C41/C48 carbons which locate below the equator of C_{60} are expected to have narrow split as being C32/C48 and C39/C41 mirrored pairs; (b) C51/C53/C56/C59 carbons which are bonded to the polar carbon locating the furthest to the addend are expected to have the smallest split as being C51/C59 and C53/C56 mirrored pairs; and (c) C3/C4/C25/C26 carbons which are on the same pentagon with the addend are expected to be widely split on [60]PCBM into C3/C26 and C4/C25 mirrored pairs. The confirmation of this

analysis from the ωB97X simulation is that the initial and the last double intensity lines have a corresponding match in the experimental spectrum (at 145.29 and 146.04 ppm), the resonance at 146.04 ppm is well-separated from the other lines in this cluster, it is readily assigned to C4/C25 line, leaving carbons C3/C26 to be the well separated pair at 145.29 ppm. The quadruple intensity line in the experimental spectrum occurs at 145.44 ppm after two double intensity lines with 0.10 ppm chemical shit difference. The corresponding simulation spectrum shows these as a set of two accidental coincidences. This indicates that, C32/C48 is coincident with C53/C56 and that C39/C41 is coincident with C51/C59. However, these assignments are not within the MAE of the simulation, and they are unlikely because the two coincidences (1) suggest that C51/C59 and C53/C56 (which are closest to the pole) have the same splitting by the asymmetry of the other addend as do C32/C48 and C39/C41(which are closest to the equator) while there appears to be a trend of the splitting increasing as the distance between the two addends decreases; and (2) C51/C59 (near the pole) has the same chemical shift as C32/C48 (near the equator). Based on this analysis, the resonances at 145.32 and 145.40 ppm are assigned to C32/C48 and C39/C41 with the order determined by simulation, and the integration 4 resonance at 145.44 ppm is assigned to C51/C59 and C53/C56. However, these latter assignments are made tentatively.

The final two double intensity fullerene lines (at 147.91 and 148.83 ppm) have already been respectively assigned earlier in the discussion to fullerene carbon atoms C5/C8 and C2/C10, on the basis of the high agreement of the simulated and experimental spectra and that they form a pair that would be symmetrically equivalent but for the asymmetry of the addend.

The fullerene sp^2 hybridized carbons assignment of [60]PCBM based on the spectra of experimental ^{13}C NMR spectroscopy and the DFT simulation of ωB97X is list in Table 3-5.

Table 3-5 The experimental ^{13}C NMR chemical shifts, integrations and atom assignments for the fullerene sp^2 carbons and carbonyl carbon of [60]PCBM based on the conclusion of ^{13}C NMR spectroscopy and ωB97X/cc-pVTZ DFT simulation.

Assignments in bold are confidently made owing to close resemblances to the experimental spectrum and full agreement across all three simulations. The others are only tentatively assigned based on the ωB97X spectrum, which was qualitatively and quantitatively closest to experiment.

Exp./ppm	Int.	Cal./ppm	Exp.–Cal.	assignment
137.95	2	137.98	-0.03	**C11/C12**
138.38	2	138.45	-0.07	**C6/C7**
141.05	2	140.93	0.12	**C15/C27**
141.30	2	141.14	0.16	**C18/C24**
142.32	2	141.93	0.39	C20/C22
142.38	2	141.96	0.42	C13/C29
142.39	2	141.99	0.40	C34/C46
142.47	2	142.05	0.42	C37/C43
143.21	2	143.00	0.21	C36/C57
143.21	2	143.08	0.13	C17/C44
143.26	2	143.11	0.15	C35/C58
143.26	1	143.32	-0.06	**C40**
143.31	2	143.23	0.08	C16/C45
143.38	1	143.42	-0.04	**C31**
144.02	2	143.98	0.04	**C38/C42**
144.02	2	144.02	0.00	**C33/C47**
144.36	2	144.52	-0.16	**C14/C28**
144.72	2	144.74	-0.02	**C54/C55**
144.72	2	144.78	-0.06	**C49/C50**
144.91	2	144.98	-0.07	C52/C60
144.95	1	145.04	-0.09	C30
145.03	2	145.00	0.03	C19/C23
145.03	1	145.08	-0.05	C21
145.29	2	145.14	0.15	**C3/C26**
145.32	2	145.55	-0.23	C32/C48
145.40	2	145.55	-0.15	C39/C41
145.44	2	145.59	-0.15	C53/C56
145.44	2	145.59	-0.15	C51/C59
146.04	2	145.80	0.24	**C4/C25**
147.91	2	148.74	-1.05	**C5/C8**
148.83	2	149.47	-0.86	**C2/C10**

3.6   Note on accuracy of the simulations

In the above discussion, the lines from the 58 sp^2-hybridised fullerene carbons were assigned based on the DFT simulations of the spectra. When there was apparent correspondence between simulated and experimental spectra coupled with agreement across all three simulations, assignments were made with confidence. Otherwise, they were made only tentatively based on the ωB97X spectrum according to its greater degree of qualitative resemblance to the experimental spectrum compared to the other simulation methods. One objective measurement that may be used to test the accuracy of simulations is the mean absolute error (MAE), which is obtained through comparing the chemical shifts of observed and simulated spectra. This parameter measures the mean of the absolute difference between each of the observes and calculated chemical shifts of the molecule. This method requires the knowledge of the assignments in the experimental spectrum. But in the case of [60]PCBM, it technically does not know the atom assignments of any of the fullerene sp^2 carbon atoms. However, as mentioned above, the areas of qualitative subjective agreement between experiment and simulation, coupled with some chemical knowledge, may lead to reasonably confident assignments. To test the objective accuracy of the DFT simulations for the chemical shifts of the 58 sp^2 hybridized carbons of the fullerene, Table 3-6 was drawn up of the experimental chemical shifts of the sp^2-bonded atoms where a confident qualitative assignment could be made together with their corresponding simulated values.

In order to draw the meaningful conclusions, the simulated spectra will need to be re-referenced. This is because in the discussion in Section 3.5, all simulated spectra were referenced such that the first line in each of the three simulated spectra

(corresponds to carbon C3 of the ester group) had the same chemical shift as that of the corresponding resonance in the experimental spectrum (22.90 ppm). However, the carbon C3 is an sp^3-hybridised carbon in the middle of an alkyl chain which would have little or no bond strain which is not the case for the fullerene carbons. In order to form the fullerene cage, not only need to consider these sp^2-hybridised, but also bond strain owing to the curvature. Hence, it is not reasonable to expect the models used by the simulation as accurately determine the value of the chemical shifts of the strained sp^2 fullerene when referenced to an unstrained sp^3 alkyl chain. This is particularly evident in the simulation of X3LYP and B3LYP which had smaller gap between the sp^2 and sp^3 regions in the spectrum, resulting in the chemical shifts for the sp^2 carbons being much lower than those of the ωB97X spectrum. This might lead to the conclusion that B3LYP (for example) has a very large MAE despite it having quite a strong resemblance to the experimental spectrum. As such it would be better to re-reference the spectra to something in the fullerene sp^2 region. Re-referencing does not in any way alter the form of the spectrum. It merely shifts the entire spectrum up or down by adding a constant. In order to minimise the effect of the arbitrariness of referencing, the following way was performed. First, Table 3-6 was drawn up of the chemical shifts of the confidently assigned fullerene carbons from each of the three simulations. Second, a value of $\delta_{exp}–\delta_{calc}$ was then obtained for each carbon from each of the three simulation methods. Third, these values were then averaged for each of the simulation methods. Finally, each of the three simulated spectra were then re-referenced by shifting them by their corresponding average difference. In this way the new re-referenced $\delta_{exp}–\delta_{calc}$ values will be the result of inconsistencies between experiment and simulation, and among the simulations for the fullerene sp^2 carbons

(that is they would be largely due to the differences in the spacings between the lines rather than their absolute values).

A list of corresponding |observed-calculated| valued as $\Delta_{\omega B97X}$, Δ_{X3LYP} and Δ_{B3LYP} was obtained and their means were determined to be: sp^2-MAE$_{\omega B97X}$ = 0.09 ppm, sp^2-MAE$_{X3LYP}$ = 0.28 ppm and sp^2-MAE$_{B3LYP}$ = 0.28 ppm as shown in Table 3-6. The subjective assessment that the ωB97X simulation bore a remarkable resemblance to the experimental spectrum for the complex fullerene sp^2 carbons part of the spectrum reflected in it having the lowest MAE of the three methods. Taking the value for the MAE of the ωB97X simulation, the tentative assignments in Section 3.5 above were re-examined. However, none of these assignments became any less tentative. This is because all previous 'confident assignments' had spacing considerably greater than the MAE, where all 'tentative assignments' had spacings substantially lower than the MAE.

Table 3-6 Table of experimental and simulated chemical shifts and their absolute differences against initial confident fullerene carbon atom assignments from Section 3.5.

Exp. (ppm)	atom assignment	ωB97X (ppm)	$\|\Delta_{\omega B97X}\|$ (ppm)	X3LYP (ppm)	$\|\Delta_{X3LYP}\|$ (ppm)	B3LYP (ppm)	$\|\Delta_{B3LYP}\|$ (ppm)
137.95	C11/C12	138.01	0.06	138.14	0.19	138.50	0.55
138.38	C6/C7	138.47	0.09	138.49	0.11	138.77	0.39
141.05	C15/C27	140.95	0.10	141.38	0.33	140.76	0.29
141.30	C18/C24	141.16	0.14	141.59	0.29	140.85	0.45
143.31	C40	143.34	0.03	143.65	0.34	143.58	0.27
143.38	C31	143.45	0.07	143.63	0.25	143.46	0.08
144.02	C38/C42	144.01	0.01	144.15	0.13	144.16	0.14
144.02	C33/C47	144.05	0.03	144.21	0.19	144.06	0.04
144.36	C14/C28	144.54	0.18	144.05	0.31	144.23	0.13
144.72	C54/C55	144.76	0.04	144.64	0.08	144.83	0.11
144.72	C49/C50	144.81	0.09	144.72	0.00	144.97	0.25
144.29	C3/C26	145.16	0.13	144.54	0.75	144.92	0.37
146.04	C4/C25	145.83	0.21	145.34	0.70	145.43	0.61
MAE			**0.09**		**0.28**		**0.28**

3.7 Conclusions

High resolution ^{13}C, ^{1}H and 2D NMR spectra of the standard organic-electronics acceptor material [60]PCBM were recorded, and resonances were identified in the ^{13}C spectrum via chemical shift and integration analysis. A 2D NMR spectrum additionally allowed for assignments of all carbons with attached hydrogens to their respective resonances. By elimination, the fullerene sp^3 carbons without hydrogens, bridgehead (C1 and C9) and bridge carbons (C61), were also unambiguously assigned. The remarkable agreement for ^{13}C NMR of the ωB97X/cc-pVTZ DFT simulation with experiment allowed for several of the resonances to be assigned with a high level of confidence. With this, the absolute mean error of the simulation was determined to be 0.09 ppm, which was lower than the 0.28 value of the commonly use B3LYP/6-31G(d,p) method. As such, the remaining resonances were tentatively assigned to their respective resonances base on the ωB97X/cc-pVTZ DFT simulation.

The ^{1}H resonances were also fully identified and assigned. Spin-spin couplings in the ^{1}H spectrum for the methyl butanoate ester group revealed strong 2nd order effects, which were assigned assuming an AA′BB′-type system for the hydrogens of methyl butanoate carbons B3 and B4 (from Figure 3-1) – revealing 7 coupling constants. As such, although being symmetrically equivalent, the two protons on each of the three carbons of the –CH$_2$–CH$_2$–CH$_2$– chain are not magnetically equivalent. This results from hindered rotation of the bonds of the alkyl chain in ester group, resulting in a 12.5:75:12.5 population ratio of the three staggered conformers about the B3–B4 bond. These conformational conclusions may provide insights into the packing behaviour of [60]PCBM in the solid state, and thereby an

understanding of the morphological interactions between [60]PCBM and its surroundings in condensed-phase organic electronic devices such as organic and perovskite photovoltaics.

4 Chemical synthesis of the bis[60]PCBM isomers mixture and its separation of 19th missing isomer by HPLC

4.1 Preamble

During the first year of my PhD, my supervisor (John Dennis) and a senior PhD student (Wenda Shi) completed much of their work on developing an HPLC method to purify 18 of the isomers of bis[60]PCBM. Together with a fellow PhD student (Xueyan Hou), I learned this method from Dr Dennis and Mr Shi and used it to purify18 of these isomers. I also determined that there should be 19 rather than 18 isomers and discovered the missing isomer F1.1. Although I learned the method from them, all bis[60]PCBM used during my PhD was synthesised and purified by myself.

4.2   Chemical synthesis of bis[60]PCBM isomers mixture

The synthesis of bis[60]PCBM was following a modification method of the discovery of [60]PCBM from Hummelen *et al*. in 1995.[1] The method involved the synthesis of methyl 4-benzoylbutyrate *p*-tosylhydrazone which was then added to C_{60} in the final stage. The modification of that methods to make bis[60]PCBM isomer mixture is that double the quantity of tosylhydrazone relative to that of C_{60} was used in [60]PCBM,[156] this could offer enough adduct to form the second addend on C_{60} cage. A detailed description of the synthesis is separated into 3 stages as follows.

4.2.1 Stage 1: Synthesis of methyl-[5-oxo-5-phenyl] pentanoate

In order to synthesis the adduct of bis[60]PCBM, methyl-[5-oxo-5-phenyl] pentanoate need to be prepared in stage 1. Firstly, 25 g of 5-oxo-5-phenylpentanoic acid was dissolved in a mixture of 100 ml of methanol and 250 ml of benzene. Once all the acid had dissolved, 3.75 g of 4-methylbenzenesulfonic acid (PTSA) was added and the resulting mixture was refluxed for 18 hours at about 90°C. This resulted in the formation of methyl-[5-oxo-5-phenyl] pentanoate, and a byproduct of water. After cooling to room temperature, the reactant mixture was added to 250 ml of ethyl acetate which dissolved the product of methyl-[5-oxo-5-phenyl] pentanoate. Then, 600 ml of 10% sodium carbonate solution in distilled water was prepared, and the reaction solution was washed three times with the sodium carbonate solution (200 ml per washing) to neutralize any unreacted acid. The washing involved mixing the organic reaction mixture with 200 ml washing solution. The mixture was allowed to stand for several hours during which the

organic and aqueous layers eventually re-separated. A separating funnel was then used to recover the organic layer which contains the methyl-[5-oxo-5-phenyl] pentanoate (the aqueous layer was discarded). This washing process was repeated three times. Next there were another three such washings, but this time in distilled water only (200 ml per wash) to dissolve the products of neutralizing the unreacted acid. Following these 6 washings, the organic layer was dried to remove any residual water with about 10 g of anhydrous magnesium sulphate. Finally, the organic solvents (any unreacted methanol, the benzene, and the ethyl ethanoate) were removed by rotary-evaporation leaving about 15 g of oily product. A scheme of this stage is shown in Figure 4-1.
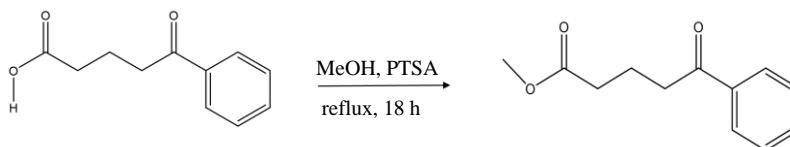
Figure 4-1 Synthesis of methyl-[5-oxo-5-phenyl] pentanoate.

4.2.2 Stage 2: Synthesis of methyl 4-benzoylbutyrate *p*-tosylhydrazone

About 15 g of the product from stage 1 (methyl-[5-oxo-5-phenyl] pentanoate) and 15.5 g of 4-methylbenzenesulfonohyzide were dissolved in 45 ml methanol, then refluxed for 6 hours at about 60°C. The reaction mixture was then allowed to cool to room temperature. After standing for 24 hours, the mixture was chilled in a freezer to –15°C. This resulted in crystals of the product of methyl 4-benzoylbutyrate *p*-tosylhydrazone in methanol. These crystals were quickly removed from the methanol by vacuum filtration after which they were washed

with ice-cold methanol, and then dried in an oven at 50°C. This gives about 10 g

of colourless crystalline product. A scheme of this stage is shown in Figure 4-2.
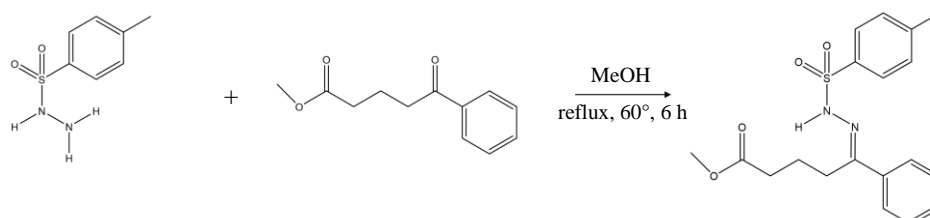
Figure 4-2 Synthesis of methyl 4-benzoylbutyrate *p*-tosylhydrazone.

4.2.3 Stage 3: Synthesis of bis[60]PCBM isomer mixture

In the last stage of the bis[60]PCBM synthesis, 1 g of the methyl 4-benzoylbutyrate

p-tosylhydrazone (from stage 2) was dissolved in 14 ml of dry pyridine in a three-

neck round bottom flask under a dry nitrogen atmosphere. Then 72 mg of sodium

methoxide was added and stirred for 20 minutes. Separately, 875 mg of C_{60} was

dissolved in 60 ml of 1,2-dichlorobenzene. This solution was degassed by a three-

step process: (1) ultra-sonification in air for 15 minutes to dissolve the C_{60} powder,

(2) vigorous rotary evaporation at room temperature for about 30 minutes followed

by (3) bubbling dry nitrogen for another 30 minutes. The degassed C_{60} solution

was then added anaerobically to the pyridine solution, after which the mixture was

heated to 85°C and irradiate with a 150 W sodium lamp overnight while stirring.

A scheme of this stage is shown in Figure 4-3. The two steps detailed reaction

mechanism of this synthesis is shown in Figure 4-4(a) and (b).
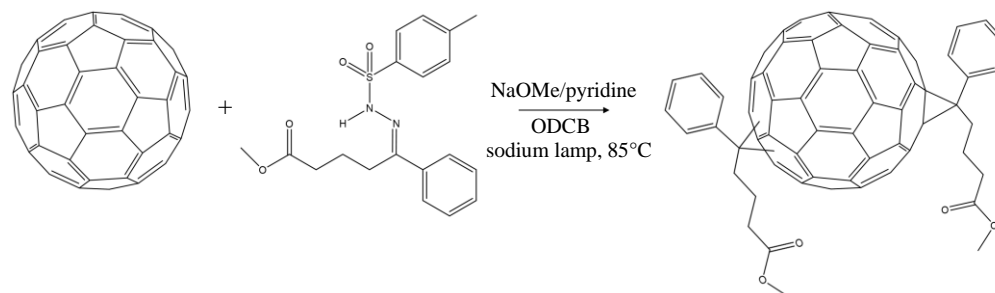
Figure 4-3 Synthesis of bis[60]PCBM from the methyl 4-benzoylbutyrate *p*-tosylhydrazone and the fullerene C$_{60}$.

After cooling to room temperature, about 10 g of silica gel was added to the mixture and shaken. This was done to remove any partially reacted homo-fullerene by-products as these adhere stronger to the silica gel than bis[60]PCBM. Then remaining solution was separated by filtration and concentrated to about 200 ml after rotary evaporation. The 200 ml product solution was then cooled to room temperature and added to 500 ml of methanol. This precipitated the bis[60]PCBM while leaving the solvents (1,2-dichlorobenzene and pyridine) dissolved in the methanol. Finally, the precipitate was removed from the liquids by vacuum filtration and dried in an oven at 50°C for 3 hours. This three-step process gave about 1 g of a fine brown power of bis[60]PCBM isomer mixture, which was dissolved in HPLC-grade toluene ready for HPLC separation into individual purified isomers.

(a)   (b)
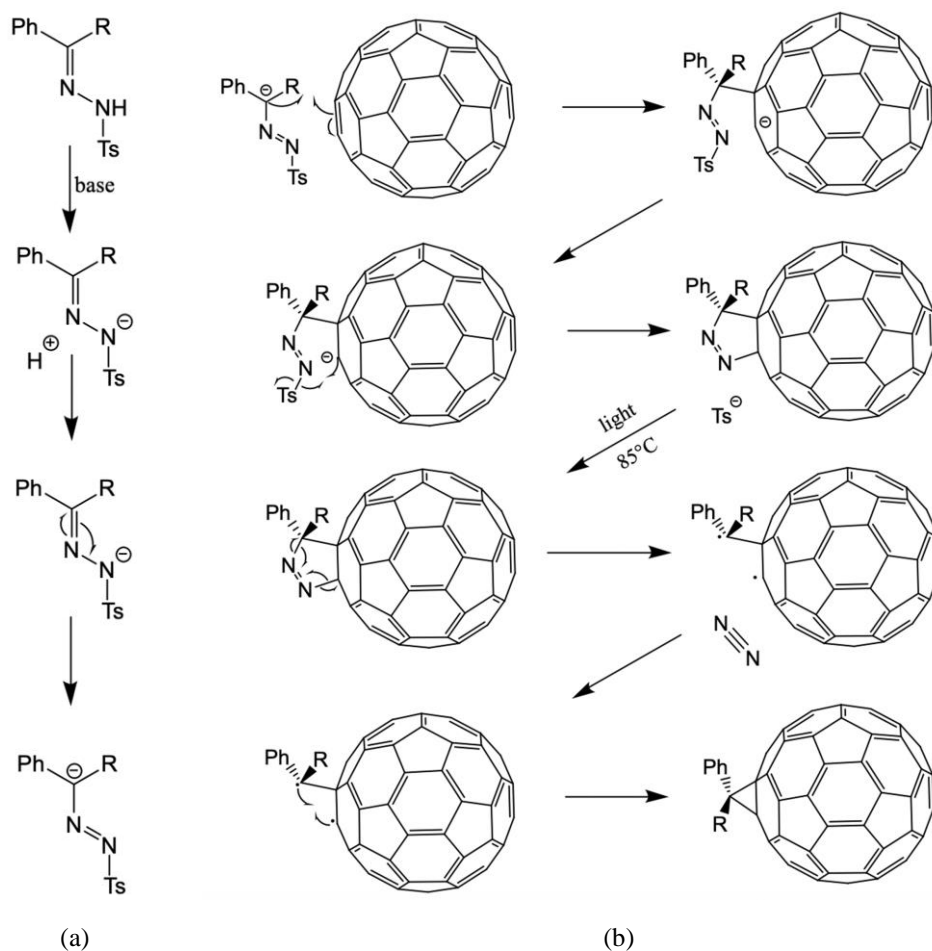
**Figure 4-4 Reaction mechanism scheme for the [3+2]-dipolar cycloaddition to
the fullerene for form [60]PCBM.**
The reaction initially proceeds (a) by abstraction of a hydrogen by a base (NaOMe)
followed by electronic rearrangement. In (b), the resulting tosylhydrazone anion
initially adds to a double bond of the fullerene. Removal of tosyl leaving group
leaves a five-membered ring, and removal of N_2 molecule leaves the three-
membered cyclopropa-ring on the fullerene. The formation of bis[60]PCBM
proceeds in the same manner except that the addition occurs at two sites on the
fullerene.

4.3 Separation of the 19th missing isomer of bis[60]PCBM by HPLC

The bis[60]PCBM isomer mixture studied in this thesis is about 4 g and that I

synthesised from four batches. For each purification, about 1 g of bis[60]PCBM

isomer mixture was dissolved in 350 ml pure toluene as the initial sample. The

purification of each batch takes about 6 months to purify the mixture into 19 pure isomers. Then the 19 samples were used for recording the ^{13}C NMR spectrum for each isomer to determine the molecular structure that presents in Chapter 5. The method of purify the bis[60]PCBM mixture into 18 isomers were firstly reported in the paper[93], then the following thesis of Shi[96]. During my purification work for structural identification and getting enough material for ^{13}C NMR spectroscopy, I found that there should be 19 isomers of bis[60]PCBM and isolated the 19th missing isomer to be one of the *trans*-1 isomer F1.1 which is conformed in UV-Vis spectrum in Section 5.2. Therefore the initial HPLC fraction F1 presented in the paper and the thesis of Shi in fact contains two subfractions, and the missing isomers resolve first from the mixture should be named F1.1, automatedly the original HPLC fraction F1 should be named F1.2.[157] This section demonstrates the purification method that how to separate the 19th missing isomers from bis[60]PCBM mixture.

The initial separation of the mixture to 7 fractions to get fraction F1 by single pass HPLC stage is on silica column. Then the multiple peak-recycling HPLC stages on 5PBB columns method were involved to separate the fractions (F1) into subfractions (F1.1 and F1.2). Peak recycling was also used for a purity test to examine if the fraction is a pure isomer in the last treatment.

Single-pass HPLC of the initial separation

In the initial separation of bis[60]PCBM, about 10 ml of the bis[60]PCBM mixture with following elution by pure toluene continuing to be at 18 ml min^{-1} was injected into the HPLC on the silica column in a single pass mode. After about 80 min, the bis[60]PCBM isomer mixture was separated and collected into 7 fractions, where

each is resolved to the baseline from its neighbours. These are labeled F1 – F7 in retention time order shown in Figure 4-5. The HPLC chromatogram of single-pass HPLC is constant to the group who is the first synthesis of bis[60]PCBM.[113] However, their work did not isolate any single isomers. As we can see from the single-pass HPLC profile for bis[60]PCBM under the 10 ml injection conditions, the residual of C_{60} with light purple colour and [60]PCBM with dark brown colour came out before 6 min which can be distinguished and removed from 7 fractions of bis[60]PCBM. The F1 of bis[60]PCBM shown as a single peak in this stage was resolved out from the mixture and collected at 8–10 min. The following F2 came out from 11–15 min as a three partially resolved peaks, and the F3 shows as a four partially resolved peaks started from 18 min for 10 min. After a six minutes gap, the next F4 shown as a well resolved single peak appear at 34–38 min, then F5 resolved out at 42–54 min as a partially resolved peak, leaving the last two single peak of F6 and F7 were collected at 62-68 min and 70–78 min. This timetable is constant for the 35 injections in total for each of the four 1 g batches. The injection of 10 ml was chosen as it was the volume of the largest injection loop that we had which still allowed for resolution to the baseline of the 7 fractions. Smaller loops (e.g., 5 ml) allowed for the resolution, but it will double the number of injections that can be avoid for the entire sample, and larger loops (e.g., 15 ml) did not give full resolution of the 7 fractions.
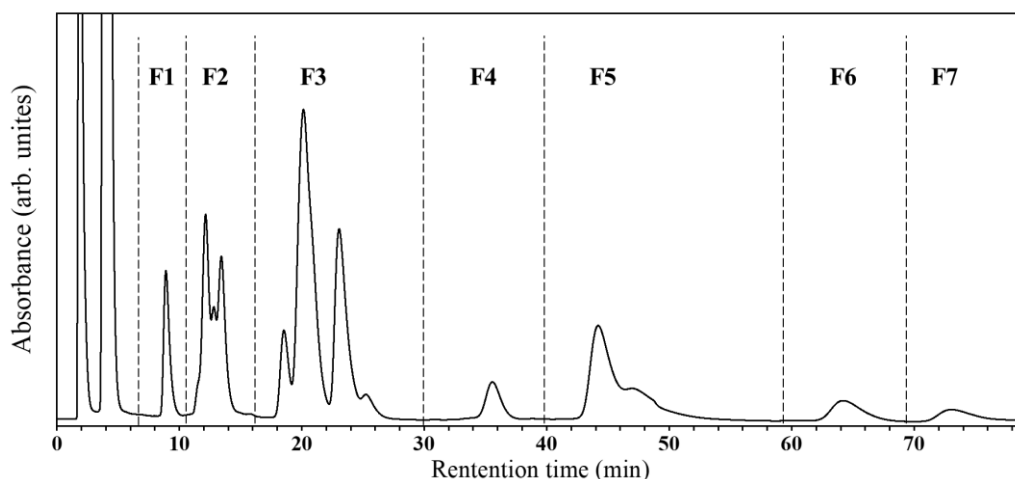
Figure 4-5 The profile of the single-pass HPLC on the silica column showing partial separation of the bis[60]PCBM isomer mixture into 7 fractions.
The peaks appear before 6 min is the residual of C_{60} with light purple colour and [60]PCBM with dark brown colour which can be distinguished from the bis[60]PCBM sample and are removed before the collection of bis[60]PCBM.

The concentration of the injected samples was about 3 mg ml^{-1}. Hence, to separate about 4 g of synthesized bis[60]PCBM into these 7 partially purified fractions required repeating this 1.5-hour single-pass HPLC technique for about 140 times.

The Examination of Figure 4-5 indicates that fractions F1, F4, F6 and F7 appear to be single component fractions in the initial separation of bis[60]PCBM isomer mixture on the single-pass HPLC mode, as these do not to show any indication of the presence of other components that would normally show up as shoulders on the peak shapes. This may be differed to F2, F3 and F5, which all indicated the presence of multiple components.

Peak-recycling HPLC of fractions F1

To test whether F1 is indeed single purified isomers from the initial separation, this fraction was injected to the first peak-recycling HPLC mode on a 5PBB column. The injection volume was reduced to 3.0 ml for the following peak-recycling stages in order to improve the resolution of the HPLC process.

Fraction F1 is seen in Figure 4-5 as a single peak appear at 8 min in the initial separation of bis[60]PCBM. However, it actually consists of two components shown from the peak-recycling HPLC mode, which appeared at about 4 min and are almost but not fully resolved after 5 cycles on 5PBB column shown in Figure 4-6. These two components are named F1.1 and F1.2 as they are subfractions of F1. Continuing to recycle beyond 5 cycles would not result in an increase in separation. This is because the F1 had become so broad by the 5th cycle that continuing to recycle would result in the onset of F1.1 on the next cycle occurring before F1.2 on the 5th cycle had fully eluted from the column. This would result in the re-mixing of F1.1 with F1.2 – ruining the separation achieved by the end of the 5th cycle.

As neither subfraction was obtained completely pure, F1.1 and F1.2 were each collected at the end of the 5th cycle at the markers in Figure 4-6. These two subfractions were then re-concentrated and each injected to a further peak-recycling HPLC treatment, which are shown in Figure 4-7 and Figure 4-8 for F1.1 and F1.2, respectively.
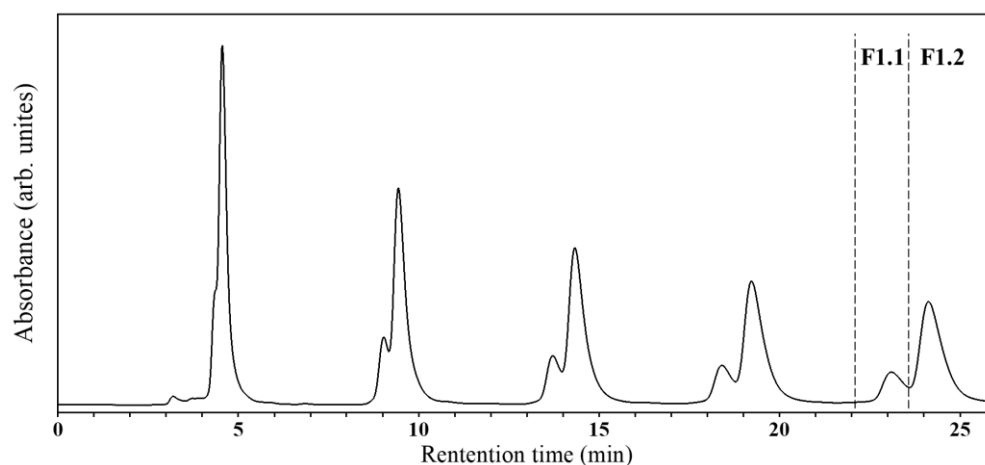
Figure 4-6 The profile of the first peak-recycling HPLC stage on the 5PBB column for the purification of fraction F1 into its subfractions F1.1 and F1.2.

For subfraction F1.1, it is seen in Figure 4-7 that there is a small residual of F1.2 in the sample, which shows as a small shoulder on the high retention time side of the main peak of F1.1. By the 5th cycle this small residual has almost separated from the main peak. Hence F1.1 was collected between the markers in Figure 4-7 as essentially pure, with the following small residual of F1.2 being removed.
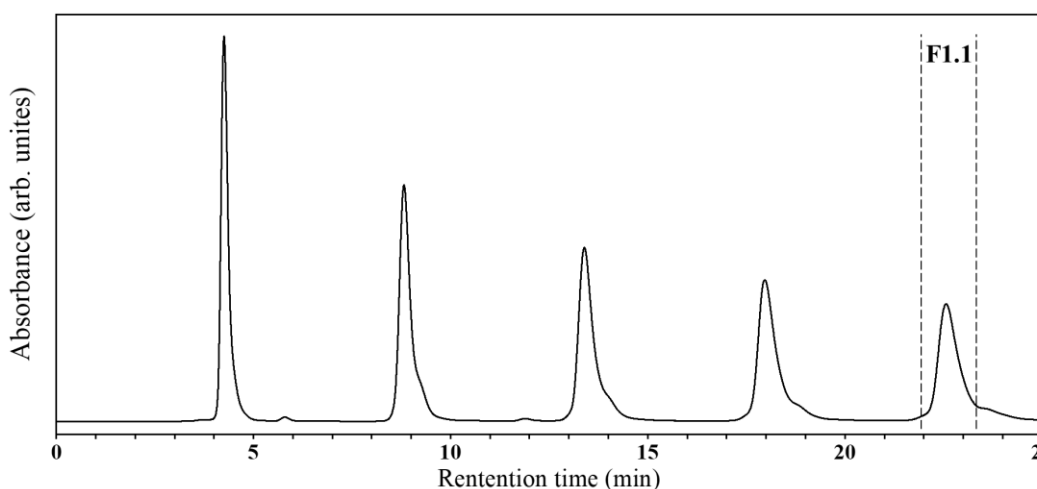
Figure 4-7 The profile of the second peak-recycling HPLC stage on the 5PBB column for the purification of subfraction F1.1 to be a pure isomer.

A similar treatment for F1.2 (Figure 4-8) shows a small residual of F1.1, this time F1.1 appears as a small shoulder on the low retention time side of the main F1.2 peak. This shoulder becomes resolved to the baseline from F1.2 by the 5th cycle, then F1.2 was collected as essentially pure on that cycle.
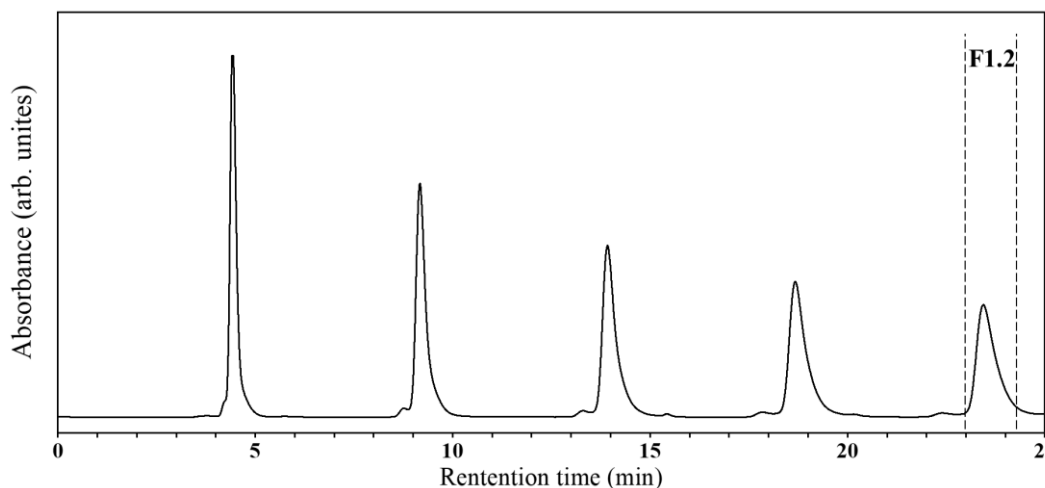
Figure 4-8 The profile of the second peak-recycling HPLC stage on the 5PBB column for the purification of subfraction F1.2 to be a pure isomer.

To test whether F1.1 and F1.2 actually had been purified, a third peak-recycling HPLC treatment was performed on each subfraction as the purity test. These are seen in Figure 4-9(a) and (b) for F1.1 and F1.2, respectively.

(a)	(b)
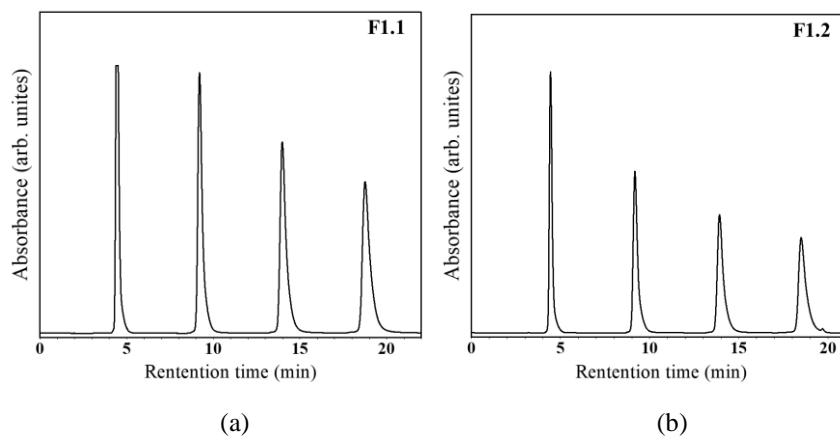
Figure 4-9 The profiles of the peak-recycling HPLC purity tests on the 5PBB column for the pure isomers (a) F1.1 and (b) F1.2.

114

Neither of the purity test of F1.1 and F1.2 show any indication of containing any sub-components. This was indicated by the smooth peaks, top, and decay of the chromatogram of the final cycle for each of these fractions. Hence, it is concluded that the apparent single peak of F1 from initial purification of bis[60]PCBM isomer mixture actually contained two isomers, F1.1 and F1.2, and that after the second peak-recycling stage each of these subfractions represented a single purified isomer of bis[60]PCBM.

The rest of 17 pure isomers separation was following the method that present in the flow chat of Figure 4-10 which fully illustrate the purification method with amending the 19th missing isomers F1.1 to the Fig 2 in previous work.[93] By using this method, all 19 isomers of bis[60]PCBM mixture were purified. These isomers were F1.1, F1.2, F2.1.1, F2.1.2, F2.2, F2.3, F3.2, F3.2.1, F3.2.2, F3.3.1, F3.3.2, F3.4, F4, F5.1, F5.2.1, F5.2.2, F5.3, F6 and F7.
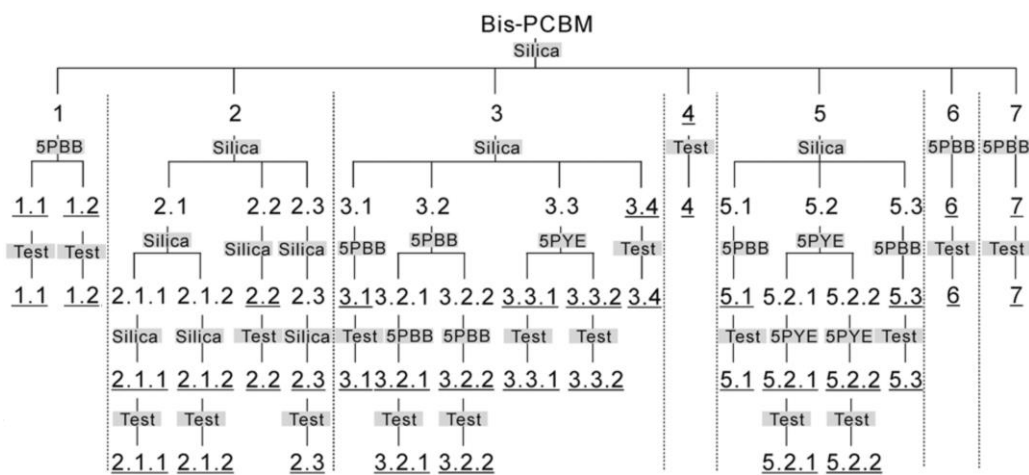
Figure 4-10 Flow chart for the complete purification of all 19 isomers of bis[60]PCBM, the column used is shown for each stage.

4.4 Conclusion

In conclusion, about 4 g of bis[60]PCBM was synthesizes following literature procedures[1], and was purified into 19 individual isomers, following a chromatographic method involving single pass mode, multi-peak-recycling and multi-columns (silica, 5PBB and 5PYE). The 19th missing isomer HPLC fraction F1.1 of bis[60]PCBM has been found, therefore the HPLC fraction F1[93] that previously determined should be sequential named F1.2. These 19 fractions were named in HPLC retention time order based on the fraction, subfraction and/or sub-subfraction from the initial single-pass HPLC method. These 19 pure isomers were F1.1, F1.2, F2.1.1, F2.1.2, F2.2, F2.3, F3.2, F3.2.1, F3.2.2, F3.3.1, F3.3.2, F3.4, F4, F5.1, F5.2.1, F5.2.2, F5.3, F6 and F7.

5 Structural identification of all 19 isomers of bis[60]PCBM by UV-Vis and ^{13}C NMR spectroscopy

5.1 The number of expected isomers of bis[60]PCBM

There are 30 double bonds on C_{60} cage. With 29 double bonds grouped in bond type shown in Table 5-1 being available for the second adduct after the first addend bridges the 1,9 bond. These could be attached giving 29 isomers of symmetric adduct. However, the asymmetric chains of bis[60]PCBM would double this number to 58 isomers because the relative orientations from two same asymmetric adducts attached on the C_{60} cage. In this case, symmetries and chiral structures could reduce this number, then the number of spectroscopically distinguishable isomers would be determined. This can be done by examining the isomers for each double bond to determine whether it gives the symmetrically equivalent isomer or an enantiomer with different numberings.

Table 5-1 The double bond number in each bond type on C$_{60}$ fullerene.

double bond type	double bond number
cis-1	2,12; 5,6; 7,8; 10,11;
cis-2	3,15; 4,18; 24,25; 26,27;
cis-3	13,14; 19,20; 22,23; 28,29;
e	16,17; 21,40; 30,31; 44,45;
trans-4	32,33; 38,39; 41,42; 47,48;
trans-3	34,35; 36,37; 43,57; 46,58;
trans-2	49,59; 50,51; 53,54; 55,56;
trans-1	52,60;

The method that was used to determine the symmetrically equivalent isomer was to swap the position of the two addends and renumbering so that the second addend is now occupying the position of the first addend (1,9 double bond), and determining the new number for the first addend. In general, resulting structure has different numbers to the original structure. However, these are not different isomers but instead different ways of numbering the same isomer.

The enantiomers were determined by reflecting the numbering of the second addend in the molecule's mirror plane to give the new numbering. As enantiomers are not spectroscopically distinguishable, these two numberings also effectively represent the same isomer. Finally, the symmetrical equivalent of the enantiomer (with its alternative numbering) are determined by swapping the two addends as before.
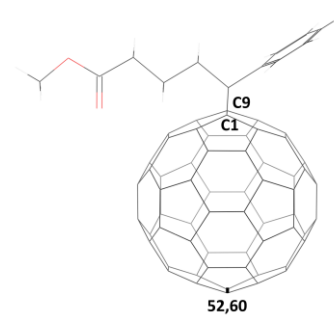
As the original isomer, its symmetrically equivalent structure, its enantiomer and the symmetrical equivalent of the enantiomer give alternative numberings for the

same isomer, following the IUPAC number system, only the isomer with the lower

initial number of the double bond should be kept. In this section, the number of the

isomers were determined for all possibilities following the order of bond type of

trans-1, *trans*-2, *trans*-3, *trans*-4, *e*, *cis-3*, *cis-2* and *cis*-1, then removing all the

alternative numbers.

5.1.1 The *trans*-1 bond

There is only one *trans*-1 bond (52,60 double bond) available on C_{60} cage in Table

5-1 and the symmetrically equivalent isomers are list in Table 5-2. It could form

two possible molecular structures which are (C_{2h})52,60-bis[60]PCBM and

(C_{2v})52,60-bis[60]PCBM by changing the orientation of the second **P**henyl **C₁**

Butyric acid **M**ethyl ester (PC₁BM) addend relative to the first addend, as shown

in Figure 5-1.

Table 5-2 The symmetrical equivalent and enantiomer from 2 possible molecular structures of *trans*-1 isomers of bis[60]PCBM.

trans-1 isomer	symmetrical equivalent	enantiomer	double bond illustration
(C_{2h})52,60	(C_{2h})52,60	--	
(C_{2v})52,60	(C_{2v})52,60	--	

Of these two unique structures, one has C_{2v} symmetry which shows the phenyl

rings from two addends are pointing to the same way, as well as the ester chains.

The other structure has C_{2h} symmetry, which shows the phenyl rings from the two

addends pointing in the opposite, as are the ester chains.

(a)   (b)
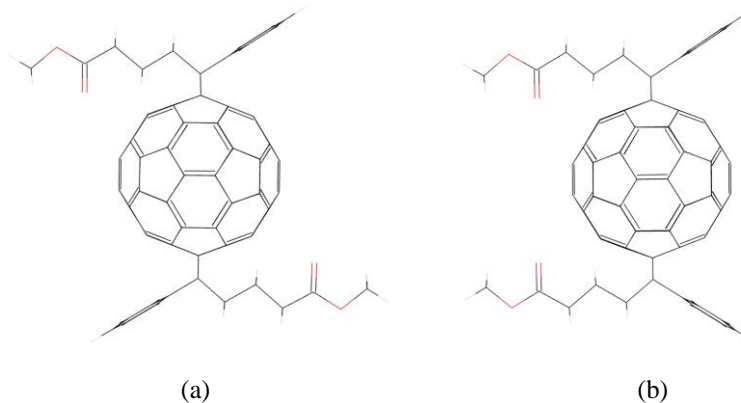
Figure 5-1 The molecular structures of the two isomers from *trans*-1 bond.
(a) (C_{2h})52,60-bis[60]PCBM, (b) (C_{2v})52,60-bis[60]PCBM.

5.1.2 The *trans*-2 bond

There are four *trans*-2 bonds (49,59; 50,51; 53,54; 55,56;) on C_{60} cage as illustrate

in the picture in Table 5-3, each of them could generate two molecular structures

because the relative orientations from the asymmetrical adducts giving an isomer

with C_1 symmetry and the other with C_2 symmetry. So, there are potentially 8 *trans*-

2 isomers which are (C_1)49,59; (C_2)49,59; (C_1)50,51; (C_2) 50,51; (C_1) 53,54; (C_2)

53,54; (C_1) 55,56 and (C_2)55,56 in total. However, the (C_2)49,59 isomer which is

symmetrically equivalent to itself and its mirror image (enantiomer) of (C_2)50,51

isomer which in turn is symmetrically equivalent to itself. Similarly, the (C_2)53,54

and (C_2)55,56 isomers are each symmetrically equivalent to themselves and are

also mirror images to each other. But the (C_2)49,59 and the (C_2)53,54 isomers are

distinguishable because 49,59 double bond is nearer to the phenyl ring of the first

addend than it is to the butyric acid methyl ester chain of that addend. Whereas,

53,54 double bond is nearer the other butyric acid methyl ester as shown in Table

120

5-3. Thus, there are two C_2 isomers, (C_2)49,59 and (C_2)53,54 represent those

equivalent isomers with C_2 symmetry by applying IUPAC naming system.

Table 5-3 The symmetrical equivalent and enantiomer from 8 possible molecular structures of *trans*-2 isomers of bis[60]PCBM.

trans-2 isomer	equivalent structure			double bond illustration
(C_2)49,59	(C_2)**49,59**	ena	(C_2)50,51	
(C_2)53,54	(C_2)**53,54**	ena	(C_2)55,56	
(C_1)49,59	(C_1)**49,59**	ena	(C_1)50,51	
	sym		sym	
	(C_1)53,54	ena	(C_1)55,56	

The (C_1)49,59 isomer is symmetry equivalent to the (C_1)53,54 isomer (by

swopping the two addends) and the enantiomer of (C_1)50,51 which is

symmetrically equivalent to (C_1)55,56 isomer. As such there is effectively only one

C_1 symmetry isomer of (C_1)49,59 for *trans*-2 bond. The equivalent isomers are

present in Table 5-3.

Therefore, the 8 potential isomers for *trans*-2 bond reduced to 3 distinguishable

molecular structures. These three *trans*-2 isomers should be named (C_2)49,59-

bis[60]PCBM, (C_1)49,59-bis[60]PCBM and (C_2)53,54-bis[60]PCBM. For the

purpose of visualising the molecular structures from the front face based on the

first addend, the structure of (C_2)49,59 is replaced by its enantiomer (C_2)50,51 and

the structure of (C_2)53,54 is replaced by its enantiomer (C_2)55,56 as shown in

Figure 5-2.

(a)   (b)   (c)
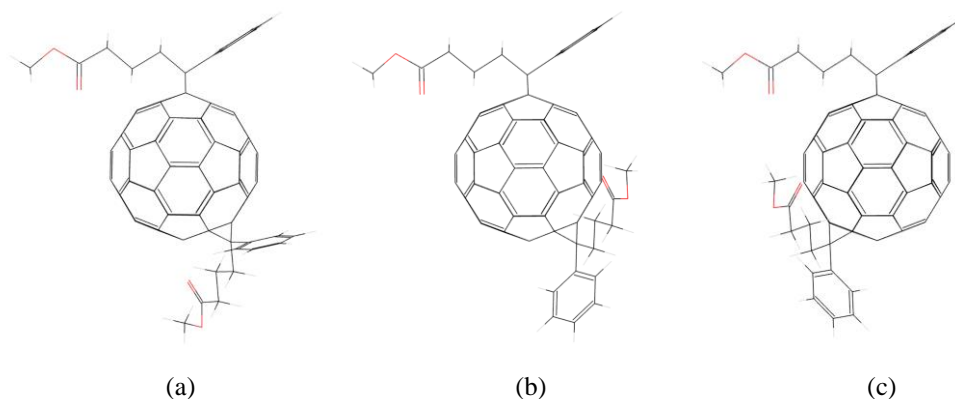
Figure 5-2 The molecular structures of the three isomers from *trans*-2 bond.
(a) (C_2)49,59-bis[60]PCBM, (b) (C_1) 49,59-bis[60]PCBM, (c) (C_2)53,54-bis[60]PCBM.

5.1.3 The *trans*-3 bond

As shown in the figure in Table 5-4, there are also four *trans*-3 bonds (34,35; 36,37; 43,57; 46,58;) on C_{60} cage, and again the two relative orientations of the addends potentially give rise to 8 *trans*-3 isomers (each of four bonds gives a C_1 and C_2 symmetry isomers), they are (C_1)34,35; (C_2)34,35; (C_1)36,37; (C_2)36,37; (C_1)43,57; (C_2)43,57; (C_1)46,58 and (C_2)46,58. As with the *trans*-2 bond, the (C_2)34,35 isomer and (C_2)46,58 isomer are enantiomers and symmetrically equivalent to itself; as the (C_2)36,37 isomer and (C_2)43,57 isomer. But the (C_2)34,35 and the (C_2)36,37 isomers are distinguishable (for the same reason for *trans*-2). Therefore, just like the *trans*-2 case, there are two C_2 isomers, (C_2)34,35 and (C_2)36,37. For the four C_1 isomers, the (C_1)34,35 isomer is symmetrically equivalent to (C_1)43,57 and enantiomer of (C_1)46,58 which is symmetrically equivalent to (C_1)36,37. According to IUPAC naming system of using smallest number for the label. These effectively lower the number of unique structures to three of ((C_2)34,35, (C_1)34,35 and (C_2)36,37) for the *trans*-3 bond as list in Table 5-4.

122

Table 5-4 The symmetrical equivalent and enantiomer from 8 possible molecular structures of *trans*-3 isomers of bis[60]PCBM.

trans-3 isomer	equivalent structure	double bond illustration
(C_2)34,35	(C_2)**34,35** ←ena→ (C_2)46,58	
(C_2)36,37	(C_2)**36,37** ←ena→ (C_2)43,57	
(C_1)34,35	(C_1)**34,35** ←ena→ (C_1)46,58 ↕sym ↕sym (C_1)43,57 ←ena→ (C_1)36,37	

Therefore, as for the *trans*-2 case, the 8 potential isomers for *trans*-3 bond reduced to three distinguishable structures which are (C_2)34,35-bis[60]PCBM, (C_1)34,35-bis[60]PCBM and (C_2)36,37-bis[60]PCBM as shown in Figure 5-3.

(a)   (b)   (c)
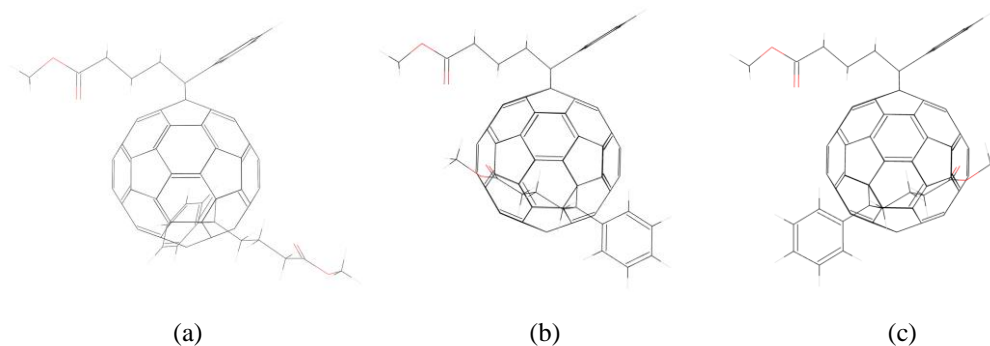
Figure 5-3 The molecular structures of the three isomers from *trans*-3 bond.
(a) (C_2)34,35-bis[60]PCBM, (b) (C_1)34,35-bis[60]PCBM and (c) (C_2)36,37-bis[60]PCBM.

5.1.4 The *trans*-4 bond

For the *trans*-4 bond type, the double bonds are located at the positions of 32,33; 38,39; 41,42; and 47,48 that are demonstrated in the figure in Table 5-5. These give

8 possible molecular structures by changing the relative orientations of two

asymmetrical addends.

**Table 5-5 The symmetrical equivalent and enantiomer from 8 possible molecular
structures of *trans*-4 isomers of bis[60]PCBM.**

trans-4 isomer	equivalent structure	double bond illustration
(C_s)32,33	(C_s)**32,33** ←ena→ / sym ← (C_s)47,48	
(C_s)38,39	(C_s)**38,39** ←ena→ / sym ← (C_s)41,42	
(C_1)32,33	(C_1)**32,33** ←ena→ (C_1)47,48	
	↕ sym ↕ sym	
	(C_1)38,39 ←ena→ (C_1)41,42	

As for the *trans*-2 and *trans*-3 bonds, four of possible molecular structures of *trans*-

4 bond have C_1 symmetry. However, the other four structures have C_s symmetry

instead of C_2 symmetry this time. They are (C_1)32,33; (C_s)32,33; (C_1)38,39;

(C_s)38,39; (C_1)41,42; (C_s)41,42; (C_1)47,48 and (C_s)47,48. Unlike the case for the

C_2 isomers of *trans*-2 and *trans*-3, where the original isomer and its symmetrical

equivalent isomer both have the same numberings, while for the C_s symmetry

isomers in *trans*-4 bond, (C_s)32,33 isomer is not only symmetrically equivalent to,

but also an enantiomer of (C_s)47,48. Hence, for C_s isomers swopping the two

addends results in a structure that is an enantiomer of the original structure. This

behaviour is also seen in the other C_s isomer, (C_s)38,39 which is symmetrically

equivalent to and an enantiomer of (C_s)41,42. These reduce the four C_s isomers to

two unique isomers of (C_s)32,33 and (C_s)38,39 according to IUPAC naming system

of using smallest number for the label. Meanwhile, (C_1)32,33 is symmetrically

equivalent to (C_1)38,39 and has an enantiomer of (C_1)47,48 which is symmetrically

equivalent to (C_1)41,42. Hence, this behaviour of the C_1 isomers is similar to previous C_1 isomers in *trans*-2 and *trans*-3 bonds, showing all four *trans*-4 bonds are effectively equivalent to each other. In total of three unique isomers (C_s)32,33-bis[60]PCBM, (C_1)32,33-bis[60]PCBM and (C_s)38,39-bis[60]PCBM of bis[60]PCBM exist of this *trans*-4 bond type as shown in Figure 5-4.

(a) (b) (c)
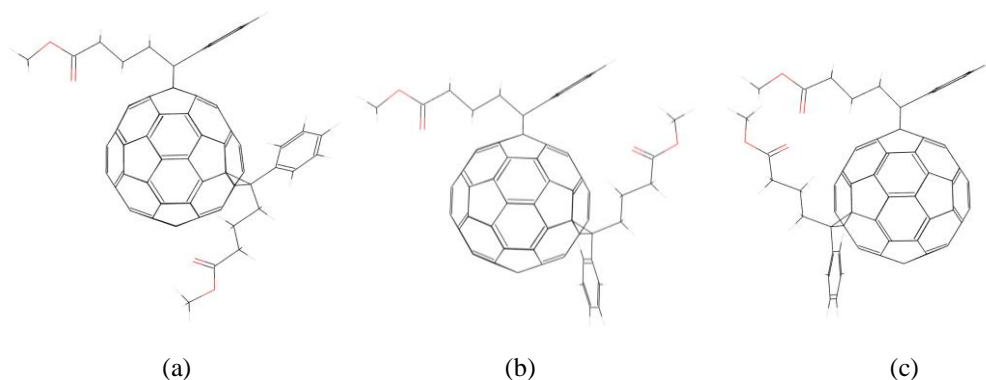
Figure 5-4 The molecular structures of the two isomers from *trans*-4 bond.
(a) (C_s)32,33-bis[60]PCBM, (b) (C_1)32,33-bis[60]PCBM and (c) (C_s)38,39-bis[60]PCBM.

5.1.5 The *e* bond

Similar rules of generating 8 possible isomers on four equatorial bonds (16,17; 21,40; 30,31 and 44,45) cannot be applied for the name of isomers according to their symmetry. This is for two main reasons. The first is that all 8 isomers have C_1 symmetry. With both PC$_1$BM groups being asymmetric there is no mirror planes, rotation axes or centres of inversion on equatorial isomers. The second is that there are two types of equatorial bonds – two horizontal equatorial double bonds (16,17 and 44,45) and two vertical equatorial double bonds (21,40 and 30,31), they are shown in Table 5-6. So *syn* and *anti* naming system must be used to distinguish the two horizontal equatorial bonds as *syn*(C_1)16,17 and *anti*(C_1)16,17, where *syn* and *anti* refer to the orientation of the phenyl ring group on the second addend relative

to that of the other addend. That is, *syn*(C_1)16,17 demonstrates the phenyl ring on the ring of the 16,17 bond and bridge carbon C62 pointing close to the first addend and butyric acid methyl ester group pointing away. On the other hand, conversely *anti*(C_1)16,17 shows the phenyl ring on the ring of the 16,17 bond and bridge carbons C62 pointing away. This *syn* and *anti* naming method could be applied on 44,45 double bond which is the mirror image of 16,17 double bond generating *syn*(C_1)44,45 and *anti*(C_1)44,45 isomers. For the two vertical equatorial double bonds (21,40 and 30,31), *syn* and *anti* naming method cannot be used to show the differences of the structures because the distances between two phenyl rings from each addend with varying orientations are equal to each other. In this case, *R* and *S* naming rules need to be used to distinguish the four possible isomers from these two vertical equatorial double bonds (21,40 and 30,31) as *R*(C_1)21,40 and *S*(C_1)21,40, and as *R*(C_1)30,31 and *S*(C_1)30,31. However, *R*(C_1)21,40 and *S*(C_1)21,40 are enantiomers; as well as *R*(C_1)30,31 and *S*(C_1)30,31. Hence, the isomers attached to the two vertical equatorial bonds may be written simply as (C_1)21,40 and (C_1)30,31.

Table 5-6 The symmetrical equivalent and enantiomer from 8 possible molecular structures of *e* isomers of bis[60]PCBM.

e isomer	equivalent structure	double bond illustration
	syn(C_1)16,17 ←ena→ *syn*(C_1)44,45	
	↑sym ↑sym	
(C_1)30,31	*R*(**C_1**)**30,31** ←ena→ *S*(C_1)30,31	
	anti(C_1)16,17 ←ena→ *anti*(C_1)44,45	
	↑sym ↑sym	
(C_1)21,40	*R*(**C_1**)**21,40** ←ena→ *S*(C_1)21,40	

The *anti*(C_1)16,17 is symmetrical equivalent of *R*(C_1)21,40 and an enantiomer of *anti*(C_1)44,45 which is symmetrically equivalent to *S*(C_1)21,40, making all four isomers are effectively equivalent to each other. The *syn*(C_1)16,17 isomer is symmetrical equivalent of *R*(C_1)30,31 and an enantiomer of *syn*(C_1)44,45 which is symmetrically equivalent to *S*(C_1)30,31, making the other four isomers are effectively equivalent to each other as simplified in Table 5-6. So, there are only two unique isomer structures which are the *syn*(C_1)16,17 and *anti*(C_1)16,17 in *e* bond type by using IUPAC naming system. However, this would introduce new continent to the naming method format as we keep using symmetry and the double bond number for the name of isomers. In order to keep the format that used here for all the isomers, I will break the IUPAC rule and use the symmetrical equivalents of these isomers. Although it is not technically correct, this system fixes the naming issue without introducing any ambiguity; as they are equally rigorous and understandable alternative names for the same things. Hence, *anti*(C_1)16,17 becomes (C_1)21,40 and *syn*(C_1)16,17 becomes (C_1)30,31 which are shown in Figure 5-5.

| (a) | (b) |
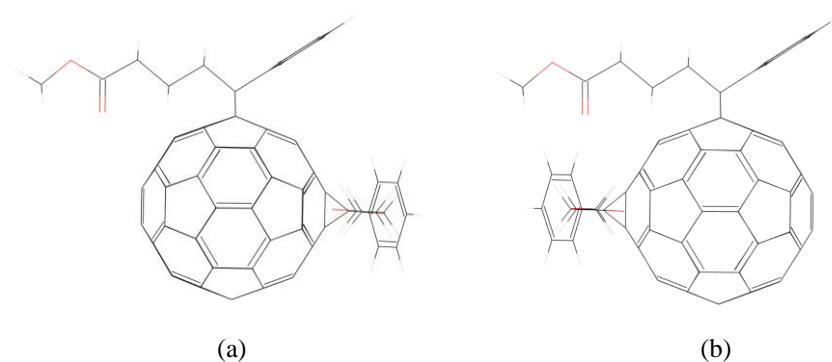
Figure 5-5 The molecular structures of the two isomers from *e* bond.
(a) (C_1)30,31-bis[60]PCBM, (b) (C_1)21,40-bis[60]PCBM.

5.1.6 The *cis*-3 bond

For the *cis*-3 bond type (in the figure in Table 5-7), there are four double bonds are

located at the positions of 13,14; 19,20; 22,23; and 28,29. Each bond could generate

two isomers with a C_1 and C_2 symmetries giving 8 possible isomers in total. As

with the *trans*-2 and *trans*-3 bonds, the (C_2)13,14 isomer and (C_2)28,29 isomer are

enantiomers and symmetrically equivalent to itself; as are the (C_2)19,20 isomer and

(C_2)22,23 isomers. But the (C_2)13,14 and the (C_2)19,20 isomers are distinguishable

(for the same reason for *trans*-2 and *trans*-3). Therefore, just like the *trans*-2 case,

there are two C_2 isomers, (C_2)13,14 and (C_2)19,20. Similar to the previous analysed

C_1 isomers, the (C_1)13,14 isomer is symmetrically equivalent to the (C_1)22,23

isomer; as are the (C_1)28,29 and the (C_1)19,20 isomers – and the (C_1)13,14 and

(C_1)28,29 isomers are enantiomers, as well as (C_1)22,23 and (C_1)19,20. This

effectively gives only one C_1 isomer as (C_1)13,14 for the *trans*-3 bond.

Table 5-7 The symmetrical equivalent and enantiomer from 8 possible molecular structures of *cis*-3 isomers of bis[60]PCBM.

cis-3 isomer	equivalent structure		double bond illustration
(C_2)13,14	(C_2)**13,14** ←ena→ (C_2)28,29		
(C_2)19,20	(C_2)**19,20** ←ena→ (C_2)22,23		
(C_1)13,14	(C_1)**13,14** ←ena→ (C_1)28,29		
	↕sym	↕sym	
	(C_1)22,23 ←ena→ (C_1)19,20		

Therefore, as for the *trans*-2 and *trans*-3 case, the 8 potential isomers for the *cis*-3

bond   reduced   to   three   distinguishable   structures   which   are (C_2)13,14-

bis[60]PCBM, (C_1)13,14-bis[60]PCBM and (C_2)19,20-bis[60]PCBM as shown in Figure 5-6.
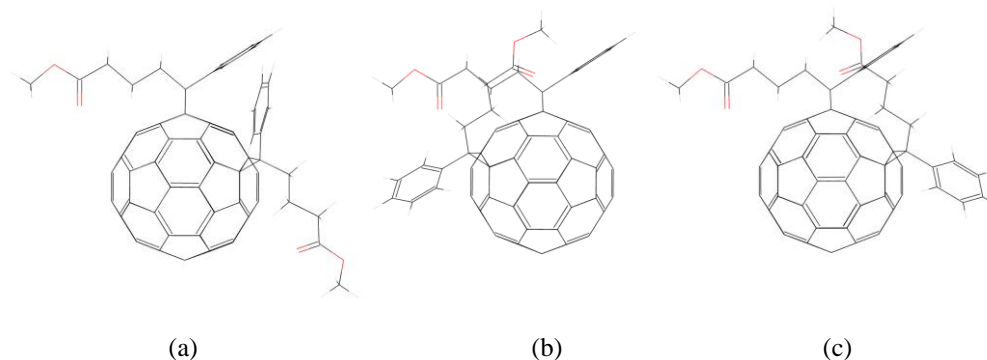
Figure 5-6 The molecular structures of the two isomers from *cis*-3 bond.
(a) (C_2)13,14-bis[60]PCBM, (b) (C_2)19,20-bis[60]PCBM, (c) (C_1)13,14-bis[60]PCBM.

5.1.7 The *cis*-2 bond

For the *cis*-2 bond type, double bonds are located at the positions of 3,15; 4,18; 24,25 and 26,27 in the figure in Table 5-8. These give 8 molecular structures. Similar to the *trans*-4 bond type rather than *trans*-2, *trans*-3 and *cis*-3 bonds, four of these have C_1 symmetry and the other four structures have C_s symmetry. They are (C_1)3,15; (C_s)3,15; (C_1)4,18; (C_s)4,18; (C_1)24,25; (C_s)24,25; (C_1)26,27 and (C_s)26,27.

For the C_s symmetry isomers in *cis*-2 bond, (C_s)3,15 isomer is not only symmetrically equivalent to, but also an enantiomer of (C_s)26,27. Hence, for C_s isomers swopping the two addends results in a structure that is an enantiomer of the original structure. This behaviour is also seen in the other C_s isomer, (C_s)4,18 which is symmetrically equivalent to and an enantiomer of (C_s)24,25. Theses give two unique C_s isomers of (C_s)3,15 and (C_s)4,18 according to IUPAC naming system that uses the smallest number for the label. Meanwhile, (C_1)3,15 is

symmetrically equivalent to (C_1)4,18 and has an enantiomer of (C_1)26,27 which is

symmetrically equivalent to (C_1)24,25. Hence, this behaviour of the C_1 isomers is

similar to previous C_1 isomers in the others bond type, showing all four C_1 isomers

are effectively equivalent to each other.

Table 5-8 The symmetrical equivalent and enantiomer from 8 possible molecular structures of *cis*-2 isomers of bis[60]PCBM.

cis-2 isomer	equivalent structure			double bond illustration
(C_s)3,15	(C_s)**3,15**	ena / sym	(C_s)26,27	
(C_s)4,18	(C_s)**4,18**	ena / sym	(C_s)24,25	
(C_1)3,15	(C_1)**3,15**	ena	(C_1)26,27	
	sym		sym	
	(C_1)4,18	ena	(C_1)24,25	

In total of three unique isomers of bis[60]PCBM exist of this bond type as shown

in Figure 5-7.

(a) (b) (c)
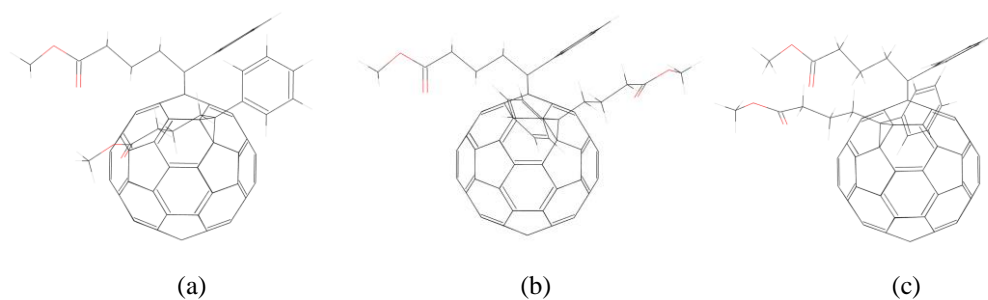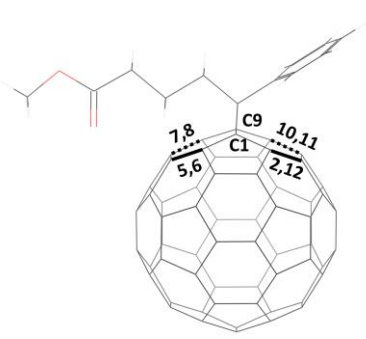
Figure 5-7 The molecular structures of the two isomers from *cis*-2 bond.
(a) (C_s)3,15-bis[60]PCBM, (b) (C_1)3,15-bis[60]PCBM and (c) (C_s)4,18-bis[60]PCBM.

5.1.8 The *cis*-1 bond

For the *cis*-1 bond type, double bonds are located at the positions of 2,12; 5,6; 7,8 and 10,11 which are equally the closest double bond to the 1,9 bond of the first addend on the same hexagon as shown in the figure in Table 5-9. These generates 8 molecular structures.

Similar to the *cis*-2 bond type, four of these structures have C_1 symmetry and the other four structures have C_s symmetry. For the C_s symmetry isomers on *cis*-1 bond, $(C_s)5,6$ isomer is not only symmetrically equivalent to, but also an enantiomer of $(C_s)7,8$ and the $(C_s)2,12$ which is symmetrically equivalent to and an enantiomer of $(C_s)10,11$. Hence, for C_s isomers swopping the two addends results in a structure that is an enantiomer of the original structure. Theses give two unique C_s isomers of $(C_s)5,6$ and $(C_s)2,12$ according to IUPAC naming system of using smallest number for the label. Meanwhile, $(C_1)2,12$ is symmetrically equivalent to $(C_1)5,6$ and has an enantiomer of $(C_1)10,11$ which is symmetrically equivalent to $(C_1)7,8$, this are demonstrated in Table 5-9.

Table 5-9 The symmetrical equivalent and enantiomer from 8 possible molecular structures of *cis*-1 isomers of bis[60]PCBM.

cis-1 isomer	equivalent structure			double bond illustration
$(C_s)2,12$	$(C_s)\mathbf{2,12}$	ena / sym	$(C_s)10,11$	
$(C_s)5,6$	$(C_s)\mathbf{5,6}$	ena / sym	$(C_s)7,8$	
$(C_1)2,12$	$(C_1)\mathbf{2,12}$	ena	$(C_1)10,11$	
	sym		sym	
	$(C_1)5,6$	ena	$(C_1)7,8$	

Hence, this behaviour of the C_1 isomers is similar to previous discussed C_1 isomers, showing all four C_1 isomers are effectively equivalent to each other. In total, there are three unique isomers of bis[60]PCBM exist of this bond type as shown in Figure 5-8.

(a)   (b)   (c)
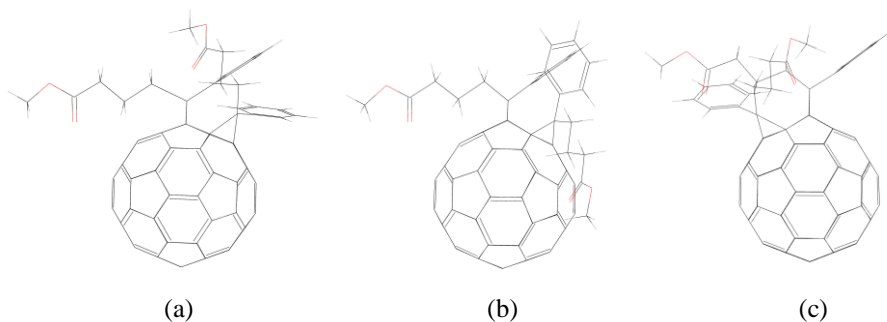
Figure 5-8 The molecular structure of the two isomers from *cis*-1 bond.
(a) (C_1)2,12-bis[60]PCBM, (b) (C_s)2,12-bis[60]PCBM and (c) (C_s)5,6-bis[60]PCBM.

5.1.9 Additional problems of previous nomenclatures

This method of determining the number and names of the bis[60]PCBM isomers removes ambiguity. The ambiguous endo-exo nomenclature method[113] led to the conclusion that there were 21 isomers, and the equally ambiguous cis-trans nomenclature of Shi led to the conclusion that there should be 18 isomers. This ambiguity might has also led Shi in his equivalent of my Table 5-10 below (Table 2.5 of his thesis[96]) to make many misassignments. Examples: trans-32,33 and trans-47,48 are not symmetrically equivalent – they are enantiomers (it is trans-38,39 that is the symmetrical equivalent of trans-32,33); trans-49,59 and trans-50,51 are not symmetrical equivalent – they are enantiomers (it is trans-53,54 that is the symmetrical equivalent of trans-49,59); cis-49,59 and cis-53,54 are not enantiomers, they are distinct isomers; cis-50,51 is not a distinct isomer, it is the

previously-misassigned enantiomer of cis-49,59; cis-34,35 and cis-44,57 are not

symmetrical equivalent – it is cis-43,57.

5.1.10 Conclusion on the number of isomers

By the above analysis, the number of potential isomers is reduced from 58 to 22 by

the application of symmetrical equivalence and chirality as list in Table 5-10. These

can be put into groups of two members from the polar and equatorial bonds and the

other bond types of three members. Further the three membered groups contain one

isomer with no symmetry (C_1) and two same symmetry isomers that are both C_s or

C_2 symmetry.

As we mentioned, the three isomers on the *cis*-1 bond which represent the closest

double bond on the same hexagon with the first addend, the structures are not likely

to be formed because there is not enough space for the two bulky addends to be

attached without touching each other. This behaviour is also be seen in other bis-

adducts for example $C_{60}(C(COOEt)_2)_2$ where the *cis*-1 isomers are missing.[112]

So, the maximum number of unique isomers of bis[60]PCBM is 19 which matches

the number of HPLC fractions from bis[60]PCBM purification in Chapter 4. This

suggests that each of the 19 HPLC fractions may correspond to a single isomer.

The remain of this chapter will assign each isomer to its corresponding HPLC

fraction by UV-Vis and ^{13}C NMR spectroscopy.

Table 5-10 All 58 nominal cyclopropa-fullerene isomers of bis[60]PCBM indicating the 22 spectroscopically distinguishable isomers, their symmetrical equivalents, their enantiomers and the symmetrical equivalents of enantiomers.

bond type	isomer	symmetrical equivalent	enantiomer	symmetrical equivalent
trans-1	(C_{2h})52,60	(C_{2h})52,60		
	(C_{2v})52,60	(C_{2v})52,60		
trans-2	(C_2)49,59	(C_2)49,59	(C_2)50,51	(C_2)50,51
	(C_1)49,59	(C_1)53,54	(C_1)50,51	(C_1)55,56
	(C_2)53,54	(C_2)53,54	(C_2)55,56	(C_2)55,56
trans-3	(C_2)34,35	(C_2)34,35	(C_2)46,58	(C_2)46,58
	(C_1)34,35	(C_1)43,57	(C_1)46,58	(C_1)36,37
	(C_2)36,37	(C_2)36,37	(C_2)43,57	(C_2)43,57
trans-4	(C_s)32,33	(C_s)47,48	(C_s)47,48	(C_s)32,33
	(C_1)32,33	(C_1)38,39	(C_1)47,48	(C_1)41,42
	(C_s)38,39	(C_s)41,42	(C_s)41,42	(C_s)38,39
e	anti(C_1)16,17	R(C_1)38,39	anti(C_1)44,45	S(C_1)21,40
	sym(C_1)16,17	R(C_1)30,31	sym(C_1)44,45	S(C_1)30,31
cis-3	(C_2)13,14	(C_2)13,14	(C_2)28,29	(C_2)28,29
	(C_1)13,14	(C_1)22,23	(C_1)28,29	(C_1)19,20
	(C_2)19,20	(C_2)19,20	(C_2)22,23	(C_2)22,23
cis-2	(C_s)3,15	(C_s)26,27	(C_s)26,27	(C_s)3,15
	(C_1)3,15	(C_1)4,18	(C_1)26,27	(C_1)24,25
	(C_s)4,18	(C_s)24,25	(C_s)24,25	(C_s)4,18
cis-1	(C_s)5,6	(C_s)7,8	(C_s)7,8	(C_s)5,6
	(C_1)2,12	(C_1)5,6	(C_1)10,11	(C_1)7,8
	(C_s)2,12	(C_s)10,11	(C_s)10,11	(C_s)2,12

5.2 The UV-Vis spectroscopy of 19 HPLC fractions of bis[60]PCBM

The UV-Vis spectrum of 18 HPLC fractions of bis[60]PCBM were firstly reported by Shi for assigning the HOMO-LUMO gap[93, 96] for each isomer without the 19th missing isomer F1.1. In this section, all 19 HPLC fractions of bis[60]PCBM with the 19th missing isomer in *trans*-1 group are re-acquired from new samples that I had purified in the range of 350-800 mm with higher resolution for determining the bond type effect on the absorption spectrum as show in Figure 5-9.
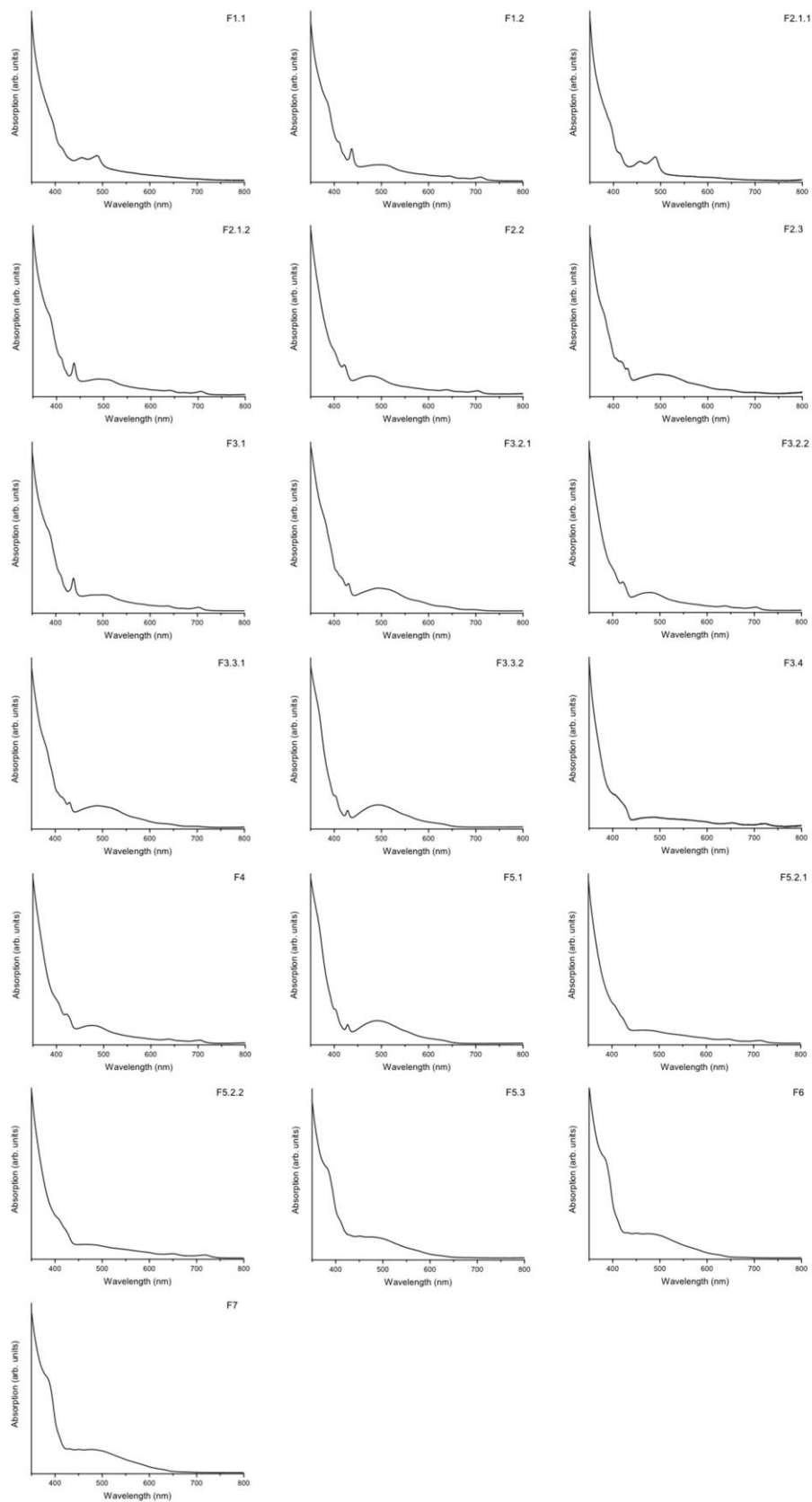
Figure 5-9 The UV-Vis spectroscopy for all 19 HPLC fractions of bis[60]PCBM in the order of HPLC fraction.

As we can see from the shape of absorption, fraction F1.1 shows two peaks near 450 nm and 500 nm which is different to fraction F1.2 with only one sharp absorption peak at 440 nm. However, fraction F2.1.1 dose have a similar shape with fraction F1.1 showing the same absorption peaks. Continuing, fraction F2.1.2 is similar to fraction F1.2, as well as fraction F3.1, but fraction F2.2 is different from all previously discussed absorption spectra. By comparing the absorption spectrum of all 19 HPLC fractions in this way, it was found that they may be classified into 7 groups (a-g in Figure 5-10) by the absorption patterns of which 5 groups have three members and 2 groups have two members.

These 7 UV-Vis groupings are the same in number and size as those of expected molecular structures that have found in section 5.2. This suggests that there may be a link between the absorption shapes of UV-Vis spectra and the bond types within bis[60]PCBM. Such a link has already been suggested in the literature for fullerene bis-adducts with symmetrical addends. Hirsch and co-authors have found that the shapes of the UV-Vis spectra of symmetric fullerene bis-adducts depends on the fullerene bond type involved rather than on the addend used.[111] There are two bis-adducts of C_{60} using the symmetrical addends – $C_{62}(COOEt)_4$ and $C_{62}(anisyl)_4$ have been purified by them. In each case they found all 7 expected isomers that give 7 unique UV-Vis spectra, and these 7 isomers are generated from different bond types (*trans*-1, *trans*-2, *trans*-3, *trans*-4, *e*, *cis*-3 and *cis*-2, the *cis*-1 isomer being missing owing to steric hindrance). With the symmetry information from each bond type isomers from ^{13}C NMR spectroscopy coupled with the expected HPLC elution order based on polarity (low to high on normal phase columns) from AM1 calculations, they could assign each UV-Vis spectrum to its corresponding bond type.[111]

In this exercise they found that the UV-Vis spectrum of the *trans*-1 isomer of the
COOEt-based molecule was very similar to the UV-Vis spectrum of *trans*-1 isomer
of anisyl-based molecule, and that the UV-Vis spectrum of the *trans*-2 isomer of
the COOEt-based was very similar to that of the *trans*-2 of anisyl-based isomers.
Indeed, they found similar close resemblances for all bond-types of both
compounds. From this, the authors concluded that, as different symmetric isomers
of the same bond type have effectively the same UV-Vis spectrum. In fact, they
went one step further and reach the same conclusion for C_{60} bis adducts with two
different symmetrical addends. For example $C_{62}(anisyl)_2(COOEt)_2$ and
$C_{61}(COOEt)_2(NCOOEt)$. For these two compounds, there are two distinguishable
equatorial isomers *e'* and *e''*. The UV-Vis spectra of the *e'* and *e''* are different in
each case, but the *e'* UV-Vis spectra of $C_{62}(anisyl)_2(COOEt)_2$ and
$C_{61}(COOEt)_2(NCOOEt)$ are similar, as are the UV-Vis spectra of *e''* isomers. The
spectra of all the other bond types are very similar between the two compounds.

In a similar way, it was found above that the 19 molecular structures of
bis[60]PCBM could be put into exactly the same 7 groups depending on bond type,
but the difference is that the asymmetric addends in bis[60]PCBM results in each
group having two or three members. As will be detailed below, by comparing the
UV-Vis spectra of those 7 groups with the spectra in Reference 74, it can be seen
that the UV-Vis absorption shapes of the 7 bis[60]PCBM groups corresponded
very closely to the shapes of 7 UV-Vis spectra of $C_{62}(COOEt)_4$ and $C_{62}(anisyl)_4$
compounds. This gives further confirmation of the hypothesis that the shapes of
the UV-Vis spectra of bis-adducts depend on the fullerene bond type involved
rather than the addend used; and extend that idea to include asymmetrical addends
of this type (dicyclopropafullerenes).

Applying these ideas to the 19 isomers of bis[60]PCBM, looking at Figure 5-10(a),

the UV-Vis spectra of HPLC fractions F1.1 and F2.1.1, it is seen that these bare a

very close resemblance to each other. There are shoulders at about 400 and 430 nm,

two broad peaks at about 450 and 480 nm, followed by a sharp decay to 500 nm

then a long decay to the unset nearly 700 nm. These two isomers can be either

trans-1 or *e* isomers as a group with two members. However, the UV-Vis pattern

shows similarity only to *trans*-1 isomers of this type (cyclopropa-fullerenes)

reported in literature, for instance, $C_{62}(COOEt)_4$ and $C_{62}(anisyl)_4$.[112] From this,

coupled with *trans*-1 isomers comprising one of the two groups with two members,

it is concluded that F1.1 and F2.1.1 are the two *trans*-1 isomers of bis[60]PCBM.

For Figure 5-10(b), the UV-Vis spectra of HPLC fractions F1.2, F2.1.2 and F3.1

bare a very close resemblance to each other. Like the *trans*-1 isomers there are two

shoulders in similar positions. However, this is where the similarity ends. What

follows is a single sharp peak at about 440 nm, a very broad peak near 500 nm,

then a very long decay which contains two weak peaks at 640 and 710 nm. As a

group with three members, it can be *trans*-2, *trans*-3, *trans*-4, *cis*-3 and *cis*-2

isomers. However, similar UV-Vis pattern was found only in *trans*-2 isomers of

$C_{62}(COOEt)_4$ and $C_{62}(anisyl)_4$ reported in Reference 74. Hence, the HPLC

fractions F1.2, F2.1.2 and F3.1 are assigned to the three *trans*-2 isomers of

bis[60]PCBM.

For Figure 5-10(c), the UV-Vis spectra of HPLC fractions F2.3, F3.2.1 and F3.3.1

show resemblance to each other, showing four shoulders following one by one

between 380 to 430 nm, then a broad peak at 500 nm but has much higher relatives

than *trans*-2 isomers, then a very long and smooth decay to the base line. Similar

absorption was found in the *trans*-3 isomers of $C_{62}(COOEt)_4$ and $C_{62}(anisyl)_4$.[111,]

[112] So the HPLC fractions F2.3, F3.2.1 and F3.3.1 are assigned to the three *trans*-3

isomers of bis[60]PCBM.

The UV-Vis spectra of HPLC fractions F2.2, F3.2.2 and F4 have a similar pattern

to *trans*-2, except that the broad peak near 500 nm has moved to 470 nm, the sharp

peak is far less pronounced and the initial shoulder can no longer be seen. A similar

pattern was found in the *trans*-4 isomers of $C_{62}(COOEt)_4$ and $C_{62}(anisyl)_4$ [112], so

the HPLC fraction F2.2, F3.2.2 and F4 can be assigned to the three *trans*-4 isomers

of bis[60]PCBM as show in Figure 5-10(d).

The UV-Vis spectra of the other group with two members, F3.3.2 and F5.1, are

supposed to be the *e* isomers – as the first group with two members is already

confirmed to be the *trans*-1 group. Confirmation of this comes from the UV-Vis

absorption spectra. These are both similar to the *trans*-2 isomers but with a less

intense sharp peak at 440 nm, the broad peak at 500 nm being more intense, and a

much quicker decay to the baseline (at 650 nm). The similarity was found in *e*

isomers of $C_{62}(COOEt)_4$ and $C_{62}(anisyl)_4$.[111, 112] Therefore, F3.3.2 and F5.1 are

indeed assigned to two *e* isomers of bis[60]PCBM as shown in Figure 5-10(e).

For Figure 5-10(f), the UV-Vis spectra of F3.4, F5.2.1 and F5.2.2 show the

resemblance to each other. There is a sharp decay from 350 to 430 nm with two

small shoulders near the end, and a long decay to the base line with two small peaks

near the end. This pattern is similar to that of *cis*-3 isomers of $C_{62}(COOEt)_4$ and

$C_{62}(anisyl)4$.[111] So F3.4, F5.2.1 and F5.2.2 are assigned to three *cis*-3 isomers of

bis[60]PCBM.
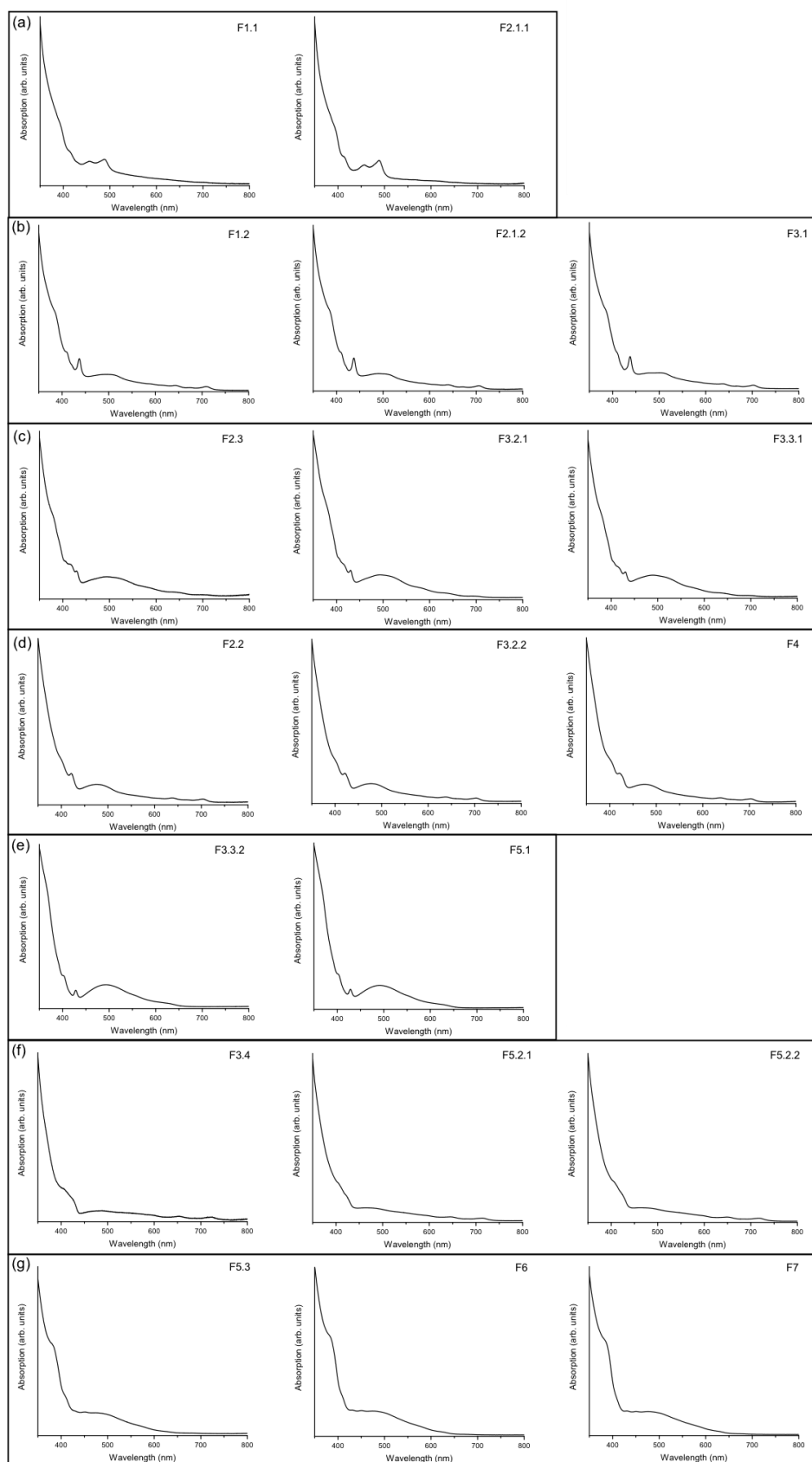
Figure 5-10 The UV-Vis spectra of 19 HPLC fractions in 7 groups.
(a) *trans*-1group, (b) *trans*-2 group, (c) *trans*-3 group, (d) *trans*-4 group, (e) *e* group,
(f) *cis*-3 group, (g) *cis*-2 group.

For Figure 5-10(g), the UV-Vis spectra of F5.3, F6 and F7 show the resemblance to each other with a sharp decay containing a pronounced shoulder to 420 nm. This is follows by a flat area up to 500 nm, then a smooth decay to the base line at 700 nm. Similar pattern was found in *cis*-2 isomers of $C_{62}(COOEt)_4$ and $C_{62}(anisyl)_4$.[111] so F5.3, F6 and F7 are assigned to three *cis*-2 isomers of bis[60]PCBM.

Although we do not expect any *cis*-1 isomers of bis[60]PCBM for steric reasons, compared with a *cis*-1 bonded cyclopropa-fullerene bisadduct, $C_{60}(NCOOEt)_2$.[111,112] The UV-Vis spectrum, of this isomer is different to that of the other 7 bond types. In addition, the spectra of those others match the bond type assignments made here, giving further confirmation for the idea that the UV-Vis spectra form a 'finger print' for the structural identification of cyclopropa-fullerene bis-adducts.

There are no isomers left which could show any clue to match the UV-Vis spectra of *cis*-1 bond type for example, $C_{60}(NCOOEt)_2$, so there are no *cis*-1 isomers exist for bis[60]PCBM.

Based on the above analysis, 7 groups of UV-Vis can be shown as follows: the two *trans*-1 isomers correspond to HPLC fractions F1.1 and F2.1.1; the three *trans*-2 isomers are F1.2, F2.1.2, and F3.1; the three *trans*-3 isomers are F2.3, F3.2.1 and F3.3.1; the three *trans*-4 isomers are F2.2, F3.2.2 and F4; the two *equatorial* isomers are F3.3.2 and F5.1; the three *cis*-3 isomers are F3.4, F5.2.1 and F5.2.2; and finally, the three *cis*-2 isomers are F5.3, F6 and F7.

Again, by the above analysis the members of the 7 bond type groups identified when determining the number of distinct isomers have been assigned to HPLC fractions. Although we now know which three of the 19 HPLC fractions involves the *trans*-2 bond F1.2, F2.1.2 and F3.1, and we also know that there are three *trans*-

2 isomers – (C_1)49,59-bis[60]PCBM, (C_2)49,59-bis[60]PCBM, and (C_2)53,54-bis[60]PCBM, we cannot assign the three *trans*-2 to their specific HPLC fraction via the UV-Vis spectra. The same thing can be said for the other six bond types. Nevertheless, the uncertainty on the identity of the isomers has been reduced from 1:19 to 1:2 or 1:3 depending on the bond type. In order to reduce the uncertainty further, the other forms of spectroscopy are required. In the next section the ^{13}C NMR spectra of the isomers will be presented and analysed. From this we can at least definitely identify the *trans*-1 isomers (i.e., distinguish isomer of (C_{2h})52,60-bis[60]PCBM from (C_{2v})52,60-bis[60]PCBM), as well as the C_1 member of each three-membered bond-type groups from the two higher symmetry members of each group (i.e., (C_1)49,59-bis[60]PCBM (*trans*-2), (C_1),34,35-bis[60]PCBM (*trans*-3), (C_1)32,33-bis[60]PCBM (*trans*-4), (C_1)13,14-bis[60]PCBM (*cis*-3) and (C_1)3,15-bis[60]PCBM (*cis*-2)).

5.3 The ^{13}C NMR spectra of 19 fractions of bis[60]PCBM

All 19 HPLC fractions of bis[60]PCBM have been characterised by ^{13}C NMR spectroscopy. Different symmetries of isomers giving different numbers of resonance and relative intensity in their ^{13}C NMR spectra. This character can be used to determine the isomer with unique symmetry in each UV-Vis group. From the discussion of the expected isomers, the isomers have been put into groups according to the bond type with different symmetries: C_{2h}, C_{2v}, C_s, C_2 and C_1. The prediction of the ^{13}C NMR line pattern for these 5 kinds of symmetries and the experimental ^{13}C NMR spectrum of 19 HPLC fractions are discussed below. Comparing the information from experimental ^{13}C NMR spectra, the molecular

structure of the isomer with the unique symmetry in each group can be certainly identified to the corresponding HPLC fraction. For instance, there are only one C_1 symmetry isomer in *trans*-2, *trans*-3, *trans*-4, *cis*-3 and *cis*-2 groups, apart from two *e* isomers both have C_1 symmetry which are identical to the line pattern of ^{13}C NMR spectrum, leaving the other two same symmetries isomers which can be identified by other techniques. This further reduced the number from 7 groups with 2 or 3 members to 7 fully identifies isomers and the remain 12 isomers in 6 groups of 2 same symmetry isomers. In this section, HPLC fractions that corresponds to the unique symmetry isomers within each group, and which two HPLC fractions correspond to the two same symmetry isomers in 6 groups will be identified.

For the ^{13}C NMR spectroscopy, toluene is used as the solvent during the HPLC purification. Despite each sample having the toluene removed by rotary evaporation to give a powder and then dissolved in carbon disulphide for the NMR experiments, all ^{13}C NMR spectra of the purified isomers showed evidence of residual toluene. These showed up as lines at 21.93, 125.73, 128.59, 129.31 and 138.21 ppm. These lines are consistent with the literature values[158] for toluene. In addition, as they are consistently at these positions in all spectra, but vary in intensity relative to the phenyl lines of the bis[60]PCBM isomers, they cannot be from the bis[60]PCBM isomers. In each spectrum presented below the resonances from the residual toluene are indicated with stars (*). The off-scale feature centred at 128.06 ppm is deuterated benzene which was used as a signal lock in the ^{13}C NMR experiment.

5.3.1 Prediction of the number of resonance and intensity from symmetry
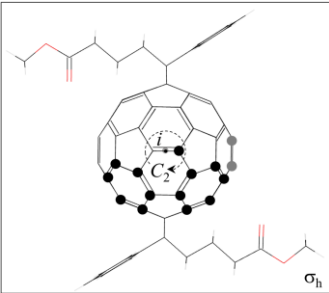
There are 5 kinds of symmetries (C_{2h}, C_{2v}, C_s, C_2 and C_1) are discovered from the 19 possible molecular structures of bis[60]PCBM. As the atoms that are symmetry-equivalent that can absorb at the same chemical shifts. According to the different symmetries, it can predict that how many resonances and their relative intensity could show up in the ^{13}C NMR spectrum for the isomers. For each symmetry, a molecular structure from the isomers as an example is given for the prediction.

C_{2h} point group symmetry

This symmetry group has a C_2 rotation axis (along the z-axis), a centre of inversion (i) and a horizontal mirror plane (σ_h).

Table 5-11 The ^{13}C NMR spectrum prediction for C_{2h} symmetry of bis[60]PCBM.

carbon	hybridization		
	sp^2	sp^3	
C$_{60}$	13×4+2×2	1×4	
phenyl ring	2×4+2×2	--	
C61/C62	--	1×2	
MB	1×2	4×2	
In total	15×4+5×2	5×2+1×4	

There are 56 sp^2 carbons on C$_{60}$ cage. Applying the horizontal mirror plane (σ_h) symmetry, the 4 carbons on the mirror plane are reflected to themselves. These could generate 4 lines with single-intensity. The other 52 carbons are each reflected to another carbon, giving 26 double-intensity resonances. Therefore, these contribute 4 single-intensity and 26 double-intensity lines from this operation. The C_2 axis passes through the centre of the double bonds (16,17) and (44,45). Hence,

there are no atoms that rotate onto themselves. As such, C_2 rotates all carbons onto another carbon – halving the number of resonances. Therefore, the combined effect is half the resonance number and double the intensity based on the horizontal mirror plane reflection, giving 2 lines of double-intensity (correspond to two dark grey carbons in the figure) and 13 lines of quadruple-intensity (correspond to 13 black carbons in the figure) for fullerene sp^2. As there is no atom on the centre of inversion (which is at the centre of the fullerene cage), inversion has no additional effect on the number of resonances because each atom maps onto another on the opposite side of the molecule, halving the number of resonances exactly as C_2 rotation axis does. Indeed, this argument applies to every carbon atom for this symmetry. There are 4 sp^3 bridgehead carbons on C_{60} cage which could give 4 single-resonance, however, this number is halved by the σ_h reflection and halved again by the C_2 rotation axis. As inversion has the same effect on the number of lines as C_2 on the carbons, this leaves 1 resonance of quadruple-intensity.

For the 6 sp^3 carbons on each phenyl ring, two of Ph1 and Ph4 carbons are lying on the mirror plane and the other 4 are bisected by it. So the number of resonance and intensity of a phenyl ring are 2×1 and 2×2. In addition, the C_2 rotation axis and inversion map one phenyl ring onto the other, hence, doubles the intensity. These give 2×2 and 2×4 resonances in 6 sp^3 region.

The two bridge carbons (C61 and C62) are reflected to themselves by the σ_h mirror plane and map onto the other by the C_2 rotation and inversion – giving 1×2 in the sp^3 region.

The two methyl butanoate (MB) groups lie entirely on the σ_h mirror plane. Hence the effect of a C_2 rotation/inversion and the reflection give the number of resonance

and intensity of 4×2 in the sp^3 region and 1×2 (from carbonyl carbons) in the sp^2
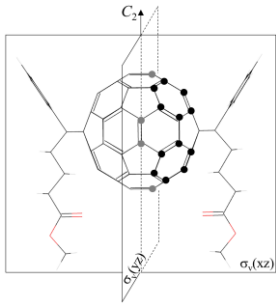
region.

In summary, the ^{13}C NMR spectrum of C_{2h}(52,60)-bis[60]PCBM is predicted to

have 15×4 and 5×2 in the sp^3 region and 5×2+1×4 in the sp^2 region as detailed in

Table 5-11.

C_{2v} point group symmetry

This symmetry group has a C_2 rotation axis (along the z-axis) and two vertical

mirror planes (σ_v(xz) and σ_v(yz)).

Table 5-12 The ^{13}C NMR spectrum prediction for C_{2v} symmetry of bis[60]PCBM.

carbon	hybridization		
	sp^2	sp^3	
C_{60}	12×4+4×2	1×4	
phenyl ring	2×4+2×2	--	
C61/C62	--	1×2	
MB	1×2	4×2	
In total	14×4+7×2	5×2+1×4	

The figure in Table 5-12 shows the effect of the two reflection operations and a

rotation axis. The non-equatorial sp^2 carbons contribute 12 resonances (correspond

to 12 black carbons in the figure) of intensity 4. This is because the 48 non-

equatorial sp^2 carbons are reflected front to back (reducing the distinct carbons to

24) from σ_v(xz) reflection, and left to right (continue reducing the distinct carbons

to 12) from σ_v(yz) reflection. The C_2 rotation axis could not further reduce this

number of the equivalent carbons from top to bottom because the inequivalence

caused by the asymmetrical addend. Of the 8 equatorial carbons, two (C16 and C17) of them can be reflected to the back (C44 and C45) by the σ_v(xz) plane, leaving the other 4 equatorial carbons (C21, C40, C30 and C31) on the σ_v(xz) plane are reflected to themselves. The two equatorial carbons on the right (C30 and C21) are equivalent to the left (C31, C40) from the σ_v(yz) reflection, making the 4 equatorial carbons (C16, C17, C44 and C45) lying on the σ_v(yz) plane are mirrored to themselves, and this symmetry is equal to the C_2 rotation applied on the equatorial carbons. Hence, the 8 equatorial carbons contribute 4 resonances (correspond to 4 carbons in dark grey in the figure) of relative intensity 2. As such, the 56 sp^2 fullerene carbons contribute 12×4 and 4×2 resonances in the sp^2 region of the spectrum. The two sp^3 fullerene bridgehead carbons of each of the two addends are mirrored on to each other by the σ_v(xz). The σ_v(yz) operation then mirrors one addend onto the other. Hence, there is only 1 resonance of relative intensity 4 from the sp^3 bridgehead carbons.

The two phenyl rings are bisected by the xz-plane. Hence, the σ_v(xz) operation (giving 2×2+2×1), which followed by the σ_v(yz) operation gives 2×4+2×2. As the symmetry of $C_2=\sigma_v$(xz)σ_v(yz), so the C_2 operation does not contribute anything new to the discussion.

The two bridge carbons (C61 and C62) which connect phenyl ring, the C_{60} cage and the methyl butanoate (MB) group are reflected onto themselves by σ_v(xz), and onto each other by σ_v(xz) or C_2 – giving 1×2 in the sp^3 region.

Finally, the two MB groups lie entirely on the xz-plane. Hence, σ_v(xz) has no effect on the number and intensity of lines. However, σ_v(yz) reflects one group onto the

other. Therefore, the combined effect (and C_2) is to give 4×2 in the sp^3 region and

1×2 (carbonyl carbon) in the sp^2 region.
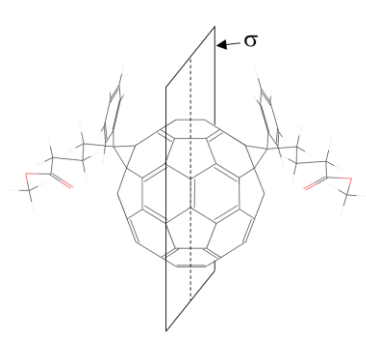
In summary, the ^{13}C NMR spectrum of C_{2v}(52,60)-bis[60]PCBM comprises 14×4

and 7×2 in the sp^3 region and 5×2+1×4 in the sp^2 region as detailed in Table 5-12.

C_s point group symmetry

This symmetry group has a mirror plane.

Table 5-13 The ^{13}C NMR spectrum prediction for C_s symmetry of bis[60]PCBM.

carbon	hybridization		
	sp^2	sp^3	
C_{60}	26×2+4×1	2×2	
phenyl ring	6×2	--	
C61/C62	--	1×2	
MB	1×2	4×2	
In total	33×2+4×1	7×2	

In the absence of the isomers in *cis*-1 group, bis[60]PCBM has 4 isomers

((C_s)32,33-bis[60]PCBM, (C_s)38,39-bis[60]PCBM, (C_s)3,15-bis[60]PCBM and

(C_s)4,18-bis[60]PCBM) with C_s symmetry. One of these is shown in the figure in

Table 5-13, which is oriented to show the mirror plane. It is seen that 4 carbon

atoms of the fullerene lie on this plane, and hence, reflect onto themselves. All

others (56) reflect onto another carbon. An example, one of the four C_s isomers in

bis[60]PCBM, (C_s)32,33-bis[60]PCBM, will be used to explain the ^{13}C NMR

prediction of the number of resonances and relative intensity.

To the 56 carbons of sp^2 on the C_{60} cage, as mentioned above four of them (C28, 29, C38 and C39) are on the mirror plane and reflect to themselves. These will generate 4 lines with single-intensity. The other 52 carbons are each reflected to another carbon, giving 26 double intensities resonances. Therefore, these contribute 4 single-intensity and 26 double-intensity lines from this operation. There are four bridgehead sp^3 carbons on C_{60} cage which could reflect to another carbon giving 2 double-intensity resonances because the mirror plane.

To the two phenyl rings, each of them has 6 sp^2 carbons. They are reflected to the other from the mirror plane giving 6 double-intensity resonances

The two bridge carbons (C61 and C62) map onto the other one by the mirror plane – giving 1×2 in the sp^3 region.

Finally, the MB groups reflected to the other by the mirror plane that gives the number of resonance and intensity of 4×2 in the sp^3 region and 1×2 in the sp^2 region.

In summary, the prediction of the ^{13}C NMR spectrum of (C_s)32,33-bis[60]PCBM comprises 7×2 in the sp^3 region and $33\times2+4\times1$ in the sp^2 region as detailed in Table 5-13. All four C_s isomers share the same number of resonances and relative intensity, but with different ppm values.

C_2 point group symmetry

This symmetry group has a C_2 rotation which is on a double bond as show in the figure in Table 5-14.

Table 5-14 The ^{13}C NMR spectrum prediction for C_2 symmetry of bis[60]PCBM.

carbon	hybridization	
	sp^2	sp^3
C_{60}	28×2	2×2
phenyl ring	6×2	--
C61/C62	--	1×2
MB	1×2	4×2
In total	35×2	7×2
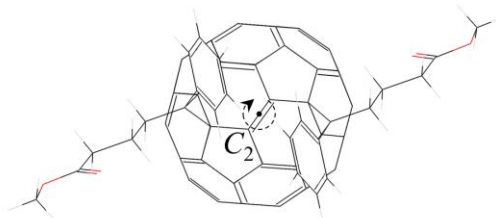
There are six expected isomers of bis[60]PCBM in C_2 symmetry, they are (C_2)13,14-bis[60]PCBM, (C_2)19,20-bis[60]PCBM, (C_2)34,35-bis[60]PCBM, (C_2)36,37-bis[60]PCBM, (C_2)49,59-bis[60]PCBM and (C_2)53,54-bis[60]PCBM. One of these $((C_2)$13,14-bis[60]PCBM as an example) is shown in the figure in Table 5-14, which is oriented to show the C_2 rotation axis. It is seen that the C_2 axis runs from the centre of a double bond, through the centre of the fullerene, to the centre of the opposing double bond. As there are no carbon atoms that transform onto themselves following the C_2 operation, all sp^2 carbon atom transform on to another sp^2 carbon atom. This means that this operation halves the number of distinct sp^2 carbon atoms on the fullerene– reducing the resonances from 56 to 28 with double-intensity, as well as four bridgehead sp^3 carbon atoms generate from 4 to 2 resonances with double-intensity.

To the two phenyl rings, all sp^2 carbon atom transform on to another by the C_2 rotation giving 6 double-intensity resonances.

The two bridge carbons (C61 and C62) map onto each other by the C_2 rotation– giving 1×2 in the sp^3 region.

150

Finally, the MB group is reflected to the other after the rotation which gives the number of resonance and intensity of 4×2 in the sp^3 region and 1×2 in the sp^2 region.

In summary, the ^{13}C NMR spectrum prediction of (C_2)13,14-bis[60]PCBM comprises 7×2 in the sp^3 region and 33×2 in the sp^2 region as detailed in Table 5-14. All six C_2 isomers of bis[60]PCBM share the same number of resonance and relative intensity, but with different ppm values.
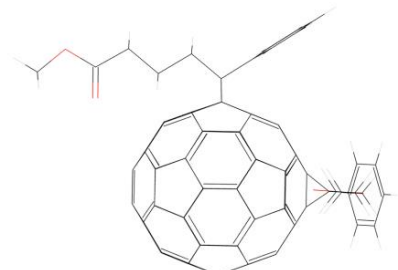
C_1 point group symmetry

This symmetry group has no symmetry.

Excluding the nonexistence cis-1 isomers, there are 7 C_1 isomers of bis[60]PCBM in 6 groups. They are (C_1)49,59-bis[60]PCBM in $trans$-2 group, (C_1)32,33-bis[60]PCBM in $trans$-3 group, (C_1)32,33-bis[60]PCBM in $trans$-4 group, (C_1)30,31-bis[60]PCBM and (C_1)21,40-bis[60]PCBM in e group, (C_1)13,14-bis[60]PCBM in cis-3 group, (C_1)3,15-bis[60]PCBM in cis-2 group. According to this asymmetric group, all 56 sp^2 fullerene carbons and all 4 sp^3 bridgehead carbons on C_{60} show as single-intensity resonances.

Table 5-15 The ^{13}C NMR spectrum prediction for C_1 symmetry of bis[60]PCBM.

carbon	hybridization	
	sp^2	sp^3
C_{60}	56×1	4×1
phenyl ring	12×1	--
C61/C62	--	2×1
MB	2×1	8×1
In total	70×1	14×1

An example ((C_1)30,31-bis[60]PCBM) is shown in the figure in Table 5-15. As no symmetry can be applied on the molecule, it gives 12 single-intensity resonances for the two phenyl rings, 2 single-intensity resonance for two the bridge carbons, 2 single intensity resonance of sp^2 and 8 single intensity resonance for the two MB groups.

In summary, the ¹³C NMR spectrum prediction of C_1 isomers comprises 14×1 in the sp^3 region and 70×2 in the sp^2 region as detailed in Table 5-15.

5.3.2 *trans*-1 isomers of bis[60]PCBM

There are two HPLC fractions, F1.1 and F2.1.1, are *trans*-1 isomers classified from UV-Vis groups in Section 5.3. Although ~10 mg of isomer F1.1 was synthesized and purified from the bis[60]PCBM mixture by HPLC, which is more than enough to record the ¹³C NMR spectrum, the solubility of this isomer is very low when purified. This behaviour was seen for all the purified isomers, whereby the solubility of the isomers when pure was considerably lower than the solubility of the isomer mixture. However, this particular isomer is the extreme case with a very strong propensity to aggregate. This is because it initially gave a dark yellow solution that within an hour became a pale yellow solution over a fine powder precipitate. This aggregation from solution unfortunately meant that the solubility of F1.1 was not high enough to record a ¹³C NMR spectrum of it, even in "high-solubility" solvents for fullerenes such as 1,2-dichlorobenzene. The solid ¹³C NMR of F1.1 also has been tried to record but the signals were so broad and overlapping to allow the structure to be determined.
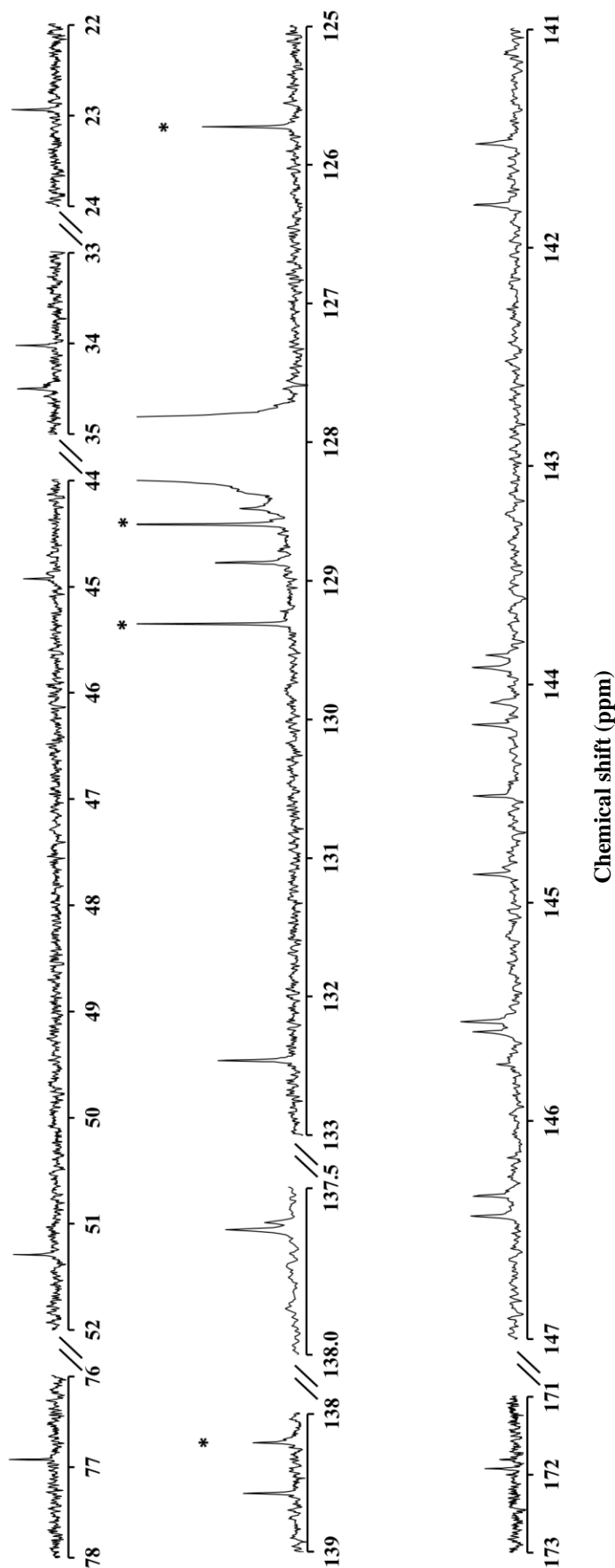
Figure 5-11 The ^{13}C NMR spectrum of HPLC fraction F2.1.1 of bis[60]PCBM.
Resonances below 78 ppm and above 125 ppm respectively originate from sp^3 and sp^2 hybridized carbons.
The resonance pattern of sp^3 and sp^2 hybridized carbon are $5\times2+1\times4$ and $14\times4+7\times2$, respectively. This is only
consistent with F2.1.1 being the (C_{2v})52,60-bis[60]PCBM isomer in *trans*-1 group.

HPLC fraction F2.1.1

The ^{13}C NMR spectrum of HPLC fraction F2.1.1 of the other *trans*-1 isomer is recorded and shown in Figure 5-11. The 6 resonances of sp^3 hybridized carbons are located from 20 to 78 ppm region, which matches the prediction that this is one of the two *trans*-1 isomers, C_{2v} or C_{2h} symmetry. It is in the pattern of 1, 2, 2, 1 with integrations of 2 except for the last one (76.91 ppm) which has an integration of 4. That is 1 resonance at 22.93 ppm, a gap, 2 resonances at 34.03 and 34.49 ppm, a gap followed by another 2 resonances at 44.92 and 51.29 ppm, then a gap to 1 resonance at 76.91 ppm as showing in Table 5-16. This pattern in sp^3 region is similar to that of [60]PCBM, which is previous discussed in Chapter 3, in which had ^{13}C, ^{1}H and 2D NMR spectra. Clearly the first 3 lines belong to the two symmetrically equivalent –CH$_2$–CH$_2$–CH$_2$– chains, with the resonance at 22.93 ppm coming from the two central carbons B3. The resonance at 34.03 ppm is slightly higher than the resonance at 34.49 ppm, and they come from the two of B2 and B4 carbons. This can be explained that the B4 carbon has a nonhydrogen neighbour could have slower relaxation giving slightly lower intensity than the B2 carbon has a carbonyl carbon neighbour. This phenomenon happens in all the other pure isomers of bis[60]PCBM. Again, similar to [60]PCBM, resonances at 44.92 and 51.29 ppm correspond to the two symmetrically equivalent bridge carbons (bis[60]PCBM carbons C61/C62), and the two symmetrically equivalent methyl groups, with the lower intensity resonance at 44.92 ppm coming from the bridge carbons, as this carbon has no hydrogens and therefore slower relaxation giving lower intensity. These also can confirm that this isomer is, like [60]PCBM, a cyclopropa-fullerene. Interestingly, the first 5 resonances of F2.1.1 discussed so far have similar chemical shifts to those found in [60]PCBM, except for the bridge

carbon. This carbon had a slightly higher chemical shift (52.19 ppm) than the

methyl carbon (51.28 ppm) in [60]PCBM. However, it occurs much lower at 44.92

ppm in the F2.1.1 isomer of bis[60]PCBM, while the methyl carbons remain near

its PCBM value of 51.28 ppm, at 51.29 ppm in the F2.1.1 isomer. The final sp^3

resonance occurs at 76.91 ppm, which according to the basis of typical "group

resonances" and similarity to [60]PCBM, is clearly the 4 symmetrically equivalent

bridge head carbons C1, C9, C52, C60 of *trans*-1 isomers. This resonance also has

slightly lower intensity than expected 4 carbons. This is because, like the bridge

carbons, the bridge head carbons also have no hydrogens attached. As mentioned

above, the single line from the bridgehead carbons confirms that this F2.1.1 is one

of the two *trans*-1 isomers, as only these two isomers have all 4 bridgehead carbons

being symmetrically equivalent. All the resonances in this region have the intensity

of 2 carbons. However, as the line pattern for the sp^3 carbons is same for both *trans*-

1 isomers, C_{2h} or C_{2v} symmetry, we need to discuss the sp^2 carbons to distinguish

them.

Table 5-16 The ^{13}C NMR chemical shift of HPLC fraction F2.1.1. The relative intensity of each resonance is labelled in the parentheses.

HPLC faction	hybridization	chemical shift (intensity)/ppm
F2.1.1	sp^3	22.93(2), 34.03(2), 34.49(2), 44.92(2), 51.29(2), 76.91(4);
	sp^2	128.47(2), 128.87(4), 132.46(4), 137.60(2), 137.63(4), 138.58(4), 141.52(4), 141.80(4), 143.87(2), 143.93(4), 144.08(2), 144.18(4), 144.51(4), 144.87(4), 145.54(4), 145.54(2), 145.59(4), 145.74(2), 146.34(4), 146.44(4), 171.92(2);

To the sp^2 hybridized carbons, apart from the off-scale feature centred on 128.06

ppm which is deuterated benzene and 4 residual toluene (labelled with stars on top)

which appear in ^{13}C NMR of [60]PCBM and other bis[60]PCBM pure isomers as

well, the first 5 lines in this region have 4 lines, 128.47, 128.87, 132.46 and 137.60 ppm, are very similar to the phenyl ring resonances in [60]PCBM which are 128.55, 128.79, 132.30 and 136.93 ppm. Hence, these are easily assigned to the phenyl ring carbons Ph4, Ph3/5, Ph2/6 and Ph1 in each of the two symmetrically equivalent phenyl groups on F2.1.1 of bis[60]PCBM, respectively. It can be confirmed by the single resonance from Ph4 at 128.55 ppm has slightly higher intensity than the Ph1 carbons with no hydrogens attached. This leaves the line at 137.60 ppm with an integration of 4 carbons as being the 1st fullerene resonance. An accidental coincidence of lines happened in the following resonances of F2.1.1, the integration analysis shows that the resonance at 145.54 ppm is of intensity 6 carbons – indicating that this resonance is a coincidence of a quadruple and a double intensity lines. Then there follows with another 11 resonances with integration 4 carbons and 4 resonances have an integration of 2 carbons, and these account for all 56 sp^2 resonances on the fullerene cage. The final resonance occurs at 171.92 ppm and has an integration of 2. This resonance may, again based on group resonances, be readily assigned to the two carbonyl carbons from the symmetrically equivalent ester groups. As such, all 84 carbons of HPLC fraction F2.1.1 of bis[60]PCBM were accounted for in this spectrum.

Observing the chemical shift of each resonance in sp^2 region from the spectrum, it can be counted that all the fullerene resonances of 56 sp^2 hybridized carbons show up as pairs, and the chemical shift difference of each pair is varied. This maybe because the 12 resonances of intensity 4 can be put into 6 pairs and 4 resonances of intensity 2 can be classified into 2 pairs, indicating that the chemical environment for each carbon atom is similar within the pair, and the chemical environment is different among the pairs. The carbons which have similar chemical

environment will show similar chemical shift, that have small difference of the chemical shift from the pairs. For the further carbon atoms identification on the C_{60} cage of this isomer, the DFTs simulation need to be involved to assign which carbon atom is which resonance, this can be further developed in the future.

According to the number of ^{13}C NMR resonances and integrations for HPLC fraction F2.1.1 which are $5\times2+1\times4$ in sp^3 region and $14\times4+7\times2$ in sp^2 region, it matches the prediction of being C_{2v} group symmetry (from section 5.4.1), and there are two isomers, (C_{2v})52,60-bis[60]PCBM and (C_{2h})52,60-bis[60]PCBM from the molecular structures of *trans*-1 bond type, so HPLC fraction F2.1.1 can be assign to the molecular structure of (C_{2v})52,60-bis[60]PCBM. We may also conclude (by elimination) that the isomer with very low solubility (HPLC fraction F1.1) must be the other *trans*-1 isomer (C_{2h})52,60-bis[60]PCBM. This is confirmed by the UV-Vis absorption spectrum of HPLC fraction F1.1, which is almost identical to that of the other *trans*-1 isomer (F2.1.1) but markedly different from the spectra of the other 17 isomers.

In conclusion for the *trans*-1 isomers, HPLC fractions F1.1 and F2.1.1 are assigned to the isomers (C_{2h})52,60-bis[60]PCBM and (C_{2v})52,60-bis[60]PCBM, respectively.

5.3.3 *trans*-2 isomers of bis[60]PCBM

The ^{13}C NMR spectra of HPLC fractions F1.2, F2.1.2 and F3.1 in *trans*-2 group are shown in Figure 5-12, Figure 5-13 and Figure 5-14, respectively. As we can see from the figures, for each of isomers, the ^{13}C NMR spectrum generates different line numbers and intensities, but similar line pattern. The details are analysed below.

157

HPLC fraction F1.2

The chemical shift of F1.2 from 20 - 80 ppm in sp^3 region from Figure 5-12 shows
that there are 7 resonances in the pattern of 1, 2, 2, 2. The resonances at 34.05 and
34.09 ppm show as a doubly degenerate line can be the case of 2 identical chemical
shifts. This occurs because these two carbons are from same position on each of
the two addends, making them symmetrically equivalent to each other. The overall
line pattern is similar to [60]PCBM in Chapter 3, the pattern for this isomer shows
the carbon atoms are: two symmetrically equivalent $-CH_2-CH_2-CH_2-$ chains, in
the order of two B3 carbons (at 23.00 ppm), two of B2 carbons at 34.05 ppm and
two of B4 carbons (at 34.09 ppm) with slightly lower intensity, following by the
two symmetrically equivalent bridge carbons at 49.37 ppm with lower intensity as
this carbon has slower relaxation without hydrogens attached, and two methyl
carbons are at 51.33 ppm, and four bridgehead carbons from both addends (at 78.93
and 79.14 ppm) which have lower intensity than the other sp^3 lines because they
each have no attached hydrogens. The two bridgehead carbons from the same
addend is not on any mirror plane, and therefore are not symmetrically equivalent.
In this case, they give two lines, as they could not be halved the number like
[60]PCBM (which has only one line for two bridgehead carbons as they are on the
mirror image). However, as there are only two bridgehead resonances, the two
bridgehead pairs are symmetrically equivalent. According to the number (7
resonances) of chemical shift of F1.2 from sp^3 region, this fraction can be assigned
to C_2 or C_s symmetry, as it has the agreement of ^{13}C NMR line prediction in Section
5.4.1 that C_2 or C_s symmetry could give 7 resonances in sp^3. However, there are
only two symmetries of C_1 and C_2 are concluded in *trans*-2 group from Section

5.2.2, F1.2 isomer can be temporally assigned to C_2 symmetry instead if C_1 which is predicted 14 lines in sp^3 region.

In the sp^2 region from 125 - 173 ppm of F1.2, the contamination caused from residual toluene at 128.59 and 129.31 ppm are labelled with stars on top of the lines. Deuterated benzene is used as the deuterium lock, giving 3 huge peaks centred on 128.06 ppm which is not counted for the resonances of the sample. Without counting the residual toluene and deuterated benzene lines, there are 35 resonances appeared in the sp^2 region. Of these 1 resonance at 171.89 ppm is from the two symmetrical carbonyl carbons, and 6 resonances are from the phenyl groups, leaving 28 resonances from the fullerene which matches the ^{13}C NMR prediction of being C_2 symmetry isomer and the chemical shifts are shown in Table 5-17. Confirmation of this comes from all 28 fullerene resonances having the same intensity (the alternative, C_s symmetry, would give 26 double-intensity resonances and 4 single-intensity resonance in sp^2 from the fullerene carbons).

There are two C_2 symmetry molecular structures which are (C_2)49,59-bis[60]PCBM and (C_2)53,54-bis[60]PCBM in *trans*-2 group, F1.2 cannot be assigned to which of them only based on ^{13}C NMR spectrum, because both isomers have the same ^{13}C NMR resonance pattern.

Figure 5-12 The ^{13}C NMR spectrum of HPLC fraction F1.2 of bis[60]PCBM.
Resonances below 80 ppm and above 125 ppm respectively originate from sp^3 and sp^2 hybridized carbons. The resonance pattern of sp^3 and sp^2 hybridized carbon are 7×2 and 35×2, respectively. This is only consistent with F1.2 being the isomer with C_2 symmetry in *trans-2* group.

Table 5-17 The ^{13}C NMR chemical shift of HPLC fractions in *trans*-2 group. The relative intensity of each resonance is labelled in the parentheses.

HPLC faction	hybridization	chemical shift (intensity)/ppm
F1.2	sp^3	23.00(2), 34.05(2), 34.09(2), 49.37(2), 51.33(2), 78.93(2), 79.14(2)
	sp^2	128.33(2), 128.66(2), 128.66(2), 132.21(2), 132.21(2), 136.43(2), 136.51(2), 137.31(2), 139.97(2), 140.31(2), 141.49(2), 142.15(2), 142.26(2), 142.36(2), 142.65(2), 142.82(2), 143.61(2), 144.02(2), 144.11(2), 144.50(2), 144.51(2), 144.83(2), 144.87(2), 145.17(2), 145.23(2), 145.55(2), 145.58(2), 145.96(2), 146.28(2), 146.33(2), 146.33(2), 147.19(2), 147.92(2), 150.99(2), 171.89(2);
F2.1.2	sp^3	22.73(1), 23.01(1), 33.87(1), 34.05(1), 34.11(1), 34.11(1), 49.31(1), 49.47(1), 51.20(1), 51.34(1), 78.91(1), 78.95(1), 79.14(1), 79.17(1);
	sp^2	128.35(1), 128.56(1), 128.70(1), 128.70(1), 128.89(1), 128.89(1), 132.24(1), 132.24(1), 132.51(1), 132.51(1), 136.46(1), 136.64(1), 136.88(1), 136.98(1), 137.29(1), 137.36(1), 137.63(1), 139.44(1), 139.98(1), 140.30(1), 140.58(1), 141.04(1), 141.57(1), 142.02(1), 142.13(1), 142.16(1), 142.38(1), 142.45(1), 142.56(1), 142.61(1), 142.64(1), 142.77(1), 142.93(1), 143.46(1), 143.61(1), 143.69(1), 143.94(1), 144.06(1), 144.23(1), 144.46(1), 144.49(1), 144.58(1), 144.76(1), 144.78(1), 144.89(1), 144.92(1), 145.21(1), 145.23(1), 145.31(1), 145.51(1), 145.58(1), 145.67(1), 145.70(1), 145.83(1), 145.92(1), 145.96(1), 146.16(1), 146.25(1), 146.28(1), 146.45(1), 146.48(1), 146.49(1), 146.68(1), 147.19(1), 147.28(1), 147.86(1), 150.96(1), 151.85(1), 171.79(1), 171.96(1);
F3.1	sp^3	22.77(2), 33.89(2), 34.14(2), 49.40(2), 51.22(2), 78.91(2), 79.17(2);
	sp^2	128.58(2), 128.90(2), 128.90(2), 132.53(2), 132.53(2), 136.91(2), 137.10(2), 137.31(2), 139.43(2), 140.56(2), 141.10(2), 141.98(2), 142.16(2), 142.53(2), 142.79(2), 142.86(2), 143.45(2), 143.73(2), 144.05(2), 144.44(2), 144.81(2), 144.81(2), 144.98(2), 145.40(2), 145.49(2), 145.81(2), 145.83(2), 146.01(2), 146.04(2), 146.26(2), 146.36(2), 146.88(2), 147.21(2), 151.80(2), 171.82(2);

HPLC fraction F2.1.2

More resonances are appeared in fraction F2.1.2 than F1.2 as can be seen in Table 5-17 and Figure 5-13, the number of resonances is doubled in both sp^3 and sp^2 region. Therefore, this isomer is the *trans*-2 isomer with C_1 symmetry, (C_1)49,59-bis[60]PCBM. For example, from 22 - 80 ppm, the number of resonances is doubled from 7 (in F1.2) to 14 (in F2.1.2), each line is splitting to be a pair. Similar to the previous discussion, the first pair resonances around 23 ppm are the two B3 carbons from the two now symmetrically inequivalent addends. Following with 3

lines which the last line is a coincidence of 2 resonances. They are two B2 and two B4 carbons on the two inequivalent –CH_2–CH_2–CH_2– chain. Here is not possible to tell which two resonances come from B2 or B4 carbons as the intensity of the coincidence is the two resonances added up, and it is not able to compare with the other two resonances. However, this is not necessary for determining the isomers. The next two pairs near 49 and 51 ppm, with the first pair having lower intensity, belong to the two hydrogen-less bridge carbons (C61/C62) and two methyl carbons, respectively. Finally, the last two pairs belong to the four bridgehead carbons which are C1/C9/C49/C59 according to (C_1)49,59-bis[60]PCBM.

In the sp^2 region a doubled number of resonances can be seen when compared to the C_2 symmetry isomer F2.1. Without counting deuterated benzene and residual toluene lines, the first two lines come from two phenyl carbon Ph4 on each symmetrically inequivalent addend. The next two pairs resonances from phenyl carbons Ph2, Ph3, Ph5 and Ph6. As these still appear as two double-intensity lines, it appears that lowering in symmetry of the molecule is not strongly felt by these phenyl carbons, as they still appear as Ph3/Ph5 and Ph2/Ph6 pairs. The final two phenyl resonances Ph1 are mixed in with the first few fullerene resonances and hence are difficult to assign. There then follows 56 lines from fullerene carbons with similar intensity. The number of these resonances and their relative intensity perfectly match the C_1 symmetry prediction. With no accidental coincidences, every fullerene sp^2 carbon is accounted for. The final pair lines near 172 ppm may be easily assigned to the two symmetrically inequivalent carbonyl carbons. Hence, the HPLC fraction F2.1.2 can be identified to the isomer (C_1)49,59-bis[60]PCBM.
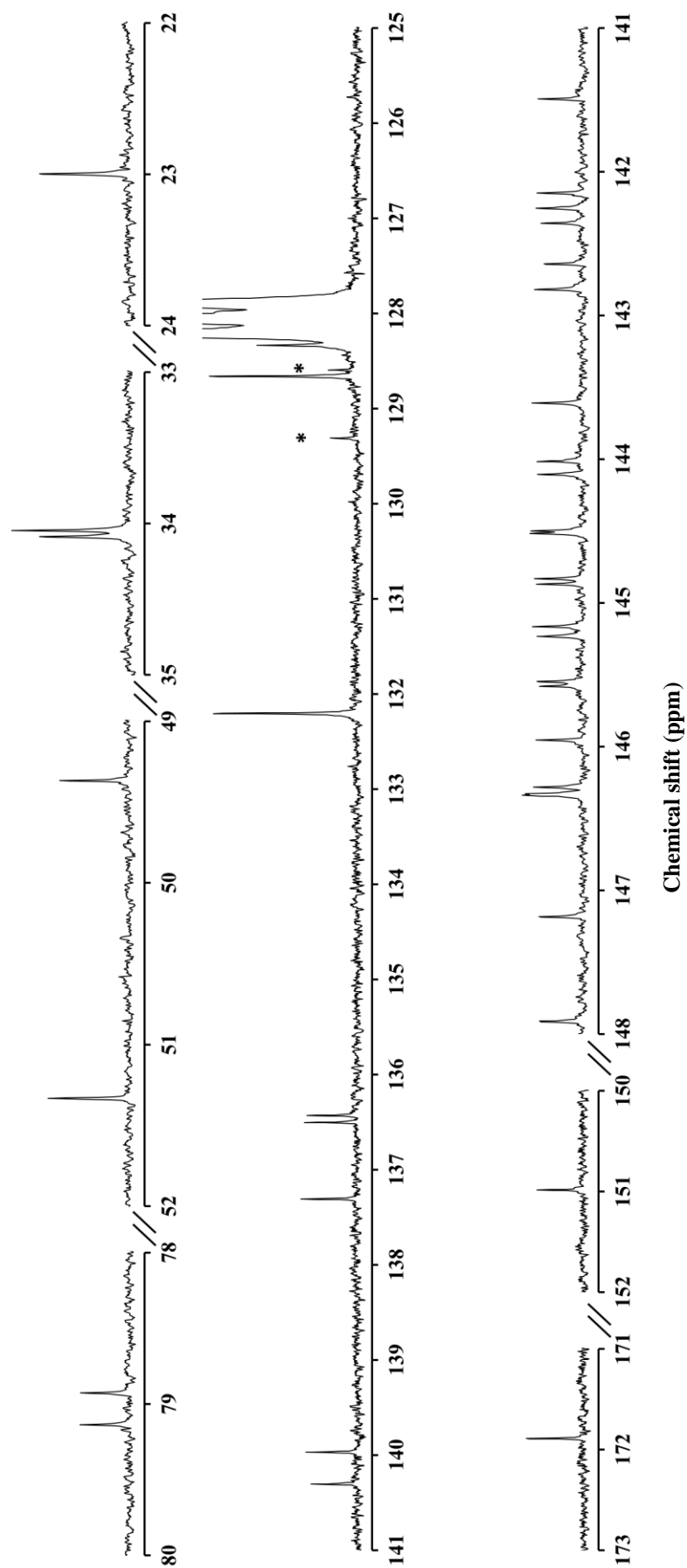
Figure 5-13 The ^{13}C NMR spectrum of HPLC fraction F2.1.2 of bis[60]PCBM.
Resonances below 80 ppm and above 125 ppm respectively originate from sp^3 and sp^2 hybridized carbons. The resonance pattern of sp^3 and sp^2 are 14×1 and 70×1, respectively. This is only consistent with F2.1.2 being the isomer (C_1)49,59-bis[60]PCBM in *trans-2* group.

163

HPLC fraction F3.1

The ^{13}C NMR resonance of F3.1 is shown in Figure 5-14. There are 7 resonances in the pattern of 1, 2, 2, 2. The chemical shifts are appeared at 22.77, 33.89, 34.14, 49.40, 51.22, 78.91 and 79.17 ppm, which are similar to the sp^3 hybridized carbon in HPLC fraction F1.2. They are the carbons from the two symmetrically equivalent –CH$_2$–CH$_2$–CH$_2$– chains, in the order of two B3 carbons at 22.77 ppm, two B2 carbons with relatively higher intensity than B4 and B4 carbons at 33.89 and 34.14 ppm. This is because, similar to [60]PCBM, both of B2 and B4 carbons sharing a same neighbour carbon of B3, and the other different neighbour carbon which is no hydrogen attached, however, the B2 carbon has a neighbour of a carbonyl carbon which could generate slightly higher intensity resonance than the B4 carbons. Then the two symmetrically equivalent bridge carbons at 49.40 ppm, and two methyl carbons (relatively higher intensity than bridge carbons) at 51.22 ppm, and 4 bridgehead carbons (lower intensity than the other sp^3 carbons) at 78.91 and 79.17 ppm (two at each). This is consistent with both C_2 and C_s, but not C_1 symmetry. As the *trans*-2 isomers do not have C_s symmetry, it is likely that this isomer has C_2 symmetry. However, the spectrum in the sp^2 region needs to be considered to confirm this.

The sp^2 hybridized carbons, have a similar pattern to that of HPLC fraction F1.2. Ignoring the deuterated benzene centred on 128.06 ppm and residual toluene line with a star (*) on top, the first 3 lines (128.58, 128.90 and 132.53 ppm) come from the two symmetrically equivalent phenyl ring groups in fact of a single height line (two symmetrically equivalent Ph4 carbons) and two double height lines (two pair of Ph3/Ph5 and Ph2/Ph6 carbons), the last phenyl line is mixed in with the initial fullerene lines. However, this time there are 27 fullerene resonances rather than the

28 expected (between 136 and 152 ppm). This problem is solved by looking at the line appear at 144.81 ppm. This line has roughly double the intensity of the other fullerene lines, suggesting that it is an accidental coincidence of two fullerene resonances. With this $26 \times 2 + 1 \times 4$ pattern, all 56 sp^2 fullerene carbons are accounted for. Again similar to F1.2, there is a gap to the final line (at 171.82 ppm), which is assigned to the pair of symmetrically equivalent carbonyl carbons. The number of lines and their relative intensity in the sp^2 region from 125 - 173 ppm are only consistent with this isomer having C_2 symmetry (C_s symmetry would produce 30 sp^2 fullerene resonances with 4 being of single-intensity and 26 of double-intensity). Therefore, this isomer is assigned to the other *trans*-2 isomer with C_2 symmetry.

In conclusion for the *trans*-2 group isomers, The HPLC fraction F2.1.2 can be uniquely assigned to the isomer (C_1)49,59-bis[60]PCBM, and HPLC fractions F1.2 and F3.1 comprise the isomers (C_2)49,59-bis[60]PCBM and (C_2)53,54-bis[60]PCBM. However, as mentioned above, the two isomers with C_2 symmetry cannot be distinguished based on the ^{13}C NMR spectra alone.

With this, the prediction based on the UV-Vis spectra that fractions F1.1 and F2.1.1 are the two *trans*-1 isomers (with C_{2h} and C_{2v} symmetries) and fractions F1.2, F2.2.1 and F3.1 are the three *trans*-2 isomers with one C_1 and two C_2 symmetries are fully confirmed by the ^{13}C NMR spectra. This gives strong confidence that the predictions from Section 5.4.1 are correct.
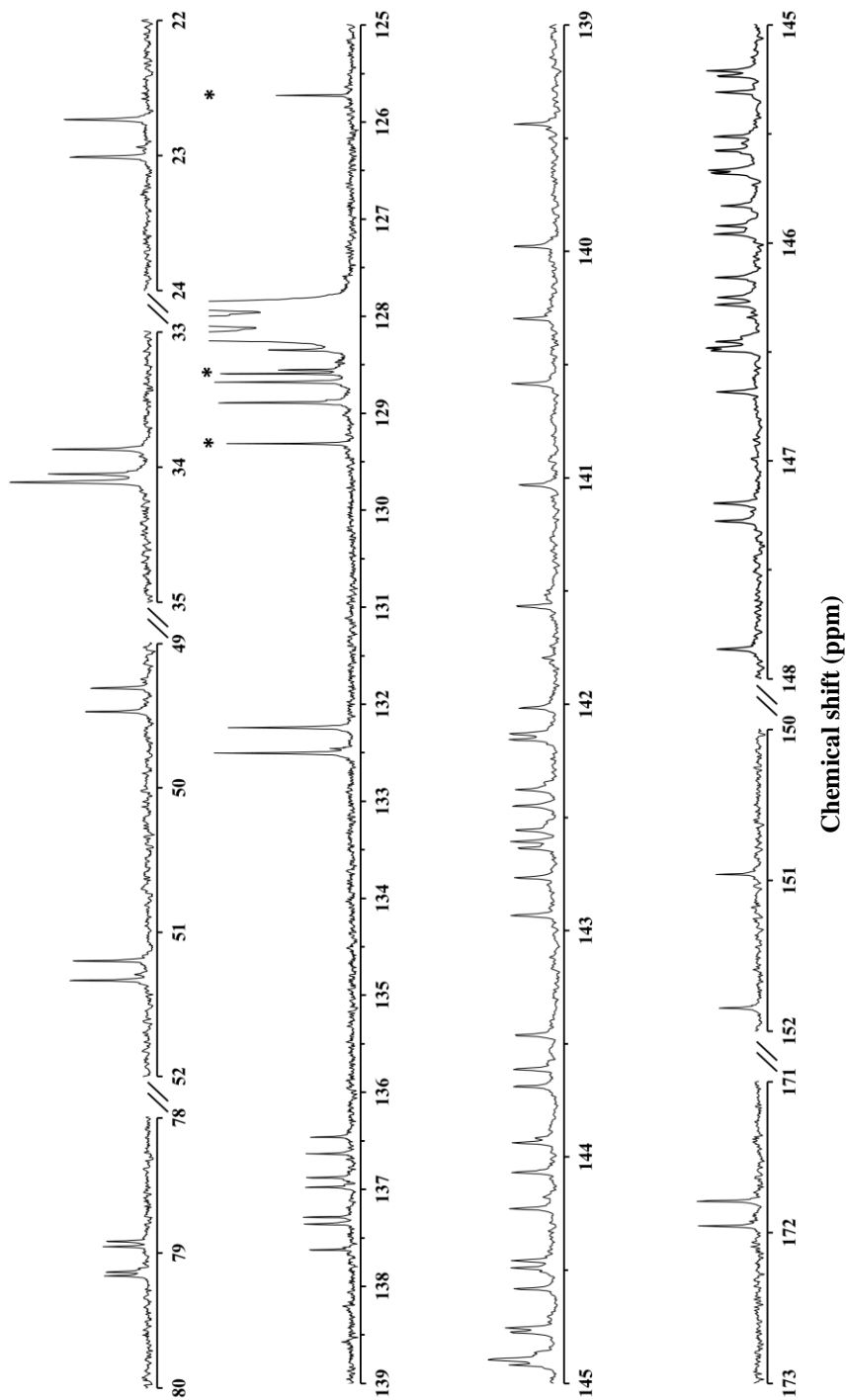
Figure 5-14 The ^{13}C NMR spectrum of HPLC fraction F3.1 of bis[60]PCBM.
Resonances below 80 ppm and above 125 ppm respectively originate from sp^3 and sp^2 hybridized carbons. The resonance pattern of sp^3 and sp^2 hybridized carbons are $7{\times}2$ and $35{\times}2$, respectively. This is only consistent with F3.1 being the isomer with C_2 symmetry in *trans*-2 group.

5.3.4 *trans*-3 isomers of bis[60]PCBM

The ^{13}C NMR spectra of *trans*-3 isomers, F2.3, F3.2.1 and F3.3.1, are show in Figure 5-15, Figure 5-16 and Figure 5-17, respectively. Their chemical shifts are list in Table 5-18. As we can see from the figures, for each isomer, the ^{13}C NMR spectra generates different line numbers and integrations, but similar line pattern. The symmetries prediction for this group are two C_2 and one C_1. The details are analysed below.

HPLC fraction F2.3

Similar to HPLC fraction F1.1, fraction F2.3 is another pure isomer with low solubility in carbon disulphide (CS_2) and has a high tendency to aggregate and precipitate out of solution. However, F2.3 has sufficient solubility in 1,2-dichlorobenzene for a spectrum to be recorded in a reasonable time (8 h signal averaging). Unfortunately, this solvent has many lines between 125 and 135 ppm, some of them cover up the lines corresponding to the phenyl groups in bis[60]PCBM. There are 5 resonances of the phenyl ring are missing in the sp^2 region.

Nevertheless, this spectrum possesses 7 lines in the sp^3 region from 22 - 81 ppm, which can only be consistent with C_2 or C_s symmetry. There are also a small line appear near 23 ppm which is a containment (labelled with star). The 7 resonances that show in the pattern of 1, 2, 2, 2 are similar to previous symmetrical isomers, they are the carbons from the two symmetrically equivalent $-CH_2-CH_2-CH_2-$ chains, in the order of two B3 carbons (at 21.26 ppm), two of B4 and B2 carbons with slightly higher intensity at higher ppm (at 33.43 and 33.55 ppm). The order of B2 and B4 carbons is different from previous isomers, as well as the two

symmetrically equivalent bridge carbons and methyl carbons. The following methyl carbons are at 50.97 ppm, and bridge carbons are at 51.06 ppm with lower intensity as this carbon has slower relaxation. The two bridgehead carbons from each symmetrically equivalent addend are at 79.44 and 79.93 ppm, they have lower intensity than the other sp^3 lines because they each have no attached hydrogens. The two bridgehead carbons from the same addend are not on any mirror plane, and therefore are not symmetrically equivalent. In this case, they give two lines. As there are only two bridgehead resonances which present for 4 bridgehead carbons, the two bridgehead pairs are symmetrically equivalent. According to the symmetry prediction in *trans*-3 group, there will have one C_1 and two C_2 symmetries, from the resonances in sp^3 region, this isomer can be possibly assign to C_2 symmetry instead if C_1, but need to be confirmed from sp^2 hybridized carbons.

In the sp^2 region from 135 to 173 ppm, there are two containment toluene lines labelled with stars. This is followed by 28 fullerene carbons and a single carbonyl resonance. This can only be consistent with C_2 symmetry, as there are 56 sp^2 fullerene carbons, the spectrum gives half this number of fullerene carbon resonances. Therefore, all lines must be doubly degenerate. Hence, despite the phenyl ring lines being covered up by the solvent, we confidently concluded that F2.3 is indeed one of the predicted isomer with C_2 symmetry in *trans*-3. That is either (C_2)34,35-bis[60]PCBM or (C_2)36,37-bis[60]PCBM.
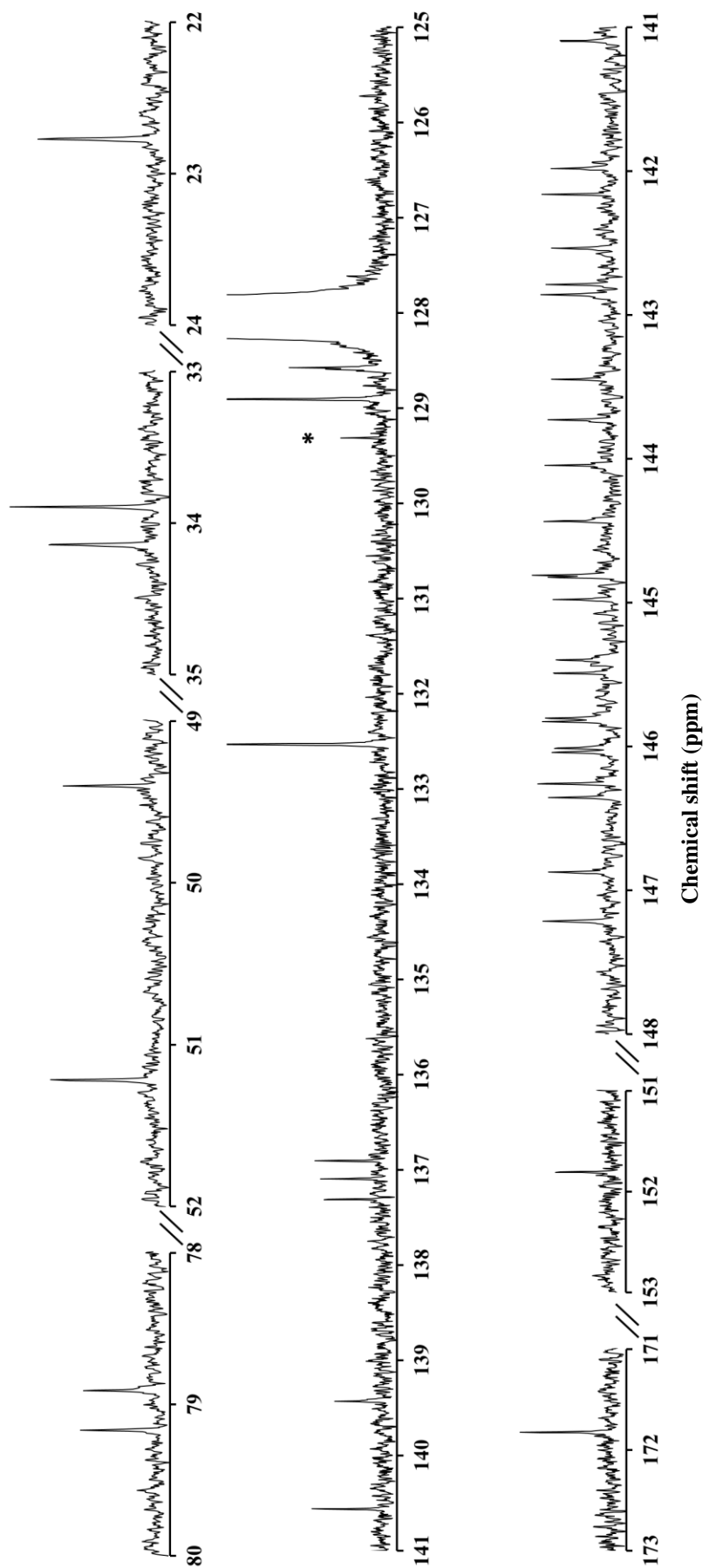
Figure 5-15 The ^{13}C NMR spectrum of HPLC fraction F2.3 of bis[60]PCBM.
Resonances below 81 ppm and above 125 ppm respectively originate from sp^3 and sp^2 hybridized carbons. The resonance pattern of sp^3 and sp^2 hybridized carbons are 7×2 and 35×2, respectively. This is only consistent with F2.3 being the isomer with C_2 symmetry in $trans$-3 group.

HPLC fraction F3.2.1

The ^{13}C NMR spectrum pattern for F3.2.1 in sp^3 region is similar to the C_1 isomer

discussed before. The resonances appear as 7 pairs. The first pair at 22.80 and 22.87

ppm are assigned to the central carbons (B3) on the two symmetrically inequivalent

$-CH_2-CH_2-CH_2-$ chains. The next two pairs occur around 34 ppm are the outer

two carbons (B2 and B4) of these chains. It is not possible to identify which of the

2 resonances near 34 ppm corresponds to which of the end CH_2 carbons according

to their relative intensity. However, for the purpose of determine the molecular

structure, this is not necessary. There then follows two pairs between 51.18 and

51.28 ppm. The resonances at 51.18 and 51.26 are assigned to the two methyl

carbons (based on their higher intensity) and those at 51.20 and 51.28 pm are

assigned to the two bridge carbons (C61/C62). The final four resonances (between

79.52 and 80.13 ppm are assigned to the 4 bridgehead carbons (C1/C9/C34/C35).

In the sp^2 region, there are 4 pairs of resonance from the two symmetrically

inequivalent phenyl ring groups, with the second and third pairs showing

coincidences near 129 and 132 ppm. These are followed by 56 sp^3 fullerene

resonances, with these at 142.03, 143.66, 144.44, 144.51 and 146.36 ppm being

accidental coincidences of double-intensity. The final two resonances at 171.77

and 171.86 ppm are from two symmetrically inequivalent carbonyl carbons. With

the number of resonances matching a *trans*-3 isomer with C_1 symmetry, this isomer

F3.2.1 can be assigned to the molecular structure of (C_1)34,35-bis[60]PCBM in

trans-3 group.

Figure 5-16 The ^{13}C NMR spectrum of HPLC fraction F3.2.1 of bis[60]PCBM.
Resonances below 81 ppm and above 125 ppm respectively originate from sp^3 and sp^2 hybridized carbons. The resonance pattern of sp^3 and sp^2 hybridized carbons are 14×1 and 70×1, respectively. This is only consistent with F3.2.1 being the isomer C_1(34,35)-bis[60]PCBM in *trans*-3 group.

Chemical shift (ppm)

171

HPLC fraction F3.3.1

The ^{13}C NMR spectrum of the last *trans*-3 isomer, F3.3.1 has the similar line pattern to C_2 symmetry isomer. Excluding deuterated benzene and residual toluene, it is 7 resonances in sp^3 region with one coincidence which is a quadruple-intensity resonance appear at 51.20 ppm to be the two symmetrically equivalent methyl carbons and bridge carbons, in this case, it cannot tell which is methyl carbons or bridge carbons as it appears as a coincidence resonance. The other symmetrically equivalent sp^3 hybridized carbons are the central carbons (B3) at 22.81 ppm and two end carbons (B2 and B4) at 33.84 and 34.17 ppm on the –CH$_2$–CH$_2$–CH$_2$– chains. The relative intensity of the resonances near 34 ppm confirms that B2 carbons corresponds to the resonance with higher intensity at lower ppm. The two bridgehead carbons from both addends (at 79.49 and 80.11ppm), they have lower intensity than the other sp^3 lines because they each have no attached hydrogens. The two bridgehead carbons from the same addend are not on any mirror plane, and therefore are not symmetrically equivalent. In this case, they give two lines. As there are only two bridgehead resonances which present for 4 bridgehead carbons, the two bridgehead pairs are symmetrically equivalent.

In the sp^2 region from 125 to 172 ppm, without counting the deuterated benzene centred on 128.06 ppm and residual toluene lines labelled with stars, this region begins with two carbons of Ph4 from both symmetrically equivalent phenyl rings at 128.47 ppm with intensity of 2 carbons. These are followed by two pairs of Ph3/Ph5 (total intensity of 4 carbons) at 128.74 ppm, and another two pairs of Ph3/Ph5 (intensity 4) at 132.29 ppm. The resonance appear at 137.10 ppm can be assigned to the last two phenyl ring carbons (Ph1). This is because it has slightly higher intensity than the other sp^2 resonances near 137 ppm.
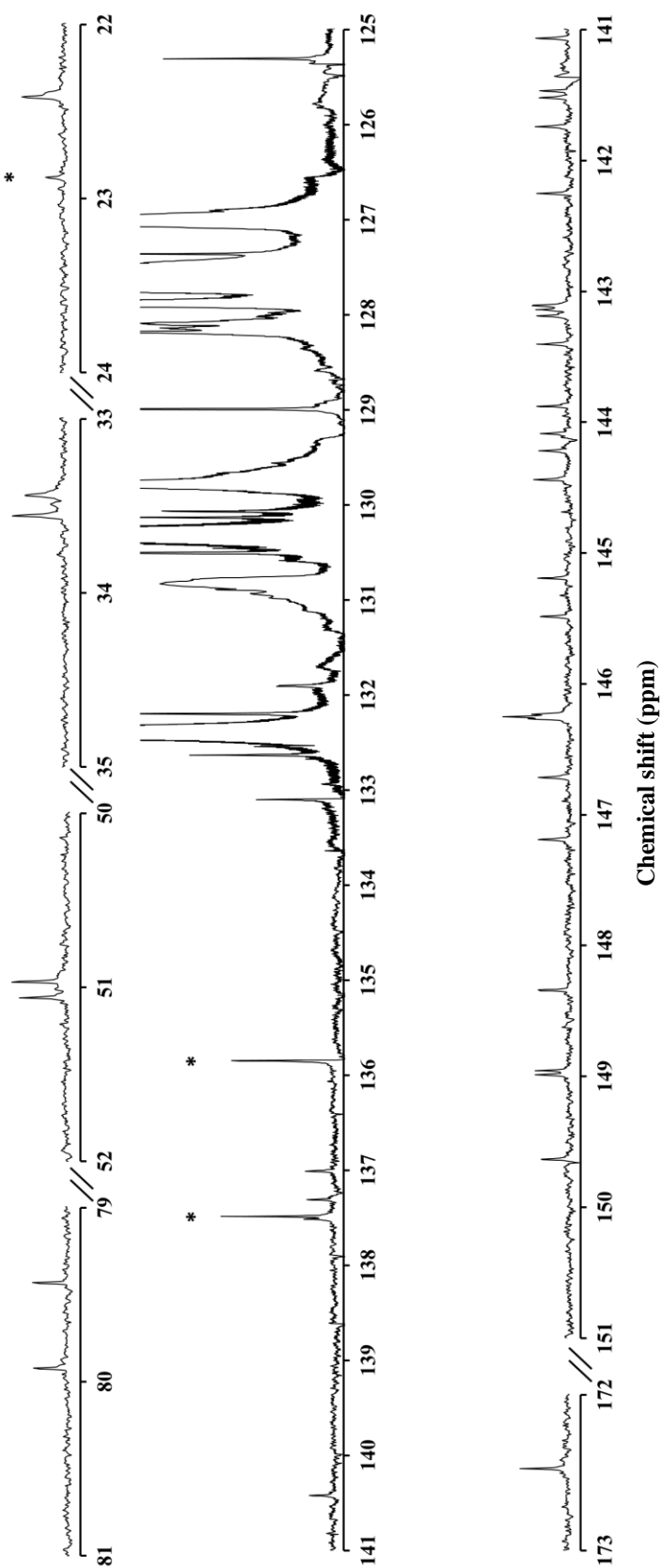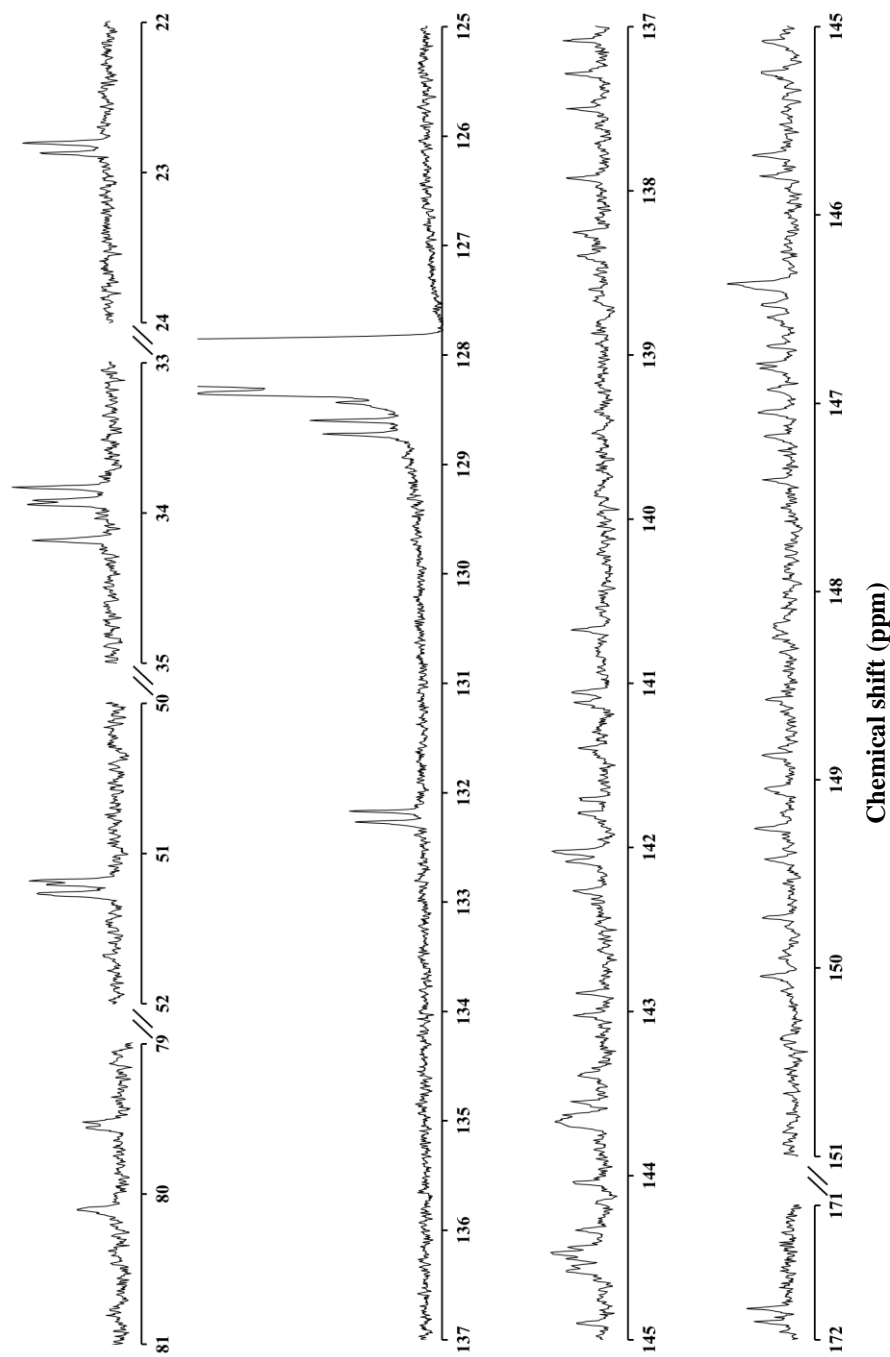
172
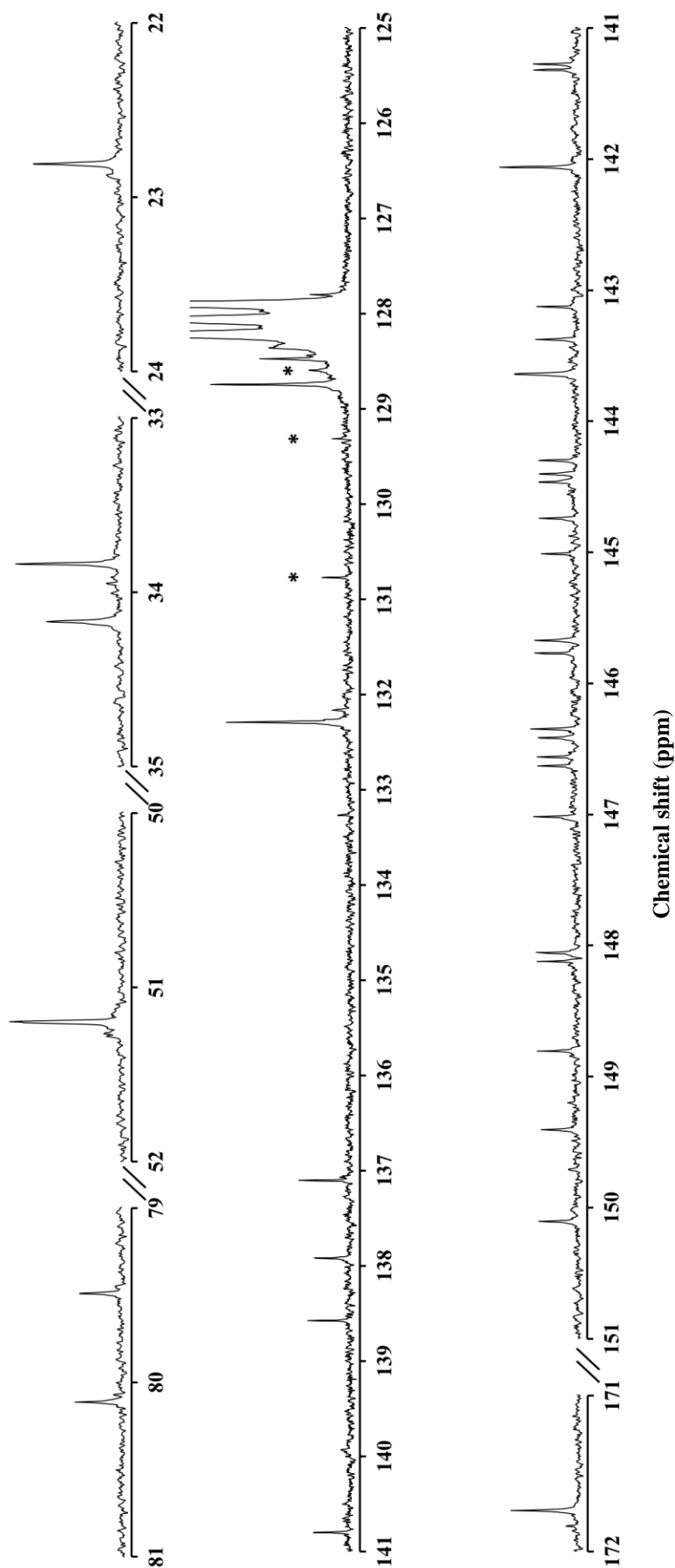
Figure 5-17 The ^{13}C NMR spectrum of HPLC fraction F3.3.1 of bis[60]PCBM.
Resonances below 81 ppm and above 125 ppm respectively originate from sp^3 and sp^2 hybridized carbons. The resonance pattern of sp^3 and sp^2 hybridized carbons are 7×2 and 35×2, respectively. This is only consistent with F3.3.1 being the isomer with C_2 symmetry in *trans-3* group.

Additional supporting evidence for this assignment is that all the other 24 fullerene resonances are all have similar intensity to each other with two coincidences that have integration of 4 carbons appear at 142.06 and 143.64 ppm, but slightly lower than the 137.10 ppm resonance. Therefore, the 137.10 ppm resonance and the other 28 resonances have difference origins with one being the phenyl carbons Ph1 and the other 28 being from the C_{60} fullerene carbons. The last resonance at 171.74 ppm can be assigned to the two symmetrically equivalent carbonyl carbons. This pattern can only be consistent with C_2 symmetry. Therefore, all lines must be doubly degenerate.

Hence, we confidently concluded that F3.3.1 is indeed one of the predicted isomer with C_2 symmetry in *trans*-3. That is either (C_2)34,35-bis[60]PCBM or (C_2)36,37-bis[60]PCBM.

Table 5-18 The ^{13}C NMR chemical shift of HPLC fractions in *trans*-3 group. The relative intensity of each resonance is labelled in the parentheses.

HPLC faction	hybridization	chemical shift (intensity)/ppm
F2.3	sp^3	21.26(2), 33.43(2), 33.55(2), 50.97(2), 51.06(2), 79.44(2), 79.93(2);
	sp^2	NO Ph. NO Ph. NO Ph. NO Ph. NO Ph. 137.01(2), 137.31(2), 137.49(2), 140.42(2), 141.07(2), 141.47(2), 141.52(2), 141.74(2), 142.25(2), 143.10(2), 143.11(2), 143.19(2), 143.40(2), 143.88(2), 144.09(2), 144.22(2), 144.44(2), 145.19(2), 145.49(2), 146.23(2), 146.25(2), 146.25(2), 146.27(2), 146.71(2), 147.19(2), 148.34(2), 148.96(2), 148.99(2), 149.64(2), 172.47(2);
F3.2.1	sp^3	22.80(1), 22.87(1), 33.83(1), 33.92(1), 33.94(1), 34.19(1), 51.18(1), 51.20(1), 51.26(1), 51.28(1), 79.52(1), 79.56(1), 80.10(1), 80.13(1);
	sp^2	128.35(1), 128.44(1), 128.60(1), 128.60(1), 128.73(1), 128.73(1), 132.17(1), 132.17(1), 132.27(1), 132.27(1), 137.09(1), 137.28(1), 137.50(1), 137.93(1), 138.26(1), 138.39(1), 140.68(1), 141.05(1), 141.12(1), 141.40(1), 141.70(1), 141.79(1), 142.03(1), 142.03(1), 142.08(1), 142.27(1), 142.88(1), 143.03(1), 143.40(1), 143.55(1), 143.64(1), 143.66(1), 143.66(1), 143.69(1), 144.04(1), 144.16(1), 144.33(1), 144.44(1), 144.44(1), 144.47(1), 144.51(1), 144.51(1), 144.55(1), 144.89(1), 145.07(1), 145.25(1), 145.68(1), 145.80(1), 146.36(1), 146.36(1), 146.48(1), 146.54(1), 146.70(1), 146.79(1), 146.81(1), 146.92(1), 147.04(1), 147.18(1), 147.40(1), 148.18(1), 148.20(1), 148.57(1), 148.87(1), 149.05(1), 149.26(1), 149.43(1), 149.73(1), 150.04(1), 171.77(1), 171.86(1);
F3.3.1	sp^3	22.81(2), 33.84(2), 34.17(2), 51.20(2), 51.20(2), 79.49(2), 80.11(2);
	sp^2	128.47(2), 128.74(2), 128.74(2), 132.29(2), 132.29(2), 137.10(2), 137.92(2), 138.58(2), 140.80(2), 141.28(2), 141.32(2), 142.06(2), 142.06(2), 143.13(2), 143.38(2), 143.64(2), 143.64(2), 144.30(2), 144.40(2), 144.46(2), 144.74(2), 145.01(2), 145.67(2), 145.77(2), 146.35(2), 146.42(2), 146.56(2), 146.63(2), 147.02(2), 148.05(2), 148.12(2), 148.81(2), 149.40(2), 150.11(2), 171.74(2);

5.3.5 *trans*-4 isomers of bis[60]PCBM

Three *trans*-4 isomers are HPLC fractions F2.2, F3.2.2 and F4. The chemical shift

of these three isomers is list in Table 5-19, and their ^{13}C NMR spectra are in the

Figure 5-18, Figure 5-19 and Figure 5-20, respectively. The spectra patterns of F2.2

and F4 have a few differences in the sp^2 region when compare to C_2 isomers in

trans-2 and *trans*-3 group. The different resonance patterns correspond to new

175

symmetry. This is expected because the isomers in *trans*-4 group are predicted to have different symmetrise of two C_s and one C_1. The details are shown below.

HPLC fraction F2.2

The spectrum of F2.2 shows that there are 7 resonances in the sp^3 region, which is consistent with C_2 and C_s symmetry. As with the symmetric isomers in the *trans*-2 and *trans*-3 groups, the first three lines come from the carbons on the two symmetrically equivalent –CH$_2$–CH$_2$–CH$_2$– chains with the first line (at 22.81 ppm) coming from the two central carbons (B3), and the others from two of B2 and B4 at 33.91 and 34.04 ppm. The different intensities indicate that the relative higher intensity resonance to be B2 carbons. The following two symmetrically equivalent bridge carbons have lower chemical shift (49.51 ppm) than the two symmetrically equivalent methyl carbons (51.30 ppm). Finally the 2 bridgehead carbon resonances at 78.50 and 78.89 ppm, that each resonance comprises two bridgehead carbons one from each addends. All 7 lines appear as double-intensity resonance.

In sp^2 region, the pattern for the phenyl carbons is different from that seen from the previous groups for the symmetric isomers. Ignoring the 'starred' toluene lines, the two quadruple-intensity phenyl ring resonances from the two symmetrically equivalent addends with their carbons Ph3/Ph5 and Ph2/Ph6 (at 128.52 and 131.97 ppm) are clearly seen, but the initial double-intensity resonance appears to be missing. However, close inspection reveals this resonance as a shoulder on the high-ppm side of the deuterated benzene signal at 128.26 ppm that comprises two Ph4 carbons. As with the other isomers, the final phenyl resonance (Ph1) is revealed by it slightly higher intensity at 137.23 ppm. This puts it after the first fullerene line for this isomer.
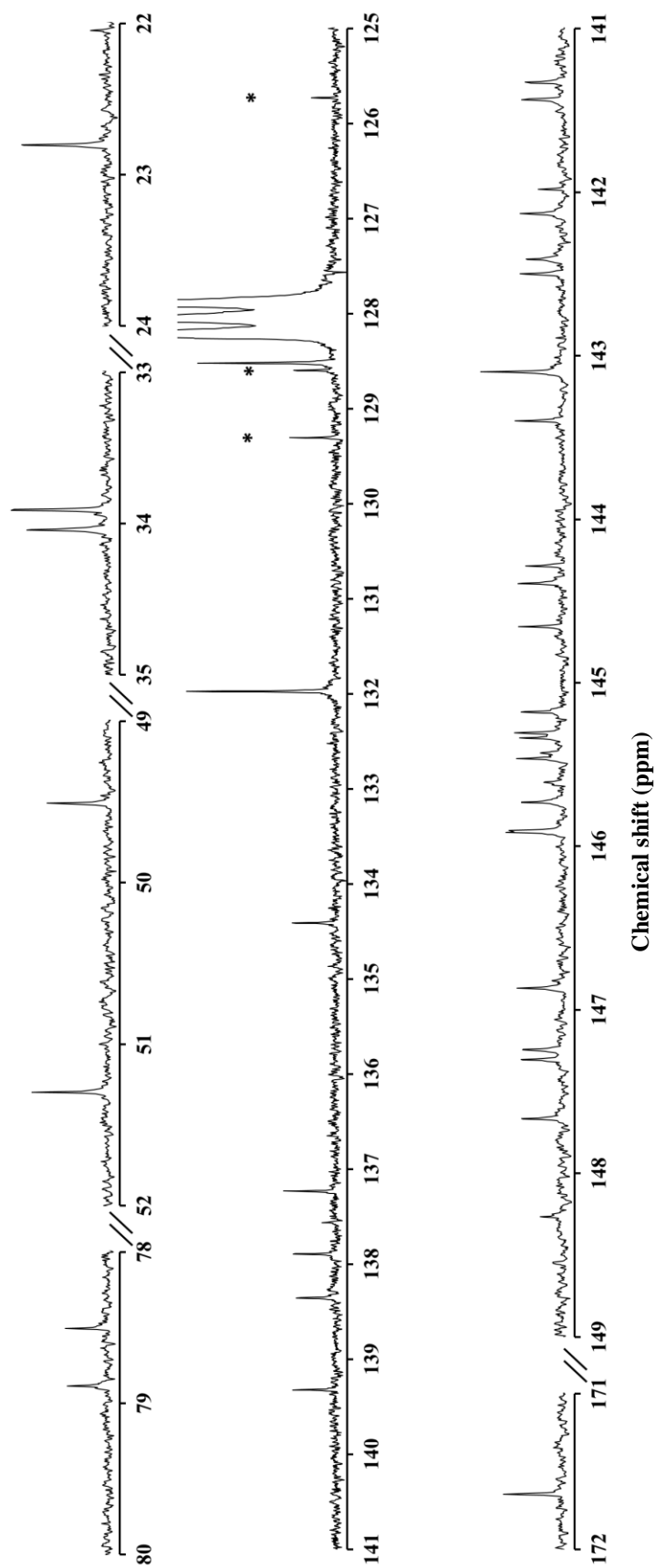
Figure 5-18 The ^{13}C NMR spectrum of HPLC fraction F2.2 of bis[60]PCBM.
Resonances below 80 ppm and above 125 ppm respectively originate from sp^3 and sp^2 hybridized carbons. The resonance pattern of sp^3 and sp^2 hybridized carbons are 7×2 and 33×2+4×1, respectively. This is only consistent with F2.2 being the isomer with C_s symmetry in *trans*-4 group.

Turning to the fullerene resonance, this is where there are major difference with the previous groups. Instead of 28 double-intensity resonances seen in the C_2 isomers, between 134 and 149 ppm there are 26 double-intensity resonances and 4 single-intensity resonances. The single-intensity lines occur at 141.98, 145.43, 145.61 and 148.26 ppm, and the lines at 143.10 ppm is an accidental coincidence of two double-intensity resonances. Finally, after a gap the resonance of the two symmetrically equivalent carbonyl carbons is seen at 171.65 ppm. In the sp^2 region, this pattern is only consistent with this isomer having C_s symmetry, hence, HPLC fraction F2.2 is assigned to be one of the C_s isomers, (C_s)32,33-bis[60]PCBM or (C_s)38,39-bi[60]PCBM, in *trans*-4 group.

Table 5-19 The ^{13}C NMR chemical shift of HPLC fractions in *trans*-4 group. The relative intensity of each resonance is labelled in the parentheses.

HPLC faction	hybridization	chemical shift (intensity)/ppm
F2.2	sp^3	22.81(2), 33.91(2), 34.04(2), 49.51(2), 51.30(2), 78.50(2), 78.89(2);
	sp^2	128.26(2), 128.52(2), 128.52(2), 131.97(2), 131.97(2), 134.41(2), 137.23(2), 137.89(2), 138.36(2), 139.32(2), 141.33(2), 141.43(2), 141.98(1), 142.13(2), 142.41(2), 142.50(2), 143.10(2), 143.10(2), 143.40(2), 144.29(2), 144.39(2), 144.66(2), 145.18(2), 145.31(2), 145.34(2), 145.43(1), 145.46(2), 145.61(1), 145.73(2), 145.91(2), 145.92(2), 146.87(2), 147.24(2), 147.31(2), 147.66(2), 148.26(1), 171.65(2);
F3.2.2	sp^3	22.72(1), 22.82(1), 33.83(1), 33.90(1), 34.08(1), 34.20(1), 49.57(1), 49.64(1), 51.13(1), 51.27(1), 78.44(1), 78.63(1), 78.97(1), 79.01(1);
	sp^2	128.27(1), 128.41(1), 128.60(1), 128.60(1), 128.75(1), 128.75(1), 132.12(1), 132.12(1), 132.16(1), 132.16(1), 134.72(1), 135.04(1), 137.26(1), 137.45(1), 137.45(1), 137.55(1), 137.79(1), 137.93(1), 138.32(1), 139.49(1), 139.84(1), 141.11(1), 141.51(1), 141.52(1), 141.74(1), 142.19(1), 142.21(1), 142.23(1), 142.33(1), 142.46(1), 142.53(1), 142.56(1), 142.90(1), 142.98(1), 143.18(1), 143.18(1), 143.40(1), 143.57(1), 143.98(1), 144.08(1), 144.30(1), 144.33(1), 145.06(1), 145.20(1), 145.30(1), 145.44(1), 145.45(1), 145.49(1), 145.52(1), 145.52(1), 145.61(1), 145.61(1), 145.64(1), 145.70(1), 145.78(1), 145.85(1), 145.86(1), 145.94(1), 145.94(1), 146.22(1), 146.43(1), 146.86(1), 147.28(1), 147.38(1), 147.43(1), 147.63(1), 148.21(1), 148.61(1), 171.66(1), 171.82(1);
F4	sp^3	22.75(2), 33.83(2), 34.28(2), 49.66(2), 51.21(2), 78.57(2), 79.08(2);
	sp^2	128.44(2), 128.77(2), 128.77(2), 132.19(2), 132.19(2), 135.33(2), 137.32(2), 137.42(2), 137.88(2), 139.99(2), 141.26(2), 141.82(2), 142.27(2), 142.40(1), 142.46(2), 142.46(2), 142.96(2), 143.05(2), 143.55(2), 143.99(2), 144.46(2), 145.06(2), 145.34(2), 145.45(2), 145.51(1), 145.55(2), 145.64(2), 145.80(2), 145.96(2), 146.10(2), 146.18(2), 146.33(1), 146.57(2), 147.33(2), 148.13(1), 148.54(2), 171.88(2);

HPLC fraction F3.2.2

The ^{13}C NMR spectrum of F3.2.2 shows a similar pattern to the previously discussed C_1 isomers as it has same number of resonances and the similar chemical shifts which appeared in the sp^3 and sp^2 regions. There are 14 lines that show up as 7 well separated pairs of resonances in the sp^3 region. The first pair of resonance appear at 22.72 and 22.82 ppm which can be assigned to the two central carbon B3

on the two symmetrically inequivalent –CH$_2$–CH$_2$–CH$_2$– chains of the ester groups, and the pair of resonances above 34 ppm to be the two B2 carbons as their relative higher intensity than the two resonances below 34 ppm which correspond to the two B4 carbons. The next two pairs near 50 and 51 ppm, with the first pair having lower intensity, belong to the two hydrogen-less bridge carbons (C61/C62) and the two methyl carbons, respectively. Finally, the last two pairs belong to the 4 bridgehead carbons which can be C1/C9/C32/C33 according to the C_1 symmetry isomer (C_1)32,33-bis[60]PCBM in *trans*-4 group, this symmetry can be confirmed from the spectrum in the sp^2 region.

In the sp^2 region from 125 to 172 ppm, ignoring the deuterated benzene centred on 128.06 ppm and residual toluene lines labelled with stars, this region begins with the carbons on the two symmetrically inequivalent phenyl rings of Ph4 at 128.27 and 128.41 ppm with intensity of one carbon. These are followed by a pair of carbons Ph3/Ph5 (total intensity of 2 carbons) at 128.60 and 128.75 ppm, and another pair of carbons Ph2/Ph6 (intensity 2) at 132.12 and 132.16 ppm. The next pair of resonances appear at 134.72 and 135.04 ppm can be assigned to the last two phenyl carbons (Ph1) with intensity 1. Then following with 51 fullerene lines with 5 coincidences of integration 2 appeared at 137.45, 143.18, 145.52, 145.61 and 145.94 ppm giving 56 resonances, and a pair of resonance from the two symmetrically inequivalent carbonyl carbons at 171.66 and 171.82 ppm. This pattern can only be consistent with C_1 symmetry. Therefore, HPLC fraction F3.2.2 can be assigned to the isomer (C_1)32,33-bis[60]PCBM in *trans*-4 group.

Figure 5-19 The ^{13}C NMR spectrum of HPLC fraction F3.2.2 of bis[60]PCBM.
Resonances below 80 ppm and above 125 ppm respectively originate from sp^3 and sp^2 hybridized carbons. The resonance pattern of sp^3 and sp^2 hybridized carbons are 14×1 and 70×1, respectively. This is only consistent with F3.2.2 being the isomer of (C_1)32,33-bis[60]PCBM in *trans*-4 group.

HPLC fraction F4

The ^{13}C NMR spectrum of F4 shows the similarity to be another C_s symmetry isomer in Figure 5-20. This matches the symmetry prediction for *trans*-4 group. For the sp^3 hybridized carbons, 7 lines in the pattern of 1, 2, 2, 2 with the chemical shift at 22.75, 33.83, 34.28, 49.66, 51.21, 78.57 and 79.08 ppm. These resonances can be assigned to the carbons on the two symmetrically equivalent –CH$_2$–CH$_2$–CH$_2$– chains, in the order of the central carbons B3, following with the two end carbons B2 with slightly higher intensity and B4. Similar to the previous C_s isomer F2.2, the hydrogen-less bridge carbons coming with lower intensity as well as the chemical shift than the following methyl carbons. Finally, the last two lines can be assigned to the 4 symmetrically equivalent bridgehead carbons. Each resonance comprises two bridgehead carbons one from each addends. All these 7 lines appear as a double-intensity resonance.

In the sp^2 region, again, ignoring the 'starred' toluene lines, the first 4 lines of phenyl ring carbons are in the pattern of double – quadruple – quadruple – double intensities in the order of the chemical shift from low-ppm to high-ppm. Similar to the previous groups for the symmetric isomers, the first double-intensity resonance at 128.44 ppm can be assigned to the two symmetrically equivalent phenyl ring carbons of Ph4, and the following two quadruple-intensity resonances at 128.77 and 132.19 ppm can be assign to the Ph3/Ph5 carbons and Ph2/Ph6 carbons. The final phenyl ring resonance (Ph1) is revealed by it slightly higher intensity at 137.32 ppm. This puts it after the first fullerene line for this isomer.

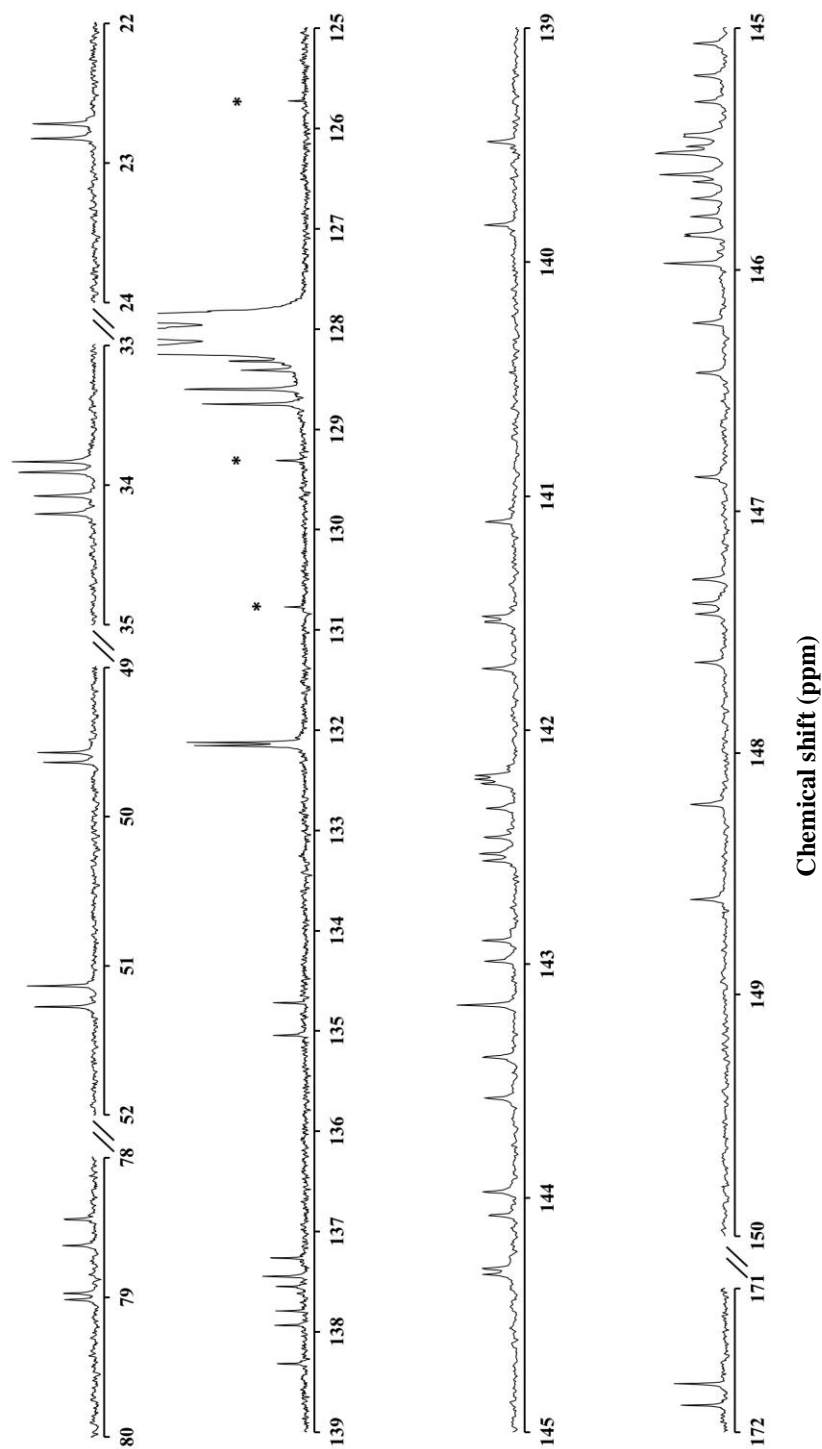**Figure 5-20 The ^{13}C NMR spectrum of HPLC fraction F4 of bis[60]PCBM.**
Resonances below 80 ppm and above 125 ppm respectively originate from sp^3 and sp^2 hybridized carbons. The resonance pattern of sp^3 and sp^2 hybridized carbons are 7×2 and 33×2+4×1, respectively. This is only consistent with F4 being the isomer with C_s symmetry in *trans–4* group.

183

The sp^2 hybridized fullerene carbons are mainly occur between 137 to 149 ppm with the first line appears at 135.33 ppm, similar to the previous C_s symmetry isomer, there are 26 double-intensity resonances that shown as 25 lines with one accidental coincidences of integration 4 occurs at 142.46 ppm, and 4 single-intensity resonances occur at 142.40, 145.51, 146.33 and 148.13 ppm. Finally, the last resonance appears at 171.88 ppm which can be assigned to the two symmetrical equivalent carbonyl carbons.

In the sp^2 region, this pattern is only consistent with this isomer having C_s symmetry. Hence, HPLC fraction F4 is assigned to be one of the C_s isomers, (C_s)32,33-bis[60]PCBM or (C_s)38,39-bis[60]PCBM, in *trans*-4 group.

5.3.6 *e* isomers of bis[60]PCBM

There are two HPLC fractions – F3.3.2 and F5.1 in the *e* group. The corresponding ^{13}C NMR spectra are in Figure 5-21 and Figure 5-22, respectively. The chemical shift of these two fractions is list in Table 5-20. The spectrum pattern of these two fractions is quite similar to each other, that means they may have same symmetries as the prediction from Section 5.4.1. The details are shown below.

HPLC fraction F3.3.2

Ignoring the contamination line occurs above 23 ppm which is labelled with a star, there are 14 resonances appear as pairs in sp^3 region. The first two lines appear at 22.66 and 22.70 ppm that can be assign to the two B3 carbons from two symmetrically inequivalent $-CH_2-CH_2-CH_2-$ chains. Then the following 4 lines appear as two close lines (at 33.83 and 33.84 ppm) in the middle of the other two lines (at 33.44 and 34.59 ppm). The inner two resonances with higher intensities

can be the two B2 carbons having faster relaxation from the neighbour carbonyl

carbon, the outer two resonances correspond to the two B4 carbons. The following

4 resonances also show the similar pattern with two slightly higher intensity

resonances (at 51.19 and 51.27 ppm) to be the two symmetrically inequivalent

bridge carbons in the middle of the other two resonances (50.96 and 53.68 ppm) to

be the two symmetrically inequivalent methyl carbons. The isomer with 14

resonances in sp^2 region can be only classified to be C_1 symmetry, this symmetry

needs to be confirmed from the sp^2 region spectrum.

In sp^2 region, the first and third lines at 128.35 and 128.55 ppm with single-

intensity come from the two symmetrically inequivalent phenyl carbons Ph4, the

second and forth resonances at 128.49 and 128.77 ppm have double-intensity are

the two of Ph3/Ph5 carbons from both addends. The following two double-intensity

resonances (131.79 and 132.16 ppm) come from the next two Ph2/Ph6 carbons.

The following two single-intensity resonances correspond to two Ph1 carbons on

the phenyl rings should be the line at 136.65 and 138.13 ppm which are relatively

higher than the other single-intensity resonances, leaving the first fullerene

resonance in the middle of Ph1 carbons. Those give 12 phenyl resonances fully

accounted. There are 53 fullerene lines appear in the sp^2 region with two accidental

coincidences occur at 142.13 ppm as a double-intensity and a triple-intensity

resonance at 144.15 ppm, giving 56 sp^2 fullerene carbons in total. The last two

single-intensity resonances at 171.61 and 171.68 ppm are assigned to the two

symmetrically inequivalent carbonyl carbons. The number of these resonances and

their relative intensity perfectly match the ^{13}C NMR prediction for C_1 symmetry.

There are only two C_1 isomers in e group, so the HPLC F3.3.2 can be assigned to

be one of the C_1 isomer, (C_1)30,31-bis[60]PCBM or (C_1)21,40-bis[60]PCBM.
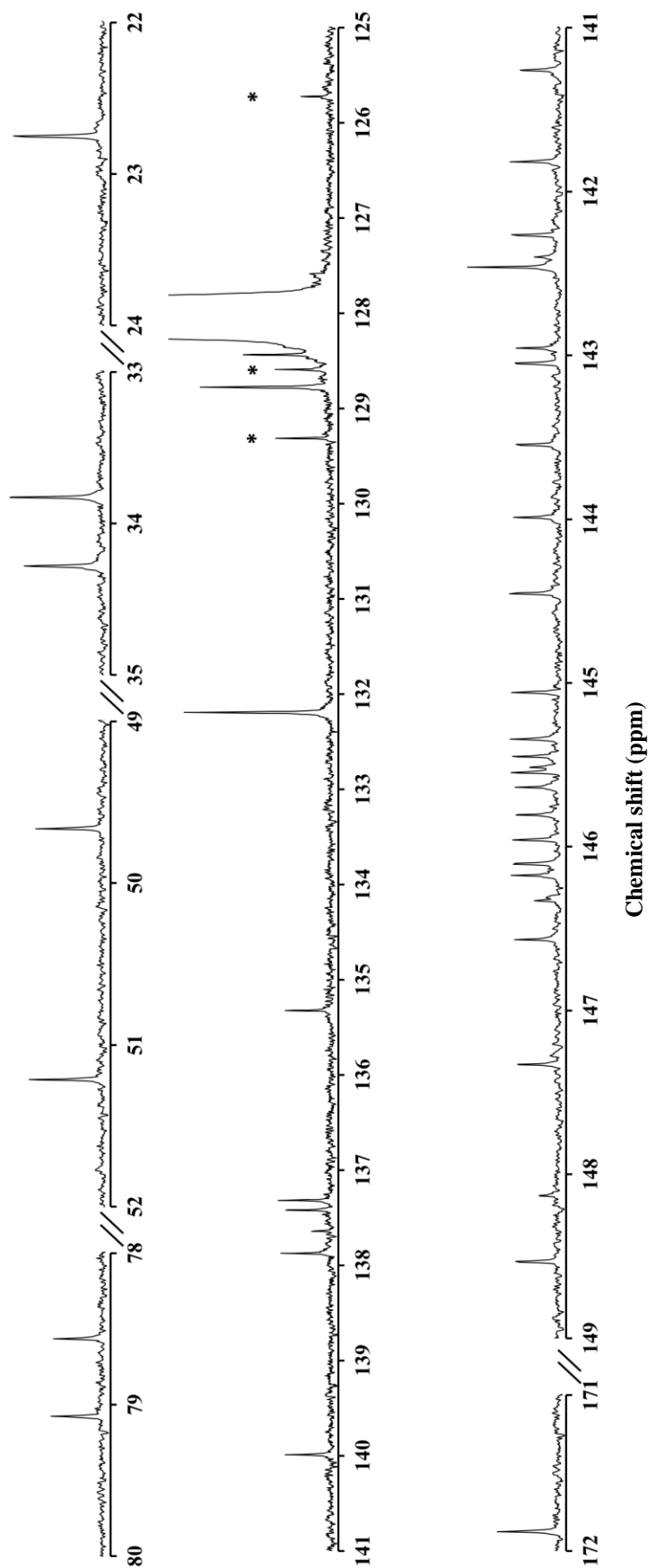
Figure 5-21 The ^{13}C NMR spectrum of HPLC fraction F3.3.2 of bis[60]PCBM.
Resonances below 81 ppm and above 125 ppm respectively originate from sp^3 and sp^2 hybridized carbons. The resonance pattern of sp^3 and sp^2 hybridized carbons are 14×1 and 70×1, respectively. This is only consistent with F3.3.2 being the isomer with C_1 symmetry in e group.

HPLC fraction F5.1

The spectrum in the sp^3 region start with the carbons on the two symmetrically inequivalent –CH$_2$–CH$_2$–CH$_2$– chains from both addends, in the order of two B3 carbons at 22.80 and 22.93 ppm. For the next two pairs of lines at 33.58, 33.82, 33.88 and 34.45 ppm, the middle two lines with relatively higher intensities can be assigned to the two B2 carbons and the outer two resonances correspond to the two B4 carbons. The following 3 lines (at 51.00, 51.22 and 53,93 ppm) ,with the line at 51.22 ppm is an accidental coincidence of a double-intensity resonance, should belong to the two symmetrically inequivalent bridge carbons and two symmetrically inequivalent methyl carbons, but it cannot tell which is which base on their relative intensity in this case. However, similar to the first C_1 isomer F3.3.2 discussed before, the two resonances appear as the accidental coincidence at 51.22 ppm possibly can be the two methyl carbons which has slightly higher intensity than the other two resonances. The last 4 lines in the sp^3 region occur at 79.32, 80.51, 80.80 and 80.86 ppm can be assigned to the four bridgehead carbons from two addends. All resonances in this region have single-intensity.

Before the analysis of sp^2 carbons from 125 - 172 ppm, there is a special line occurs at 128.59 ppm which should be a coincidence of a residual toluene line and a single-intensity carbon that comes from a phenyl ring carbon Ph4, this is because the residual toluene lines occur at 125.73, 128.59 and 129.31 ppm existed in many isomer spectra as a set, and the intensity of the toluene line at 128.59 ppm should be similar to the line at 129.31 ppm rather than doubled as show in the spectrum, and slightly higher than the line at 125.73 ppm.
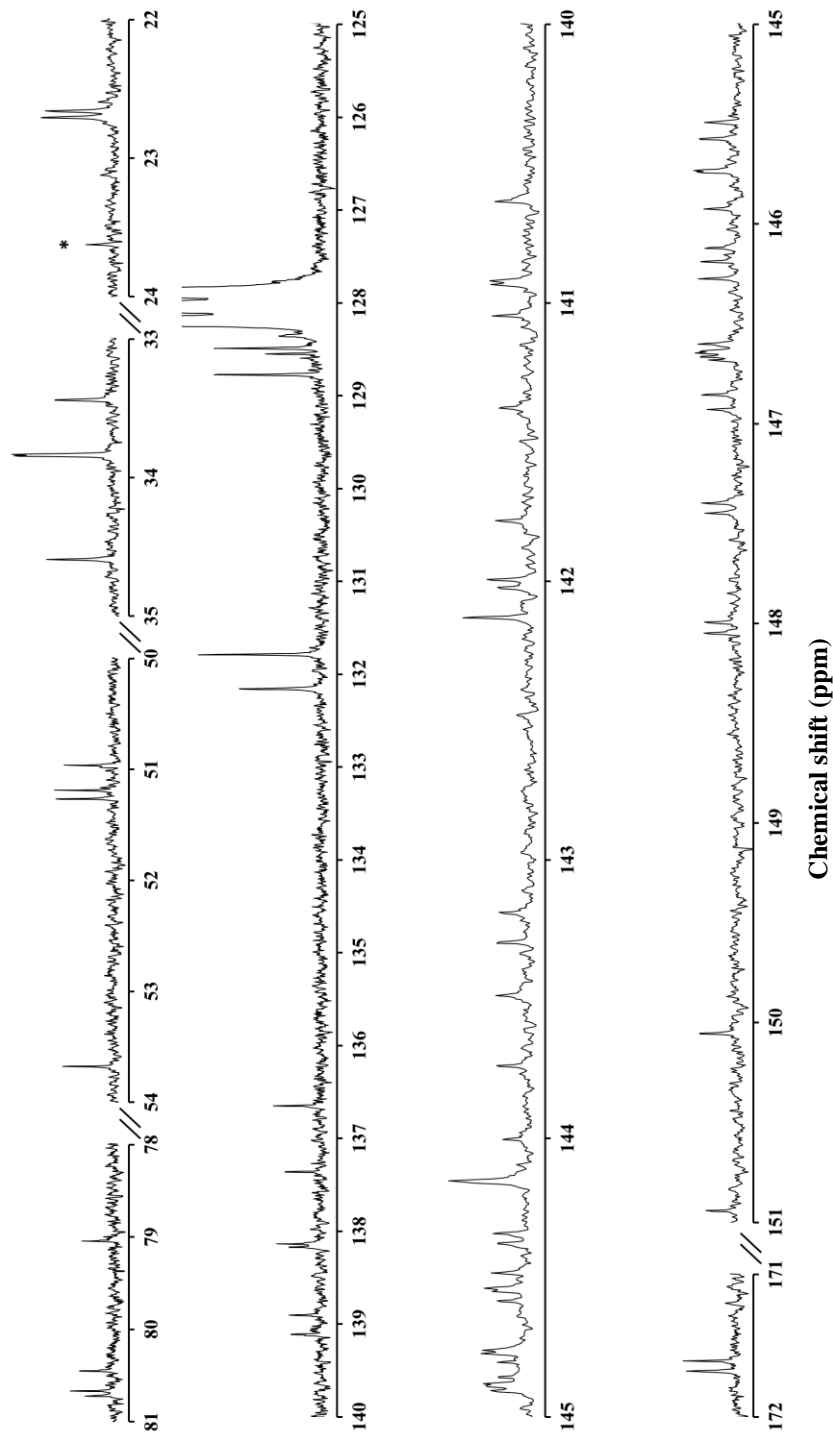
Figure 5-22 The ^{13}C NMR spectrum of HPLC fraction F5.1 of bis[60]PCBM.
Resonances below 81 ppm and above 125 ppm respectively originate from sp^3 and sp^2 hybridized carbons. The resonance pattern of sp^3 and sp^2 hybridized carbons are 14×1 and 70×1, respectively. This is only consistent with F5.1 being the isomer with C_1 symmetry in e group.

Another Ph4 carbon on the other phenyl ring appears at 128.41 ppm as a single-

intensity appears after a double-intensity resonance at 128.35 ppm which can be

assigned to the Ph3/Ph5 carbons together with another double-intensity resonance

at 128.68 ppm. After a gap, a pair of double-intensity resonances at 131.99 and

132.24 ppm come from the two symmetrically inequivalent phenyl ring carbons

Ph2/Ph6.

Table 5-20 The ^{13}C NMR chemical shift of HPLC fractions in *e* group. The relative intensity of each resonance is labelled in the parentheses.

HPLC faction	hybridization	chemical shift (intensity)/ppm
F3.3.2	sp^3	22.66(1), 22.70(1), 33.44(1), 33.83(1), 33.84(1), 34.59(1), 50.96(1), 51.19(1), 51.27(1), 53.68(1), 79.04(1), 80.45(1), 80.67(1), 80.72(1);
	sp^2	128.35(1), 128.49(1), 128.49(1), 128.55(1), 128.77(1), 128.77(1), 131.79(1), 131.79(1), 132.16(1), 132.16(1), 136.65(1), 137.35(1), 138.13(1), 138.17(1), 138.91(1), 139.11(1), 140.63(1), 140.92(1), 140.93(1), 141.04(1), 141.38(1), 141.79(1), 141.99(1), 142.03(1), 142.13(1), 142.13(1), 143.19(1), 143.30(1), 143.49(1), 143.74(1), 144.04(1), 144.15(1), 144.15(1), 144.15(1), 144.34(1), 144.37(1), 144.48(1), 144.54(1), 144.55(1), 144.58(1), 144.76(1), 144.78(1), 144.80(1), 144.86(1), 144.88(1), 144.89(1), 144.90(1), 145.49(1), 145.58(1), 145.73(1), 145.74(1), 145.93(1), 146.12(1), 146.19(1), 146.27(1), 146.60(1), 146.63(1), 146.64(1), 146.66(1), 146.68(1), 146.85(1), 146.93(1), 147.40(1), 147.45(1), 148.00(1), 148.05(1), 150.05(1), 150.94(1), 171.61(1), 171.68(1);
F5.1	sp^3	22.80(1), 22.93(1), 33.58(1), 33.82(1), 33.88(1), 34.45(1), 51.00(1), 51.22(1), 51.22(1), 53.93(1), 79.32(1), 80.51(1), 80.80(1), 80.86(1);
	sp^2	128.35(1), 128.35(1), 128.41(1), 128.59(1), 128.68(1), 128.68(1), 131.99(1), 131.99(1), 132.24(1), 132.24(1), 136.87(1), 137.47(1), 137.82(1), 137.85(1), 139.18(1), 139.39(1), 140.62(1), 141.07(1), 141.22(1), 141.39(1), 141.62(1), 141.79(1), 141.89(1), 142.02(1), 142.14(1), 142.24(1), 143.29(1), 143.40(1), 143.51(1), 143.74(1), 143.92(1), 144.07(1), 144.20(1), 144.20(1), 144.22(1), 144.26(1), 144.51(1), 144.57(1), 144.60(1), 144.77(1), 144.80(1), 144.84(1), 144.87(1), 144.89(1), 144.91(1), 145.07(1), 145.07(1), 145.20(1), 145.49(1), 145.58(1), 145.61(1), 146.00(1), 146.12(1), 146.22(1), 146.30(1), 146.31(1), 146.36(1), 146.60(1), 146.80(1), 146.91(1), 147.04(1), 147.09(1), 147.31(1), 147.36(1), 147.50(1), 147.54(1), 149.97(1), 150.81(1), 171.72(1), 171.72(1);

The following two single resonances appear at 136.87 and 137.47 ppm should be

the last two phenyl ring carbons Ph1 as they have slightly higher intensity than the

next fullerene carbons. Again, two accidental coincidences of double-intensity

lines appear at 144.20 and 145.07 ppm which give rise to 56 sp^2 fullerene single-intensity resonances, and another line at 171.72 ppm which can be assigned to the last coincidence of the two symmetrically inequivalent carbonyl carbons. This resonance pattern is only consistent to be an isomer with C_1 symmetry. Hence, the HPLC fraction F5.1 in e group can be one of the C_1 isomers, (C_1)30,31-bis[60]PCBM or (C_1)21,40-bis[60]PCBM.

5.3.7 *cis*-3 isomers of bis[60]PCBM

There are three HPLC fractions, F3.4, F5.2.1 and F5.2.2 in *cis*-3 group, their ^{13}C NMR spectra are shown in Figure 5-23 to Figure 5-25, respectively. Their chemical shifts are list in Table 5-21. Similar to the other three members group, these isomers are predicted to have two same symmetry of C_2 and one unique symmetry of C_1.

HPLC fraction F3.4

The ^{13}C NMR spectrum of F3.4 shows clearly that there are 7 lines in the sp^3 region in the pattern of 1, 2, 2, 2 which keeps this isomer to be a C_2 or C_s symmetry. The first 3 lines at 22.51, 33.61 and 33.84 ppm can be assigned to the two B3 carbons, and two of B4 and B2 carbons as the B2 carbons with a carbonyl neighbour should generate slightly higher intensity resonance than B4 carbons on the two symmetrically equivalent –CH$_2$–CH$_2$–CH$_2$– chains. The following two lines at 47.29 and 51.16 ppm come from the two symmetrically equivalent bridge carbons which have slightly lower intensity as the hydrogen-less carbon and methyl carbons. The last two lines at 77.00 and 80.32 ppm with lower intensity than the other sp^3 resonances can be assigned to the two pair of nonhydrogen attached bridgehead carbons from both addends. All these resonances have the intensity of 2 carbons.
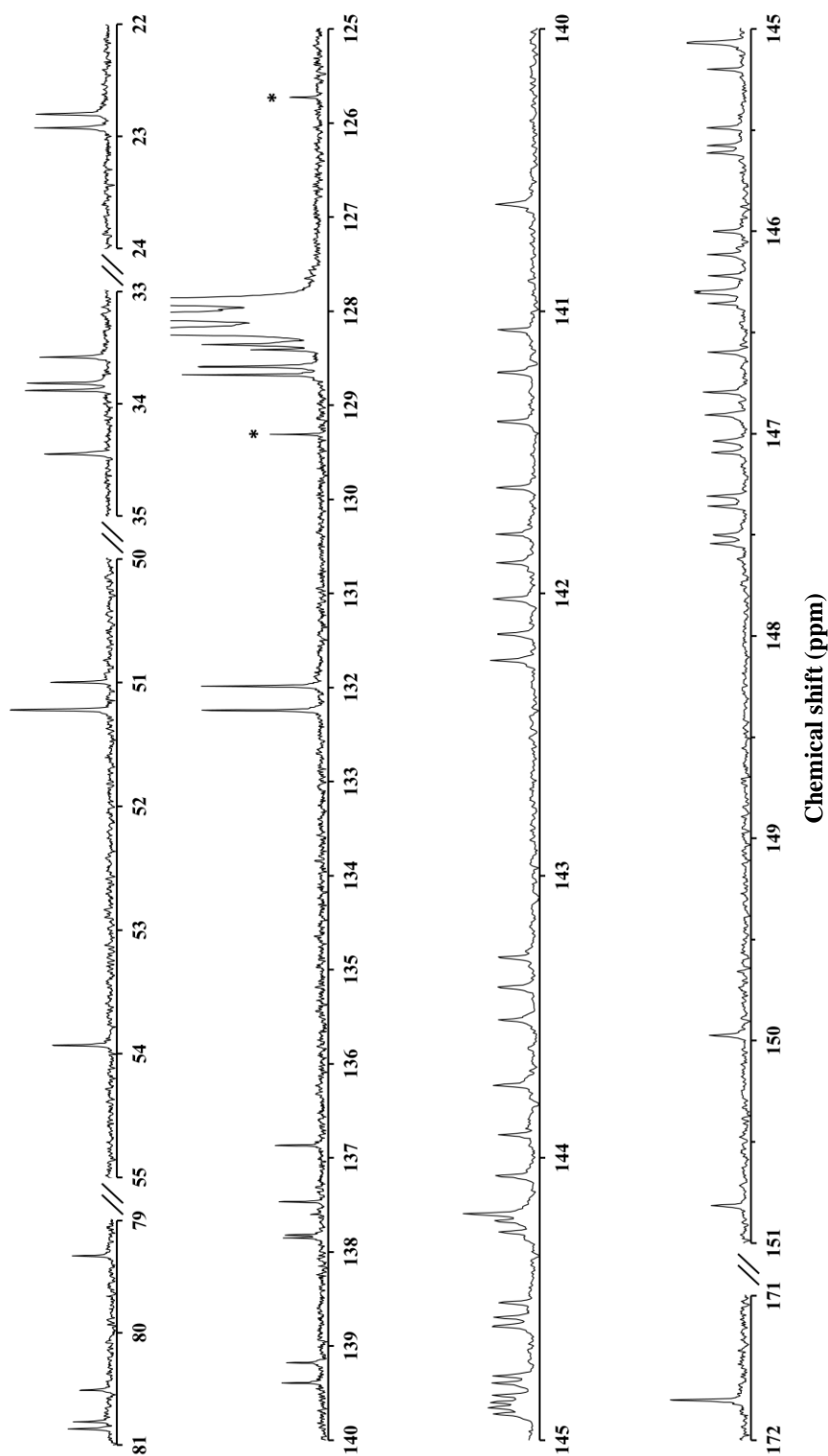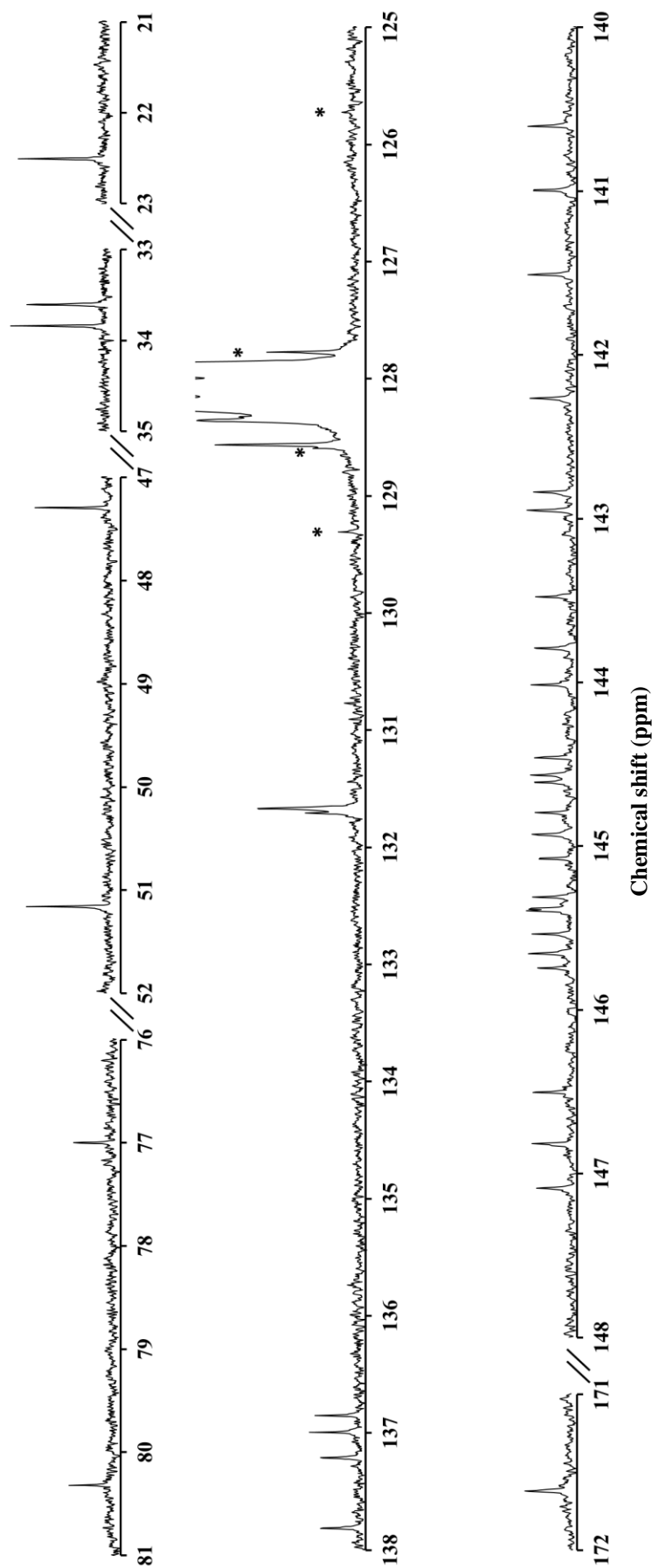
Figure 5-23 The ^{13}C NMR spectrum of HPLC fraction F3.4 of bis[60]PCBM.
Resonances below 81 ppm and above 125 ppm respectively originate from sp^3 and sp^2 hybridized carbons. The resonance pattern of sp^3 and sp^2 hybridized carbons are 7×2 and 35×2, respectively. This is only consistent with F3.4 being the isomer with C_2 symmetry in cis-3 group.

In the sp^2 region, ignoring the deuterated benzene centred on 128.06 and residual

toluene lines, the first resonance (intensity of 2 carbons) appears at 128.35 ppm is

contaminated with a sideband line coming from the carbons (Ph4) on the two

symmetrically equivalent phenyl rings. Then the following 2 lines at 128.57 and

131.67 ppm with doubled height intensity (intensity of 4 carbons) come from

Ph3/Ph5 and Ph2/Ph6 carbons from both addends. There is a resonance (at 131.71

ppm) besides the Ph2/Ph6 carbons is the last two phenyl ring carbons (Ph1). After

a gap, there are 28 resonances that all have the same intensity of 2 carbons appear

from 136-148 ppm correspond to C_{60} fullerene carbons. This number of fullerene

resonance matches the ^{13}C NMR prediction of being C_2 symmetry isomer. Finally,

a line appear at 171.62 ppm can be assigned to the two symmetrically equivalent

carbonyl carbons. As there are two C_2 isomers, (C_2)13,14-bis[60]PCBM and

(C_2)19,20-bis [60]PCBM in *cis*-3 group, the HPLC fraction F3.4 can be one of

these C_2 isomers.

Table 5-21 The ^{13}C NMR chemical shift of HPLC fractions in *cis*-3 group. The relative intensity of each resonance is labelled in the parentheses.

HPLC faction	hybridization	chemical shift (intensity)/ppm
F3.4	*sp^3*	22.51(2), 33.61(2), 33.84(2), 47.29(2), 51.16(2), 77.00(2), 80.32(2);
	sp^2	128.35(2), 128.57(2), 128.57(2), 131.67(2), 131.67(2), 131.71(2), 136.85(2), 137.00(2), 137.21(2), 137.81(2), 140.60(2), 140.99(2), 141.51(2), 142.26(2), 142.84(2), 142.95(2), 143.48(2), 143.79(2), 144.02(2), 144.46(2), 144.56(2), 144.61(2), 144.80(2), 144.93(2), 145.07(2), 145.31(2), 145.32(2), 145.38(2), 145.54(2), 145.65(2), 145.75(2), 146.50(2), 146.82(2), 147.09(2), 171.62(2);
F5.2.1	*sp^3*	22.51(2), 33.59(2), 33.92(2), 47.90(2), 51.18(2), 76.72(2), 80.30(2);
	sp^2	128.72(2), 130.77(2), 130.77(2), 132.29(2), 132.29(2), 137.03(2), 137.09(2), 137.46(2), 137.62(2), 137.83(2), 141.05(2), 141.16(2), 141.21(2), 141.90(2), 142.65(2), 142.89(2), 143.63(2), 143.78(2), 144.63(2), 144.69(2), 144.77(2), 144.80(2), 144.86(2), 144.96(2), 145.06(2), 145.19(2), 145.21(2), 145.26(2), 145.48(2), 145.66(2), 145.92(2), 146.30(2), 146.45(2), 146.62(2), 171.97(2);
F5.2.2	*sp^3*	21.93(1), 22.69(1), 33.37(1), 33.54(1), 33.87(1), 34.27(1), 47.53(1), 47.66(1), 51.24(1), 51.24(1), 76.57(1), 77.14(1), 80.03(1), 80.29(1);
	sp^2	Ph4(1), Ph4(1), 128.49(1), 128.49(1), 128.63(1), 128.63(1), 130.79(1), 131.81(1), 131.81(1), 132.17(1), 132.17(1), 132.40(1), 136.86(1), 136.88(1), 137.18(1), 137.24(1), 137.40(1), 137.40(1), 137.42(1), 137.89(1), 140.74(1), 140.83(1), 140.87(1), 141.22(1), 141.39(1), 141.43(1), 141.63(1), 142.42(1), 142.72(1), 142.80(1), 142.85(1), 142.97(1), 143.51(1), 143.55(1), 143.77(1), 143.78(1), 143.88(1), 144.38(1), 144.59(1), 144.61(1), 144.63(1), 144.67(1), 144.68(1), 144.74(1), 144.87(1), 144.88(1), 144.91(1), 144.93(1), 145.11(1), 145.11(1), 145.20(1), 145.26(1), 145.28(1), 145.29(1), 145.31(1), 145.37(1), 145.38(1), 145.55(1), 145.59(1), 145.63(1), 145.79(1), 145.86(1), 146.07(1), 146.43(1), 146.52(1), 146.70(1), 146.72(1), 147.39(1), 171.76(1), 171.79(1);

HPLC fraction F5.2.1

Excluding a residual toluene line (labelled with a star) at 21.93 ppm, there are 7 lines appear in the *sp^3* region in the pattern of 1, 2, 2, 2 which is constant to be C_2 or C_s symmetry. Similar to the other symmetrical isomers, the first 3 lines can be assigned from the two symmetrically equivalent –CH$_2$–CH$_2$–CH$_2$– chains, in the order of two B3 carbons at 22.51 ppm, and two B4 and B2 carbons at 33.59 and 33.92 ppm from the relative intensity. A wide gap is well separated the two

symmetrically equivalent bridge carbons (at 47.90) from higher intensity resonance of methyl carbons at 51.18 ppm. Finally, the last two lines at 76.72 and 80.30 ppm can be assigned to the 4 bridgehead carbons. They have lower intensity than the other sp^3 lines because they each have no attached hydrogens. The two bridgehead carbons from the same addend are not on any mirror plane, and therefore are not symmetrically equivalent. In this case, they give two lines. As there are only two bridgehead resonances which present for 4 bridgehead carbons, the two bridgehead pairs are symmetrically equivalent. All these 7 resonances have the intensity of 2 carbons.

In the sp^2 region, there are multiple contaminations labelled with stars appeared in the range of phenyl rings lines. However, it is still possible to identify the phenyl ring lines based on the spectra from previous analysed C_2 and C_s symmetrical isomers. There should have 4 lines in the intensity pattern of double-quadruple-quadruple-double come from the carbons on the two symmetrically equivalent phenyl rings in the order of Ph4 carbons, Ph3/Ph5 carbons, Ph2/Ph6 carbons and Ph1 carbons, because this pattern appeared in all the isomers which have C_2 or C_s symmetry. Excluding the residual benzene and residual toluene lines, the first short line (intensity of 2) at 22.51 ppm can be assigned to the Ph4 carbons, then the next two higher lines (intensity of 4) appear at 130.77 and 132.29 ppm can only be the Ph3/Ph5 and Ph2/Ph6 carbons. Therefore, the first 3 resonances from two symmetrically equivalent phenyl rings are fully identified.

Figure 5-24 The ^{13}C NMR spectrum of HPLC fraction F5.2.1 of bis[60]PCBM.
Resonances below 81 ppm and above 125 ppm respectively originate from sp^3 and sp^2 hybridized carbons. The resonance pattern of sp^3 and sp^2 hybridized carbons are 7×2 and 35×2, respectively. This is only consistent with F5.2.1 being the isomer with C_2 symmetry in cis-3 group.

The last phenyl ring line is mixed in with the initial fullerene lines. There are 28 fullerene resonances between 137 and 147 ppm with equally intensity suggest that this isomer is having C_2 symmetry instead of C_s, and those resonances are double-intensity giving fully 56 sp^2 fullerene carbons. Finally, the last line at 171.97 ppm comes from the two symmetrically equivalent carbonyl carbons. Hence, HPLC fraction F5.2.1 can be one of the two C_2 isomers, (C_2)13,14-bis[60]PCBM or (C_2)19,20-bis [60]PCBM in *cis*-3 group.

HPLC fraction F5.2.2

From the ^{13}C NMR spectrum of F5.2.2, there are 13 lines appeared instead of 14 expected for C_1 symmetry isomer in the sp^3 region. This problem is solved by looking at the line at 51.24 ppm. This line has roughly double the intensity than the other sp^3 lines, suggesting that it can be an accidental coincidence of two resonances. Similar to the other C_1 isomers, the first pair of resonances at 21.93 and 22.69 ppm can be assigned to the two B3 carbons on the two symmetrically inequivalent –CH$_2$–CH$_2$–CH$_2$– chains, and the next two pairs resonances are at 33.37, 33.54, 33.87 and 34.27 ppm, with the first pair (at 33.37 and 33.54 ppm) having higher intensity can be assigned to the two B2 carbons and the other pair resonances to be B4 carbons. There is an accidental coincidence appear at 51.24 ppm in the group of bridge carbons and methyl carbons. According to the line pattern of bridge carbons and methyl carbons from the other C$_1$ isomers, it can temporally assign that the first two lines and the coincidence are correspond to a pair of bridge carbons and methyl carbons. Here is not possible and unnecessary to tell which of the resonances is which of the bridge or methyl carbons for the molecular structure determination. However, the resonance of bridge carbons appear at sp^3 region can still be the evidence that this isomer is cyclopropa-

fullerene. Finally, the last four lines come from 4 bridgehead carbons are appear at 76.57, 77.14, 80.03 and 80.29 ppm. Hence, F5.2.2 can be identified to be a C_1 isomer. This conclusion also can be confirmed from the spectrum in the sp^2 region.

In the sp^2 region, without counting the deuterated benzene and residual toluene lines labelled with stars, the first line is of high intensity and occurs at 128.49 ppm. It belongs to a coincidence of Ph3 and Ph5 carbons from one of the two symmetrically inequivalent phenyl rings. The next resonance is at 128.63 ppm can be assigned to the Ph3 and Ph5 carbons from one of the other phenyl ring group. However, the intensity of this line is lower than the first, which is accounted for by it being broader. This suggests that the Ph3 and Ph5 carbons on this ring are less chemically equivalent than these carbons are on the first ring – resulting in less of a coincidence. In the spectra of the other isomers the first group of line in the sp^2 region belongs to the phenyl Ph4 carbon(s), whereas in this spectrum the first line comes from the Ph3/Ph5 carbons (which is the second group of line in the other isomers). As there is no evidence of a resonance from Ph4 carbon after the first line, it can be concluded that this resonance does, as usual, come before the Ph3/Ph5, but cannot be seen as it is merged with the very intense line from the deuterated benzene signal lock. Indeed, close inspection of the trailing edge of the benzene lines reveals a small shoulder, which is likely to be from one of the two symmetrically inequivalent Ph4 carbon, with the other Ph4 carbon being unseen as it occurs completely under the benzene resonance. The resonances from the two symmetrically inequivalent Ph2/Ph6 phenyl pairs occur at 131.81 and 132.16 ppm. Similarly, the two Ph3/Ph5 pairs, one pair is more intense than the other owing to one being broader than the other.
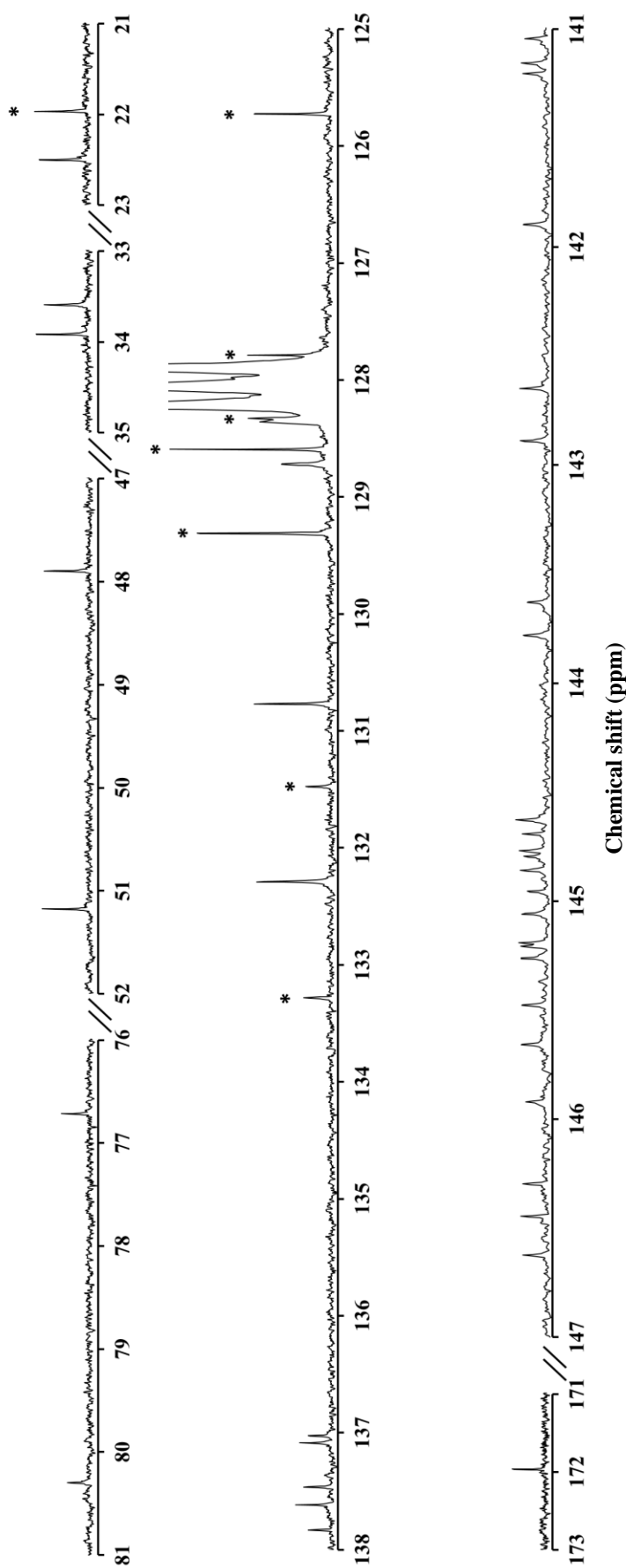
Figure 5-25 The ^{13}C NMR spectrum of HPLC fraction F5.2.2 of bis[60]PCBM.
Resonances below 81 ppm and above 125 ppm respectively originate from sp^3 and sp^2 hybridized carbons. The resonance pattern of sp^3 and sp^2 hybridized carbons are 14×1 and 70×1, respectively. This is only consistent with F5.2.2 being the isomer (C_1)13,14-bis[60]PCBM in cis-3 group.

The reason for this is likely to be the same, whereby the members from one of the two Ph2/Ph6 pairs are in more chemically equivalent environment than the members of the other pair. The resonances of Ph1 carbons from the two symmetrically inequivalent phenyl rings are mix with 54 fullerene lines. Mixed with the phenyl resonances are two fullerene resonances at 130.79 and 132.40 ppm. For the remaining fullerene resonances there are two accidental coincidences occur at 137.40 and 145.11 ppm which have the intensity of 2 carbons, and 52 single intensity resonances, which account for all 56 sp^2 fullerene carbons to be sure that F5.2.2 is the isomer that has C_1 symmetry. Finally, the carbonyl carbons are occur at 171.76 and 171.79 ppm. Hence, HPLC fraction F5.2.2 can be only assigned to the unique isomer (C_1)13,14-bis[60]PCBM in *cis*-3 group.

5.3.8 *cis*-2 isomers of bis[60]PCBM

There are 3 HPLC fractions, F5.3, F6 and F7 in *cis*-2 group. The ^{13}C NMR spectra of these three isomers are shown in Figure 5-26, Figure 5-27 and Figure 5-28, respectively. The chemical shifts are list in Table 5-2. This is the last three members group which is predicted to have two C_s and one C_1 symmetries. The details are shown below.

HPLC fraction F5.3

The sp^3 region spectra of F5.3 gives 7 lines in the pattern of 1, 2, 2, 2 which can determine that this isomer has C_s or C_2 symmetry. The first 3 of these lines appear at 22.93, 33.60 and 33.71 ppm can be assigned to the carbons on the two symmetrically equivalent –CH$_2$–CH$_2$–CH$_2$– chains, in the order of two B3 carbons, and two of B4 and B2 carbons as the B2 carbons has relative higher intensity. The

next two lines can be assigned to the two symmetrical hydrogen-less bridge carbons at 49.64 ppm and the symmetrical methyl carbons at 51.23 ppm. Finally, the four bridgehead carbons are showing as two lines at 75.49 and 78.13 ppm under the symmetry of C_s or C_2. All 7 lines have the intensity of 2 carbons.

The varying intensities of the spectrum from the fullerene carbons in sp^2 region show a clue to identify the symmetry for this isomer. Without counting the deuterated benzene and residual toluene lines, the resonance from the two symmetrically equivalent phenyl ring carbons Ph4 is not clearly seen as it is coincident with the much higher intensity benzene signal. There are only 2 high integration lines in the range of phenyl rings resonances (128 – 138 ppm) which appear in all the other isomers, together with 2 very short lines which may come from the fullerene carbons. However, the intensity of the first of these lines, which occurs at 128.69 ppm and is assigned to the Ph3/Ph5 pair from the two symmetrically equivalent phenyl ring groups, has a slightly lower intensity (owing to being broader) than the other high integration line. This second phenyl ring line occurs at 132.32 ppm and is assigned to the two Ph2/Ph6 pairs. The explanation for the Ph3/Ph5 pair being broader than the Ph2/Ph6 pair is that the chemical environments of the Ph2/Ph6 pair are more similar in the two phenyl rings than the two Ph3/Ph5 pairs. For the resonances of fullerene carbons, they are appeared between 130 – 151 ppm which mixed with one phenyl ring resonance from Ph1 carbons.
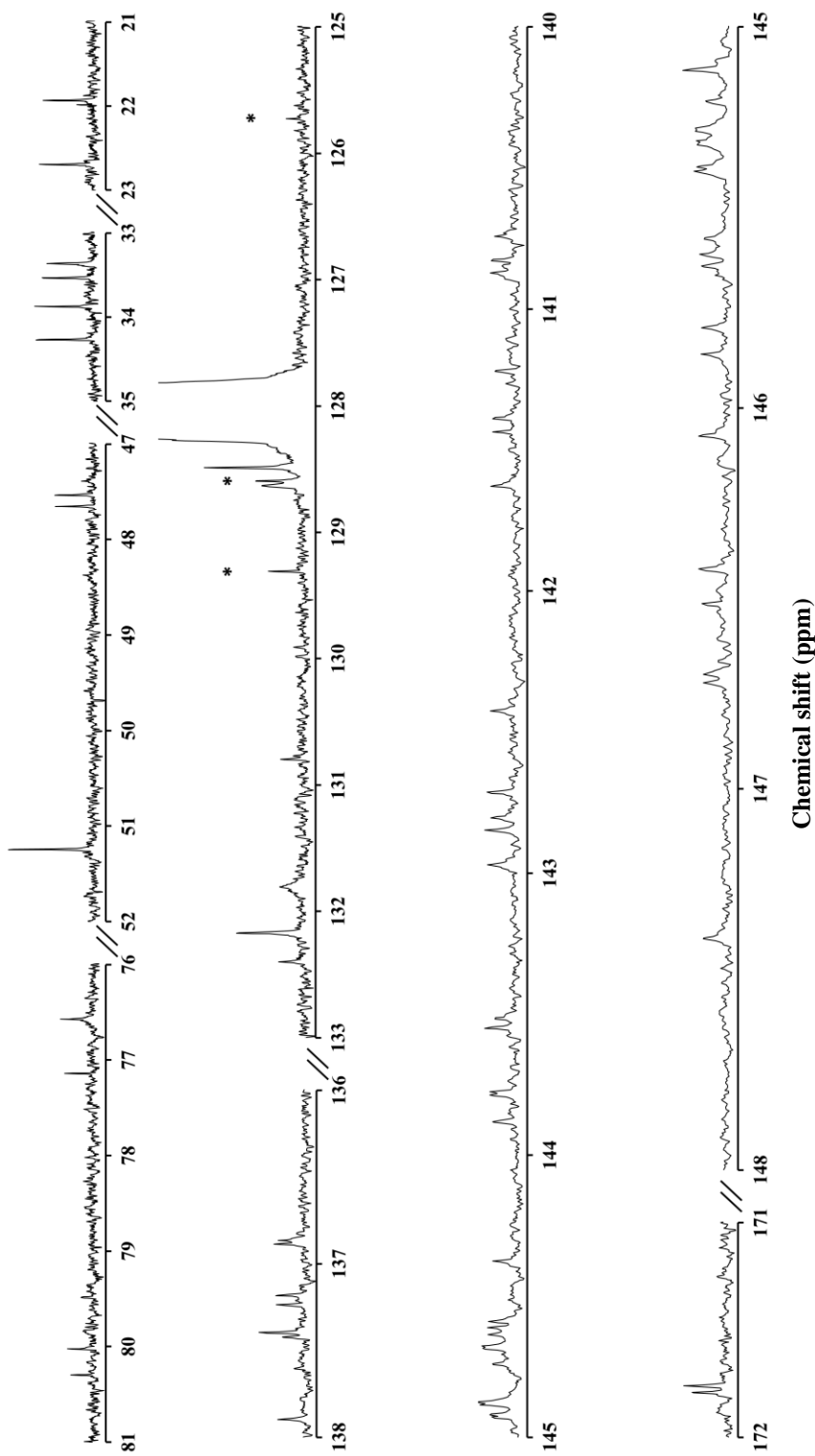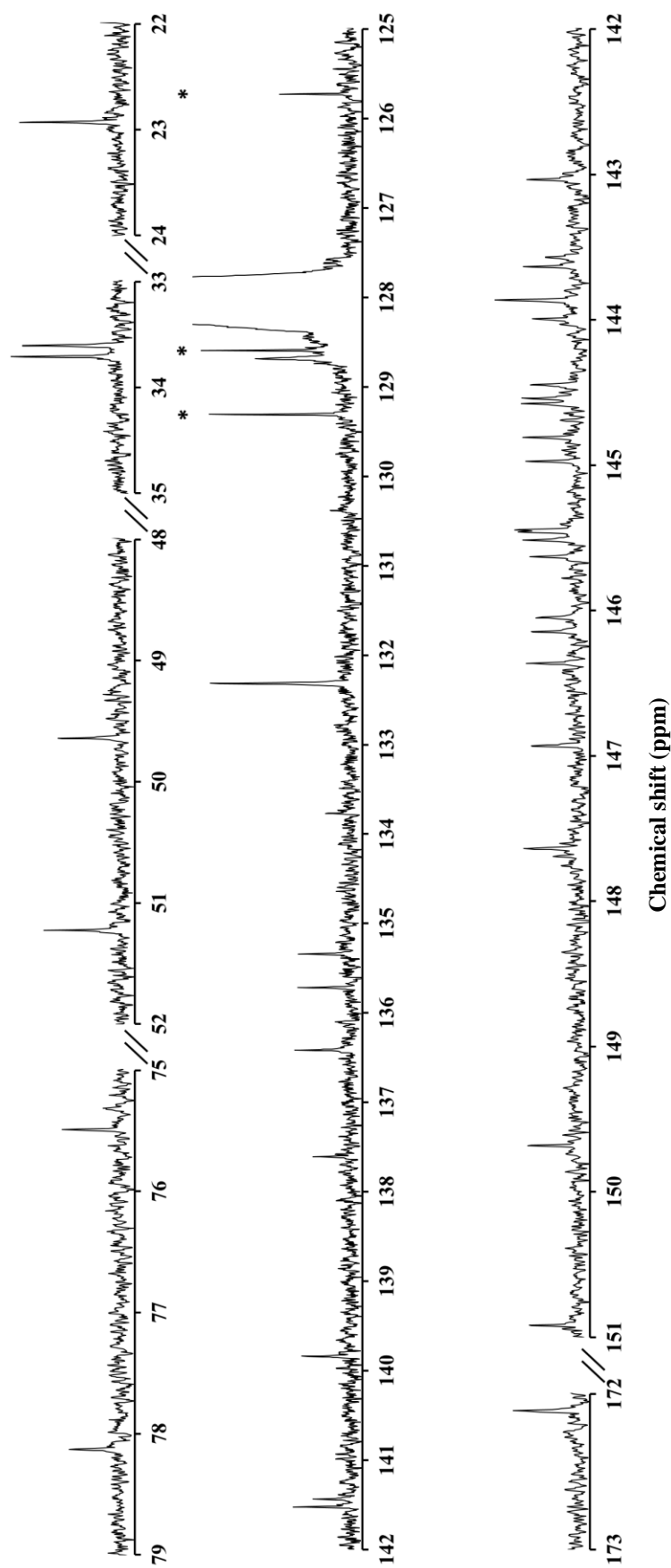
Figure 5-26 The ^{13}C NMR spectrum of HPLC fraction F5.3 of bis[60]PCBM.
Resonances below 79 ppm and above 125 ppm respectively originate from sp^3 and sp^2 hybridized carbons. The resonance pattern of sp^3 and sp^2 hybridized carbons are 7×2 and 33×2+4×1, respectively. This is only consistent with F5.3 being the isomer with C_s symmetry in cis-2 group.

There are single and double intensity lines exist in the fullerene range, but the number of lines is not very clear to match the C_s symmetry in this isomer. However, there are much less lines than 56 to be a C_1 isomer and more lines than 28 to be a C_2 isomer, and looking the integration of the line at 143.87 ppm, it shows that the intensity of 3 carbons which could explain that this accidental coincidence resonance comprises an e carbon and two symmetrically equivalent carbons on the C_{60} fullerene. With the other 3 single-intensity lines appear at 130.38, 133.77 and 143.57 ppm, all four e carbons are fully counted. Putting together with the remaining 26 double intensity resonances, all 56 sp^2 fullerene carbons are identified. The last line at 172.11 ppm can be assigned to the two symmetrically equivalent methyl carbons.

The resonance format of this isomer illustrates that it has C_s symmetry. As there are two predicted C_s molecular structures, (C_s)3,15-bis[60]PCBM and (C_s)4,18-bis[60]PCBM in *cis*-2 group, we could not to identify F5.3 to be which C_s isomer based on the ^{13}C NMR spectrum.

Table 5-22 The ^{13}C NMR chemical shift of HPLC fractions in *cis*-2 group. The relative intensity of each resonance is labelled in the parentheses.

HPLC faction	hybridization	chemical shift (intensity)/ppm
F5.3	sp^3	22.93(2), 33.60(2), 33.71(2), 49.64(2), 51.23(2), 75.49(2), 78.13(2);
	sp^2	Ph4(2),　128.69(2), 128.69(2), 130.38(1), 132.32(2), 132.32(2), 133.77(1), 135.34(2), 135.72(2), 136.42(2), 137.61(2), 139.84(2), 141.43(2), 141.53(2), 143.03(2), 143.57(1), 143.64(2), 143.87(1), 143.87(2), 144.00(2), 144.45(2), 144.54(2), 144.58(2), 144.81(2), 144.98(2), 145.44(2), 145.46(2), 145.52(2), 145.63(2), 146.05(2), 146.14(2), 146.36(2), 146.93(2), 147.64(2), 149.69(2), 150.92(2), 172.11(2);
F6	sp^3	22.55(1), 23.11(1), 32.77(1), 33.42(1), 33.61(1), 34.09(1), 49.14(1), 49.51(1), 51.25(1), 51.28(1), 74.73(1), 75.40(1), 78.23(1), 78.35(1);
	sp^2	128.31(1), 128.46(1), 128.60(1), 128.60(1), 128.66(1), 128.66(1), 130.78(1), 131.76(1), 131.76(1), 132.31(1), 132.31(1), 133.26(1), 133.27(1), 135.68(1), 135.76(1), 136.09(1), 136.15(1), 136.66(1), 139.15(1), 139.69(1), 141.32(1), 141.53(1), 141.57(1), 141.79(1), 142.82(1), 142.86(1), 143.64(1), 143.80(1), 143.81(1), 143.85(1), 143.94(1), 143.95(1), 143.99(1), 144.00(1), 144.02(1), 144.28(1), 144.46(1), 144.47(1), 144.55(1), 144.55(1), 144.55(1), 144.62(1), 144.68(1), 144.97(1), 145.34(1), 145.44(1), 145.49(1), 145.49(1), 145.53(1), 145.56(1), 145.73(1), 145.76(1), 146.06(1), 146.07(1), 146.08(1), 146.13(1), 146.20(1), 146.26(1), 146.36(1), 146.87(1), 147.60(1), 147.61(1), 147.72(1), 147.78(1), 148.91(1), 150.04(1), 150.57(1), 152.13(1), 171.67(1), 171.85(1);
F7	sp^3	22.53(2), 32.90(2), 33.70(2), 49.02(2), 51.22(2), 74.66(2), 78.67(2);
	sp^2	128.44(2), 128.44(2), 128.44(2), 130.77(1), 131.51(2), 131.51(2), 132.73(1), 135.98(2), 136.00(2), 136.33(2), 139.33(2), 141.39(2), 141.91(2), 142.76(2), 143.56(2), 144.01(2), 144.03(2), 144.08(2), 144.11(2), 144.48(2), 144.66(2), 145.35(2), 145.38(2), 145.51(2), 145.54(2), 145.57(2), 145.91(2), 145.91(2), 146.11(2), 146.16(2), 146.30(2), 147.55(1), 147.71(2), 147.79(1), 149.37(2), 151.86(2), 171.66(2);

HPLC fraction F6

The ^{13}C NMR spectrum of F6 shows 14 lines in pairs in the sp^3 region from 22 – 79 ppm. Those lines keep same pattern to the other C_1 isomers. The first pair of lines at 22.55 and 23.11 ppm come from the two central B3 carbons on the two symmetrically inequivalent –CH$_2$–CH$_2$–CH$_2$– chains, followed by two of B4 carbons at 32.77 and 33.42 ppm having relative lower intensity than the two of B2

carbons at 33.61 and 34.09 ppm. The next four lines group as two pairs which can be assigned to the two nonhydrogen bridge carbons at 49.51 and 51.25 ppm with lower intensity, leaving another pair at 51.28 and 74.73 ppm to be the two symmetrically inequivalent methyl carbons. Finally, the last 4 lines with lower intensity than other sp^2 resonances can be identified to be the 4 bridgehead carbons that have no hydrogen attached from both addends, therefore, under C_1 symmetry.

All these 14 singe-intensity resonances appeared in the sp^3 region show that this isomer has C_1 symmetry. It means that we expect to see 56 sp^2 fullerene lines, 2 carbonyl lines, and the resonances of phenyl ring carbons may exist like the previous C_1 isomers that giving 4 pairs of resonances in the intensity pattern of single–double–double–single from Ph4, Ph3/Ph5, Ph2/Ph6, Ph1 carbons. Excluding the deuterated benzene and toluene lines, the first two single-intensity resonances at 128.31 and 128.46 ppm can be assigned to the two Ph4 carbons on the two symmetrically inequivalent phenyl ring groups. The first of these two lines is raised in intensity because it appears overlapped with the tail of the third benzene line. The following two double-intensity resonances at 128.60 and 128.66 ppm are the two Ph3/Ph5 carbons, as one of the residual toluene often appears at 128.59 ppm which is merged together with the line at 128.60 ppm, making the resonance at 128.60 slightly higher than the resonance at 128.66 ppm. The next two double-intensity resonances on phenyl ring groups from Ph2/Ph6 are appear at 131.76 and 132.31 ppm. However, the intensity of these two double-intensity resonances are lower than the first pair, which are accounted for by it being broader. This suggests that the Ph2 and Ph6 carbons on both rings are less chemically equivalent than Ph3/Ph5 carbons, and the resonance at 131.76 ppm of Ph2/Ph6 carbons on one of the phenyl ring is even broader than the other – resulting in less of a coincidence.

Figure 5-27 The ^{13}C NMR spectrum of HPLC fraction F6 of bis[60]PCBM.
Resonances below 79 ppm and above 125 ppm respectively originate from sp^3 and sp^2 hybridized carbons. The resonance pattern of sp^3 and sp^2 hybridized carbons are 14×1 and 70×1, respectively. This is only consistent with F6 being the isomer (C_1)3,15-bis[60]PCBM in cis-2 group.

This maybe because the phenyl ring attached to carbon C61 is near to the ester
group that attached to C62 whereas the phenyl attached C62 is oriented away from
the ester on C61, this is can be seen in the Figure 5-7(b). The next two single-
intensity resonances for the Ph1 carbons are mixed with fullerene lines from 135 –
137 ppm where they are 5 single-intensity resonances from carbons with no
attached hydrogens. As the fullerene and Ph1 resonances would have similar
intensities, we cannot tell which of the 5 lines come from the two Ph1 carbons.
Allowing for a coincidence of 3 resonances at 144.55 ppm and a coincidence of 2
resonances at 145.49 ppm, the line pattern is consistent with C_1 symmetry as there
are 56 sp^2 fullerene single-intensity resonances. The two carbonyl carbons occur at
171.67 and 171.85 ppm. Therefore, the HPLC fraction F6 is assigned to the *cis*-2
isomer with C_1 symmetry, (C_1)3,15-bis[60]PCBM.

HPLC fraction F7

In the sp^3 region, the spectrum of F7 shows 7 lines in the pattern of 1, 2, 2, 2 which
illustrate this isomer may has C_s or C_2 symmetry. According to the previous
discussion, these 7 double-intensity resonances are assigned to the carbons on the
two symmetrically equivalent $-CH_2-CH_2-CH_2-$ chains, in the order of two B3
carbons at 22.53 ppm, and two of B4 and B2 carbons at 32.90 and 33.70 ppm based
on their relative intensity. The resonance from B2 carbons are slightly higher than
that of B4 carbons because the carbonyl carbon as a neighbour of B2 carbons gives
faster relaxation than the no hydrogen attached carbon neighbour of B4 carbons.
Then the next two lines (at 49.02 ppm) can be assigned to the two symmetrically
equivalent hydrogen-less bridge carbons with slightly lower intensity than the two
symmetrically equivalent methyl carbons at 51.22 ppm. Finally, the four
bridgehead carbons appear as two lines at 74.66 and 78.67 ppm having lower

intensity than the other sp^3 lines because each of them has no attached hydrogens. The two bridgehead carbons from the same addend are not on any mirror plane, and therefore are not symmetrically equivalent. In this case, they give two lines. As there are only two bridgehead resonances which present for 4 bridgehead carbons, the two bridgehead pairs are symmetrically equivalent. To know what symmetry this isomer has, the spectrum in sp^2 region need to be analysed.

Ignoring the deuterated benzene and residual toluene lines labelled with stars, the first lines at 128.44 ppm is quite high than any other lines in this sp^2 region. The integration shows it is a resonance of intensity of 6 carbons illustrating that it is a coincidence of two Ph4 carbons and two pairs of Ph3/Ph5 carbons from the two symmetrically equivalent phenyl ring groups. The resonances appears at 131.51 ppm of integration 4 can be assigned to the two pairs of Ph2/Ph6 carbons from symmetrically equivalent phenyl ring groups. As with the other isomers, the resonance of Ph1 carbons maybe the line at 136.33 ppm according to the relative higher intensity than fullerene resonances and is mixed with the fullerene resonances. The fullerene resonances occur between 130 and 152 ppm. With a coincidence of two pairs of symmetrically equivalent resonances appear at 145.91 ppm, and four single-intensity resonance at 130.77, 132.73, 147.55 and 147.79 ppm, the overall pattern for fullerene carbons is the same as that for F5.3, which is 26 double-intensity resonances and 4 single-intensity resonances, indicating that this isomers has C_s symmetry. The final resonance gives a single line of integration 2 from the two symmetrically equivalent carbonyl at 171.66 ppm. There are two C_s isomers in cis-2 group as predicted, (C_s)3,15-bis[60]PCBM and (C_s)4,18-bis[60]PCBM. Hence, F7 can be the other of these two isomers.
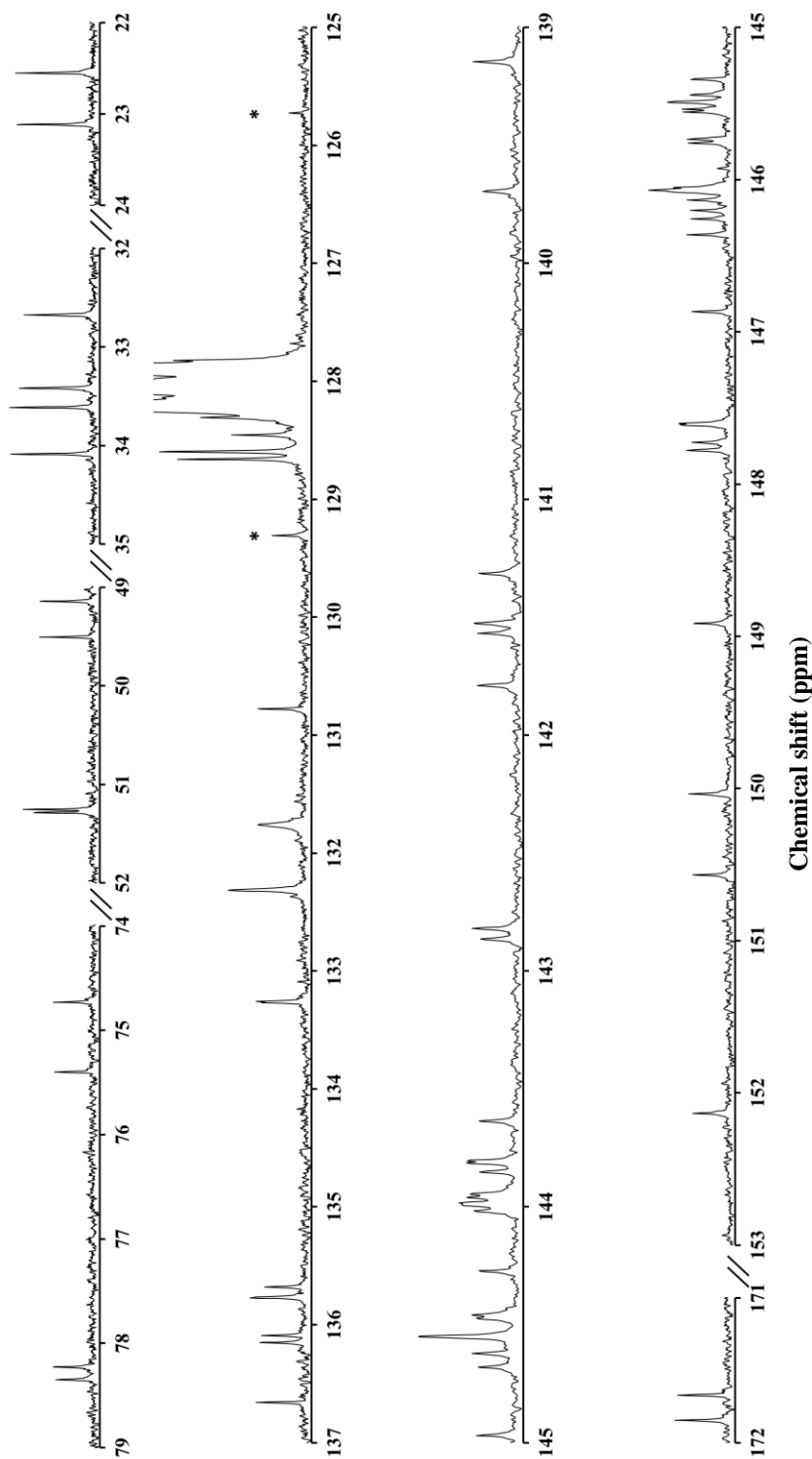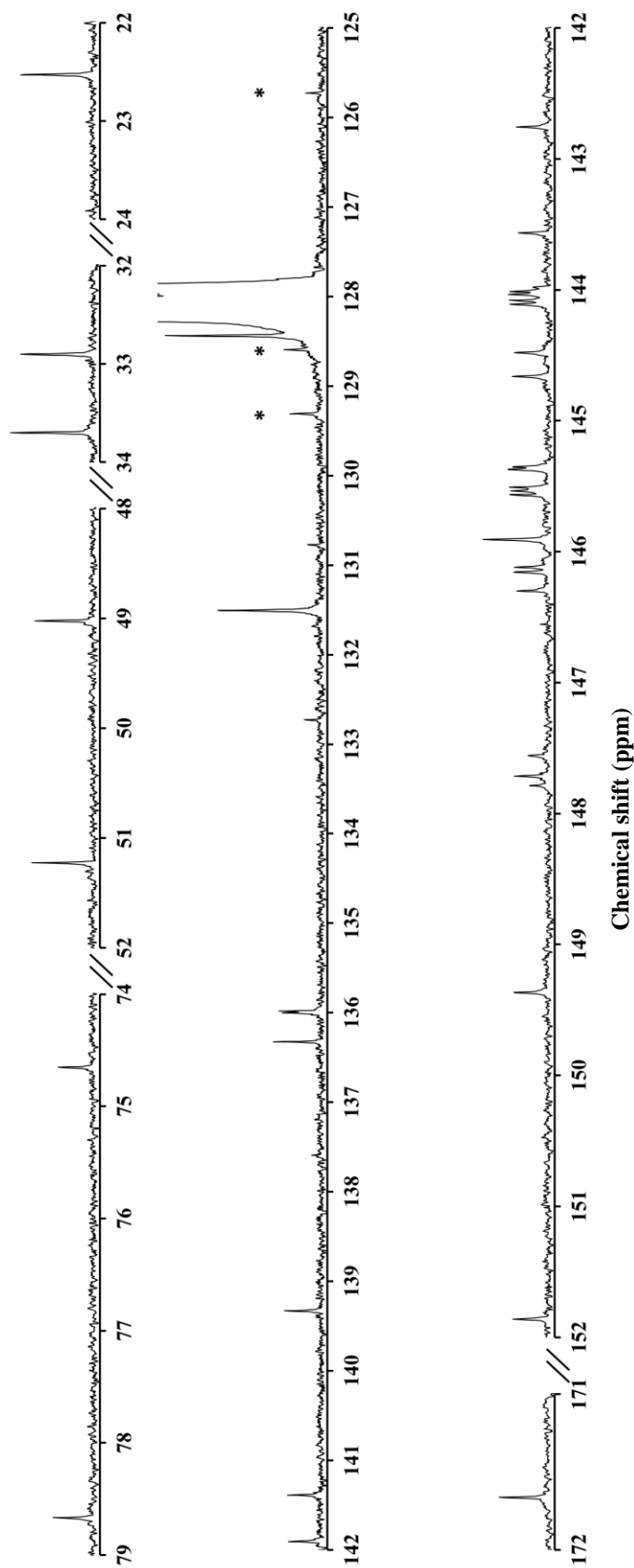
Figure 5-28 The ^{13}C NMR spectrum of HPLC fraction F7 of bis[60]PCBM.
Resonances below 79 ppm and above 125 ppm respectively originate from sp^3 and sp^2 hybridized carbons. The resonance pattern of sp^3 and sp^2 hybridized carbons are 14×1 and 70×1, respectively. This is only consistent with F7 being the isomer with C_s symmetry in cis-2 group.

Chemical shift (ppm)

5.3.9 Conclusion of 19 isomers of bis[60]PCBM

By the above examination of the resonances from ^{13}C NMR spectra, it confirms with the expected isomers that 1) all the isomers are cyclopropa-fullerene; 2) there are two isomers in C_2 symmetry and one isomer in C_1 symmetry in the groups of *trans*-2, *trans*-3 and *cis*-3, then two C_s and a C_1 isomers in the groups of *trans*-4 and *cis*-2 of the three members groups. For the two members groups, *trans*-1 does have a C_{2v} and by elimination a C_{2h} isomers, and two isomers both have C_1 symmetry in *e* group. Therefore, the isomer which has the unique symmetry (C_{2v} and C_1) in the groups of *trans*-1, *trans*-2, *trans*-3, *trans*-4, *cis*-3 and *cis*-2 can be identified (list in Table 5-23), leaving the two indistinguishable symmetric HPLC fractions in the same group cannot be determined.

Looking at the symmetry patterns from Table 5-23, we have found that: 1) from the three members groups except *cis*-3, it is *symmetric – asymmetric – symmetric* format by following the HPLC fraction order which is the retention time for each isomer need to be collected from the purification stage; and 2) the HPLC fraction order of the 7 so far uniquely identified isomers is inversely correlate with the distance between the addends. That is, a shortest retention time corresponds to an isomer that the second addend is the furthers apart from the first addend on the C_{60} cage, and vice versa.

Table 5-23 The structural assignment for unique symmetry isomer in each bond type by ^{13}C NMR spectroscopy.

bond type	HPLC fraction	symmetry	isomer assignment
trans-1	F1.1	C_{2h}	(C_{2h})52,60-bis[60]PCBM
	F2.1.1	C_{2v}	(C_{2v})52,60-bis[60]PCBM
trans-2	F1.2	C_2	-
	F2.1.2	C_1	(C_1)49,59-bis[60]PCBM
	F3.1	C_2	-
trans-3	F2.3	C_2	-
	F3.2.1	C_1	(C_1)34,35-bis[60]PCBM
	F3.3.1	C_2	-
trans-4	F2.2	C_s	-
	F3.2.2	C_1	(C_1)32,33-bis[60]PCBM
	F4	C_s	-
e	F3.3.2	C_1	-
	F5.1	C_1	-
cis-3	F3.4	C_2	-
	F5.2.1	C_2	-
	F5.2.2	C_1	(C_1)13,14-bis[60]PCBM
cis-2	F5.3	C_s	-
	F6	C_1	(C_1)3,15-bis[60]PCBM
	F7	C_s	-

5.4 Correlation of same symmetry isomers by HPLC fraction order

To aid in the isomer assignments, density functional theory (DFT) calculations were used. Reasonable input geometries were made by drawing the molecular structure of each of the 19 isomers using the Discovery Studio software[159] followed by an initial 'molecular mechanics' geometry optimisation. These geometries were used as the input geometries for the DFT optimisations. These were performed using the High-Performance Computing facility at Queen Mary University of London with tight cut-offs within the Gaussian 16 package[140] at the B3LYP/cc-pVTZ level coupled with Grimme D3 empirical dispersion with Beck-Johnson

dampening on a superfine grid (Route Section keywords "opt=tight B3LYP/cc-pVTZ empiricaldispersion=gd3bj int=grid=superfine"). The resulting direct-line spacing between the two ester B4 carbons of each of the 19 isomers was measured using the Gaussview v6.0 Software.[160] In the traditional normal-phase chromatography, the stationary phase is constructed from a polar material (e.g., silica or alumina) while the mobile phase is non-polar solvent such as hexane. In the reversed phase chromatography, it is the opposite. The stationary phase is non-polar and the mobile phase is polar. With this, in the normal-phase chromatography low-polarity materials tend to be held in the non-polar solvent solutions better than high-polarity materials. Similarly, high-polarity eluents adsorb onto the polar mobile phase better than low-polarity eluents. The combination of these two effects is that the least polar compound elutes first and the most polar compound elute last. Conversely, in the reverse-phase chromatography high-polarity materials tend to be held in the polar solvent solutions better than low-polarity materials, and low-polarity eluents adsorb better onto the low-polarity mobile phase than high-polarity eluents. This time the combination of these two effects means that the more polar compounds elutes first and the least polar compounds elute last. However, such behaviour is not seen in chromatography of fullerenes.

Fullerenes are sparsely soluble in polar solvents, and hence are separated in non-polar solvents. Early work on fullerene chromatography employed the alumina as the stationary phase. Therefore, it was a traditional form of the normal-phase chromatography. However, having C_{60} elutes before C_{70} in normal-phase chromatography cannot be explained because of dipolar interactions with either the mobile or stationary phases. This is because I_h-C_{60} and $D_{5h(6)}$-C_{70} both have zero simulated dipole moment (from B3LYP/cc-pVTZ optimized geometry). Indeed,

C_{60} also elutes before C_{70} on non-polar (the reverse-phase) columns, but elution orders should be reversed between normal-phase and reverse-phase chromatography.

However, there is a general pattern within fullerene HPLC showing that the more curved surface of the fullerene the shorter its retention time. There is an increase in retention time as the size of the fullerene increases for reasonable spherical fullerenes. For example, the I_h-C_{60}, D_2(IV)-C_{84} and D_{2d}(II)-C_{84} are among the most 'spherical' fullerenes (as their aspect ratios are very nearly identical). The retention time of the two C_{84} isomers are longer than that of C_{60} owing to the two C_{84} isomers having a larger radius of curvature than C_{60}, but they are almost equal to each other, the difference is about just 6 seconds over retention times of about 20 minutes.[120]

In a similar way, the retention time of isomers of the same fullerene increases as the curvature of the surface decreases. As an example of this, Figure 5-29(a) and (b) show the two isomers of the fullerene C_{84} that have same D_{2d} symmetry, D_{2d}(I)-C_{84} and D_{2d} (II)-C_{84}, with the z-axis (the principle C_2 axis) horizontal and in the plane of the paper. In these orientations the two molecules look quite dissimilar with one being reasonably oval while the other is reasonably round. Like I_h-C_{60} and $D_{5h(6)}$-C_{70}, both D_{2d} isomers of C_{84} have zero calculated electric dipole moment. However, the round isomer (b) is the first of the 10 known isomers of C_{84}[120, 121, 161] to elute from the HPLC column; whereas the oval isomer (a) is the last of the C_{84} isomers to elute from the column (eluting after the larger fullerene C_{86}[121].

As explained in the Section 2.1.4 of the Theory Chapter, columns developed for fullerene separation are designed to take advantage of $\pi-\pi$ interactions between the π-bonds of the fullerene and those of the stationary-phase coating (for example, a tri-dinitrophenyl-based unit for the Buckyclutcher[128], a pyrene-based unit for the

buckyprep and PYE columns[129] columns and a pentabromobenzene-based unit for the PBB[130] column). With this, the retention-time behaviour of fullerenes can be understood. That is, for a particular fullerene, those with reasonably low-curvature areas on their surfaces will have the longer retention times than those with more curved surfaces, and that the larger the low-curvature area of the fullerene the longer the retention times.

(a)   (b)
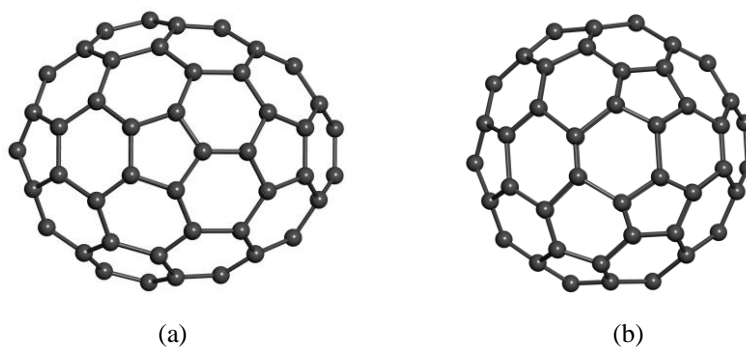
Figure 5-29 The two isomers of the fullerene C$_{84}$ that have D_{2d} symmetry.
(a) D_{2d}(I)-C$_{84}$ and (b) D_{2d}(II)-C$_{84}$. Both of them have zero calculated electric dipole moment, D_{2d}(I)-C$_{84}$ and D_{2d} (II)-C$_{84}$ are the first and last of the 10 known isomers of C$_{84}$ to elute from the reverse-phase buckprep column, respectively. This wide difference in HPLC behaviour may be explained by the large low-curvature areas at the top and bottom of D_{2d}(I)-C$_{84}$ in the figure. This results in stronger $\pi-\pi$ interactions between the fullerene and the pyrene unit of the stationary phase (compared with D_{2d}(II)-C$_{84}$) which gives a longer retention time).

The word 'polarity' is often used in the literature to describe retention-time behaviour of fullerenes. However, this polarity cannot be related to the electric dipole moment. A striking example of the 'polarity' not being the expected electric dipole comes from the two *trans*-1 isomers of bis[60]PCBM. One of these isomers, (C_{2h})52,60-bis[60]PCBM, has the lowest calculated (by B3LYP/cc-pVTZ optimization) electric dipole moment of any of the 19 isomers of bis[60]PCBM at zero as shown in Table 5-24. In seeming agreement with the usual normal-phase principle that the lower the dipole moment the lower the retention time, this isomer has is the first to elute from the normal-phase silica column. On the other hand, the

other polar isomer, (C_{2v})52,60-bis[60]PCBM, has the highest calculated electric

dipole moment of the isomers (4.56 debyes). However, rather than being the last

of the 19 isomer to elute (which the calculated electric dipole would predict),

(C_{2v})52,60-bis[60]PCBM is only the third of the 19 isomers to elute - and it is so

on both the normal-phase silica column and the two different reverse-phase

columns (PYE and PBB) used in this thesis.

At the other end of the HPLC retention-time range, the final three isomers to elute

from all columns used here are the three *cis*-2 isomers. The calculated electric

dipole moments of these isomers are: 4.15, 1.59 and 1.46 debyes for (C_1)3,15-

bis[60]PCBM, (C_s)3,15-bis[60]PCBM and (C_s)3,18-bis[60]PCBM, respectively.

This again shows no retention-time correlation with the calculated electric dipole

moment. For example, of the three *cis*-2 isomers, the two with the widest retention-

time separation have the same dipole moment (about 1.5 D), and the one with the

largest dipole moment (4.15 D) elutes in between them.

To illustrate the point that HPLC retention time of these fullerene derivatives is

based on a shape-based 'dipole', Figure 5-30 shows (a) a *trans*-1 isomer (low

polarity/early eluting), (b) an equatorial isomer (medium polarity/mid eluting) and

(c) a *cis*-2 isomer (high polarity/late eluting). By this it means that if the addend

attached to the 1,9 bond is placed at the top of the molecule then *cis*-2 isomers have

high shape-polarity as the top (with two very close addends) is different from the

bottom (with no addends at all), whereas the *trans*-1 isomers have low shape-

polarity because the top (with its attached addend) is similar to the diametrically

opposite bottom (with its attached addend). The equatorial isomers have the end

addend roughly midway between these two extremes.

<div align="center">(a)   (b)   (c)</div>
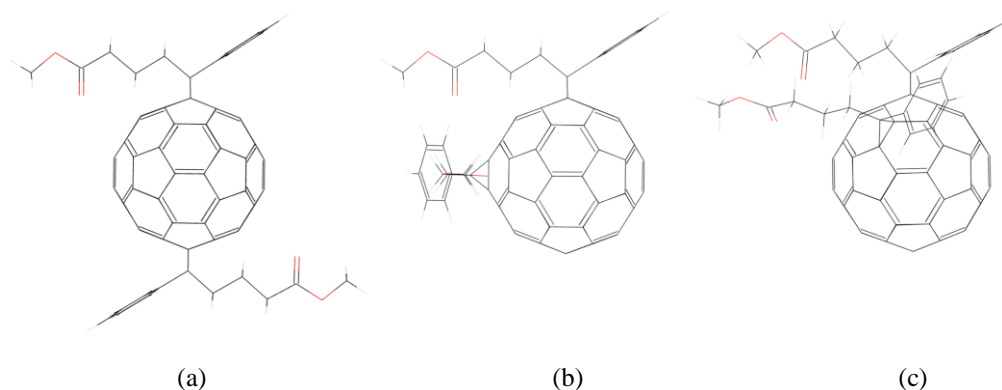
Figure 5-30 The shape-polarity of fullerenes and their derivatives.
(a) a *trans*-1 isomer, (b) an *e* isomer and (c) a *cis*-2 isomer of bis[60]PCBM. The
cis-2 isomer is considered to be of high polarity owing to it having one end that is
markedly different to the other, which is not the case for the low polarity *trans*-1
isomer (as both are the same). The *e* isomer is of mid polarity.

When comparing the HPLC behaviour of all the isomers, it is noted that there is a
relationship between HPLC retention time and bond type. For example, the first 4
isomers to come off the HPLC column all involve either the *trans*-1 or the *trans*-2
bond type (i.e., the isomers with the most widely spaced and the second-most
widely spaced bond types), whereas, as mentioned above the last three isomers to
come off the column are the three *cis*-2 isomers, which have the three closest
spaced bond type. The two *e* isomers have intermediate retention time being the
11th and 14th isomers to come off the column. Such behaviour is consistent with the
general behaviour of fullerenes column as the order goes in order of increasing
shape-based polarity. Such an explanation fits in with the notion that greater $\pi-\pi$
interactions between the fullerene and stationary phase give longer retention times.
For the *cis*-2 isomers, both addends are very close together leaving a large amount
of the fullerene π-rich surface exposed to interact with π-network of the pyrene or
pentabromobenzene units on their respective columns, which results in relatively
long retention times. On the other hand, for the *trans*-1 isomers, these $\pi-\pi$
interactions are blocked at both the top and the bottom of the molecule by the two

addends. This results in reduced $\pi-\pi$ interactions, which leads to shorter retention

times. The *e* isomers are seen to be intermediate in blocking the $\pi-\pi$ interactions.

Extending this observation to all bond types, from the ^{13}C NMR analysis for

bis[60]PCBM isomers, the retention time of the known C_1 isomer from each of the

bond-type groups is in the order of *trans*-2, *trans*-3, *trans*-4, *e*, *e*, *cis*-3 and *cis*-2.

Hence, it is seen that the retention time order of the isomers is dependent on the

separation of the two addends. All 7 C_1 isomers follow this pattern. It is also noted

that the two *trans*-1 isomers also follows this pattern with the (C_{2h})52,60-

bis[60]PCBM isomer eluting before the (C_{2v})52,60-bis[60]PCBM isomer. With

this, all 9 known isomers following this pattern without exception. This lends

strong support to the idea that the retention time of the bis[60]PCBM isomers is

inversely correlated to the separation between the two addends.

Another observation that can be made about the HPLC behaviour of the isomers

which can be obtained from the ^{13}C NMR analysis is that within each three

membered group the isomers come off the HPLC column in the order of *symmetric*

– asymmetric – symmetric as mentioned above from Table 5-23. For example, the

order for the three *trans*-2 isomers is $C_2 - C_1 - C_2$, and the order of the three *cis*-2

isomers is $C_s - C_1 - C_s$. As such, the two same-symmetry isomers appear to be well

separated in HPLC retention order. For example, the two *trans*-4 isomers with C_s

symmetry are the 5th and 13th isomers to come of the column with the C_1 isomer

being intermediate – the 9th isomer to come off the column. Given the analysis of

Figure 5-30 that the retention time on the column depends on the separation of the

two addends. It seems reasonable to conclude that the first of the two same

symmetry isomers of a group to come of the column has its two addends further

apart than those of the other same symmetry isomer. Again, using the *trans*-4

216

isomers as an example, the C_s-symmetry *trans*-4 isomer that is the 5th purified

fraction to come of the column has more widely spaced addends than the C_s-

symmetry *trans*-4 isomer that is the 13th isomer to come off the column, and that

the 9th isomer to come off the column – (C_1)32,33-bis[60]PCBM – has intermediate

addend separation. Hence, it is hypothesised here that the two same symmetry

isomers may be distinguished by their HPLC behaviour based on their addend

separations.

As a rough measure of the separation of the two addends, the distance between the

two ester groups was used in this thesis. The ester was chosen over the phenyl

group because the ester extends the furtherer in space, and hence should have a

larger effect on disrupting the fullerene/stationary phase $\pi-\pi$ interactions. As such,

in the following analysis the separation of the B4 carbons of the two ester groups

is used as a relative measure of isomer polarity. B4 is chosen because the ester

group is flexible through rotation of the C-C single bonds. However, B4 carbon is

fixed in its orientation from its respective the bridge carbons (C61 or C62). Hence,

the effect of the flexibility occurs after B4. This argument also applies to the two

bridge carbons. However, for each bond type the bridge-bridge′ separation is the

same for all isomers of that bond type (the C61-C62 distance is the same for all

three *trans*-3 isomers) but the B4-B4′ distance depends on the isomer. The resulting

direct-line spacing between the two ester B4 carbons of each of the 19 isomers was

measured from the DFT geometry optimisations using the Gaussview v6.0

Software.

trans-1 isomers

The B4 spacings of (C_{2h})52,60-bis[60]PCBM and (C_{2v})52,60-bis[60]PCBM isomers are 11.85 and 11.55 Å, respectively. From this, on the basis that the ester groups are further apart for the C_{2h} isomer than the C_{2v} isomer shown in Figure 5-31, we would predict that the C_{2h} isomer would come of the column before the C_{2v} isomer. This prediction is consistent with the observation that the C_{2h} and C_{2v} isomers are the 1st and 3rd isomers to come off the column.

(a)   (b)

Figure 5-31 Diagrams of two trans-1 isomers in order of decreasing B4-B4' separation.
The order agrees with the HPLC retention time observation of the two isomers and suggests that the first C_{2h} isomer (F1.1) is (a) (C_{2h})52,60-bis[60]PCBM and that the second C_{2v} isomer (F2.1.1) is (b) (C_{2v})52,60-bis[60]PCBM.

trans-2 isomers

For the trans-2 isomers in Figure 5-32 the B4 spacings in decreasing order are 11.75, 11.20 and 10.43 Å from the isomers of (C_2)49,59-bis[60]PCBM], (C_1)49,59-bis[60]PCBM] and (C_2)53,54-bis[60]PCBM], respectively.

(a)	(b)	(c)

Figure 5-32 Diagrams of three *trans*-2 isomers in order of decreasing B4-B4' separation.
The order agrees with the HPLC retention time observation of the three isomers and suggests that the first C_2 isomer (F1.2) is (a) (C_2)49,59-bis[60]PCBM and that the second C_2 isomer (F3.1) is (c) (C_2)53,54-bis[60]PCBM. It also predicts that the central isomer (F2.1.1) is (b) (C_1)49,59-bis[60]PCBM, which has already been confirmed by ^{13}C NMR spectroscopy.

These spacings accurately predict the observed $C_2 - C_1 - C_2$ HPLC retention order of the *trans*-2 isomers. They are also consistent with the overall HPLC fraction order as (C_2)49,59-bis[60]PCBM, with a spacing of 11.75 Å, is in between the two *trans*-1 isomers – giving the observed (C_{2h})52,60-bis[60]PCBM – (C_2)49,59-bis[60]PCBM – (C_{2v})52,60-bis[60]PCBM – (C_1)49,59-bis[60]PCBM order for the first four isomers in HPLC order. Hence, confidently assign the 1st *trans*-2 isomer (F1.2) to be (C_2)49,49-bis[60]PCBM, and the latter (F3.1) to be (C_2)53,54-bis[60]PCBM. It also predicts that the central isomer (F2.1.1) is (C_1)49,59-bis[60]PCBM, which has already been confirmed by ^{13}C NMR spectroscopy.

trans-3 isomers

For the *trans*-3 isomers in Figure 5-33 the B4 spacings are 10.77, 10.08 and 9.91 Å from the isomers of (C_2)34,35-bis[60]PCBM and (C_1)34,35-bis[60]PCBM and (C_2)36,37-bis[60]PCBM, respectively.
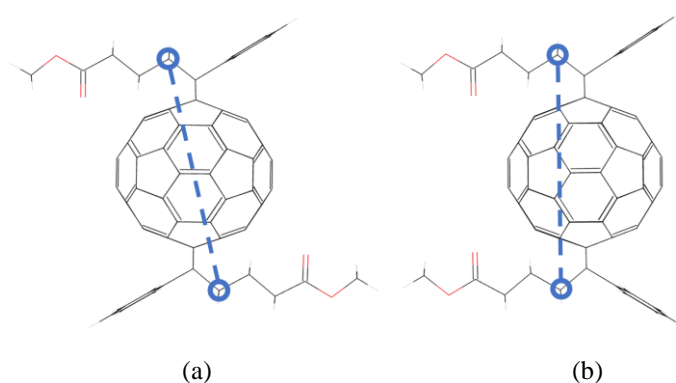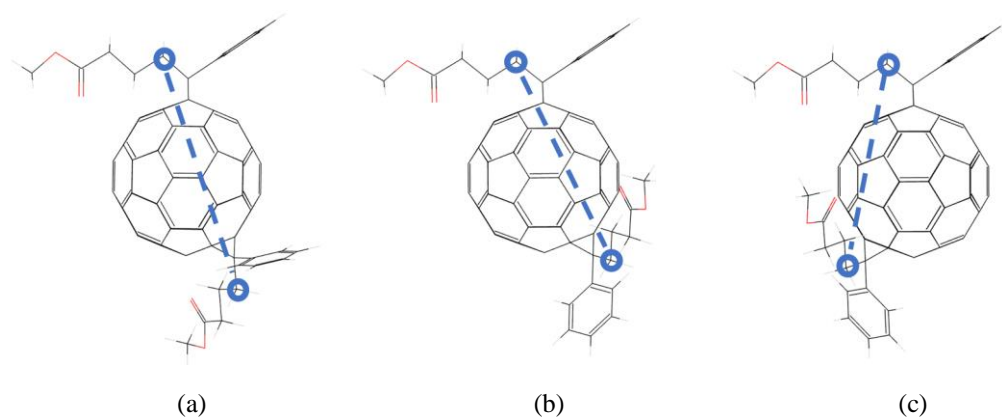
(a) (b) (c)

**Figure 5-33 Diagrams of three *trans*-3 isomers in order of decreasing B4-B4'
separation.**
The order agrees with the HPLC retention time observation of the three isomers and
suggests that the first C_2 isomer (F2.3) is (a) (C_2)34,35-bis[60]PCBM and that the
second C_2 isomer (F3.3.1) is (c) (C_2)36,37-bis[60]PCBM. It also predicts that the
central isomer (F3.2.1) is (b) (C_1)34,35-bis[60]PCBM, which has already been
confirmed by ^{13}C NMR spectroscopy.

As with the *trans*-2 bond-type, these spacings accurately predict the observed C_2 –

C_1 – C_2 HPLC order of the *trans*-3 isomers – again giving confidence to out B4

spacing method of determining the widely spaced same symmetry isomers of each

bond type. Hence, the 1st *trans*-3 isomer (F2.3) to is assigned to be (C_2)34,35-

bis[60]PCBM, and the latter (F3.3.1) to be (C_2)36,37-bis[60]PCBM. It also

predicts that the central isomer (F3.2.1) is (C_1)34,35-bis[60]PCBM, which has

already been confirmed by ^{13}C NMR spectroscopy.

trans-4 isomers

In decreasing order, the B4 spacings shown in Figure 5-34 for the *trans*-4 isomers

are 10.64, 9.61 and 8.05 Å from the isomers of (C_s)32,32-bis[60]PCBM, (C_1)32,32-

bis[60]PCBM and (C_s)38,38-bis[60]PCBM, respectively.

The spacings accurately predict the C_s – C_1 – C_s HPLC order of *trans*-4 isomers.

So the 1st *trans*-4 isomer (F2.2) is assigned to be (C_s)32,33-bis[60]PCBM and the

latter (F4) to be (C_s)38,39-bis[60]PCBM. It also predicts the central isomer (F3.2.2)

is (C_1)32,33-bis[60]PCBM which has confirmed by ^{13}C NMR spectroscopy.
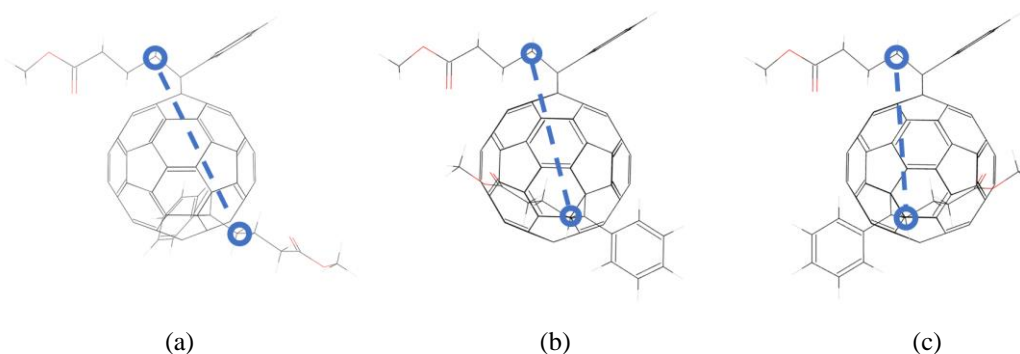
(a)   (b)   (c)

**Figure 5-34 Diagrams of three *trans*-4 isomers in order of decreasing B4-B4'
separation.**
The order agrees with the HPLC retention time observation of the three isomers and
suggests that the first C_s isomer (F2.2) is (a) (C_s)32,33-bis[60]PCBM and that the
second C_s isomer (F4) is (c) (C_s)38,39-bis[60]PCBM. It also predicts that the central
isomer (F3.2.2) is (b) (C_1)32,33-bis[60]PCBM, which has already been confirmed by
^{13}C NMR spectroscopy.

e isomers

Both *e* isomers have C_1 symmetry, which means that unlike the other two
membered-group (*trans*-1) or any of the three membered groups, none of these
isomers can be assigned to their respective isomer based on the ^{13}C NMR data.
However, we can only assign them based on our addend B4 spacing method. The
B4 carbons spacings of (C_1)30,31-bis[60]PCBM and (C_1)21,40-bis[60]PCBM
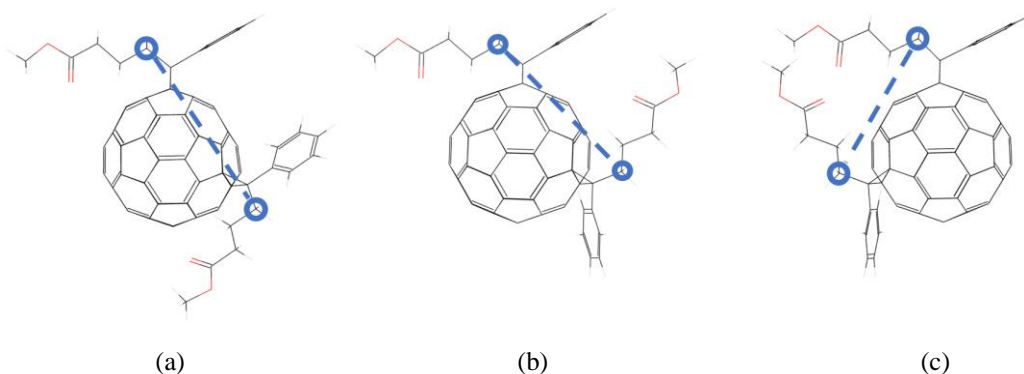isomers are 9.71 and 7.83 Å shown in Figure 5-35, respectively.
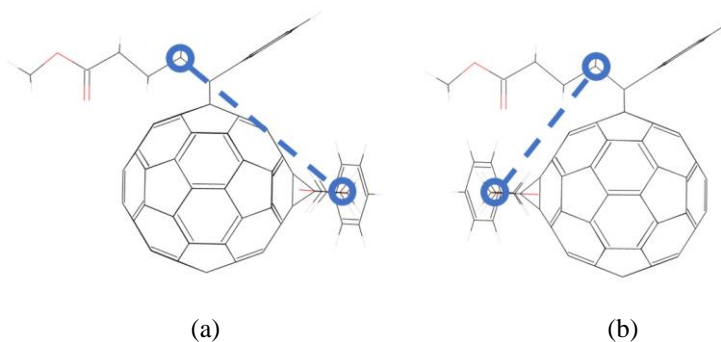

(a)   (b)

**Figure 5-35 Diagrams of two *e* isomers in order of decreasing B4-B4'
separation.**
The order agrees with the HPLC retention time observation of the two isomers and
suggests that the first C_1 isomer (F3.3.2) is (a) (C_1)30,31-bis[60]PCBM and that
the second C_1 isomer (F5.1) is (b) (C_1)21,40-bis[60]PCBM.

221

These isomers represent the 11th and 14th isomers to come off the column. Although

there are only two isomers between them, they are however still widely spaced in

HPLC retention time. This is because there is a large retention time gap between

F3 (which contains one of the equatorial isomers) and F4 and another wide gap

until fraction F5 (which contains the other equatorial isomers). Hence, based on

this wide HPLC separation the first isomer to come off the column, fraction F3.2.2

is assigned to (C_1)30,31-bis[60]PCBM on the basis of having the large ester B4

separation, and the latter isomer, F5.1 is assigned to (C_1)21,40-bis[60]PCBM.

cis-3 isomers

For the *cis*-3 isomers in Figure 5-36, the B4 spacings are 8.63, 5.64 and 6.89 Å

from the isomers of (C_2)13,14-bis[60]PCBM, (C_2)19,20-bis[60]PCBM and

(C_1)13,14-bis[60]PCBM, respectively.

(a)   (b)   (c)
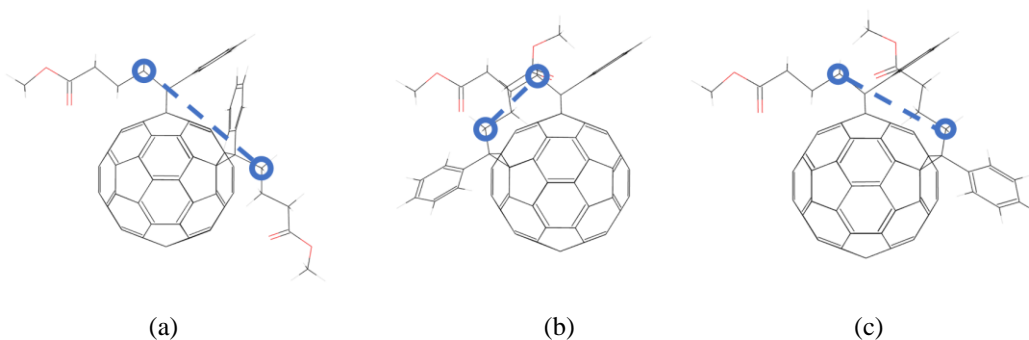
Figure 5-36 Diagrams of three *cis*-3 isomers of B4-B4' separation.
The order agrees with the HPLC retention-time observation of the three isomers and
suggests that the first C_2 isomer (F3.4) is (a) (C_2)13,14-bis[60]PCBM and that the
second C_2 isomer (F5.2.1) is (b) (C_2)19,20-bis[60]PCBM. It also predicts that the last
isomer (F5.2.2) is (c) (C_1)13,14-bis[60]PCBM, which has already been confirmed by
^{13}C NMR spectroscopy.

Again, these spacings accurately predict the observed $C_2 - C_2 - C_1$ HPLC order of

the *cis*-3 isomers. Hence, the 1st *cis*-3 isomer (F3.4) is assigned to be (C_2)13,14-

bis[60]PCBM, and F5.2.1 to be (C_2)19,20-bis[60]PCBM. It also predicts that the

last isomer (F5.2.2) is (C_1)13,14-bis[60]PCBM, which has already been confirmed

by ^{13}C NMR spectroscopy.

cis-2 isomers

In decreasing order, the B4 spacings for the *cis*-2 isomers are 6.64, 6.29 and 5.08

Å from the isomers of (C_s)3,15-bis[60]PCBM, (C_1)3,15-bis[60]PCBM and

(C_s)4,18-bis[60]PCBM, respectively. As demonstrates in Figure 5-37.

| (a) | (b) | (c) |
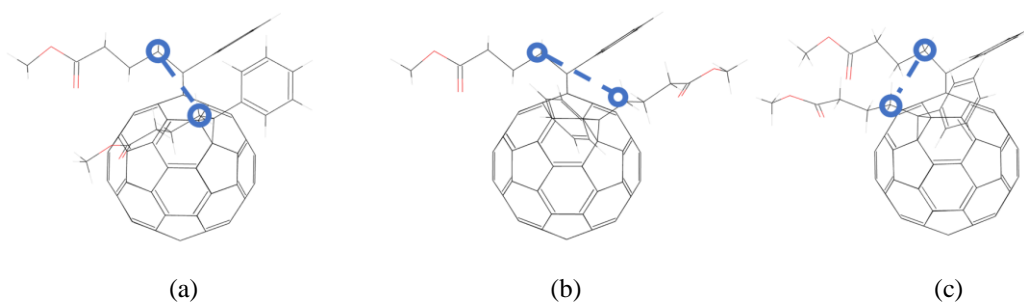
Figure 5-37 Diagrams of three *cis*-2 isomers in order of decreasing B4-B4' separation.
The order agrees with the HPLC retention-time observation of the three isomers and suggests that the first C_s isomer (F5.3) is (a) (C_s)3,15-bis[60]PCBM and that the second C_s isomer (F7) is (c) (C_s)4,18-bis[60]PCBM. It also predicts that the central isomer (F6) is (b) (C_1)3,15-bis[60]PCBM, which has already been confirmed by ^{13}C NMR spectroscopy.

Again, these spacings accurately predict the observed $C_s - C_1 - C_s$ HPLC order of

the *cis*-2 isomers. Hence, the 1st *cis*-2 isomer (F5.3) to is assigned to be (C_s)3,15-

bis[60]PCBM, and the latter, F7, to be (C_s)4,18-bis[60]PCBM. It also predicts that

the central isomer (F6) is (C_1)3,15-bis[60]PCBM, which has already been

confirmed by ^{13}C NMR spectroscopy.

5.5 Conclusion

At the beginning of this chapter we had 19 isomer-pure HPLC fractions of
bis[60]PCBM. However, we had no idea which HPLC fraction corresponded to
which isomers – or even how many isomers there should be.

By assuming that all isomers of bis[60]PCBM were, like [60]PCBM, cyclopropa-
fullerenes, it was determined that there were 58 nominal isomers originating from
29 remaining double bonds on [60]PCBM to which the second addend could add
in two different relative orientations. By inspection of these 58 isomers it was found
that several of them were symmetrically equivalent to each other, which reduced
the number of isomers to 36. By considering that most of the isomers are chiral,
and that enantiomers cannot be spectroscopically distinguished or separated in
normal columns, the number of effective isomers was determined to be 22. Finally,
by noting that isomers whereby both addends were attached to adjacent double
bonds on the same hexagonal rings were so close that they interfered with each
other and hence could not form for steric reasons, the number of formable isomer
was determined to be 19 – exactly the same number of the HPLC fractions.

By noting similarities and differences between the UV-Vis absorption spectra we
were able to place the HPLC fractions into 5 groups of three members and 2 groups
of two members. In addition, by considering all possible cyclopropa-fullerene
isomers of bis[60]PCBM we were able to place the isomers into 6 groups of three
members and 2 groups of two members based on their bond-type (*trans*-1, *trans*-2,
trans-3, *trans*-4, *e*, *cis*-3, *cis*-2 and *cis*-1). By noting that *cis*-1 isomers were unable
to form for steric reasons, we were left with 5 groups of three members and 2
groups of two members. The number of groups and the numbers of members of the

bond-type groups were exactly the same as the number of groups and the number of members as the UV-Vis spectral groups. This suggested that there was a link between the bond-types of the isomers and their UV-Vis spectra. By consulting the literature on molecular structure and UV-Vis absorption spectra of other fullerene bis-adducts, we were able to identify the bond types associated with each spectral type for bis[60]PCBM. This reduced the uncertainty of a particular isomer corresponding to a particular HPLC fraction from one in nineteen to one in two or three depending on the bond type. By employing ^{13}C NMR spectroscopy, we were able to unambiguously identify 7 of the isomers, and reduce the uncertainty in the assignment of all remaining isomers to one in two; where in each case the two members of each uncertain group had the same molecular symmetry. Finally, by noting that HPLC retention time is inversely correlated with addend separation, and by noting that the two uncertain same symmetry isomers within each two membered group had widely different HPLC retention times, we were able to assign each same symmetry isomer within each group to its particular isomer based on addend separation of the two same symmetry isomers within each group. It was also noted that there was no correlation between retention time and electric dipole moment, which is normally the property that governs HPLC behaviour in both normal-phase and reverse phase. This suggests that addend separation is the primary consideration for HPLC behaviour of fullerene bis-adducts Therefore, by a combination of HPLC retention time analysis, UV-Vis absorption spectroscopy and ^{13}C NMR spectroscopy, we were able to uniquely identify which specific isomer corresponded to which specific HPLC fraction. These findings are summarised in the Table 5-24. As a result of this work, we are now in the position to supply anyone with any specific isomer they desire.

Table 5-24 Complete isomer assignments to HPLC fractions based on a combination of isomer type (from UV−Vis spectra), ^{13}C NMR line patterns, HPLC retention time and calculated electric dipole moment.

bond type	isomer assignment	electric dipole/D	spacing/Å	HPLC fraction	^{13}C NMR pattern
trans-1	(C_{2h})52,60-bis[60]PCBM	0	11.85	F1.1	10×2+14×4
	(C_{2v})52,60-bis[60]PCBM	4.56	11.55	F2.1.1	12×2+15×4
trans-2	(C_2)49,59-bis[60]PCBM	1.36	11.75	F1.2	42×2
	(C_1)49,59-bis[60]PCBM	0.87	11.20	F2.1.2	84×1
	(C_2)53,54-bis[60]PCBM	0.79	10.43	F3.1	42×2
trans-3	(C_2)34,35-bis[60]PCBM	0.79	10.77	F2.3	42×2
	(C_1)34,35-bis[60]PCBM	0.82	10.08	F3.2.1	84×1
	(C_2)36,37-bis[60]PCBM	0.64	9.91	F3.3.1	42×2
trans-4	(C_s)32,33-bis[60]PCBM	1.51	10.64	F2.2	4×1+40×2
	(C_1)32,33-bis[60]PCBM	1.29	9.61	F3.2.2	84×1
	(C_s)38,39-bis[60]PCBM	0.93	8.05	F4	4×1+40×2
e	(C_1)30,31-bis[60]PCBM	1.55	9.71	F3.3.2	84×1
	(C_1)21,40-bis[60]PCBM	1.28	7.83	F5.1	84×1
cis-3	(C_2)13,14-bis[60]PCBM	1.44	8.63	F3.4	42×2
	(C_2)19,20-bis[60]PCBM	1.33	6.89	F5.2.1	42×2
	(C_1)13,14-bis[60]PCBM	1.41	5.64	F5.2.2	84×1
cis-2	(C_s)3,15-bis[60]PCBM	1.59	6.64	F5.3	4×1+40×2
	(C_1)3,15-bis[60]PCBM	4.15	6.29	F6	84×1
	(C_s)4,18-bis[60]PCBM	1.46	5.08	F7	4×1+40×2

6 Conclusions and recommendations

6.1 ^{1}H, ^{13}C and 2D NMR spectra for [60]PCBM

The high resolution of ^{1}H, ^{13}C and 2D NMR spectra were recorded for the typical organic electronics acceptor material [60]PCBM. Based on the analysis of chemical shift and integration from ^{13}C spectrum, the resonances from every carbon atom of the butyric acid methyl ester group, the phenyl ring group and the fullerene were identified. According to the 2D NMR spectrum, all carbon atoms with attached hydrogens were assigned to their respective resonances. By a process of elimination, the fullerene sp^3 carbons, bridgehead carbons (C1 and C9) and the bridge carbon (C61), were also unambiguously assigned.

The ωB97X DFT simulation of the ^{13}C NMR spectrum by employing a triple zeta Dunning basis set gave such a remarkable agreement with the experimental ^{13}C NMR spectrum, showing than the remaining fullerene resonances, and the ester carbonyl resonance were assigned to their respective resonances to a high level of

confidence. These confident assignments of carbon atoms suggest that this computational combination is highly suited for the simulation of the ^{13}C NMR spectra of fullerene derivatives.

The ^{1}H NMR resonances of [60]PCBM were also fully identified and assigned. Interestingly, the spin-spin couplings for the butyric acid methyl ester group were not as expected at 1st order in the ^{1}H NMR spectrum. Actually, the spectrum revealed clearly 2nd order couplings. This means that the two protons on each of the three carbons of the $-CH_2-CH_2-CH_2-$ chain are not magnetically equivalent apart from being symmetrically equivalent. It is indicated that there is not free rotation of the sigma bond of the alkyl chain in butyric acid methyl ester group, although rotation becomes free at larger distance from the fullerene bridge carbon (C61). Therefore, an AA′BB′-type system was used for the 2nd order couplings analysis. The hydrogens attached on carbons B3 and B4 from butyric acid methyl ester group revealed 7 coupling constants were determined. It was also determined that there was hindered rotation about the ester B3-B4 bond which yielded a 12.5 : 75 : 12.5 population ratio of the three staggered conformers (*gauche-anti-gauche'*) about this bond. These hindered rotational and conformational conclusions may also provide insights into the packing behavior of [60]PCBM in the solid state, and perhaps more importantly, it may assist in the understanding of the morphological interactions between [60]PCBM and its surroundings in condensed-phase organic electronic devices such as organic and perovskite photovoltaics.

6.2 Purification of bis[60]PCBM mixture into its constituent isomers

The as-produced bis[60]PCBM mixture was separated into its 19 constituted isomers by peak-recycling HPLC method. Firstly, an initial single-pass HPLC method was devised to partially purify the mixture of bis[60]PCBM into 7 multi-component fractions using a bare silica column. This column had the advantage of giving relatively long retention times over the columns which usually used for fullerenes. The longer retention time ranged from 5 to 70 minutes from the first to the last isomer. The 'fullerene' columns of 5PYE and 5PBB on the other hand both gave retention time that range about 3 to 5 minutes for all isomers – effectively appearing as a single broad multi-shouldered peak for the bis[60]PCBM mixture. Once the mixture was separated into the 7 fractions, multi-stage peak-recycling HPLC methods were used to purify each of the fractions into their subfractions, and even sub-subfractions in order to obtain individual samples of each isomer which is exceeding 99.0% purity. Once a fraction or subfraction was reduced to the stage where it only comprised two isomers, the 'fullerene' columns were used as they are more efficient than the bare silica column. A total of 19 isomers were purified out of the mixture and given working names based on their fraction, subfraction and sub-subfraction numbers, as appropriate.

6.3 Structural identification of all 19 isomers of bis[60]PCBM

58 possible molecular structures of bis-adducts have been reduced to 22 by the symmetry equivalent and chirality. Furthermore, 3 of these isomers of bis[60]PCBM cannot be formed because steric hindrance reasons – leaving 19

isomers. Aiming to determine the molecular structure of each of these 19 isomers purified from bis[60]PCBM mixture, they were characterised by UV-Vis absorption spectroscopy and ^{13}C NMR spectroscopy. Based on comparisons with known UV-Vis absorption spectra of analogous fullerene bis-adducts, the 19 isomers were places into 7 structural groups that depend on the bond-type of the 2nd addend location named as *trans*-1, *trans*-2, *trans*-3, *trans*-4, *e*, *cis*-3 and *cis*-2. As expected, there were no members of the 8th group which is *cis*-1 for steric reasons. These 7 groups respectively had 2, 3, 3, 3, 2, 3, and 3 members, which are the number of expected spectroscopically distinguishable isomers for each bond type group. These provided that all isomers were cyclopropa-fullerenes.

As the IUPAC systematic names of these isomers are very long and difficult to be determined, a naming system was proposed for these isomers. The new naming system keeps the commonly-used bis[60]PCBM, then replaces the *trans*-1, *cis*-2, etc., labels and their inconsistent as well as ill-defined sub-labels for the variants of each bond-type with the unambiguous fullerene carbon atom numbering from the IUPAC system. This system also negates the high difficulty of determining the stereochemistry (R/S isomerism) which posed by the presence of six chiral centres per isomer through employing the isomer's point group symmetry.

The ^{13}C NMR results show that all 19 isomers are cyclopropa-fullerenes (and conversely that none of them are homo-fullerenes which would involve single bonds, double bonds or a combination of both). Leaving aside the 3 *cis*-1 isomers which cannot form for steric hindrance reasons, the results also show that the mixture contains every one of the 19 possible spectroscopically distinguishable isomers. Based on the number of resonance and relative intensity from the ^{13}C

NMR spectra, it is allowed for the two *trans*-1 isomers, and the sole C_1 symmetry isomers from each of the 5 three-membered bond-type groups to be unambiguously assigned to their respective HPLC fraction. The two same symmetry isomers in each of the 6 remaining groups (*trans*-2, *trans*-3, *trans*-4, *e*, *cis*-3 and *cis*-2) cannot be distinguished by ^{13}C NMR spectroscopy. However, in each group of these 6 groups, it was noted that the two same symmetry isomers were widely separated in HPLC retention – being the 1st and last isomer in each group to come off the HPLC column. With the HPLC columns separating isomers based on their shape (such that the more polar the isomer the shorter its retention time), and with this polarity being related to the separation of the two addends (such that the closer the addend the more polar the isomer), the isomer with the larger addend separation was assigned to the HPLC fraction with the shorter retention time in each of the 6 groups. In this way, the remaining 12 isomers (two same symmetry isomers per group) were assigned to their respective HPLC fractions.

With these findings, each purified HPLC fraction was assigned to a specific structural isomer. This information is crucial to those who fabricate photovoltaic devices using purified bis[60]PCBM isomers which have varied energy levels. This is because they can now know which specific structural isomer is being employed in their devices. Or conversely, if a researcher requires a specific isomer, this isomer can be purified from the mixture as the target. With this information, photovoltaic devices based on purified bis[60]PCBM isomers may now be associated with a specific structural isomer. Thereby, a deeper understanding of the energetic and morphological order/disorder within the acceptor phase of bulk heterojunction OPVs and the electron extraction layer of perovskite solar cells may be further developed by researchers on the field.

231

6.4   Recommended future work

Further DTF work: Benchmarking of a range-separated DFT methods for the simulation of ^{13}C NMR spectra of fullerene derivatives initially with a reasonably large basis set. Benchmarking basis sets for the more successful DFT methods. Optimization of the parameters within the more successful DFT/basis set combinations. For example, within ωB97X the rate of change from pure DFT exchange energy for each electron pair at a separation of $r_{1,2} = 0$ to pure Hartree-Fock exchange at $r_{1,2}$ = infinity may be optimize by varying the range-separation parameter ω; and the fraction of Hartree-Fock exchange at $r_{1,2} = 0$ may be varied from 0 to 1 through the short-range Hartree-Fock coefficient, c_x in ωB97X.

Further NMR work: The ^{1}H NMR spectroscopy of each of the bis[60]PCBM isomers needs to be performed and analyzed. This thesis concentrated on the ^{13}C NMR spectra of these for their molecular structure information. The low natural abundance of ^{13}C meant the samples needed to be highly concentrated in order to obtain sufficient signal of ^{13}C NMR in a reasonable amount of time. Unfortunately, this meant that the ^{1}H spectra were generally of poor quality with line broadening artefacts. For example, the methyl hydrogens showing at unresolved 1:2:3 triplets in most isomers.

Future work on OPV devices: Combining the work of Shi and co-authors[93, 96] that the isomer mixture of bis[60]PCBM may be separated into their individual constituent isomers and known the frontier orbital energies of each purified HPLC fraction. Now with this thesis, those who follow and make OPV devices with the purified isomers may also know which specific isomer they are putting in their devices. With that, they will be able to make meaningful conclusions on what

structural properties of bis[60]PCBM isomers are useful. For example on which combinations of regio and stereo isomerism are beneficial and which are detrimental to OPV performance – both from improving energetic disorder and morphology disorder point of view. With 19 closely related but systematically varied species, with subtle differences, a considerable amount of information may be obtained. Then armed with this information, chemists can perform targeted synthesis to produce only isomer with beneficial properties (or suppress the synthesis of isomers with detrimental properties). Another form of future work would go beyond bis[60]PCBM. That is, the new analogous molecules with all the beneficial properties and without any of the detrimental properties (as obtained through isomer-pure bis[60]PCBM studies) could be synthesized and employed in OPV devices rather than targeted synthesis of good bis[60]PCBM isomers.

Reference

1.   J. C. Hummelen, B. W. Knight, F. Lepeq, F. Wudl, J. Yao and C. L. Wilkins, *J. Org. Chem.*, 1995, **60**, 532-538.

2.   C. J. Brabec, F. Padinger, N. S. Sariciftci and J. C. Hummelen, *J. Appl. Phys.*, 1999, **85**, 6866-6872.

3.   F. B. Kooistra, V. D. Mihailetchi, L. M. Popescu, D. Kronholm, P. W. M. Blom and J. C. Hummelen, *Chem. Mater.*, 2006, **18**, 3068-3073.

4.   P. R. Berger and M. Kim, *J. Renew. Sustain. Ener.*, 2018, **10**.

5.   Y. Z. Lin and X. W. Zhan, *Mater. Horiz.*, 2014, **1**, 470-488.

6.   N. D. Treat and M. L. Chabinyc, *Annu. Rev. Phys. Chem.*, 2014, **65**, 59-81.

7.   T. Ameri, P. Khoram, J. Min and C. J. Brabec, *Adv. Mater.*, 2013, **25**, 4245-4266.

8.   C. Groves, O. G. Reid and D. S. Ginger, *Acc. Chem. Res.*, 2010, **43**, 612-620.

9.   O. Inganas, F. L. Zhang and M. R. Andersson, *Acc. Chem. Res.*, 2009, **42**, 1731-1739.

10.   R. Kroon, M. Lenes, J. C. Hummelen, P. W. M. Blom and B. De Boer, *Polym. Rev.*, 2008, **48**, 531-582.

11.   T. Hamasaki, T. Morimune, H. Kajii, S. Minakata, R. Tsuruoka, T. Nagamachi and Y. Ohmori, *Thin Solid Films*, 2009, **518**, 548-550.

12.   X. M. Zhao, T. J. Liu, X. Y. Hou, Z. L. Liu, W. D. Shi and T. J. S. Dennis, *J. Mater. Chem. C*, 2018, **6**, 5489-5496.

13.   Y. L. Shen, D. J. Yu, X. Wang, C. X. Huo, Y. Wu, Z. F. Zhu and H. B. Zeng, *Nanotechnology*, 2018, **29**.

14.   Z. Tang, Z. F. Ma, A. Sanchez-Diaz, S. Ullbrich, Y. Liu, B. Siegmund, A. Mischok, K. Leo, M. Campoy-Quiles, W. W. Li and K. Vandewal, *Adv. Mater.*, 2017, **29**.

15.   B. R. Sutherland, A. K. Johnston, A. H. Ip, J. X. Xu, V. Adinolfi, P. Kanjanaboos and E. H. Sargent, *Acs Photonics*, 2015, **2**, 1117-1123.

16.   H. H. Xu, J. Li, B. H. K. Leung, C. C. Y. Poon, B. S. Ong, Y. T. Zhang and N. Zhao, *Nanoscale*, 2013, **5**, 11850-11855.

17.   X. H. Wang, O. Hofmann, R. Das, E. M. Barrett, A. J. Demello, J. C. Demello and D. D. C. Bradley, *Lab on a Chip*, 2007, **7**, 58-63.

18.   T. T. Do, S. Chavhan, J. Subbiah, T. H. Ou, S. Manzhos, D. Jones, J. M. Bell, J. H. Jou and P. Sonar, *New J. Chem.*, 2019, **43**, 9243-9254.

19.   L. Vasilak, S. M. T. Halirn, H. Das Gupta, J. Yang, M. Karnperman and A. Turak, *Acs Appl. Mater. Inter.*, 2017, **9**, 13347-13356.

20. Q. M. Zhang, L. J. Chen, W. Y. Jia, Y. L. Lei and Z. H. Xiong, *Org. Electron.*, 2016, **39**, 318-322.

21. J. Jimenez-Loppez and E. Palomares, *Chem*, 2019, **5**, 748-749.

22. A. Mahmood, J. Y. Hu, B. Xiao, A. L. Tang, X. C. Wang and E. J. Zhou, *J. Mater. Chem. A*, 2018, **6**, 16769-16797.

23. A. W. Hains, C. Ramanan, M. D. Irwin, J. Liu, M. R. Wasielewski and T. J. Marks, *Acs Appl. Mater. Inter.*, 2010, **2**, 175-185.

24. A. B. Tamayo, B. Walker and T. Q. Nguyen, *J. Phys. Chem. C*, 2008, **112**, 11545-11551.

25. B. C. Thompson, Y. G. Kim, T. D. McCarley and J. R. Reynolds, *J. Am. Chem. Soc.*, 2006, **128**, 12714-12725.

26. A. N. Aleshin, I. P. Shcherbakov, I. N. Trapeznikova and V. N. Petrov, *Phys. Solid State*, 2016, **58**, 1882-1890.

27. M. A. Faist, P. E. Keivanidis, S. Foster, P. H. Wobkenberg, T. D. Anthopoulos, D. D. C. Bradley, J. R. Durrant and J. Nelson, *J. Polym. Sci. Pol. Phys.*, 2011, **49**, 45-51.

28. T. Lan, F. Soavi, M. Marcaccio, P. L. Brunner, J. Sayago and C. Santato, *Chem. Commun.*, 2018, **54**, 5490-5493.

29. B. Park, *Thin Solid Films*, 2015, **578**, 156-160.

30. B. Z. Yang, Y. S. Lin and J. M. Wu, *Appl. Mater. Today*, 2017, **9**, 96-103.

31. C. H. Chiang and C. G. Wu, *Nat. Photonics*, 2016, **10**, 196-200.

32. J. H. Heo, H. J. Han, D. Kim, T. K. Ahn and S. H. Im, *Energ. Environ. Sci.*, 2015, **8**, 1602-1608.

33. J. Y. Jeng, K. C. Chen, T. Y. Chiang, P. Y. Lin, T. D. Tsai, Y. C. Chang, T. F. Guo, P. Chen, T. C. Wen and Y. J. Hsu, *Adv. Mater.*, 2014, **26**, 4107-4113.

34. J. Seo, S. Park, Y. C. Kim, N. J. Jeon, J. H. Noh, S. C. Yoon and S. I. Sang, *Energ. Environ. Sci.*, 2014, **7**, 2642-2646.

35. J. Xu, A. Buin, A. H. Ip, W. Li, O. Voznyy, R. Comin, M. J. Yuan, S. Jeon, Z. J. Ning, J. J. McDowell, P. Kanjanaboos, J. P. Sun, X. Z. Lan, L. N. Quan, D. H. Kim, I. G. Hill, P. Maksymovych and E. H. Sargent, *Nat. Commun.*, 2015, **6**.

36. J. B. You, Z. R. Hong, Y. Yang, Q. Chen, M. Cai, T. B. Song, C. C. Chen, S. R. Lu, Y. S. Liu and H. P. Zhou, *Acs Nano*, 2014, **8**, 1674-1680.

37. J. Nelson, *The physics of solar cells*, Imperial College Press, 2003.

38. D. S. Bethune, G. Meijer, W. C. Tang, H. J. Rosen, W. G. Golden, H. Seki, C. A. Brown and M. S. Devries, *Chem. Phys. Lett.*, 1991, **179**, 181-186.

39. J. P. Hare, T. J. Dennis, H. W. Kroto, R. Taylor, A. W. Allaf, S. Balm and D. R. M. Walton, *J. Chem. Soc. Chem. Commun.*, 1991, 412-413.

40. T. J. Dennis, J. P. Hare, H. W. Kroto, R. Taylor, D. R. M. Walton and P. J. Hendra, *Spectrochim. Acta. A*, 1991, **47**, 1289-1292.

41. J. A. Mikroyannidis, A. N. Kabanakis, S. S. Sharma and G. D. Sharma, *Adv. Funct. Mater.*, 2011, **21**, 746-755.

42. S. Shoaee, S. Subramaniyan, H. Xin, C. Keiderling, P. S. Tuladhar, F. Jamieson, S. A. Jenekhe and J. R. Durrant, *Adv. Funct. Mater.*, 2013, **23**, 3286-3298.

43. T. Umeyama, T. Miyata, A. C. Jakowetz, S. Shibata, K. Kurotobi, T. Higashino, T. Koganezawa, M. Tsujimoto, S. Gelinas, W. Matsuda, S. Seki, R. H. Friend and H. Imahori, *Chem. Sci.*, 2017, **8**, 181-188.

44. L. Ye, S. Q. Zhang, D. P. Qian, Q. Wang and J. H. Hou, *J. Phys. Chem. C*, 2013, **117**, 25360-25366.

45. Y. J. He, H. Y. Chen, J. H. Hou and Y. F. Li, *J. Am. Chem. Soc.*, 2010, **132**, 1377-1382.

46. S. Leach, M. Vervloet, A. Despres, E. Breheret, J. P. Hare, T. J. Dennis, H. W. Kroto, R. Taylor and D. R. M. Walton, *Chem. Phys.*, 1992, **160**, 451-466.

47. W. I. F. David, R. M. Ibberson, J. C. Matthewman, K. Prassides, T. J. S. Dennis, J. P. Hare, H. W. Kroto, R. Taylor and D. R. M. Walton, *Nature*, 1991, **353**, 147-149.

48. R. S. Ruoff, D. S. Tse, R. Malhotra and D. C. Lorents, *J. Phys. Chem.*, 1993, **97**, 3379-3383.

49. N. S. Sariciftci, L. Smilowitz, A. J. Heeger and F. Wudl, *Science*, 1992, **258**, 1474-1476.

50. J. P. Hare, H. W. Kroto and R. Taylor, *Chem. Phys. Lett.*, 1991, **177**, 394-398.

51. R. Taylor, J. P. Hare, A. K. Abdulsada and H. W. Kroto, *J. Chem. Soc., Chem. Commun.*, 1990, 1423-1424.

52. Z. Xu, L. M. Chen, G. W. Yang, C. H. Huang, J. H. Hou, Y. Wu, G. Li, C. S. Hsu and Y. Yang, *Adv. Funct. Mater.*, 2009, **19**, 1227-1234.

53. Z. Xu, L. M. Chen, M. H. Chen, G. Li and Y. Yang, *Appl. Phys. Lett.*, 2009, **95**.

54. G. Yu, J. Gao, J. C. Hummelen, F. Wudl and A. J. Heeger, *Science*, 1995, **270**, 1789-1791.

55. M. M. Wienk, J. M. Kroon, W. J. H. Verhees, J. Knol, J. C. Hummelen, P. A. van Hal and R. A. J. Janssen, *Angew. Chem. Int. Edit.*, 2003, **42**, 3371-3375.

56. T. D. Anthopoulos, D. M. de Leeuw, E. Cantatore, P. van 't Hof, J. Alma and J. C. Hummelen, *J. Appl. Phys.*, 2005, **98**.

57. M. A. Faist, S. Shoaee, S. Tuladhar, G. F. A. Dibb, S. Foster, W. Gong, T. Kirchartz, D. D. C. Bradley, J. R. Durrant and J. Nelson, *Adv. Energy Mater.*, 2013, **3**, 744-752.

58. C. Yang, J. Y. Kim, S. Cho, J. K. Lee, A. J. Heeger and F. Wudl, *J. Am. Chem. Soc.*, 2008, **130**, 6444-6450.

59. C. Liu, Y. J. Li, C. H. Li, W. W. Li, C. J. Zhou, H. B. Liu, Z. S. Bo and Y. L. Li, *J. Phys. Chem. C*, 2009, **113**, 21970-21975.

60. P. A. Troshin, H. Hoppe, J. Renz, M. Egginger, J. Y. Mayorova, A. E. Goryochev, A. S. Peregudov, R. N. Lyubovskaya, G. Gobsch, N. S. Sariciftci and V. F. Razumov, *Adv. Funct. Mater.*, 2009, **19**, 779-788.

61. Y. Zhang, H. L. Yip, O. Acton, S. K. Hau, F. Huang and A. K. Y. Jen, *Chem. Mater.*, 2009, **21**, 2598-2600.

62. H. U. Kim, J. H. Kim, H. Kang, A. C. Grimsdale, B. J. Kim, S. C. Yoon and D. H. Hwang, *Acs Appl. Mater. Inter.*, 2014, **6**, 20776-20785.

63. G. J. Zhao, Y. J. He, Z. Xu, J. H. Hou, M. J. Zhang, J. Min, H. Y. Chen, M. F. Ye, Z. R. Hong, Y. Yang and Y. F. Li, *Adv. Funct. Mater.*, 2010, **20**, 1480-1487.

64. L. P. Zheng, Q. M. Zhou, X. Y. Deng, M. Yuan, G. Yu and Y. Cao, *J. Phys. Chem. B*, 2004, **108**, 11921-11926.

65. J. A. Mikroyannidis, A. N. Kabanakis, P. Suresh and G. D. Sharma, *J. Phys. Chem. C*, 2011, **115**, 7056-7066.

66. J. A. Mikroyannidis, D. V. Tsagkournos, P. Balraju and G. D. Sharma, *Sol. Energy Mater. Sol. Cells*, 2011, **95**, 3025-3035.

67. J. A. Mikroyannidis, D. V. Tsagkournos, S. S. Sharma and G. D. Sharma, *J. Phys. Chem. C*, 2011, **115**, 7806-7816.

68. S. O. Kim, D. S. Chung, H. Cha, J. W. Jang, Y. H. Kim, J. W. Kang, Y. S. Jeong, C. E. Park and S. K. Kwon, *Sol. Energy Mater. Sol. Cells*, 2011, **95**, 432-439.

69. I. Yamada, M. Pandey, Y. Hayashi, N. Shibata, T. Soga and T. Toru, *9th International Conference on Nano-Molecular Electronics*, 2011, **14**.

70. M. Seri, E. Rossi, T. Carofiglio, S. Antonello, G. Ruani, M. Maggini and M. Muccini, *J. Mater. Chem.*, 2011, **21**, 18308-18316.

71. P. Nagarjuna, A. Bagui, J. H. Hou and S. P. Singh, *J. Phys. Chem. C*, 2016, **120**, 13390-13397.

72. J. Liu, X. Guo, Y. J. Qin, S. D. Liang, Z. X. Guo and Y. F. Li, *J. Mater. Chem.*, 2012, **22**, 1758-1761.

73. Y. Yu, B. Jin, R. F. Peng, L. S. Fan, L. H. Cai, B. Fan and S. J. Chu, *Synth. Met.*, 2016, **212**, 44-50.

74. M. F. Wang, E. Chesnut, Y. M. Sun, M. H. Tong, M. Guide, Y. Zhang, N. D. Treat, A. Varotto, A. Mayer, M. L. Chabinyc, T. Q. Nguyen and F. Wudl, *J. Phys. Chem. C*, 2012, **116**, 1313-1321.

75. H. U. Kim, D. Mi, J. H. Kim, J. B. Park, S. C. Yoon, U. C. Yoon and D. H. Hwang, *Sol. Energy Mater. Sol. Cells*, 2012, **105**, 6-14.

76. C. Liu, S. Q. Xiao, X. P. Shu, Y. J. Li, L. Xu, T. F. Liu, Y. W. Yu, L. Zhang, H. B. Liu and Y. L. Li, *Acs Appl. Mater. Inter.*, 2012, **4**, 1065-1071.

77. J. Ge, J. Liu, X. Guo, Y. J. Qin, H. X. Luo, Z. X. Guo and Y. F. Li, *Chem. Phys. Lett.*, 2012, **535**, 100-105.

78. M. L. Lv, M. Lei, J. Zhu, T. Hirai and X. W. Chen, *Acs Appl. Mater. Inter.*, 2014, **6**, 5844-5851.

79. G. M. Lin, R. L. Cui, H. Huang, X. H. Guo, S. Y. Yang, C. Li, J. Q. Dong and B. Y. Sun, *Tetrahedron*, 2015, **71**, 7998-8002.

80. X. Y. Meng, W. Q. Zhang, Z. A. Tan, C. Du, C. H. Li, Z. S. Bo, Y. F. Li, X. L. Yang, M. M. Zhen, F. Jiang, J. P. Zheng, T. S. Wang, L. Jiang, C. Y. Shu and C. R. Wang, *Chem. Commun.*, 2012, **48**, 425-427.

81. L. L. Deng, J. Feng, L. C. Sun, S. Wang, S. L. Xie, S. Y. Xie, R. B. Huang and L. S. Zheng, *Sol. Energy Mater. Sol. Cells*, 2012, **104**, 113-120.

82. X. Y. Meng, W. Q. Zhang, Z. A. Tan, Y. F. Li, Y. H. Ma, T. S. Wang, L. Jiang, C. Y. Shu and C. R. Wang, *Adv. Funct. Mater.*, 2012, **22**, 2187-2193.

83. H. P. Zeng, T. T. Wang, A. S. D. Sandanayaka, Y. Araki and O. Ito, *J. Phys. Chem. A*, 2005, **109**, 4713-4720.

84. J. L. Segura, E. M. Priego, N. Martin, C. P. Luo and D. M. Guldi, *Org. Lett.*, 2000, **2**, 4021-4024.

85. G. Possamai, S. Marcuz, M. Maggini, E. Menna, L. Franco, M. Ruzzi, S. Ceola, C. Corvaja, G. Ridolfi, A. Geri, N. Camaioni, D. M. Guldi, R. Sens and T. Gessner, *Chem. Eur. J.*, 2005, **11**, 5765-5776.

86. G. D. Blanco, A. J. Hiltunen, G. N. Lim, C. B. Kc, K. M. Kaunisto, T. K. Vuorinen, V. N. Nesterov, H. J. Lemmetyinen and F. D'Souza, *Acs Appl. Mater. Inter.*, 2016, **8**, 8481-8490.

87. C. L. Chochos, N. Tagmatarchis and V. G. Gregoriou, *Rsc Adv.*, 2013, **3**, 7160-7181.

88. E. Voroshazi, K. Vasseur, T. Aernouts, P. Heremans, A. Baumann, C. Deibel, X. Xue, A. J. Herring, A. J. Athans, T. A. Lada, H. Richter and B. P. Rand, *J. Mater. Chem.*, 2011, **21**, 17345-17352.

89. C. Y. Zhang, S. Chen, Z. Xiao, Q. Q. Zuo and L. M. Ding, *Org. Lett.*, 2012, **14**, 1508-1511.

90. S. Chen, G. Ye, Z. Xiao and L. M. Ding, *J. Mater. Chem. A*, 2013, **1**, 5562-5566.

91. P. Sakthivel, T. W. Ban, S. Kim, Y. S. Gal, E. A. Chae, W. S. Shin, S. J. Moon, J. C. Lee and S. H. Jin, *Sol. Energy Mater. Sol. Cells*, 2013, **113**, 13-19.

92. A. Hirsch and M. Brettreich, *Fullerenes*, Wiley-VCH, Weinheim, 2005.

93. W. Shi, X. Hou, T. Liu, X. Zhao, A. B. Sieval, J. C. Hummelen and T. J. S. Dennis, *Chem. Commun.*, 2017, **53**, 975-978.

94. T. T. Cao, N. Chen, G. X. Liu, Y. B. Wan, J. D. Perea, Y. J. Xia, Z. W. Wang, B. Song, N. Li, X. H. Li, Y. Zhou, C. J. Brabec and Y. F. Li, *J. Mater. Chem. A*, 2017, **5**, 10206-10219.

95. L. H. Hu, R. L. Cui, H. Huang, G. M. Lin, X. H. Guo, S. Y. Yang, Y. F. Lian, J. Q. Dong and B. Y. Sun, *J. Nanosci. Nanotechno.*, 2015, **15**, 5285-5290.

96. W. Shi, *Fullerene isomers for organic photovoltaics*, Queen Mary University of London, 2016.

97. E. Osawa, *Kagaku*, 1970, 854.

98. Z. Yoshida and E. Osawa, *Aromaticity*, 1971.

99. D. E. H. Jones, *New Sci.*, 1966, **32**, 245.

100. D. H. E. Jones, *The Inventions of Daedalus*, Freeman, 1982.

101. D. A. Bochvar and E. G. Galpern, *Doklady Akademii Nauk Sssr*, 1973, **209**, 610-612.

102. R. A. Davidson, *Theor. Chim. Acta*, 1981, **58**, 193-231.

103. H. W. Kroto, *Chem. Soc. Rev.*, 1982, **11**, 435-491.

104. W. W. Dudley and D. A. Williams, *interstellar chemistry*, Academic Press, London, 1984.

105. J. August, H. W. Kroto and N. Trinajstic, *Astrophys. Space Sci.*, 1986, **128**, 411-419.

106. E. A. Rohlfing, D. M. Cox, A. Kaldor and K. H. Johnson, *J. Chem. Phys.*, 1984, **81**, 3846-3851.

107. H. W. Kroto, J. R. Heath, S. C. Obrien, R. F. Curl and R. E. Smalley, *Nature*, 1985, **318**, 162-163.

108. W. Kratschmer, L. D. Lamb, K. Fostiropoulos and D. R. Huffman, *Nature*, 1990, **347**, 354-358.

109. J. R. Heath, S. C. Obrien, Q. Zhang, Y. Liu, R. F. Curl, H. W. Kroto, F. K. Tittel and R. E. Smalley, *J. Am. Chem. Soc.*, 1985, **107**, 7779-7780.

110. F. Wudl, R. E. Smalley, A. B. Smith, R. Taylor, E. Wasserman and E. W. Godly, *Pure Appl. Chem.*, 1997, **69**, 1412-1434.

111. A. Hirsch, I. Lamparth and H. R. Karfunkel, *Angew. Chem. Int. Ed. Engl.*, 1994, **33**, 437-438.

112. F. Djojo, A. Herzog, I. Lamparth, F. Hampel and A. Hirsch, *Chem. Eur. J.*, 1996, **2**, 1537-1547.

113. R. K. M. Bouwer, *Fullerene bisadducts for organic photovoltaic*, University of Groningen, 2012.

114. X. Hou, *Purification and characterisation of Bis[60]PCBM isomers and study of the degradation of organic solar cells based on them*, Queen Mary University of London, 2019.

115. S. Fanali, P. Haddad, C. Poole, P. Schoenmakers and P. Lioyd, *Liquid Chromatography*, Elsevier, 2013.

116. M. L. Zhang and H. D. Qiu, *Trac-Trends Anal. Chem.*, 2015, **65**, 107-121.

117. E. E. Maroto, M. Izquierdo, S. Reboredo, J. Marco-Martinez, S. Filippone and N. Martin, *Acc. Chem. Res.*, 2014, **47**, 2660-2670.

118. J. Y. Zhang, S. Stevenson and H. C. Dorn, *Acc. Chem. Res.*, 2013, **46**, 1548-1557.

119. C. Thilgen and F. Diederich, *Fullerenes and Related Structures*, 1999, **199**, 135-171.

120. T. J. S. Dennis, T. Kai, T. Tomiyama and H. Shinohara, *Chem. Commun.*, 1998, 619-620.

121. T. J. S. Dennis, T. Kai, K. Asato, T. Tomiyama, H. Shinohara, T. Yoshida, Y. Kobayashi, H. Ishiwatari, Y. Miyake, K. Kikuchi and Y. Achiba, *J. Phys. Chem. A*, 1999, **103**, 8747-8752.

122. R. Taylor, G. J. Langley, A. G. Avent, T. J. S. Dennis, H. W. Kroto and D. R. M. Walton, *J. Chem. Soc. Perk. Trans. 2*, 1993, 1029-1036.

123. M. V. R., *Practical High-Performance Liquid Chromatography*, Wiley-Blackwell, 2010.

124. N. U. D., *HPLC Columns: Theory, Technology, and Practice*, Wiley-VCH, 1997.

125. D. C. Harris, *Quantitative Chemical Analysis*, W. H. Freeman and Company, New York, 2010.

126. C. M. Varma, J. Zaanen and K. Raghavachari, *Science*, 1991, **254**, 989-992.

127. C. C. Chen, S. P. Kelty and C. M. Lieber, *Science*, 1991, **253**, 886-888.

128. C. J. Welch, S. R. Perrin and D. Kuechl, *Abstracts of Papers of the American Chemical Society*, 1993, **206**, 40-ORGN.

129. A. G. Avent, D. Dubois, A. Penicaud and R. Taylor, *J. Chem. Soc. Perk. Trans. 2*, 1997, 1907-1910.

130. O. V. Boltalina and T. Nakajima, *New Fluorinated Carbons: Fundamentals and Applications*, Elsevier Inc., 2017.

131. U. Sahoo, A. K. Seth and R. Chawla, *UV/Visible Spectroscopy: Absorption Spectroscopy*, LAP LAMBERT Academic Publishing, 2012.

132. H. Günther, *NMR Spectroscopy: Basic Principles, Concepts and Applications in Chemistry*, Wiley-VCH, 2013.

133. W. Kemp, *NMR in Chemistry: A Multinuclear Approach*, Macmillan, London, 1986.

134. E. W. Garbisch, *J. Chem. Educ.*, 1968, 480-493

135. H. J. Reich, *J. Chem. Educ.*, 1995, **72(12)**, 1086.

136. A. Navarro-Vazquez, J. C. Cobas, F. J. Sardina, J. Casanueva and E. Diez, *J. Chem. Inf. Comput. Sci.*, 2004, **44**, 1680-1685.

137. W. J. Colucci, S. J. Jungk and R. D. Gandour, *Magn. Reson. Chem.*, 1985, **23**, 335-343.

138. C. Y. Yang, J. G. Hu and A. J. Heeger, *J. Am. Chem. Soc.*, 2006, **128**, 12007-12013.

139. R. Mens, S. Chambon, S. Bertho, G. Reggers, B. Ruttens, J. D'Haen, J. Manca, R. Carleer, D. Vanderzande and P. Adriaensens, *Magn. Reson. Chem.*, 2011, **49**, 242-247.

140. M. J. Frisch, G. W. Trucks, H. B. Schlegel, G. E. Scuseria, M. A. Robb, J. R. Cheeseman, G. Scalmani, V. Barone, G. A. Petersson, H. Nakatsuji, X. Li, M. Caricato, A. V. Marenich, J. Bloino, B. G. Janesko, R. Gomperts, B. Mennucci, H. P. Hratchian, J. V. Ortiz, A. F. Izmaylov, J. L. Sonnenberg, D. Williams-Young, F. Ding, F. Lipparini, F. Egidi, J. Goings, B. Peng, A. Petrone, T. Henderson, D. Ranasinghe, V. G. Zakrzewski, J. Gao, N. Rega, G. Zheng, W. Liang, M. Hada, M. Ehara, K. Toyota, R. Fukuda, J. Hasegawa, M. Ishida, T. Nakajima, Y. Honda, O. Kitao, H. Nakai, T. Vreven, K. Throssell, J. A. Montgomery, Jr., J. E. Peralta, F. Ogliaro, M. J. Bearpark, J. J. Heyd, E. N. Brothers, K. N. Kudin, V. N. Staroverov, T. A. Keith, R. Kobayashi, J. Normand, K. Raghavachari, A. P. Rendell, J. C. Burant, S. S. Iyengar, J. Tomasi, M. Cossi, J. M. Millam, M. Klene, C. Adamo, R. Cammi, J. W. Ochterski, R. L. Martin, K. Morokuma, O. Farkas, J. B. Foresman and D. J. Fox, *Gaussian 16, Revision C.01*, Gaussian, Inc., Wallingford CT, 2016.

141. J. D. Chai and M. Head-Gordon, *J. Chem. Phys.*, 2008, **128**, 084106.

142. T. H. Dunning, *J. Chem. Phys.*, 1989, **90**, 1007-1023.

143. A. D. Becke, *J. Chem. Phys.*, 1993, **98**, 5648-5652.

144. S. Bennia, R. Milad, S. Messaoudi, M. de Person, F. Moussa, M. Abderrabba and D. Merlet, *Plos One*, 2018, **13**.

145. P. A. Christy, A. J. Peter and C. W. Lee, *Solid State Commun.*, 2018, **283**, 22-26.

146. P. A. Christy, A. J. Peter and C. W. Lee, *Physica B*, 2019, **555**, 9-17.

147. S. Dheivamalar, L. Sugi, K. Ravichandran and S. Sriram, *Spectrochim. Acta. A*, 2018, **202**, 333-345.

148. G. Colherinhas, E. E. Fileti and T. Malaspina, *J. Mol. Model.*, 2018, **24**.

149. A. R. Tulyabaev, I. I. Kiryanov, I. S. Samigullin and L. M. Khalilov, *Int. J. Quantum Chem.*, 2017, **117**, 7-14.

150. S. Nayak, S. Paul, A. Bauri, A. Ray and S. Bhattacharya, *J. Mol. Liq.*, 2018, **272**, 137-150.

151. C. Schneider, H. Nishimura, J. Lee, L. T. Scott, A. Wakamiya, R. Forbes and P. E. Georghiou, *Supramol. Chem.*, 2018, **30**, 575-582.

152. A. Miralrio, L. E. Sansores, B. King and A. Munoz-Castro, *Phys. Chem. Chem. Phys.*, 2018, **20**, 26325-26332.

153. X. Xu and W. A. Goddard, *Proc. Natl. Acad. Sci. U.S.A.*, 2004, **101**, 2673-2677.

154. M. S. Meier, H. P. Spielmann, R. G. Bergosh and M. C. Tetreau, *J. Org. Chem.*, 2003, **68**, 7867-7870.

155. X. Camps and A. Hirsch, *J. Chem. Soc. Perk. Trans. 1*, 1997, 1595-1596.

156. M. Lenes, G. Wetzelaer, F. B. Kooistra, S. C. Veenstra, J. C. Hummelen and P. W. M. Blom, *Adv. Mater.*, 2008, **20**, 2116-2119.

157. T. Liu, I. Abrahams and T. J. S. Dennis, *J. Phys. Chem. A*, 2018, **122**, 4138-4152.

158. H. E. Gottlieb, V. Kotlyar and A. Nudelman, *J. Org. Chem.*, 1997, **62**, 7512-7515.

159. *Dassault Systèmes BIOVIA*, *Discovery studio 4.5 Client*, *San Diego: Dassault Systèmes*, 2019.

160. R. Dennington, T. A. Keith and J. M. Millam, *GaussView, Version 6*, Semichem Inc. Shawnee Mission KS, 2019.

161. N. Tagmatarchis, A. G. Avent, K. Prassides, T. J. S. Dennis and H. Shinohara, *Chem. Commun.*, 1999, 1023-1024.